

University of Strathclyde
Design, Manufacture & Engineering Management

Reducing the environmental impact of hydraulic fracturing pumps

Aleksandar Josifović

A thesis presented in fulfilment of the requirements
for the degree of Doctor of Philosophy

2016

Declaration of author's rights

This thesis is the result of the author's original research. It has been composed by the author and has not been previously submitted for examination which has led to the award of a degree.

The copyright of this thesis belongs to the author under the terms of the United Kingdom Copyright Acts as qualified by University of Strathclyde Regulation 3.50. Due acknowledgement must always be made of the use of any material contained in, or derived from, this thesis.

Aleksandar Josifović

September 2016

Abstract

The current approach to hydraulic fracturing requires large amounts of industrial hardware to be transported, installed and operated in temporary locations. Typically 70% of the mass of this equipment is comprised of the fleet of truck-mounted pumps required to provide the high pressures and flows necessary for well stimulation. The established design of these pumps were developed for the shale gas extraction industry in North America, where the environmental, geological, regulatory and social constraints are very different from Europe. Consequently the engineering choices made in the current pump designs did not focus on minimising the physical and environmental footprint of the operation. These aspects are of paramount importance for the emerging hydraulic fracturing industry in Europe, so it is timely to address these factors when considering the design of future high-pressure pumps for European shale resources.

This thesis develops and applies a methodology for environmental optimisation of the key mechanical design parameters for the high-pressure pumps that are central to hydraulic fracturing operations. Before describing the optimisation methodology the thesis provides an overview of the industrial plant required to carry out a hydraulic fracturing operation, and an estimate of the functional requirements (i.e. pressure and flow) of the equipment.

The computational model, central to the optimisation process, is validated by using field data from a hydraulic fracturing site in North America and an experimental test rig.

The optimisation analysis concludes that reducing the plunger diameter and running the pump at higher angular velocity, with lower forces, can increase pump efficiency by up to 4.6%. Furthermore the modification of the pump's parameters would result in several environmental benefits beyond the obvious economic gains of lower fuel con-

sumption. Previous studies have shown that over 90% of the emissions of CO_2 and other pollutants that occur during a hydraulic fracturing operation are associated with the pumps and their prime movers. Consequently, any increase in pumping efficiency will also reduce the greenhouse gas emissions and improve local air quality (CO_2 , NO_x and other pollutants). Additionally, the reduction in plunger diameter will reduce the amplitude of fatigue stresses and so increase the life of the units and allow their overall mass to be reduced. More reliable pumps could decrease the number of standby (i.e. backup) units necessary, and so reduce procurement costs and site traffic, including the overall site footprint.

The concluding system optimisation study suggests that the highest level of direct on-site emission is due to the inefficient and asynchronous operation of multiple frac-truck assemblies. Reducing the number of frac-truck assemblies subsequently affects pump traffic lowering the nuisance effects to the local community such as noise, road damage and road traffic risk.

Contents

Abstract	i
Contents	iii
List of Figures	ix
List of Tables	xiv
Nomenclature	xvi
1 Introduction	1
1.1 Motivation	2
1.1.1 Research Aims and Objectives	4
1.2 Thesis outline	4
2 Literature review	8
2.1 Geological overview of the processes	8
2.1.1 Oil Formation	9
2.1.2 Fundamental rock theory	10
2.1.3 Conventional Oil and Gas	12
2.1.4 Unconventional Oil and Gas	16
2.2 Hydraulic fracturing implementation	19
2.2.1 Well preparation	20
2.2.2 Single pumping stage	22
2.2.3 Multi-stage hydraulic fracturing of the entire well	23
2.2.4 Pressure, flow requirements and fluid composition	23

2.3	Process equipment	34
2.3.1	Transporting and storage equipment	34
2.3.2	Fluid mixing equipment	36
2.3.3	Pipeline - Manifold trailer	38
2.3.4	High-pressure PD pumps	39
2.4	Drive train assembly	41
2.4.1	Diesel Engine	42
2.4.2	Transmission	44
2.5	Positive displacement pump	46
2.5.1	Operating principle of PD pump	49
2.5.2	Power End design	50
2.5.3	Fluid End design	52
2.6	Environmental impact	54
2.7	Generation of improvement concepts	56
2.8	Summary	59
3	Methodology	61
3.1	Research mode and strategy	61
3.2	Research domain	62
3.3	Research technique	63
3.3.1	Methodology for development of computational model	65
3.3.2	Methodology for model validation	66
3.3.3	Methodology for pump and system optimisation	67
4	The Computational Model	69
4.1	Drive train modelling	69
4.1.1	Drive train overview	70
4.1.2	Drive train theory	72
4.2	Single cylinder model	75
4.2.1	Validation	76
4.2.2	Results produced by the single cylinder model	78
4.2.3	Discussion of a single cylinder model	79

4.3	Valve dynamics model	80
4.3.1	Aims and objectives of the valve model	81
4.3.2	Valve system overview	82
4.3.3	Valve computational modelling and model validation	82
4.3.4	Results of valve model	86
4.3.5	Discussion of valve model	86
4.4	Multi-cylinder model	89
4.4.1	Modelling of a multi-cylinder PD pump	90
4.4.2	Results of a multi-cylinder PD pump model	92
4.4.3	Power evaluation	94
4.4.4	Discussion of a multi-cylinder PD pump model	96
4.5	Summary	97
5	Field data	98
5.1	Data acquisition methodology	98
5.1.1	Sensor data	98
5.1.2	Location and well details	99
5.1.3	IMS gateway	99
5.1.4	Acquisition and data storage	101
5.1.5	Data transfer method	102
5.2	Data analysis	102
5.2.1	Methodology	102
5.2.2	State one overview	104
5.2.3	Data analysis summary	108
5.3	Conclusion	110
6	Pump test rig data	112
6.1	Test rig components	112
6.1.1	Pump	113
6.1.2	Motor	114
6.1.3	Inverter drive	114
6.1.4	Solenoid valve	114

6.1.5	Tank	115
6.1.6	Pipework	115
6.2	System requirements	115
6.3	Instrumentation and data acquisition	116
6.3.1	Process control	117
6.3.2	Sensor implementation	118
6.3.3	Safety and failure prevention	119
6.3.4	Data acquisition	119
6.4	Data analysis	120
6.4.1	Suction pressure	120
6.4.2	Discharge pressure	125
6.4.3	Internal chamber	127
6.4.4	Flow rate	129
6.5	Summary	131
7	Validation	133
7.1	Problems and Opportunities	133
7.2	Methodology	133
7.3	Statistical model	133
7.4	Data analysis	135
7.4.1	Suction pressure	135
7.4.2	Chamber pressure	138
7.4.3	Discharge pressure	141
7.4.4	Outlet flow rate	144
7.5	Summary	146
8	Optimisation study	149
8.1	Hydraulic fracturing: functional requirements	150
8.1.1	Pumping period	150
8.1.2	Pump pressure	151
8.1.3	Flow rate	151
8.1.4	Pump Requirements	152

8.1.5	Environmental Footprint	152
8.1.6	Case study summary	153
8.2	Single pump optimisation	154
8.2.1	Current design	154
8.2.2	Model	154
8.2.3	Coarse grid exploration study	156
8.2.4	PD pump design space results	157
8.2.5	Monte Carlo optimization	159
8.2.6	Mass reduction	162
8.2.7	PD pump design space discussion	163
8.3	Multi-pump system optimisation	164
8.3.1	Methodology	164
8.3.2	Multi-pump system modelling	165
8.3.3	Boundary conditions	166
8.3.4	Defining objective function	167
8.3.5	Optimised model	170
8.3.6	Multi-pump system optimisation summary	172
8.4	Assessing environmental impact	172
8.4.1	Input data - assumptions	172
8.4.2	Results	174
8.5	Summary	178
9	Discussion and conclusion	180
9.1	Key developments	183
9.2	Contribution to knowledge	184
9.3	Future work	184
	References	187
A	Appendix	1
A.1	Field data	1
A.1.1	Power End Tri-axial accelerometer	4
A.1.2	Fluid End Tri-axial accelerometer	4

A.2 Operational states two, three and four	7
B Test rig components	12
C Validation	16

List of Figures

1.1	Schematic representation of equipment interaction	2
1.2	Overall structure of research	5
2.1	Structure of literature review	9
2.2	Cycle of rocks	11
2.3	Permeability for tight gas reservoirs	17
2.4	Wellbore constriction	18
2.5	Wireline tools	21
2.6	Single stage of hydraulic fracturing	22
2.7	Multi-stage hydraulic fracturing	24
2.8	Mathematical solution to the stress distribution around the wellbore . .	25
2.9	Stress field distribution around the wellbore section	25
2.10	Further analysis of the stress fields	26
2.11	Fluid Composition Chart	31
2.12	Global overview of hydraulic fracturing equipment	33
2.13	On-site pipework schematic	35
2.14	Blender control panel mounted on the blender unit	37
2.15	Blender control software used in the control van	38
2.16	Manifold trailer and the fluid distribution	39
2.17	Sensor location on the frac-trailer assembly	40
2.18	Pump control software used in the control van	40
2.19	Composition of a frac-truck assembly	42
2.20	Diesel engine, component details	43
2.21	Engine and transmission combined performance curves	45

2.22	Transmission unit	46
2.23	Mechanical subsystems in positive displacement pump	47
2.24	Triplex positive displacement pump	47
2.25	PD pump operational summary	48
2.26	Operating principle of a PD pump	49
2.27	PD pump's power-end subassembly	50
2.28	PD pump's fluid-end subassembly	52
3.1	Framework of research methodology	62
3.2	Methodology for optimisation development	64
3.3	MatLab computational model and alternative tools	65
3.4	Computational model validation methodology	67
3.5	Summary of optimisation methodology	68
4.1	Mass flow rate from a positive displacement pump	71
4.2	Extracted engine's operational data	72
4.3	PD pump's plunger kinematics	75
4.4	Hydrodynamic transmission in MatLab powering PD pump operation	75
4.5	MatLab model pressure validation	77
4.6	MatLab model flow validation	78
4.7	Pump Speed Inputs	79
4.8	Results: Flow Rates at different rotational speed	80
4.9	Suction and discharge valve actuation and timing	85
4.10	Valve operating states	86
4.11	Mass flow rate in discharge stroke	87
4.12	Pressure during discharge stroke using remodelled valve dynamics	87
4.13	Single cylinder pump using lumped parameter model.	90
4.14	Triplex (three-cylinder) pump using lumped parameter model.	91
4.15	Lumped parameter and experimental model in one chamber	93
4.16	Pressure comparison in common manifold chamber	93
4.17	Power evaluation using lumped parameter model	95
4.18	Power comparison in one chamber	95

5.1	Sensor placement on the field unit	99
5.2	Typical well data from Pearsall basin	100
5.3	Field data acquisition unit	100
5.4	Methodology for data acquisition from the PD pump unit on site.	100
5.5	Pump metrics obtained during one pumping stage	103
5.6	Identifying transitional parts of the stage	103
5.7	Pump metrics during formation breakdown - state one	105
5.8	Collection of PD pump field metrics	105
5.9	Suction pressure during one pumping stroke	106
5.10	Frequency spectrum of the suction pressure	107
5.11	Pressure field in PD pump's discharge plenum	108
5.12	High amplitude variation of the discharge pressure	109
5.13	Frequency spectrum of the discharge pressure	109
5.14	Summary of the collected field data	110
6.1	Essential operating parameters from the test pump	113
6.2	Skid assembly with major components	115
6.3	PD pump assembly with regulating pneumatic valve	115
6.4	Test rig assembly	115
6.5	Test rig schematics and essential sensor information	116
6.6	Test rig inlet pressure variation	123
6.7	Inlet pressure during one pumping stroke in Test No. 18	124
6.8	Frequency spectrum of the inlet pressure	124
6.9	Test rig outlet pressure variation	125
6.10	Outlet pressure during one pumping stroke in Test No. 6	127
6.11	Frequency spectrum of the outlet pressure	128
6.12	Test rig chamber pressure from all cylinders	128
6.13	Test rig chamber pressure in one cylinder	129
6.14	Frequency analysis in a single pressure chamber	130
6.15	Test rig overall volumetric flow rate	130
7.1	Theory of correlation coefficient	134

7.2	Problems with correlation coefficient in cyclic systems	135
7.3	Comparison between the test rig data and the computational model . . .	137
7.4	Comparison between the field data and the computational model	137
7.5	Cylinder pressure comparison	139
7.6	Single cylinder pressure comparison	139
7.7	Triplex pump pressure field comparison	141
7.8	Outlet pressure comparison, test rig and the model	142
7.9	Outlet pressure recorded in the field and the computational model . . .	143
7.10	Comparing the computational model's flow rate response to the CFD . .	144
7.11	Comparing the flow rate from the test rig to the computational model .	145
8.1	Process map for optimisation development	150
8.2	Experimental case study values	154
8.3	Defining PD pump's operating range	155
8.4	Exploration of parameter design space	158
8.5	Histogram of the evaluated data	160
8.6	Effect of vehicle mass on fuel consumption in HGVs	162
8.7	Engine performance was modelled using manufacturer's data	168
8.8	Defining pump simulation input data	168
8.9	Histograms of the optimisation results	169
8.10	Quantified savings from the PD pump and the system optimisation . . .	177
A.1	Orientation of accelerometers on the PD pump	1
A.2	Pump metrics during formation breakdown - state one	2
A.3	Pump metrics prior to formation breakdown	3
A.4	Crankshaft accelerometer and data metrics	5
A.5	Power-end frequency analysis	5
A.6	Accelerometer's kinematic derivations	6
A.7	Fluid-end frequency analysis	6
A.8	Operating metrics in the state two	8
A.9	Operating metrics in the state two - one second data	9
A.10	Operating metrics in the state three	10

A.11 Operating metrics in the state four	11
B.1 Pneumatically actuated pressure adjusting valve	13
B.2 P&ID schematic of the test rig	14
B.3 Sensor calibration certificate	15
C.1 Factory test rig data from full size experiment conducted in the USA. .	16

List of Tables

1.1	Quantification of equipment footprint on site	3
2.1	Experimental flow rate data during hydraulic fracturing	30
2.2	Morphological chart of future hydraulic fracturing development	58
4.1	Summary of the power consumption from a single plunger	96
5.1	Suction pressure operational metrics	106
5.2	Discharge pressure	107
6.1	Electric motor performance specification	114
6.2	Variable frequency drive performance specification	114
6.3	Pressures sensors selected for this experimental setup	117
6.4	Data acquisition characteristics	120
6.5	Test outline	121
6.6	Inlet pressure	122
6.7	Outlet pressure	126
7.1	Suction pressure correlation, test rig and model	136
7.2	Suction pressure correlation, field data and model	136
7.3	Simplex pump chamber pressure correlation	138
7.4	Chamber pressure correlation, model and experimental	138
7.5	Discharge pressure correlation, model and experimental	141
7.6	Discharge pressure correlation, model and field data	143
7.7	Chamber flow rate correlation, model and experimental	145
7.8	Discharge flow rate comparison, model and experimental	145

8.1	List of shale formation properties	151
8.2	Defining optimisation's boundary conditions	155
8.3	Results from PD pump optimisation	161
8.4	Frac site and engine boundary conditions	167
8.5	Optimisation results for site management	171
8.6	Environmental optimisation in hydraulic fracturing - input data	173
8.7	Environmental optimisation in hydraulic fracturing - results	175
8.8	Environmental optimisation in hydraulic fracturing - results	176
A.1	Accelerometer located on the PD pump's Power End	4
A.2	Accelerometer located on the PD pump's Fluid End	5

Acronyms

API	American petroleum institute
BDC	bottom dead centre
BSFC	brake specific fuel consumption
DAQ	Data acquisition system
DECC	Department of Energy & Climate Change
EPA	environmental protection agency
FE	fluid end
FM	Flowmaster software
HP	horse power
LPG	Liquefied Petroleum Gas
MD	measured depth
NPSH	Net positive suction head
OEM	Original Equipment Manufacturer
PD	positive displacement
PE	power end
RF	recovery factor
RMS	root mean square
RMSE	root mean square error
SBC	Single Board Computer
SSD	solid state drive
TDC	top dead centre
TDS	total dissolved solids
TVD	true vertical depth

Published papers

The work from this thesis has contributed to the following list of publications:

1. Josifovic, Aleksandar, Jennifer Roberts, Jonathan Corney, Bruce Davies and Zoe Shipton. Reducing the environmental impact of hydraulic fracturing through design optimisation of positive displacement pumps. In print. *Energy*, 2016.
2. Josifovic, Aleksandar and Jonathan Corney. Development of industrial process characterisation through data mining. IEEE Symposium Series on Computational Intelligence Accepted. *IEEE SSCI*, 2016.
3. Josifovic, Aleksandar, Jonathan Corney, and Bruce Davies. Valve dynamics in multi-cylinder positive displacement pump model. *Advanced Intelligent Mechatronics (AIM), 2015 IEEE/ASME International Conference on*. IEEE, 2015, DOI:<http://dx.doi.org/10.1109/aim.2015.7222505>.
4. Josifovic, Aleksandar, Jonathan Corney, and Bruce Davies. Modelling dynamic response in multi-cylinder positive displacement pump. *CONTECH' - 14 Control Engineering Conference on Mechatronics, Advanced Manufacturing Technologies, Automatic Control Systems and Information Technology. Istanbul, Turkey*, 2014.
5. Josifovic, Aleksandar, Jonathan Corney, and Bruce Davies. Modeling a variable speed drive for positive displacement pump. *Advanced Intelligent Mechatronics (AIM), 2014 IEEE/ASME International Conference on*. IEEE, 2014, DOI:<http://dx.doi.org/10.1109/aim.2014.6878248>.

Papers currently under review:

1. Josifovic, Aleksandar, Aldo Iannetti, Jonathan Corney and Matthew Stickland. A new engineering procedure for Positive Displacement Pump performance analysis based on 1D and 3D CFD commercial codes. *Journal of Dynamic Systems, Measurement and Control, DS-16-1415*.
2. Josifovic, Aleksandar, Jennifer Roberts, Jonathan Corney and Zoe Shipton. Process optimisation and environmental assessment in hydraulic fracturing systems. *PNAS* prepared for submission.

Chapter 1

Introduction

The International Energy Agency (IEA) [1] has estimated that, by 2035, gas demand will have increased by 50% of 2011 levels. Such growth would impact on the global energy mix and see gas overtake coal as the second-largest energy source after oil. The same report also suggested that after 2020 unconventional gas extraction will account for 32% of the total gas production worldwide (currently, this figure is estimated to be about 14%). If the figures suggested by the IEA report are to be realised, gas extraction from unconventional sources will have to double by 2020. Interest in unconventional sources of hydrocarbons has also been motivated by the desire to ensure the security of Europe's gas supply [2].

Although surveys suggest there are significant potential shale gas reserves in Europe (e.g. Britain [3], France and Poland [4]), exploration has been limited and, to date, no large-scale extraction operations have commenced. This is largely because of concerns about a range of environmental and social impacts that has prevented the granting of legal licences for the process in a number of countries. While there are some potential subsurface risks (such as well integrity failure leading to groundwater pollution, or earth tremors from the hydraulic fracturing process), arguably, surface installations pose the greatest potential environmental and social risks [5]. These risks include surface water pollution, light and noise pollution, traffic, and air quality. In the UK, for example, operators have been refused licences to carry out hydraulic fracturing operations because of concerns about the noise of the machinery [6] and road traffic [7]. Thus the potential environmental impacts of the topside equipment must be minimised

if shale gas extraction operations are to become widespread in Europe.

1.1 Motivation

The process of hydraulic fracturing involves numerous mobile units designed to transport, store, mix and propel fluid down a wellbore. An operational “frac-site” in North America is reported to typically occupy approximately 3000 m^2 , of which two-thirds of all the units on site are frac-truck assemblies, (Table 1.1). In other words, the frac-truck assemblies dominate the equipment used in terms of their share of a site’s power consumption, transported mass and surface footprint. The frac-truck assemblies are comprised of a prime mover (diesel engine), transmission and PD pump as shown in Figure 1.1. The performance of each individual element in the chain is non-linear with efficiencies that vary with operating conditions.

Although positive displacement pumps, similar to those installed on frac-truck assemblies, have high mechanical efficiency, 90% [8] the overall efficiency of the operation (i.e. from power generation to high-pressure flow) is rarely considered. For example [9] suggests potential development routes for positive displacement plunger pumps.

This thesis analyses the on-site equipment in detail and identifies opportunities for improvement in the mechanical design that will result in quantifiable benefits.

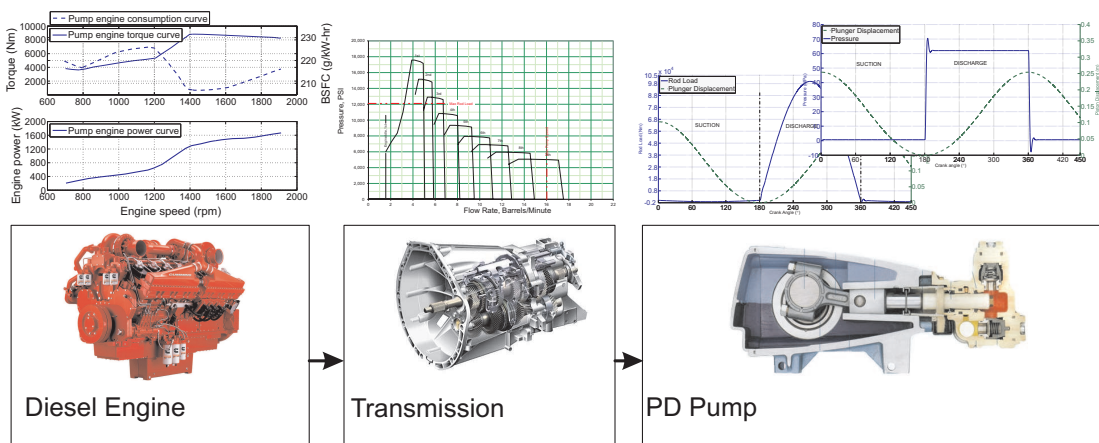


Figure 1.1: Schematic representation of equipment interaction in a frac-truck assembly

Although this work is focused on the needs of a specific pump, used in a particular operation, the wider significance is clear when history of reciprocating machinery and

Table 1.1: Quantification of equipment footprint on site

	Number of units	Area [m^2]	Engine power [kW]	Total area [m^2]	Total power [kW]
Blender	1	136	354	136 (6.2%)	354 (1.4%)
Control van	1	40	56	40 (1.8%)	56 (0.2%)
Frac-pump assembly	14	100	1678	1400 (64%)	23492 (95%)
Hydration assembly	1	128	354	128 (5.8%)	354 (1.4%)
Sand conveyors	2	200	90	400 (18.2%)	180 (0.8%)
Water transport	1	90	286	90 (4%)	572 (1.2%)
Total	20			2194 (100%)	24722 (100%)

the economics of pumping are considered.

Pumps are ubiquitous in industrial, commercial and domestic application around the world and power consumption from pumps in Europe, according to ETSU report [10] and energy efficiency study conducted by Fleiter et al. [11], accounts for 20% of the overall use of electric energy. Their effective function is critical in a vast range of applications in pharmaceutical [12], chemical process industries and medicine (high precision micro dosing pumps) [13]. Pump designs vary with the most common being centrifugal and positive displacement [8]. Given their widespread importance, even small improvements in energy efficiency can be economically significant. In order to improve energy efficiency of the equipment, it is necessary to study operating condition and pumping performance thoroughly.

The potential for improving the performance of reciprocating machinery through optimisation is illustrated by the history of the internal combustion engines. For example, around early 1900s Rolls Royce car engines were significantly larger in size (4118cc, 4 cylinder) but produced only 15 kW. In contrast, today's Formula 1 engines are 1600cc turbocharged V6 machines and produce up to 450 kW [14]. A process of continuous refinement of the basic function of the engine components has seen the adoption of electronic regulation, valve timing, precision manufacturing and the iterative system optimisation.

Given the context it would not be surprising if optimisation of the reciprocating pumps used in hydraulic fracturing resulted in significant benefits.

1.1.1 Research Aims and Objectives

The aim of this work is to analyse functional requirements of hydraulic fracturing equipment and identify ways to reduce the overall environmental impact.

Thus the aim can be stated as, “Reduce the environmental impact and improve operational efficiency of hydraulic fracturing.”

This aim is associated with the following objectives:

1. Assess the relative environmental impacts of equipment used in hydraulic fracturing
2. Identify the opportunities for system improvement
3. Identify the best candidate for detailed study
4. Quantify the potential benefits that would arise from a specific set of design parameters.

These initial objectives are developed when the specific focus of the work has been established. The outputs, associated with each of these objectives, define the contribution to knowledge arising from this work and are detailed in the conclusions 9.2.

1.2 Thesis outline

Figure 1.2 shows the structure of the thesis schematically. Each thesis chapter commences with a brief introduction outlining the contribution of the chapter to the overall thesis.

Chapter 2: Literature review

The literature review introduces the fundamental processes of oil and gas formation, evaluation and production. In the main part of the review, the motivation for hydraulic fracturing is established by emphasizing the different downhole properties of conventional and unconventional wells. The mechanics of well stimulation is presented by establishing required equipment output in terms of pressure, flow rate, density and fluid composition.

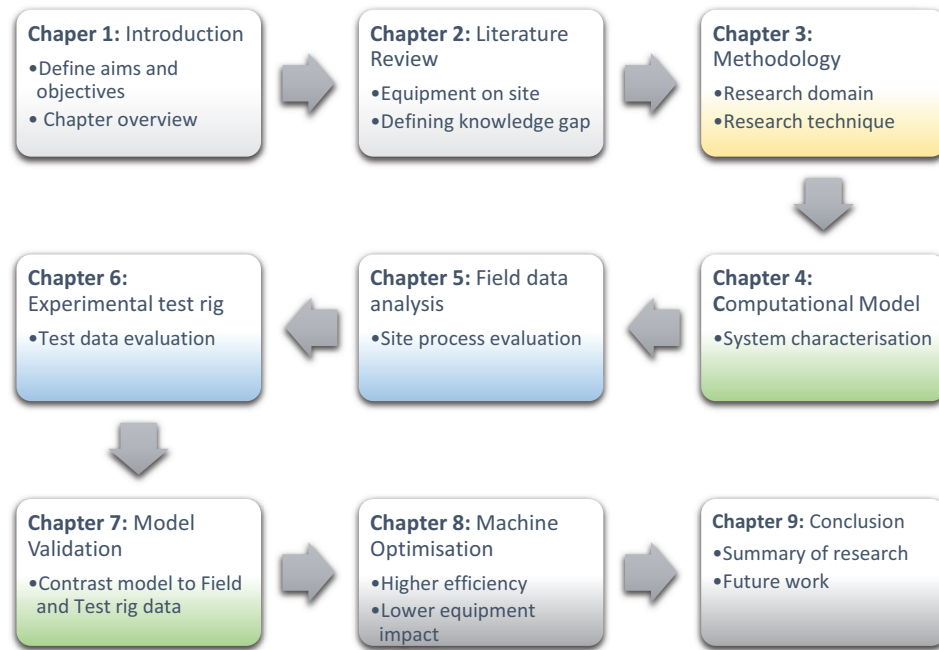


Figure 1.2: Overall structure of research

The second part of the literature review focuses on the top surface equipment including slurry mixers (blender), flow control equipment and frac-truck assemblies. Detailed analysis of the equipment operation is illustrated in the later sections by discussing high-pressure slurry pumps and the associated drives. The environmental concerns related to hydraulic fracturing are discussed in the context of equipment operation and the environmental consequences.

The final part of the review section summarises the options identified by the literature review for reduction of the environmental impact. A concept evaluation process is used to identify the most promising option for the research to focus on.

Chapter 3: Methodology

Based on the improvement concept, identified in the previous chapter, the methodology section identifies suitable approaches for the research. The research strategies review the advantages of different experimental and analytical methods for optimising complex multivariable mechanical systems and process validation [15]. The use of Monte Carlo sensitivity analysis is identified as a suitable approach for the application.

Chapter 4: Computational model development

The computational model of a frac-truck assembly is developed to support an analytical process for optimising the pump and system design in hydraulic fracturing. The interaction between different mechanical systems is modelled to enable an effective representation of the system dynamics. The functionality of the model is established by using lookup tables, kinematic principles and the results of previously conducted high fidelity (CFD) computational studies.

Chapter 5: Field data

The process data logged for one pump while performing a single stage of hydraulic fracturing job is detailed. In chapter 7 this field data is quantitatively compared with the behaviour of the test rig and the analytical model.

Chapter 6: Pump test rig data

Although the field data characterises the behaviour of a pump performance on a working frac-site it is limited in the variation of parameter values it can explore. To investigate the pump behaviour in response to a range of conditions a scaled test rig is developed. The test rig exploits the geometrical similarities between the equipment employed in the current hydraulic fracturing processes and much smaller high-pressure pumps. The ability to operate and study different aspects of design and control, presents a powerful tool in the optimisation studies.

Chapter 7: Validation

Statistical methods are used to compare the computational model with both field and experimental data. The model shows satisfactory level of consistency with the experimental analysis and provides the discussion of the engineering challenges.

Chapter 8: Optimisation study

The validated computational model is used to optimise the proportions of the PD pump to minimise energy and mass. The model is further developed to assess the

performance gains in hydraulic fracturing by examining different operating regimes for frac-truck assemblies on site. Finally, an environmental analysis of the modified design of hydraulic fracturing PD pumps is conducted to quantify impacts of the proposed changes.

Chapter 9: Discussion and conclusion

A summary of the thesis is presented in the final concluding chapter which reflects on the aims and objectives of the work together with the resulting contributions to knowledge. Future work outlines next steps for further research and development.

Chapter 2

Literature review

The requirements, constraints and functions of the machinery involved in hydraulic fracturing arise from several different bodies of knowledge:

- Geology and geomechanics,
- Petroleum engineering,
- Mechanical engineering,
- Chemical engineering,
- Environmental engineering

This chapter provides an overview of each of these topics which have been organised in subcategories as illustrated in Figure 2.1. The chapter ends with a brief discussion of possible approaches to reducing environmental impact and justifies the choice of the mechanical design optimisation.

2.1 Geological overview of the processes

The development of hydraulic fracturing technology was motivated by the opportunity to extract hydrocarbons that were previously beyond reach for conventional recovery methods. Understanding of the hydraulic fracturing process has to start from an application of the basic principles of oil formation, maturation process, settling process inside the source rock and the methods for enhanced oil recovery.

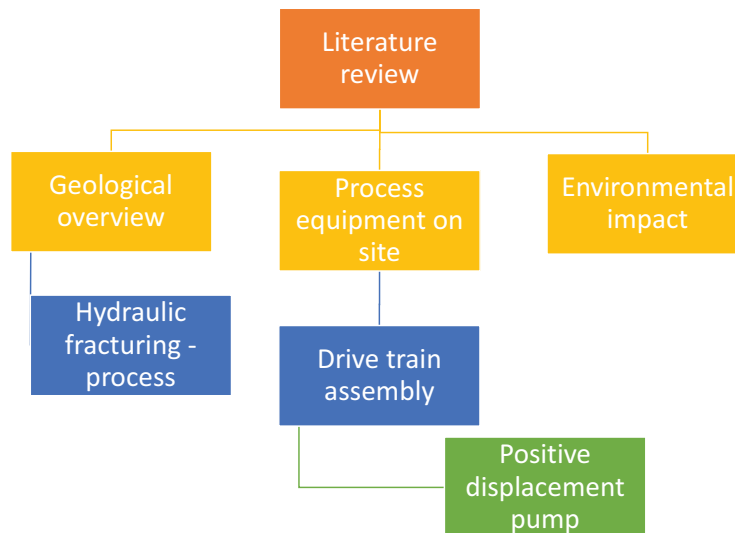


Figure 2.1: Literature review structure

2.1.1 Oil Formation

The first step is to understand the resource, its location, its relationship to surrounding rocks, vertical distance from the water table (aquifers), and other factors.

Deposition of the organic material over extensive time periods (millions of years ago) has resulted in creation of sediment layer on the ocean seabed. The formed sediment consist of plankton, anaerobic bacteria and mud which form a layer also known as sapropel. The gradual settling process continually covers the original sapropel layer with younger sediments. Through chemical processes sapropel is transformed into kerogen at approximately 50°C which is the equivalent of 2 km burial depth [16].

The gradual increase of burial depth results in higher temperature to which kerogen is being subjected. According to Seewald, (2003) [17] thermal degradation of kerogen yields hydrocarbons at temperatures of approximately 60°C . Maturation of kerogen occurs at different temperature ranges which produces hydrocarbons in different physical states. Therefore, kerogen can be subdivided into four types. Kerogen types I and II, as per Seewald, (2003) [17], produce oil at temperature range between 60°C and 160°C . Natural gas, condensate and waxy oil are derived from kerogen type III whereas methane (CH_4) and carbon dioxide (CO_2) are product of kerogen type IV. Extracting petroleum from the source rock has inherent difficulty by which very high percent (roughly 85%) of hydrocarbons are being retained in the source rock [18].

Earth's tectonic movements may cause the layers of sediments to experience physical impacts such as geological folding and faulting. These processes can see accumulation of the additional layers of strata on top of the underlying kerogen which causes the temperature to rise and alter maturation process. Liquid petroleum is formed from kerogen at temperatures between 80-120°C which indicates burial depth of about 3-5 km. Oil as a liquid derivative of kerogen naturally migrates into sandstone reservoir. At higher maturation temperatures, specifically 120-150°C, kerogen is converted into natural gas which filters through the liquid and settles in sandstone. Migration of gas is normally restricted by the impermeable rock which prevents the gas seeping towards lower pressure. In particular cases, salty water may also get stored inside the sandstone reservoir by underlying gas and liquid hydrocarbons.

2.1.2 Fundamental rock theory

Downhole geology is heterogeneous and isotropic. The host rock is divided into layers and pre-existing fracture networks can have an order of magnitude variations in strength and permeability. This gives rise to complex interactions between injection pressure, fluid flow and the mechanical response of the downhole rock. Feedback from the subterranean zone to the topside operation during the progress of hydraulic fracturing is limited to the variations in the water pressure measured at the well-head.

Earth's crust is formed of different rock materials which can be unconsolidated (loose) such as sand, gravel, volcanic material and clay or consolidated (solid) such as granite, sandstone and limestone. The shaping of Earth's crust is done through three different processes: volcanism; erosion and sedimentation; and metamorphism. Each of these processes leads to the formation of a different type of rock as shown in Figure 2.2. The rock types are accordingly classified into three major categories: igneous, sedimentary, and metamorphic. Reservoir rocks are of sedimentary origin and can be further classified as sandstones, carbonates and shale.

Sandstones are fragmental rock consisting of sand grains. The main constituent of sandstones is quartz.

Carbonates are composed of calcite and dolomite. If the main material is calcite, carbonate rock is referred to as limestone. Dolomite is secondary rock formed from

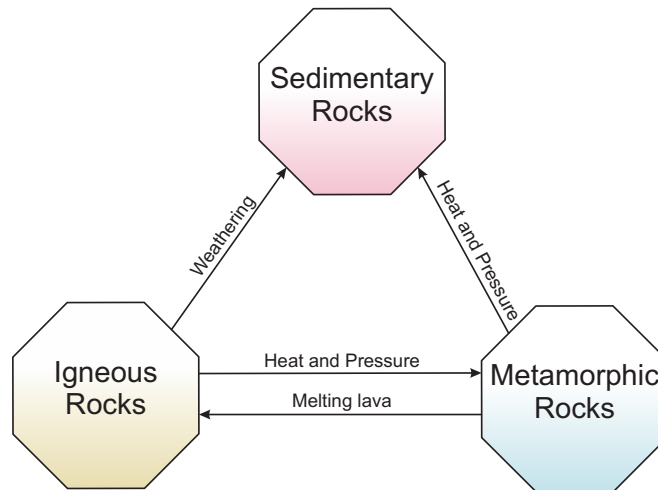


Figure 2.2: Igneous rocks are formed after cooling and solidifying of volcanic material that has moved to the Earth's surface. Sedimentary rocks (layered) are those that have been deposited by water, wind or ice and whose particles have come from the destruction of previous source material (sandstone and shale) or chemically precipitated by water (limestone). Metamorphic rocks (changed rocks) form as a result of the recrystallization of a previously existing rock [19].

limestone by replacing calcium in calcite with magnesium.

Shale consists of compacted beds of clay and fine-grained minerals. Shale is generally tight, impervious rock which acts as a sealing cap rock for sandstone or carbonate reservoirs. It frequently forms streaks and intercalation in hydrocarbon reservoirs that may have a complex effect on flow characteristics. Shale is the most abundant reservoir rock, 50% of all sedimentary rock is shale [20].

Because even the consolidated rock structures are not absolutely solid their microstructure can be further analysed by understanding following material properties.

Porosity is the ability of the reservoir rock to store fluids. If bulk volume of a piece of rock is presented by V_b and the pore volume V_p , porosity then is given by:

$$\phi = \frac{V_p}{V_b} \quad (2.1)$$

The porosity of most commercial hydrocarbon reservoirs is between 10 and 25%[21].

Viscosity defines the internal friction of the moving fluid. Low viscosity of the fluid signifies a lower resistance to flow. The coefficient of viscous flow is a rock property dependent on the shape and the size of the interconnected pore network.

Permeability is a complex function, derived from experimental analysis, which de-

describes the pore structure of a rock. A governing factor is the average pore diameter of the rock. Estimation of rock's permeability can be done by calculation using the squared average of pore diameter. The permeability of producing reservoirs are in the range of 100 to 1000 mD (millidarcy) and these values may be identified as good. On the other hand, permeability of the shale rock is approximately 0.001 mD [22].

Resistivity is a measurement of the formation's capability to transmit current by means of the interstitial and the adsorbed water it contains. The level of water in reservoir will affect the measurement due to its different conductivity properties to oil. Therefore the detection of hydrocarbon zones is done by measuring formation resistivity which is a function of water saturation [23].

Caprock acts as a seal entrapping subsurface gas. Shale gas and oil are essentially lighter than water and, if unobstructed, would flow up to the surface. Caprock is more impermeable type of rock which seals the hydrocarbon flow passage.

Structural traps can be divided into three forms: anticline trap, fault trap, and salt dome traps. Anticline traps are formed by folding, causing isolation of reservoirs at high points. Fault traps are formed by faulting with parallel rock sections moving so that impermeable rock types trap the migrating fluids within a reservoir. Salt dome reservoirs are formed by salt domes intruding into sedimentary layers, therefore, isolating areas along the flanks of the salt structure [24].

2.1.3 Conventional Oil and Gas

Conventional oil and gas, as a term, applies to well types that start producing hydrocarbons straight after drilling and completion processes. Several enhancing oil recovery (EOR) methods are employed to increase the production of the well. Even though methods such as water injection, gas injection or artificial lift are often used they are all considered and categorised as conventional production enhancement methods.

Achieving the goal of maximising hydrocarbon production is done by using three recovery methods, primary, secondary and tertiary.

Primary recovery

Primary recovery relies on the natural energy formed in the reservoir. In the oil textbooks it may be found that this value is estimated to be around 10% of the total contents of the well [25]. Since the introduction of horizontal drilling, this value has increased and the average value ranges from up to 17% [26]. The source of a natural drive can be divided into following categories.

Solution gas drive is considered to be the most common primary drive. This natural drive mechanism is present in one third of all reservoirs and the recovery factor (RF) is 5-30% (average 15-17%). Solution gas mechanism utilises volatility of the gas, naturally forming on top of oil, as a drive mechanism for oil recovery [27].

Water drive is a primary recovery mechanism in which the pressure from free water is sufficient to move hydrocarbons out of the reservoir, into the wellbore and up to the surface. Water drive reservoirs can have bottom water-drive or edge-water drive. In a bottom water-drive reservoir, water is located beneath the oil accumulation, while in an edge-water reservoir, water is located on the edges of the reservoir. Water drive method is generally applicable if adjacent aquifers are available. Recovery factor for this type of drive mechanism is usually around 40% [28]. Water drive mechanism is used in one-third of all reservoirs.

Gas cap drive presents a type of drive mechanism where oil and gas are formed at lower pressure. The energy that drives this system comes from expanding gas which occurs as the oil is being produced. Producing only oil at first, as the pressure in the reservoir drops, gas expands and helps maintain pressure in the well. At optimal conditions, recovery factor can be estimated to be from 20% to 40% [28].

Gravity drainage drive mechanism is implemented in reservoirs where the pressure had already been depleted. This drive mechanism usually occurs in reservoirs with high permeability and usually in conjunction with other drive mechanisms. Recovery rates of this drive system are high (50-70%) over extended periods [28].

Compaction natural drive mechanism is most frequently found in high (≈ 40 MPa) pressure reservoirs. In practice, these types of wells are not very common, mostly found in the North Sea. Compressibility of the gas at reservoir condition drives the gas movement to the surface where gas expands thereby $1\text{ m}^3 @ 35\text{ MPa}$ equals $340\text{ m}^3 @ \text{surface}$

condition. Recovery factor is up to 70% [29].

Secondary Recovery

Water flooding is a secondary recovery method, the most frequent and commonly used after the depletion of hydrocarbons using primary recovery. Recovery method relies on the different physical properties of oil and water. Since oil and water do not mix, increasing the volume of water in the reservoir will displace the oil pushing it out of the reservoir. Flooding, as a stimulation method, performs best with lighter oils with $API > 30$ [30].

Thermal recovery method is based on injecting heat into the formation to reduce the viscosity of the oil thereby allowing it to flow more readily into the producing well. Thermal recovery is preferred for heavier oils with API value above 20 [31]. There are three main techniques for thermal recovery:

- Steam flooding involves injection of steam that is produced at the surface and delivered into the formation. As the heavy oil is heated, steam cools and condenses into hot water. Heat reduces the viscosity of the oil and it allows it to be pushed towards the producing well. From the application perspective, steam flooding can be successful in shallow reservoirs when injection well drilling is economic.
- Cyclic steam method (aka. huff and puff) is the most successful form of thermal recovery. In this method, a well will act as an injector well and as a producing well at different times in the cycle. Cyclic steam is considered economical and does not require a large number of tightly spaced wells. It is a sustainable method and can be used repeatedly for several years.
- Fire flooding delivers compressed air from the surface into the injection well providing oxygen to ignite oil in the formation. Fire is controlled by the amount of oxygen being injected. Heavy oil is heated in the combustion process thereby reducing its viscosity. This method is somewhat uneconomical as it consumes oil and produces char. In the industry, it is commonly used as a final recovery system.

Tertiary Recovery

Tertiary recovery is used after depletion of secondary recovery. It relies on continuation and injection of different types of man-made energy. The main difference between this type of recovery and secondary recovery is that this uses chemical agents to enhance hydrocarbon production.

Miscible flooding method is based on fluids that mix with oil, therefore, making them less viscous. Miscible fluids are, by definition, fluid types that mix but do not change molecular structure. As an example water mixes with milk by diluting the milk or making it watery, it does not change its molecular structure. CO_2 (Carbon dioxide) is miscible with oil and is pumped downhole to change reservoir characteristics. It can lower the oil viscosity which allows fluid to penetrate deeper into the recesses of the reservoir lowering the trapped oil's viscosity and thereby allowing the oil to flow more easily [32]. Major expenses in this method are the investments in surface facilities that separate CO_2 from hydrocarbons. Fortunately, once CO_2 has been separated it can be compressed and reused. Other miscible fluids include:

- LPGs (Liquefied Petroleum Gases), although they result in high recovery using LPG is too expensive especially when LPG market price is high.
- Flue gases, naturally occurring waste released in industrial processes where oil/gas or coal is combusted. Use of flue gases is limited to their availability.
- Nitrogen extracted from air. A limitation of this method is that nitrogen is only miscible in deep, high-pressure reservoirs.
- Detergents, usually pumped into the formation followed by a water sweep. Although high recoveries are possible the cost of detergent is a crucial limiting factor.
- Alkaline or caustic substances (sodium hydroxide), can have high recovery rate but handling these chemicals can be dangerous. Like detergents, these substances are also expensive.

Mobility ratio method for well stimulation is based on polymers (long chain of chemical substances) which are injected into the well to help reduce friction or decrease

surface tension between oil and water molecules and the rock surface. Polymers have shown promise when coupled with water flooding. The high cost of polymers is the limiting factor.

Microbial flood is the method of injecting bacteria into the well. As bacteria consumes the oil it produces methane gas as a by-product which is miscible. The release of methane pushes the less viscous oil out toward the producing well.

In conclusion, using miscible flooding and microbial flooding can be effective in carbon situations but its cost and accessibility limit its usage.

2.1.4 Unconventional Oil and Gas

Depletion of the conventional reserves naturally triggers the need for accessing remaining hydrocarbons using alternative sources. The term unconventional stands for types of reservoirs that require implementation of different well stimulation methods to improve well production. Because of the different rock structures', producing gas from the unconventional resources requires higher technological development. This increases the cost of the system.

Types of rock considered as unconventional sources of oil and gas include:

- tight gas sands
- coal bed methane
- shale gas
- gas hydrates

Unconventional rocks have significantly lower permeability compared to the conventional hydrocarbon reserves which is illustrated in Figure 2.3. It can be seen that values vary by several orders of magnitude from high quality conventional to more challenging coal bed methane, gas shales and gas hydrates.

Function of Stimulation

Producing from unconventional wells requires stimulation treatment to enhance connectivity between reservoir fluid and the wellbore. Stimulation treatment enforces the

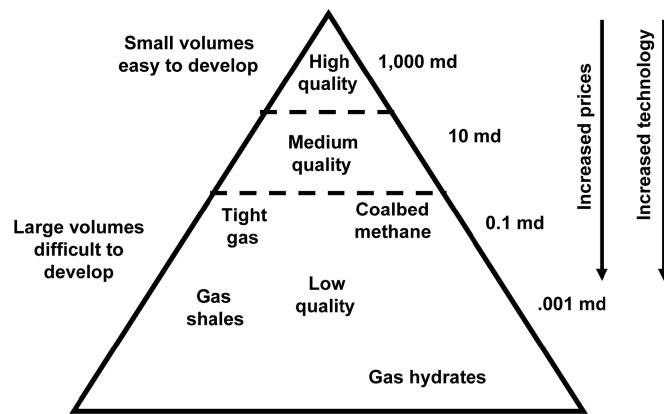


Figure 2.3: Permeability for tight gas reservoirs[22]

fluid to flow from the formations with low permeability. Methods such as acid injection or hydraulic fracturing can increase production rates up to four times [33], [34].

In Figure 2.4 geometry of the radial flow is given. As the flow approaches the wellbore the flow pattern (annotated using arrows) begins to act restrictively, thereby hindering conductivity. This constriction reduces the pressure drop which results in the decrease of fluid volume that reaches internal parts of the wellbore. Zones with lower permeability are more affected by the flow restriction which results in lower production rates.

In addition to natural restriction, formation damage can also occur preventing free fluid flow. Formation damage occurs when formation rock comes into contact with the drilling mud. It comes in two forms; first, in formations containing clays, drill mud is absorbed and expanded hampering permeability, secondly, solids in the mud are reducing permeability by becoming entrapped in the pores of the formation. Both occurrences can create unwanted bottlenecks in the immediate vicinity of the wellbore that can impact the well's production rate. Stimulation treating operations include:

- Matrix acidizing
- Hydraulic fracturing
- Fracturing acidizing

In all stimulation operations treating liquids are pumped from the surface, down the well, inside tubing anchored by a packer, out through the perforations and into the

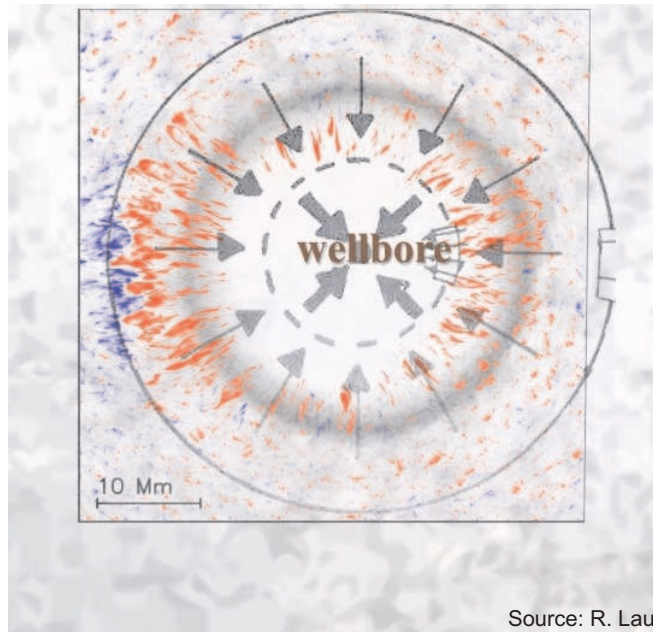


Figure 2.4: Wellbore constriction

formation. In hydraulic fracturing and fracture acidizing several hundred bars of surface pressure is also introduced into formation along with the treating liquids. The type of treating liquids, pressure amplitudes and flow rates are determined by the formation and its permeability in the pay zone.

Matrix acidizing

In matrix acidizing different compositions of acid are used to increase the number of fractures. Hydrofluoric acid is used in sandstone while hydrochloric acid has a better result in limestone reservoirs[35]. To avoid formation fracture in unproductive ways, throughout the matrix acidizing of the reservoir, no undue additional pressure must be acting on the reservoir rock.

Hydraulic fracturing overview

Hydraulic fracturing is an effective treatment to enhance hydrocarbon recovery from so-called “tight” sandstone formations i.e. formations that have low permeabilities. In this treatment pumps on the surface generate surface pressure of up to 100 MPa that is subsequently channelled into the wellbore to initiate formation breakdown.

Once the fracture is extended far enough a propping agent, often large rounded sand grains are introduced into the pumped slurry stream. Continual pumping is maintained until formation is fully saturated after which surface pumping stops. As the artificially induced pressure is declining, the well establishes its normal pressure conditions, newly formed fractures would normally close but are instead held open by the proppant. These fractures now filled, with proppant particles, form an excellent flow path for the oil and gas.

Fracture Acidizing

Fracture acidizing is the method for combining matrix acidizing and hydraulic fracturing. It is used to stimulate the production in limestone and dolomite reservoirs. Because limestone and dolomite are composed largely of calcium carbonate, they will dissolve in hydrochloric acid (HCl). In this operation, HCl is injected at a high enough pressure inside the formation in order to initiate fracture in a roughly vertical direction. As the pressure of the pumped acid propagates the fractures it chemically etches or dissolves the irregular surfaces which create high volume flow channel towards the wellbore. As in hydraulic fracturing, after the stimulation process, fractures would close but in reality, newly formed etched channels remain open. This action changes the flow characteristic from radial to a high volume lateral.

2.2 Hydraulic fracturing implementation

The technology enabling global transformation of energy has evolved from a well stimulation procedure invented just after the end of Second World War. The first experimental “hydrofrac” (i.e. hydraulic fracturing) was carried out in 1947 in Grant Country, Kansas, US when approximately 3,800 litres of naphthenic acid and palm oil were injected into a well bore 800 metres deep. By 1949 the process was patented and an exclusive licence granted to the Halliburton Oil Well Company. The same year saw the first two commercial fracturing treatments performed in Oklahoma and Texas using crude oil, gasoline and sand. By the end of 1949 a total of 332 oil wells had been hydraulically fractured with an average increase in production of 75%. Given this dramatic effect it is not surprising that within a few years (1950s) up to 300 wells were

treated every month [36]. In parallel with the growth of well stimulation operations the 1970s also saw the emergence of horizontal drilling technologies although it would be almost 30 years before the two technologies were combined [37]. The process of hydraulic fracturing was progressively refined and extended from oil to gas fields. By the 1990s the application of hydraulic fracturing made drilling for gas in Texas's Barnett Shale commercially viable for the first time. The Barnett shale was also the location of a step change in the process capability when in 2004 hydraulic fracturing and horizontal drilling were combined for the first time. In 2010 the opportunity for hydraulic fracturing expanded again with the identification of large oil and gas shale reserves in both the US and Europe. Despite the rapid downhole technology development, the on-site operation has seen only incremental changes since 1960s [38]. Equipment used on-site has remained conceptually the same even though the process requirement was showing increasing process demands by moving to higher treating pressures.

The following sections present technical overview of hydraulic fracturing stimulation process from shale geophysics to mechanical on-site setup. The first section presents challenges and well preparation methods prior to hydraulic fracturing.

Sections 2.2.2 and 2.2.3 provide an overview of the process during hydraulic fracturing. Initially, a single "stage" of hydraulic fracturing is examined, before discussing how the process is conducted across a number of stages covering the entire "pay zone" of the well. Typical values for the major process parameters (e.g. speed, pressure, flow, time etc.) are presented for each step. These have been obtained from site visits and available literature (both commercial and academic), which are identified in the text.

Section 2.2.4 of the literature review will be examining calculation methods for establishing pressure and flow requirements. Using first-principle equations of fracture mechanics breakdown pressure will be determined based on different well characteristics. Stimulation flow rates will be calculated using typical operational practices in the North America.

2.2.1 Well preparation

Following well cementing process, the internal volume of the wellbore needs to be connected to the surrounding geology structure. Hydraulic fracturing design involves

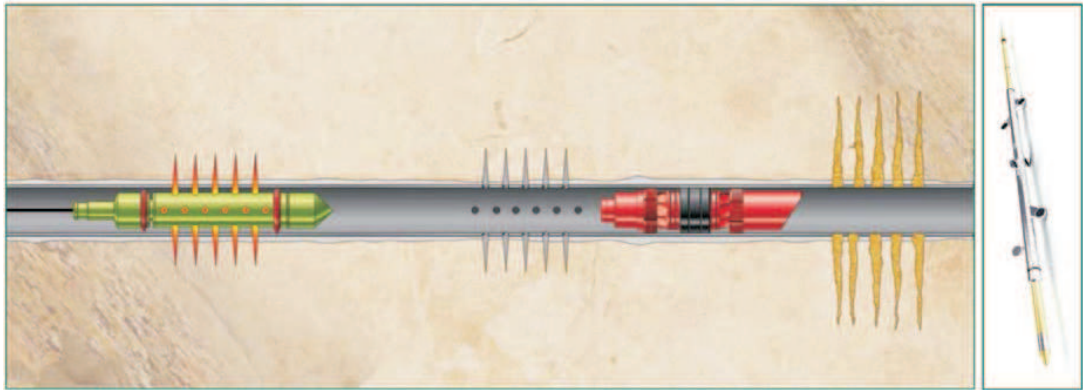


Figure 2.5: Wireline tools - perforating gun and plug [39]

planning which includes isolation of the potential pay zone. Prior to fluid injection downhole wireline is lowered into the well with a setting tool that carries perforating gun and a plug. The electric signal is sent to the very top of the setting tool to position the plug in place. Once the plug is set wireline sends the signal which activates perforation guns with positive and negative charges. Perforating is the process of blasting through (1) walls of the casing, (2) the cement sheath, (3) about a meter into the formation rock. It is through these holes that hydrocarbons fluids will pass to the surface when production begins. Jet perforators are set to blast on average 8-16 jet holes per metre with each shot being rotated 90° - 180° throughout the pay zone. Steel constructed casing guns, operated on an electric wireline, are both retrievable and reusable.

Perforation can be done in overbalanced and underbalanced conditions. On a well being hydraulically fractured underbalanced perforation has advantage of immediately being placed under production, or stimulation. As well as saving time and money, underbalanced (through-tubing) perforating can also reduce any formation damage or enable access for down hole equipment.

Once placed inside the target zone perforating gun will fire, connecting the internal wellbore geometry with the well formation, and retrieve. Injection of slurry will then begin through the production tubing.

In Figure 2.5 a perforating gun is shown on the left and a plug which is set in place.

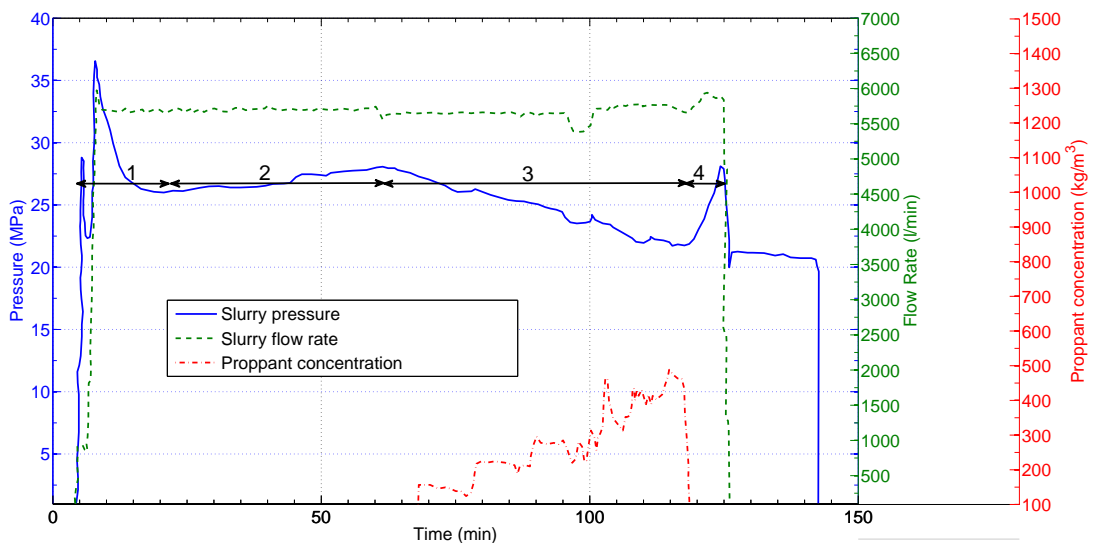


Figure 2.6: The process of hydraulic fracturing can be characterised by the four combinations of flow rate, pressure and proppant seen during a typical stage, (adapted from [40]). In the phase 1 water is pumped at high pressure to initiate cracks in the well. Phase 2 delivers a high flow rate at a reduced pressure and in this phase formed cracks are enlarged and expanded. Proppant is introduced in the phase 3 and finally, in phase 4 water is recirculated through the bore to displace proppant.

2.2.2 Single pumping stage

In order to hydraulically fracture a well, fluids (comprised mostly of water) are injected under high pressure to stress the rock until it cracks. Once hairline fractures have formed they need to be held open for gas to flow out, otherwise rock will close due to the pressure exerted by the weight of the rock above (referred to as overburden pressure). To do this the fractures are propped open with sand (or other proppant), that is added to the frac-fluid [41]. Gas then flows from the rock into the well bore, via these propped fractures, once fluid pressure is reduced (usually by pumping). After a clean-up phase (e.g. pumping of the frac water from the well, clearing of site, removal of earth works, etc. which may take up to 40 days [42]) the well is ready for production.

The hydraulic fracturing process can be illustrated concisely by referring to one of the performance monitoring graphs recorded in the control truck. On the right-hand axis of the Figure 2.6 slurry (i.e. frac-fluid) and proppant concentration (i.e. sand) flow rate are plotted against time during a two and a half hour fracturing operation. On the left-hand axis, treating pressure is plotted. The slurry rate in Figure 2.6 refers to total flow (litres/min) of slurry (frac-fluid) from the pump array. Proppant concentration

refers to the percent of sand combined with the slurry (frac-fluid) [41].

The pressure plot in Figure 2.6 reaches its peak (fracture initiation) early in the stage after which it reduces and is maintained constant to guarantee desired fracture propagation. Flow rate is also held constant from the moment the cracks are initiated to ensure correct fracture size (i.e. desired width, height and length). Proppant is introduced towards the middle of the cycle. The particle size of the proppant is systematically varied during the hydraulic fracturing process, starting with larger and ending with finer grain size. Proppant concentration increases continually while the grain size is reduced. This is necessary so that the established fissures are “propped” open with the grains supporting the overburden (i.e. the geological strata above the fracture).

2.2.3 Multi-stage hydraulic fracturing of the entire well

Wells are rarely fractured in only one place. The well is divided into a number of isolated sections, known as stages, which are then fractured individually. The number of sections (stages) depends on the length of the well, and can range from 1 to 50 stages. Wells are fractured in stages to ensure fractures are created along the length of the bore (rather than only in the weakest area of the rock). To enable pressure containment within the desired area, a section of the well bore is closed off using packers [37]. Once that section is fractured and propped, the completed stage needs to be isolated to ensure that the next area is not affected by the previous stage [41].

Figure 2.7 illustrates the process for an entire well where the boxed areas represent a single stage, described earlier in Figure 2.6. Hydraulic fracturing starts from the far end of the well (i.e. right-hand side of Figure 2.7) and progressively moves to the heel of the wellbore, stage by stage. At the end of the hydraulic fracturing process (i.e. once all the stages have been hydraulically fractured) all the internal parts (packers, perforating gun, etc) are removed, and the frac-fluid first flows to surface (due to the high pressure in the well bore).

2.2.4 Pressure, flow requirements and fluid composition

Any investigation into the mechanical redesign of hydraulic fracturing equipment must start by considering the necessary performance requirements. Field work and technical

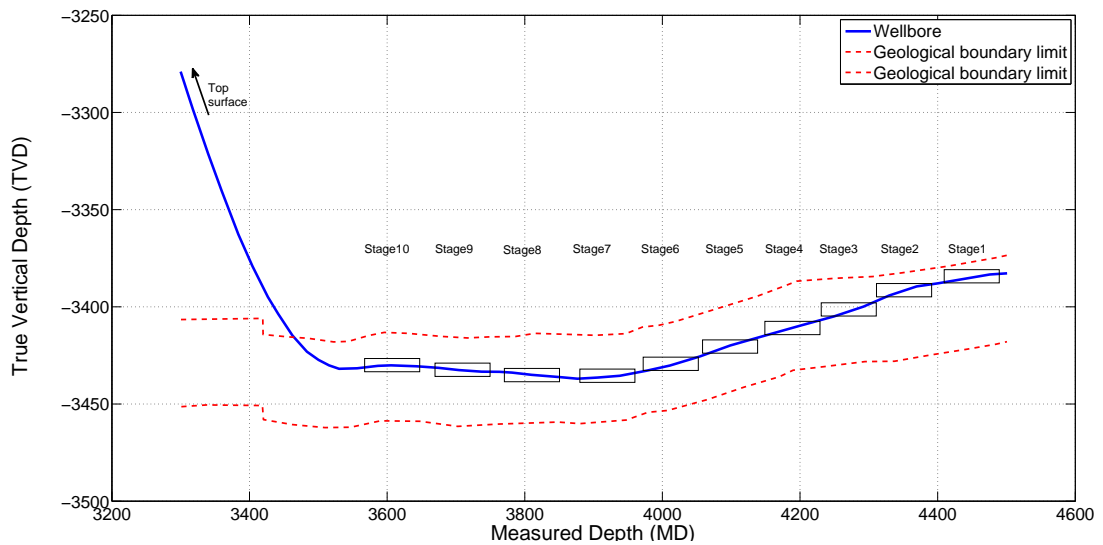


Figure 2.7: The single stage stimulation process (shown in Figure 2.6) is repeated along the length of the ‘target zone’ of a well in a sequence of operations that progresses from the end of the wellbore towards the surface. The figure is a reproduction of the original well data obtained from field trials[43].

engineering literature [44] has enabled global understanding of the downhole processes. The following section provides engineering evaluation of the pressures and flow rates typically required to stimulate a shale reservoir successfully. The final section presents fluids used in hydraulic fracturing processes.

Pressure

In order to establish the pressure needed to fracture a rock, the relationship between the depth and the properties of the target rock formation must be analysed. Although the structure of rock is very variable, the typical density, porosity and compressive stress values that define the material can be used to illustrate the order of magnitude of these parameters [42]. Even in the same basin, the depth of the prospective formations will vary significantly in terms of the upper and lower limits. For instance, in the Bowland basin (UK), the upper limit of the formation range is around 1,000 meters with the maximum thickness up to 4,000 meters [45]. Furthermore, the properties (e.g. strength, density, etc.) will vary within the basin due to heterogeneities in the rock itself caused by natural variations in its formation, therefore the treating pressure is not simply a function of depth.

Haimson and Fairhurst presented the following solution for fracture initiation and

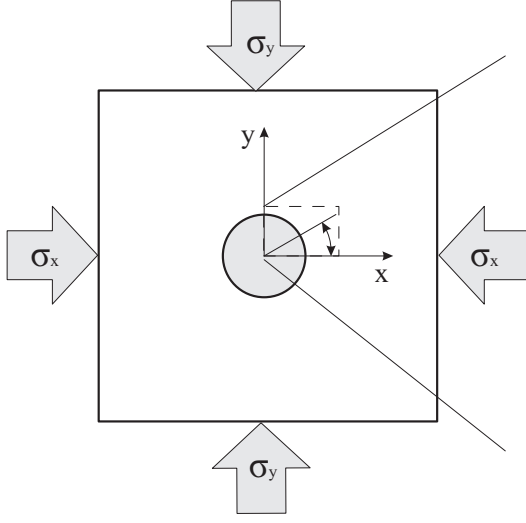


Figure 2.8: Mathematical solution to the stress distribution around the wellbore

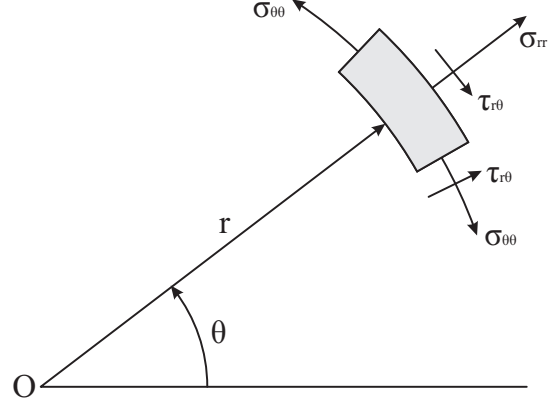


Figure 2.9: Stress field distribution around the wellbore section

extension [46]. Assuming an isotropic, homogenous, linear elastic rock the stresses in the formation prior to any stimulation, shown in Figure 2.8, can be expressed as in equation 2.2. This expression supposes that a vertical wellbore radius, r_w , is drilled in the z -axis (σ_z direction) and also that radial stress is σ_{rr} , tangential stress is $\sigma_{\theta\theta}$ and $\tau_{r\sigma}$ is shear stress that exists around the wellbore. Radial distance is r and angle measured from the σ_z direction is θ , Figure 2.9.

$$\begin{aligned}
 \sigma_{rr} &= \frac{\sigma_x + \sigma_y}{2} \left(1 - \frac{r_w^2}{r^2} \right) \\
 &\quad + \frac{\sigma_x - \sigma_y}{2} \left(1 + 3\frac{r_w^4}{r^4} - 4\frac{r_w^2}{r^2} \right) \cos 2\theta \\
 \sigma_{\theta\theta} &= \frac{\sigma_x + \sigma_y}{2} \left(1 + \frac{r_w^2}{r^2} \right) - \frac{\sigma_x - \sigma_y}{2} \left(1 + 3\frac{r_w^4}{r^4} \right) \cos 2\theta \\
 \tau_{r\sigma} &= \frac{\sigma_x - \sigma_y}{2} \left(1 - 3\frac{r_w^4}{r^4} + 2\frac{r_w^2}{r^2} \right) \sin 2\theta
 \end{aligned} \tag{2.2}$$

As a first approximation, let us assume $r = r_w$. Substituting this in equation 2.2 it can be concluded that $\sigma_{rr} = 0$ and $\tau_{r\sigma} = 0$. So the tangential stress in the rock, $\sigma_{\theta\theta}$ can be expressed using equation 2.3.

$$\sigma_{\theta\theta} = \sigma_x + \sigma_y - 2(\sigma_x - \sigma_y) \cos 2\theta \tag{2.3}$$

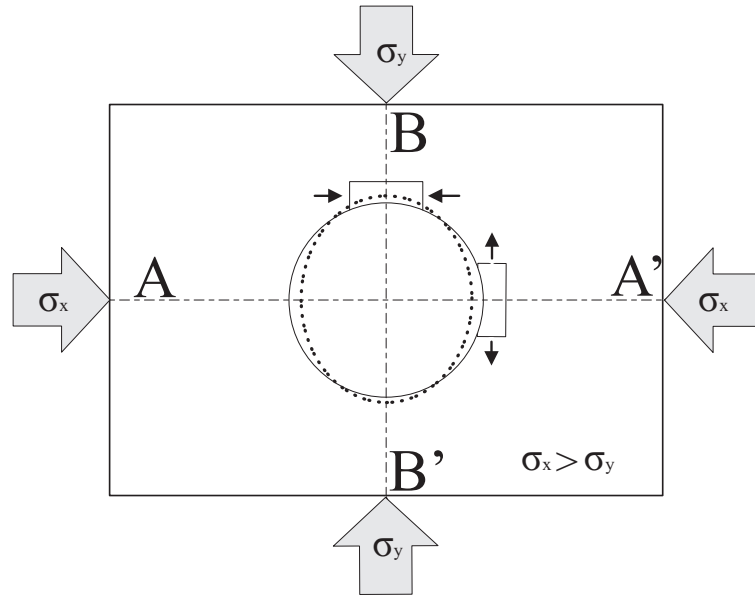


Figure 2.10: Further analysis of the stress fields shown in figures 2.8 and 2.8 considers stress distribution in XY direction in cases where σ_x is greater than σ_y

Thus, if σ_z is acting in vertical direction the common impact of both σ_x and σ_y stresses can be estimated. These stresses are present in the entire reservoir.

Figure 2.10 shows the borehole deformation due to stresses acting in X and Y direction. If σ_x is assumed to be greater than σ_y the direction of fracture propagation can be determined. Material particles close to A-A' are under tension while particles close to B-B' are under compression. Solid mechanics suggests that fracture initiates at a point, or points, of maximum tensile stress and that additional cracks will propagate in the direction of the maximum principle stress. Furthermore, it is known that rock is almost an order of magnitude weaker in tension than in compression [47] which is clear that fracture will initiate in the A-A' direction.

Stress in A-A' section, when $\theta = 0^\circ$:

$$\begin{aligned}\sigma_{\theta\theta} &= \sigma_x + \sigma_y - 2(\sigma_x - \sigma_y)(1) \\ \sigma_{\theta\theta} &= 3\sigma_y - \sigma_x\end{aligned}\tag{2.4}$$

Stress in B-B' section, when $\theta = 90^\circ$:

$$\begin{aligned}\sigma_{\theta\theta} &= \sigma_x + \sigma_y - 2(\sigma_x - \sigma_y)(-1) \\ \sigma_{\theta\theta} &= 3\sigma_x - \sigma_y\end{aligned}\tag{2.5}$$

In order for a fracture to occur in the well the maximum tensile stress induced around the wellbore must be greater than tensile strength of the formation. Indeed, if $\sigma_{\theta\theta} = 3\sigma_y - \sigma_x$ (the stress caused by the weight of the rock above the bore) exceeds the tensile strength of the formation then a fracture will occur in the process of drilling and hydraulic fracturing may not be necessary. However, if $\sigma_{\theta\theta}$ is not sufficient, fluid pressure must be applied to induce additional tensile stress in the wellbore. Stresses generated by internal fluid pressure can be estimated by applying equation 2.6. Pressure differential inside the wellbore (Δp) is the difference between the bottomhole pressure (p_w) and the reservoir pressure (p_r).

$$\begin{aligned}\sigma_{rr} &= (p_w - p_r)\frac{r_w^2}{r^2} = \Delta p\frac{r_w^2}{r^2} \\ \sigma_{\theta\theta} &= -(p_w - p_r)\frac{r_w^2}{r^2} = -\Delta p\frac{r_w^2}{r^2} \\ \tau_{r\theta} &= 0\end{aligned}\tag{2.6}$$

So if tensile strength of the formation is considered it can be concluded that fracturing will occur whenever $\sigma_{\theta\theta}$ is equal to the tensile strength of the rock (T).

The effect of pore pressure (p_r) also needs to be accounted for. In 1923, Terzaghi introduced the concept of effective stress stating that the weight of the overburden is carried by the rock material (i.e. grains) and the pore pressure (the pressure of the fluid in the pore spaces between the rock grains). To refine this concept in 1941, Biot introduced a poroelastic constant, β , that describes the efficiency of fluid pressure [48]. The poroelastic constant β can be obtained experimentally.

Equation 2.2 can now be developed to include additional factors reflecting fluid pressure, equation 2.6, tensile strength of the rock (T) and Terzaghi/Biot stress distribution (βp_r). Finally, the breakdown pressure required to cause formation failure (p_b) can be expressed by equation 2.7.

Breakdown pressure (p_b) is the first phase of hydraulic fracturing. Once formation breakdown occurs, the overall pressure is predominately reduced by 20-30% [49], as

shown in Figure 2.6. This phenomenon was explained by Haimson et al. [46] and Hubbert et al. [47] who also identifies the basic driving factors for fracture initiation during hydraulic fracturing.

$$p_b = 3\sigma_{Hmin} - \sigma_{Hmax} + T - \beta p_r \quad (2.7)$$

Having established the driving factors for the overall stress state, the most influential factors can be examined and discussed further. From the equation 2.7 it is apparent that all the variables show linear correlation. However, σ_{Hmin} , (due to the multiplication factor 3) has the highest impact. The least principal horizontal stress σ_{Hmin} is a direct result of the overburden stress and the Poisson's ratio of the material (ν) determines how much vertical stress will be transmitted in the horizontal direction. Rocks with a high Poisson's ratio will have higher horizontal stress. Taking into account both the overburden carried by the rock grain and the overburden carried by the pore pressure (βp_r) the total horizontal stress equation can be expressed by equation 2.8.

$$\sigma_{Hmin} = \left(\frac{\nu}{1 - \nu} \right) (\sigma_V - \beta p_r) + \beta p_r \quad (2.8)$$

Furthermore, equation 2.8 states that horizontal stress (σ_{Hmin}) is affected by vertical stresses of the overlying formation (σ_V) and pore pressure (βp_r) in the horizontal direction.

Poisson's ratio (ν), poroelastic constant (β) and pore pressure (p_r) can all be derived by experimental analysis of the core samples [50]. Vertical stress (σ_V) is naturally affected by the height of the overburden layer (H) and the average density (ρ) of the overlying strata, expressed by equation 2.9.

$$\sigma_V = \rho H \quad (2.9)$$

$$22.62 \frac{kPa}{m} \leq \sigma_V \leq 24.88 \frac{kPa}{m} \quad (2.10)$$

A logging tool could be used to measure formation density of the individual layers in the overburden. However, due to the well depth and time involved it is more common to use an average pressure factor gradient as expressed in equation 2.10.

It can be concluded that, for formations that haven't experienced significant deformation, depth is the principal factor for determining the pressure requirements of the well if no dominating structural faults are present. The case study in section 8.1 will evaluate sets of data using these theoretical equations.

Summarising presented fracture initiation mechanics it can be seen that breakdown pressure can be determined based on the geological properties and the location of the source rock. Analysis of stress field has demonstrated that fracture orientation is also a known function that can be established analytically.

Volume

Having established the theoretical breakdown pressure required to initiate rock fracture, the second operating variable, fluid volume, can also be investigated. There is no single property of shale rock being hydraulically fractured that is able to describe accurately the volume of water required for each individual well. Due to geological differences in the properties of the rock, structural and the relative location of the prospective shale layers, predictions need to be adjusted appropriately. Currently, only North American shale data is available to estimate the properties of the European equivalent shales. The magnitude of the liquid volume required is established by the API (American Petroleum Institute) guideline which states that volume of water required to successfully hydraulically fracture well is between 9 million and 18 million liters [51], academic literature predominantly confirms these numbers [52].

Volume requirement can be divided into two quantities. First, the amount of water needed to fill all the hoses, pipelines and well casing up to the target zone (i.e. stage to be fractured). Second, the water absorbed in the cracked rock during the hydraulic fracturing. This approach requires both quantitative and qualitative assessment of the actual water requirement depending on the changes in the well properties (i.e. depth

and shale rock characteristics). To calculate the volume required to fill the pipe work and bore on site it is necessary to examine all the lines leading from the water storage units on site to the shale reservoir rock (well depths are rarely shallower than 1,000 m). Because surface leads and lines are measured in tens of meters (at least two orders of magnitude smaller than the well depth) the following discussion focuses only on steel casing volume.

The outer wall of the bore is formed by casing strings run in sequence. Bigger diameter pipes are used in the beginning and as the well length progresses casing pipe diameter becomes smaller [49]. The internal wall of the bore is created by a uniform production casing throughout the entire well. Since diameter is consistent from the surface to the end internal well bore volume can be calculated using equation 2.11. Measured depth (MD) is the true well length from the surface to the end of the well, Figure 2.7. Pipe's inside diameter is denoted by D_w .

$$V_w = \frac{D_w^2 \pi}{4} MD \quad (2.11)$$

To evaluate the second volume of the water needed during hydraulic fracturing it is necessary to examine actual field data.

The field data was collected from three different hydraulic fracturing operations in structurally different basins during April 2013. In each case operational time of the hydraulic fracture for a single stage was between 60 and 210 minutes. A number of flow rates were recorded during operations but for brevity this section will present only one stage per well (Table 2.1).

Table 2.1: Experimental flow rate data during hydraulic fracturing [53]

Well No.	Time (min)	Flow rate (l/min)	Average rate (l/min)	Total Volume (l)
Well 1	57	1,908 - 8,904	6,698	381,759
Well 2	97	1,590 - 7,950	6,376	618,510
Well 3	210	1,590 - 16,224	13,144	2,472,100

Although only loosely correlated it can be observed that the average volume flow rate per stage is between 6,000 and 10,000 l/min. The volume of fluid needed to fill the

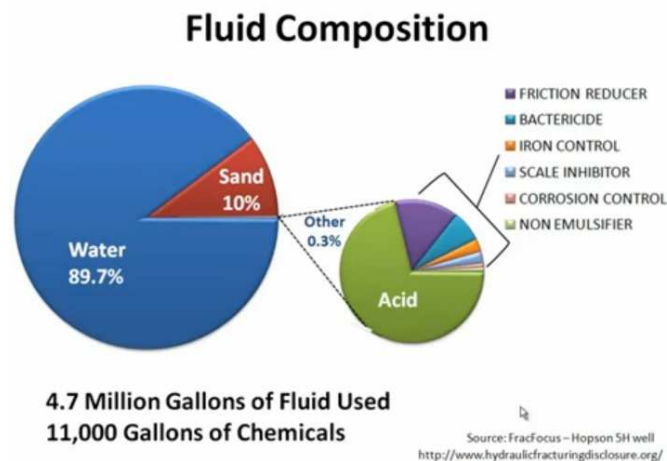


Figure 2.11: Fluid Composition Chart

casing, equation 2.11, would typically only be measured in tens of thousands of litres (e.g. 20,000l) which are clearly a negligible factor for the overall requirements.

In conclusion, this section has demonstrated how volume requirements can be estimated in hydraulic fracturing applications. Two individual parts of the system were considered, volume of process machinery (pipes, hoses, steel casing...) and the volumetric flow rates released into the formation. It was demonstrated how experimental data from field locations can complement the analytical analysis and published guidelines.

Fluid composition

Slurry or frac-fluid is a mixture of water, chemicals and sand or other manmade grain particles commonly referred to as proppant. In recent years industry has disclosed specific details about precise chemicals that are being used. Figure 2.11 was created by the “Ground Water Protection Council” in collaboration with companies involved in frac-fluid industry. The specific well, shown in Figure 2.11, indicates that injected slurry composition has 0.3% of chemical present. Hydrochloric acid is the dominant chemical injected to clean out the well after perforation blast. Other components are included to change the properties of the slurry by altering its viscosity, density and bacteria resilience to name a few.

The function of each of the added chemicals is fully defined and introduced into slurry to produce a desired effect. Acid composition is hydrochloric and its purpose is

to dissolve minerals and initiate cracks. The second most common additive is a friction reducer that helps to maintain low friction between fluid/pipe surface. To increase viscosity of the fluid, and thereby sustain proppant in the slurry, isopropanol is added. To prevent pipe damage due to scale formation or corrosion inhibitors are frequently added. Bacteria formation is counteracted by use of biocide [52].

Sand is the most common type of proppant used in the industry. It is cheaper than manmade alternatives and it varies in sizes, chemical and mechanical properties. In the industry size of proppant is measured using mesh standard size system (100 mesh, 10/20 mesh, etc...). Manmade proppant can be synthetic, ceramic, plastic or resin coated and each has different application for different hydrocarbons [40].

Flowback water (aka backflow water) is the murky, salty water from hydraulic fracturing of natural gas wells. It consists of frac-fluid which returns to the surface (aka the frac load recovery) as well as produced water. This water contains clay, dirt, metals, chemicals and even diesel that may have been added. The frac load recovery can be anywhere from 10-70% of the volume of fluid that is injected [54],[55]. Transition point occurs when recovering of frac-fluid is substituted with produced water. Usually, this point is difficult to distinguish, yet may be discerned from the different chemical signatures of the frac water versus the naturally occurring water produced by the formation. In the initial 3-4 weeks of post-fracturing flowback of frac-fluids is estimated to be around $1,000\text{ m}^3/\text{day}$ [52] after which an additional 8,000 to 22,000 m^3 of produced water may flowback for up to two years [55].

Flowback water may be characterised as having high salinity and total dissolved solids (TDS). It is laden with the same chemicals that were pumped into the well, in addition to any unique contaminants that are present in the rock formation water deep below. In addition to natural salinity of water in the formation, any fresh water that is forced down a well will tend to dissolve salts in the formation thus giving the recovered water very high salinity.

Produced reservoir water and recycled flowback water can be treated and reused for fracturing, depending on the quality of the water. Natural formation water has been in contact with the reservoir formation for millions of years and thus contains minerals native to the reservoir rock. Some of this formation water is recovered with the flowback

water after hydraulic fracturing, so that both contribute to the characteristics of the flow back water. The salinity, TDS, and overall quality of this formation/flow back water mixture can vary by geologic basin and specific rock strata. For example, water salinity can range from brackish (5% (5,000 parts per million (ppm)) to 3.5%), to saline (3.5-5%), to supersaturated brine (5-20%). Other water quality characteristics that may influence water management options for fracturing operations include concentrations of hydrocarbons (analysed as oil and grease), suspended solids, soluble organics, iron, calcium, magnesium, and trace constituents such as benzene, boron, silicates, and possibly other constituents [56].

The returning fluid is predominately collected in metal tanks, open pools, lagoons or pits lined with layers of plastic. Temporary storage pits are depleted and water is usually either recycled for fracturing additional wells or trucked off-site to a waste water disposal facility. Containment pits, or open-air ponds can become points of failure if liners get cracked or damaged in which case contaminated fluids can then leach into ground water.

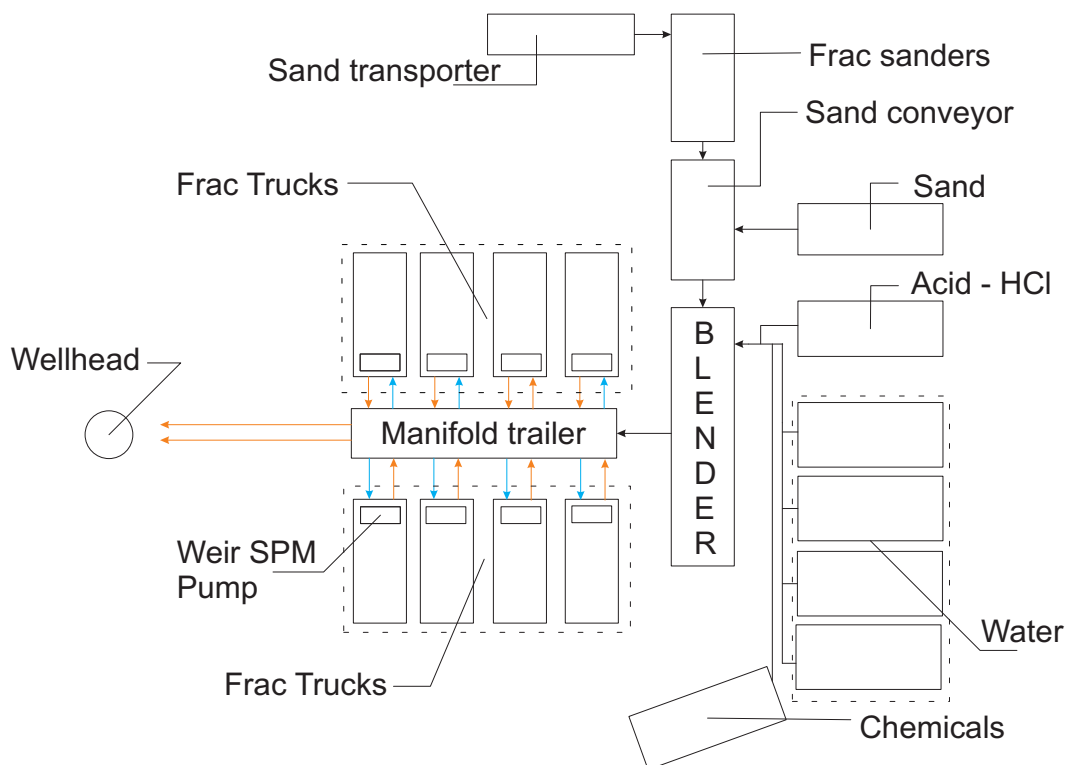


Figure 2.12: Global overview of hydraulic fracturing equipment

2.3 Process equipment

This section discusses the machinery on-site and equipment used in the process of hydraulic fracturing. Water and chemical storage units are covered in a section 2.3.1 dedicated to transport and fluid handling. Subsequent sections 2.3.2 and 2.3.3 discuss fluid mixing and flow distribution to and from positive displacement pumps. In section 2.3.4 an introduction to the topic of PD pumps and control on site is given.

This figure 2.12 shows a simplified schematic of a typical frac site. On the right side of the schematic all the consumables, such as water, chemical, sand, are stored on site before being mixed inside the blender. Fluid is then transferred to the manifold trailer that ultimately supplies each individual pump with frac-fluid. On this schematic red and blue lines represent high and low-pressure lines, respectively.

Figure 2.13 shows pipework schematic of a typical hydraulic fracturing site. Figure shows the connections between blender, chemical and water facilities, as well as additional units such as centrifugal pumps found on the blender unit and various safety valves common to most hydraulic installations.

The control van is a physical unit present on the frac-site that acquires and processes information coming from the ongoing work. It also issues commands to maintain or change operational state.

Machinery used during hydraulic fracturing can be separated into several categories:

- Transporting and storage equipment,
- Fluid mixing equipment,
- Pipeline - manifold trailer,
- High-pressure positive displacement pumps.

2.3.1 Transporting and storage equipment

Equipment used for hydraulic fracturing is designed to be mobile. Pumps, blenders and pipelines are all mounted on trailers. Similarly, water, chemicals and sand are transported to site in separate containers. Well stimulation is just one of many procedures used to prepare a well for production so the equipment is only temporarily deployed

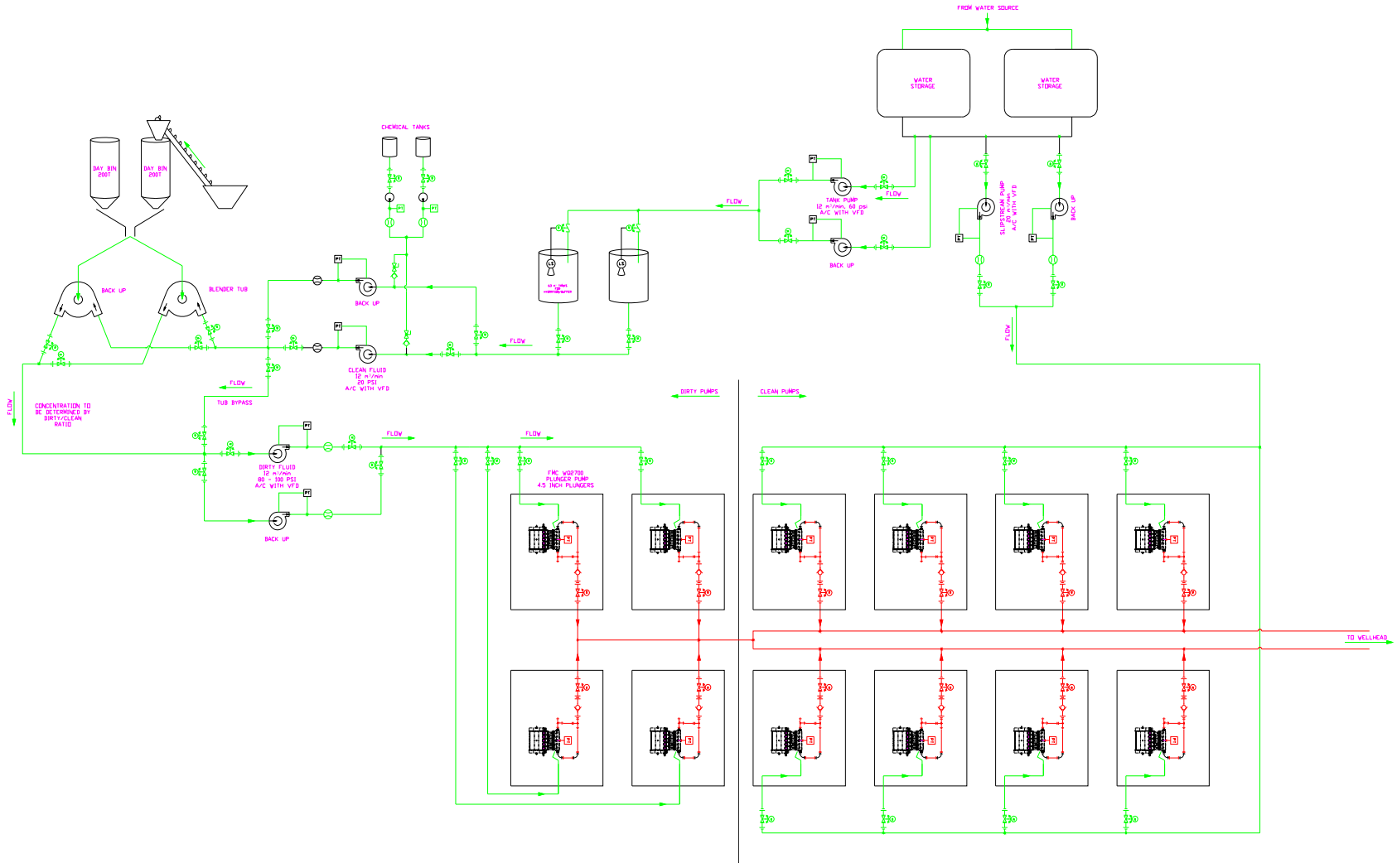


Figure 2.13: Pipework schematic [39]

to site. The size of the well, number of stages, well properties and the number of wells on a single pad will determine the length of the process. Upon hydraulic fracturing completion all the machinery is removed.

Size and weight of the individual assemblies is a deciding factor as to whether equipment will be used on-site. In the U.S. different states have different laws when it comes to allowable load. For instance, in California road weight legislation [57] is different to Texas weight limits [58]. This indicates that alternative design could benefit from lighter and therefore more practical components. In the sections 2.4 and 2.5 additional information will be presented.

Physical dimensions of individual trucks may vary as long as it aligns with state legislation. For example, a frac-trailer, that has a PD pump mounted on it has length, width and height of 14, 2.6 and 4.1 metres, respectively. In configuration where triplex pump is assembled frac-trailer weights 25,000 kg [59]. A tanker, in accordance with EU road legislation [60], is able to transport a maximum of 32,000 litres of water or petrol (this volume is limited by mass restrictions).

Proppant is supplied to site by similar transport methods. Overall load restriction will limit the individual tanker. It can be concluded that the same mass limit of proppant on the truck is the same as water, 32,000 kg. The capacity of upright storage silos is $100 m^3$ of proppant. From silos blender is supplied via gravity drive and does not require hydraulic power to operate. Because of the silos' capacity, eliminating truck movement is advantageous for most treatments.

Depending on the chemical property of the material consumables can be stored in plastic or steel containers where once delivered, components are ready to be used.

2.3.2 Fluid mixing equipment

A blender is used to mix all the components such as water, chemicals and proppant into one consistent fluid. This fluid is commonly referred to as “slurry” or “frac-fluid”. Depending on the desired effect downhole this fluid may be more or less viscous than water. Sand is transported into the blender tub using augers while chemicals and water use separate supply lines. Once the slurry is created, centrifugal pumps conduct fluid transfer to a common pipeline (manifold trailer), at pressure of ($\approx 7.00 \text{ bar}$), also



Figure 2.14: Blender control panel mounted on the blender unit

referred to as priming.

Blender control is one of the critical phases of the on-site processing plant. In order to ensure proper fluid mixture is pumped into the borehole a number of parameters such as mass, flow rate, temperature need be accounted for. Ingredients going into the blender are water, proppant and chemicals but the fluid coming out of the pump is one consistent blend. The control board is located on the blender unit itself. All the information is fed back to the control van. Figure 2.14 show the on-site control panel. The operator is assigned and located inside the blender control cabin. Blender has a number of mechanical components such as augers, for transporting sand, and centrifugal pumps that drive slurry mixture to the manifold trailer. An operator in the blender control cabin monitors and manually operates speed of the sand augers. If required, manual control of the slurry mixture can be executed from inside the blender control cabin.

In the control van, the second operator will have specialised software, provided by the blender unit manufacturer [61], while being in constant communication with the operator on the blender unit itself thereby making sure the data feeding into the control van corresponds to the readings on the blender control panel. Operator in charge of running the blender from inside the control van will have one of his screens displaying information as shown on Figure 2.15. This provides direct control of fluid mixture, properties of the fluid (i.e. Density, Composition) as well as flow properties. Driving operational changes in the software make direct blender adjustment.

One of the important parameters on the blender unit is the tub level, shown on the

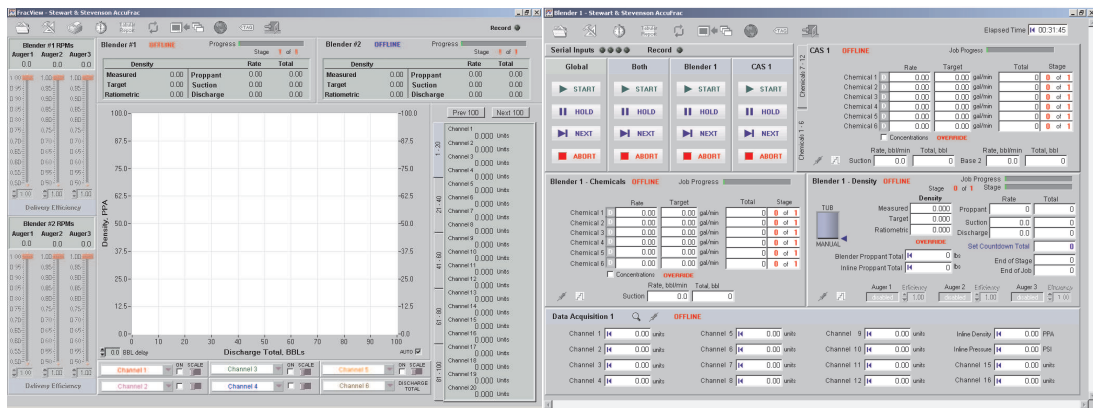


Figure 2.15: Blender control software used in the control van[61]

right window of Figure 2.15. The operator must maintain sufficient amount of fluid in the tub while hydraulic fracturing is in progress. Failing to maintain the adequate flow causes damaging effect on the equipment allocated after the blender, predominantly the positive displacement pumps.

2.3.3 Pipeline - Manifold trailer

The manifold trailer (aka missile trailer) unit is located amid the array of PD pumps, Figure 2.12, and is designed to transport fluid from blender to suction side of PD pumps. Blue line shown in Figure 2.12 is leading the flow from the blender to PD pumps at low pressure. Photograph of a typical manifold trailer is illustrated in Figure 2.16. The inlet side of the manifold trailer is leading from the blender and, as previously discussed in section 2.3.2, slurry is pressurised to $\approx 7.00 \text{ bar}$ [62]. Ports on the inlet side of the manifold trailer are operated by butterfly valves.

The manifold trailer also handles the fluid coming out from the PD pumps and distributing towards the wellhead. A high-pressure line is positioned underneath a low-pressure line, as shown in Figure 2.16. A hydraulic fracturing site may have up to 20 independent PD pumps and each pump is capable of generating pressure up to $\approx 100 \text{ MPa}$ (15,000 *psi*). High energy generated in the pumping process has to be constrained following special procedures designed to ensure safe operation. Restraining rings and restraining ropes on the manifold trailer are designed to immobilise high-pressure lines leading fluid from discharge side of the pump to the manifold trailer.



Figure 2.16: Manifold trailer is a flow distributor that supplies PD pumps on site with low pressure slurry from the blender and handles high-pressure discharge slurry from PD pump towards the wellhead.

2.3.4 High-pressure PD pumps

Positive displacement (PD) pumps have variable speeds which allows them to deliver the desired flow rates. Pumps are powered by diesel engines and the power is delivered to the transmission. Output shaft from the transmission gearbox is connected to input shaft of the PD pump.

High-pressure pumps are sized up to 2,200 kW [63] and fully mounted on the truck trailer making it a mobile unit ready to be transported to and from any service location.

Inside the control van, pump driver system is focused on delivering optimum flow rates during hydraulic fracturing. Sensors are located throughout frac-trailer unit and monitor changes in the system. Precise sensor location is shown in Figure 2.17 and the sensor output is forwarded to the control van.

Pump driving software, as used in control van, can be seen in Figure 2.18. Examining screens in Figure 2.18 suggests different grouping of the systems, window on the left shows all the pumps on a frac site. Summary of essential parameters are shown in the window on the left, including pressure in *psi*, flow rate in *bbbl/min*, engine speed

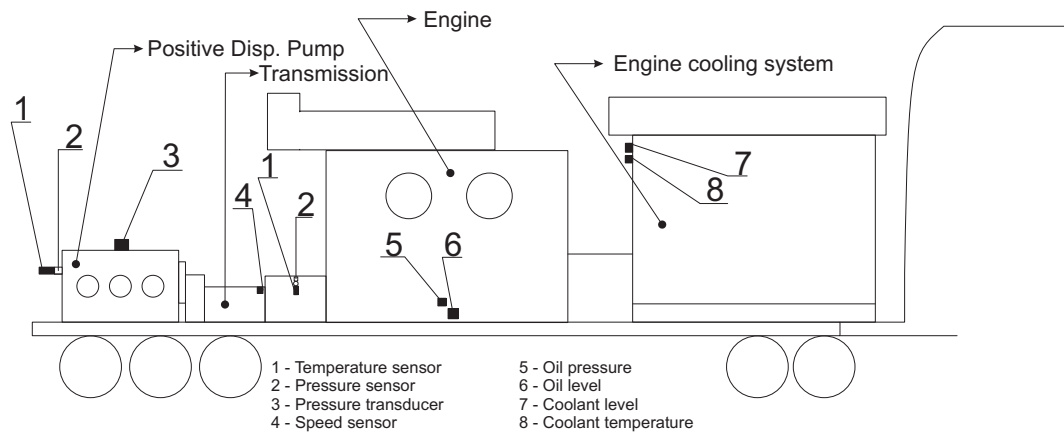


Figure 2.17: Sensor location on the frac-trailer assembly

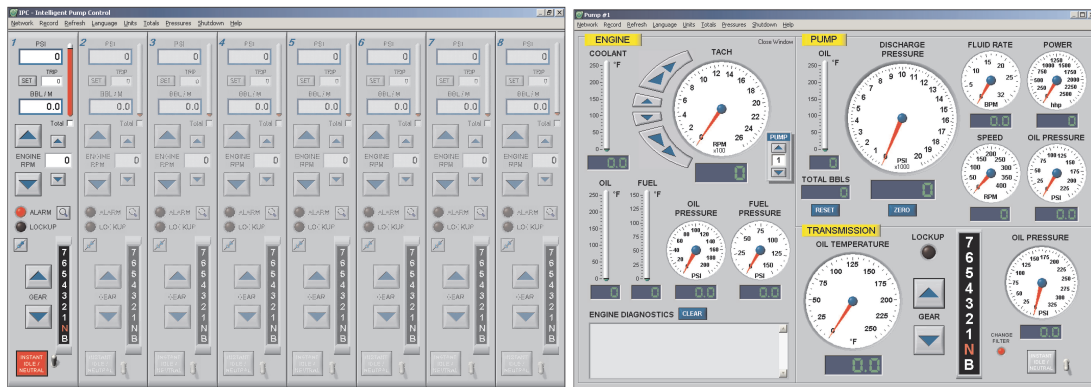


Figure 2.18: Pump control software used in the control van [64]

and transmission gear. Window on the right shows in more detail a single frac-trailer assembly with a single pump. The graphical representation shows separate sections for ‘Pump’, ‘Engine’ and ‘Transmission’. Specific parameters are displayed in addition to oil pressures and temperatures gauges and fuel levels. If an operator experiences any suspicious pump behaviour, accessing detailed reading can help towards malfunction diagnostics.

Prior to any pumping downhole, it is mandatory to ensure pressure conservancy within equipment on site. Any leaks in the system will affect pressure reading in the control van and by doing so convey a false image of pressure trend downhole. Pressure

tests are conducted prior to every hydraulic fracturing stage. Similar to blender control validation, discussed in section 2.3.2, pressure reading from individual pump is to be validated by using sensor data acquired in the control van. Each pump is equipped with an analogue pressure gauge to increase the safety factor of the process control.

Whilst hydraulic fracturing is being performed the pressure response from the well and adjusting pump speed are constantly recorded. In case of pressure drop, with the same number of pumps running, decline occurred because fluid downhole reached more porous zone and is leaking off. Naturally, this is true assuming that there are no leaks in the surface equipment. Pressure spikes can be encountered as well, which indicates that the fluid propagation downhole has reached a harder, more impermeable zone. The rock formation is highly heterogeneous, as discussed in 2.1, which means that at specific depth pumping system may encounter different well properties. It is therefore absolutely essential to track pressure trend and act in accordance with the well response.

2.4 Drive train assembly

Frac-truck assembly is a major component of the hydraulic fracturing system comprised of a high-pressure PD pump and drive mechanism that pressurises fluid up to ≈ 100 MPa (15,000 psi). Hydraulic energy is delivered by converting power from the diesel engine to the in-line motion of the cylinders. One of the challenges lies in the operating fluid itself due to its inert and incompressible nature. Physical properties of slurry composition can vary so the more viscous the fluid the more it will increase the drive unit's power requirements.

Stresses inside the pump, during a pumping cycle, are critical for the mechanical integrity of the system. Rod load limit of a typical triplex pump is approximately 1 MN as specified by the equipment's manufacturer [65]. The internal geometry of the pump is in direct contact with the fluid's high-pressure gradient. Typical slurry also carries sand grain particles which, in high-pressure conditions, have damaging effect on a pump. Erosion, cavitation and corrosion in specific pumping regimes can easily lead to valve, sealing mechanisms or even pump fluid block failure.

Figure 2.19 shows a typical frac-truck assembly which consists of drive system,

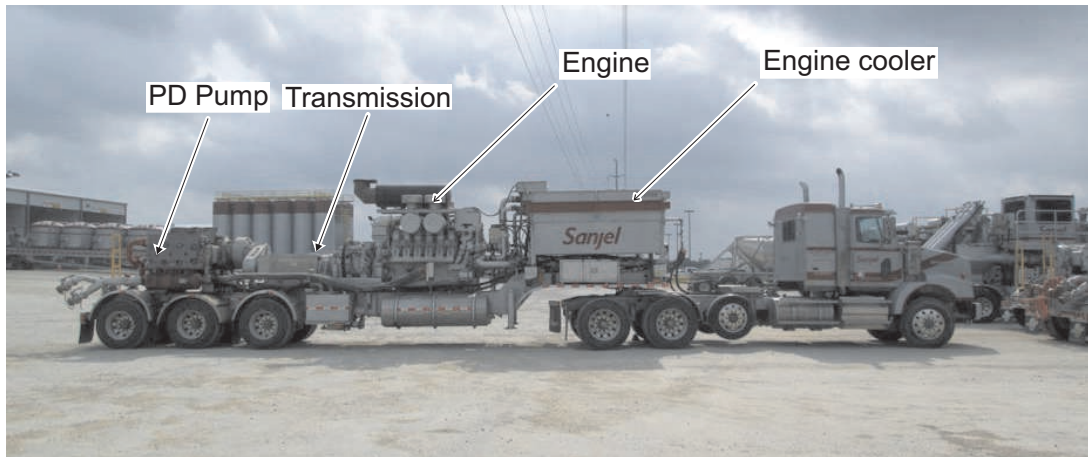


Figure 2.19: Frac-truck assembly is comprised of individual systems such as PD pump, transmission, diesel engine and the auxiliary cooling system

transmission and PD pump [66]. Normal operation requires additional systems such as cooling and lubrication systems.

In this section literature review will focus on the frac-truck assembly by discussing following systems; Diesel engine, Transmission and PD pump assembly.

2.4.1 Diesel Engine

Engines mounted on the frac truck vary in size depending on the size of the pump and the consumption of additional components. Choosing the right size of pump is determined first of all by examining PD pump requirements. Common diesel engine sizes, depending on the manufacturer, go up to 3,000 kW. A typical pump engine is a CAT 3512C HD, 1678 kW @ 1900rpm. This engine is continuous duty rated, Tier II 4-stroke, V style, engine displacement volume is 58.91 [67].

The truck shown in Figure 2.19 is designed to transport the frac-truck assembly to and from a site. In this analysis the engine selected is a typical heavy duty freight engine, Mercedes-Benz OM 501LA, 290kW @ 1800rpm, engine displacement 11.95l. This engine has Euro 3 emissions levels [68].

Figure 2.20 displays physical setup of diesel engine mounted on the frac-trailer. Pump engine is mounted adjacent to the truck cabin separated by an engine cooler compartment, Figure 2.20 (left). Instrumentation present on this vehicle, Figure 2.20 (centre) shows oil pressure and temperature readings. This unit displays pressures and



Figure 2.20: Left: Engine mounted on the Frac-trailer assembly, Centre: Pressure and temperature control gauges, Right: Oil filters

temperatures in the transmission system. The pump's power-end lubrication system is also connected. Every skid has an on-board computer that records operation metrics, allocated on the same side as the Pressure/Temperature control panel. Due to its more sensitive construction it needs to be protected from outside conditions. A touch-screen display and computer are therefore kept in an aluminium casing adjacent to the control panel. Basic operational metrics include the number of hours in operation, pressure readings and properties of the lubrication system. The software has a multitude of input options that include user specified parts of the frac-truck assembly, an example of which is the pump's suction and discharge valves replacement. These consumables need to be inspected and replaced at regular intervals to ensure proper operation of the PD pump. The on-board computer can store installation and replacement data from the operator enabling good economic prediction as well as operational history.

Frac-trucks are often operating in a remote or demanding environment. Depending on the altitude and temperature conditions adequate additional equipment must be present and engines must be set up for particular atmospheric conditions. Fracturing in Texas means there is not enough vegetation to prevent excess sand and dust accumulation. This requires upgrading the filtering system. Figure 2.20 (right) shows additional oil filters installed on this diesel engine.

The cooling compartment is located in-between the engine and the driver's cabin. The cooling system is comprised of a horizontal radiator and hydraulically driven fan. Cooling circuits are used for engine coolant, aftercooler, PD pump lubrication oil, fuel and hydraulic fan drive.

2.4.2 Transmission

The rotational power of the engine's drive shaft does not have the required speed and torque for PD pump's operation. Consequently speed reduction is implemented to ensure optimal performance from the PD pump. In the oil and gas industry eight and nine gear speed gearboxes are widely used. Connection between gearbox and the engine is achieved via torque converter which is designed to establish flexible fluid coupling between the engine and the gearbox.

Torque Converter - is a transmission unit that transmits power from engine to gearbox. Unlike conventional gearboxes, that use pairing up of the gears to transfer torque and speed, torque converters use hydraulics as a transfer medium. These units employ hydrodynamic coupling, specifically oil, to create flexible connection between output shaft from the diesel engine and the input shaft of the conventional gearbox. Torque converter's prime function is to multiply torque from the source unit (engine) while decreasing rotational speed. The gradual build-up of power is an additional benefit; when the engine is at low speed the torque multiplication will be lower, as the engine accelerates torque multiplication will gradually increase up to its efficiency peak.

Power from the source (diesel engine - prime mover) is absorbed in the impeller, fluid is accelerated from relatively low-velocity present near the centre to a high velocity that is at the outer diameter. Power capacity is proportional to impeller's speed and outside diameter. Torque capacity is also proportional to impeller's speed and the outer diameter. Work done by the engine, in accelerating fluid from low to high velocity, is turned into kinetic energy which is transmitted to the turbine. Inside the turbine, fluid loses its speed while being guided back towards the centre of the chamber. From the turbine it enters the stator element that changes direction of the return flow between the turbine and the impeller. This direction change increases the momentum of the fluid, thereby increasing the torque capacity. From stator it enters impeller in a continuous process. Reaction torque presents a share of the total torque that resulted from the change in fluid direction. The amount of reaction torque is determined by the shape, angle and configuration of the blades. More than one reaction member can be employed whereas units are marked as single, two or three-stage converters in accordance with

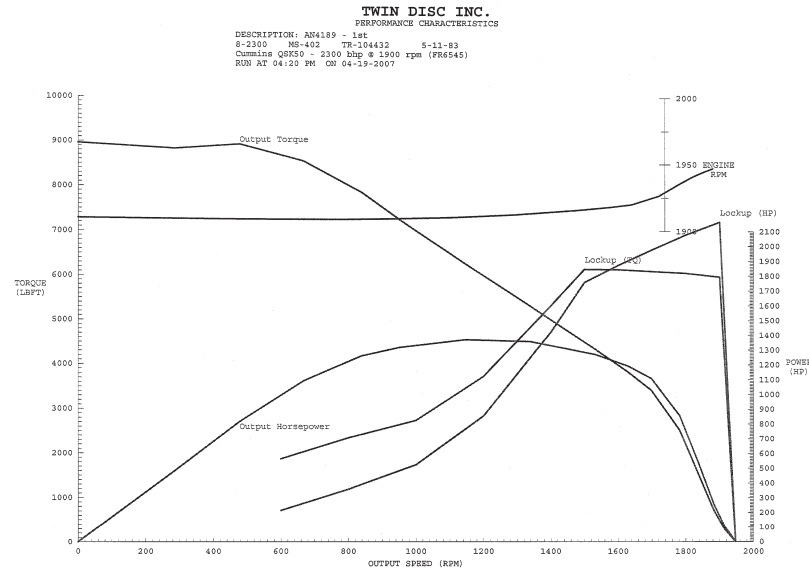


Figure 2.21: Combined performance curves between engine and torque converter compiled by TwinDiscInc. [71].

the number of stages in the turbine [69].

In this literature review Twin Disc 8500 [70] was selected for demonstration. Chosen torque converter is assembled on a wide array of fracturing trailers and is considered to be the industry standard.

Based on an engine's output performance and selected torque-converter collective power and torque output can be calculated based on the individual input data. In Figure 2.21 combined plot shows sole engine's power and torque over a range of speeds and the same power/torque metrics of engine and torque converter combined.

The gearbox - is comprised of eight gears which allows the pump to operate over a range of speeds. The gearbox will start building up from lower to higher gear (with the initiation of the pumping process). Allison Transmission 9800 Series [72] is one of the most commonly used in hydraulic fracturing. Input power size varies depending on the model starting from 1,200 kW to 1,800 kW. Acceptable full load engine governed speed is 1,800-2,100 rpm with minimum engine idle speed (with transmission in 'drive') of 550 rpm [72]. Since the drive train is powering PD pump operation, it only needs to rotate in one direction, there is no need for reverse gear. Figure 2.22 shows a gearbox

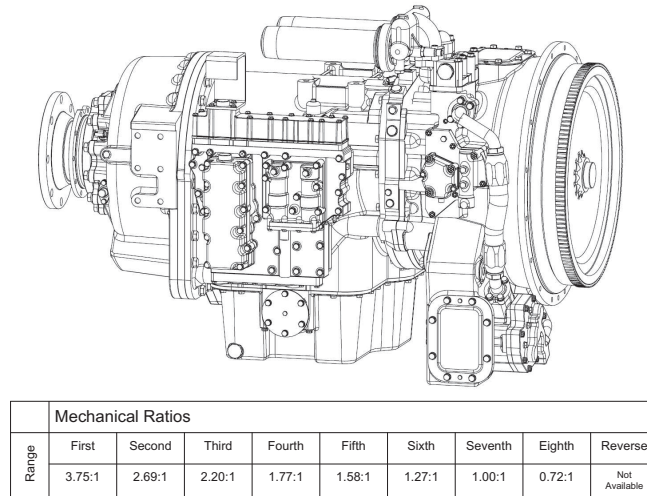


Figure 2.22: Transmission unit connecting diesel engine to positive displacement pump is shown. Table beneath gives reduction ratios for selected gearbox unit [72].

schematic on a frac-truck assembly with a table of different speed ratios.

2.5 Positive displacement pump

Pumps used in hydraulic fracturing applications operate by using the reciprocating motion of the plunger to pressurise the fluid. Plunger movement from bottom-dead-centre to top-dead-centre compresses fluid inside the chamber until it reaches the outlet (wellhead) pressure. A typical reciprocating pump has a fixed pumping stroke. Flow rate capacity is defined by considering the internal chamber volume (plunger diameter and plunger stroke) and pump speed.

The pump is comprised of two main sections; power-end (PE) has a crankshaft mechanism that transfers rotational movement from transmission to linear motion of plungers and fluid-end (FE) stands for an enclosed chamber in which the fluid is pressurized. Depending on the configuration, PD pumps can have either three or five cylinders (or chambers), also known as triplex and quintuplex respectively.

Pump chosen for further analysis is WeirSPM TWS2250HD shown in Figure 2.23. This pump has a triplex setup (three plungers) and is available in multiple plunger sizes offering flow rate up to 2,300 l/min and pressure as high as 130 MPa [73].

High-pressure pumping equipment is required to pump large volumes of frac-fluid

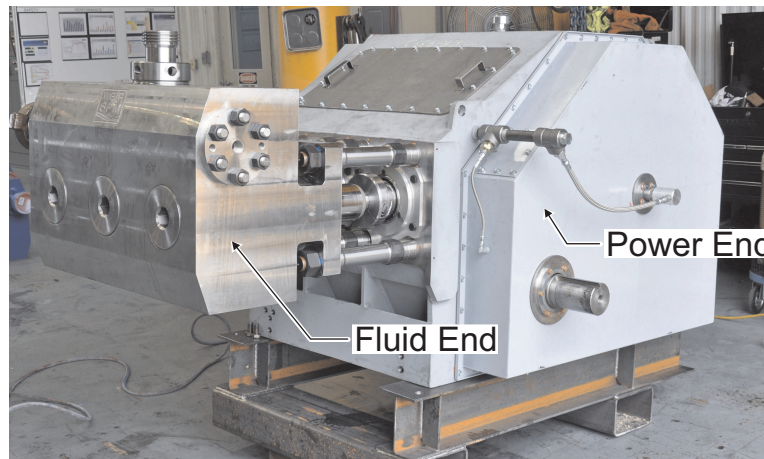


Figure 2.23: Positive displacement pump is mounted on the back of the trailer skid. It is comprised of two sections, power-end with mechanical crankshaft and fluid-end in which slurry is pressurised.



Performance specifications:

Specification	Design	Value
Mech. horsepower	HP_m (kW)	1,677
Max. rod load capacity	F_{max} (kg)	108,214
Max. engine RPM	RPM_{eng}	1,950
Gear ratio	r_g	6.353:1
Stroke length	L (m)	0.204
Plunger diameter	D (m)	0.111
Number of cylinders	N_{cyl}	3
Mech. efficiency	ME (%)	90

Figure 2.24: Left image shows typical 3-cylinder positive displacement pump employed in hydraulic fracturing [73]. To the right, the table details the performance specification of a typical pump.

to pressurise the well formation until the surrounding rock fractures. After fracturing has occurred, pumps are needed to propel and deposit proppant into the newly opened fissures in the rock to keep the formation open. Some pump types, such as a centrifugal or rotary pump, decline in performance once operated outside the point of peak efficiency. However, positive displacement pumps have a broader operating range and are able to provide both high flow rates and pressure for sustained periods [74]. A typical 3-cylinder pump is shown in Figure 2.24.

The fundamental physics of fluid movement means that all pumps are designed to operate in predefined ranges as shown in Figure 2.25b. Operating pumps outside their design range can lead to premature failure caused by over stressing their structures [75].

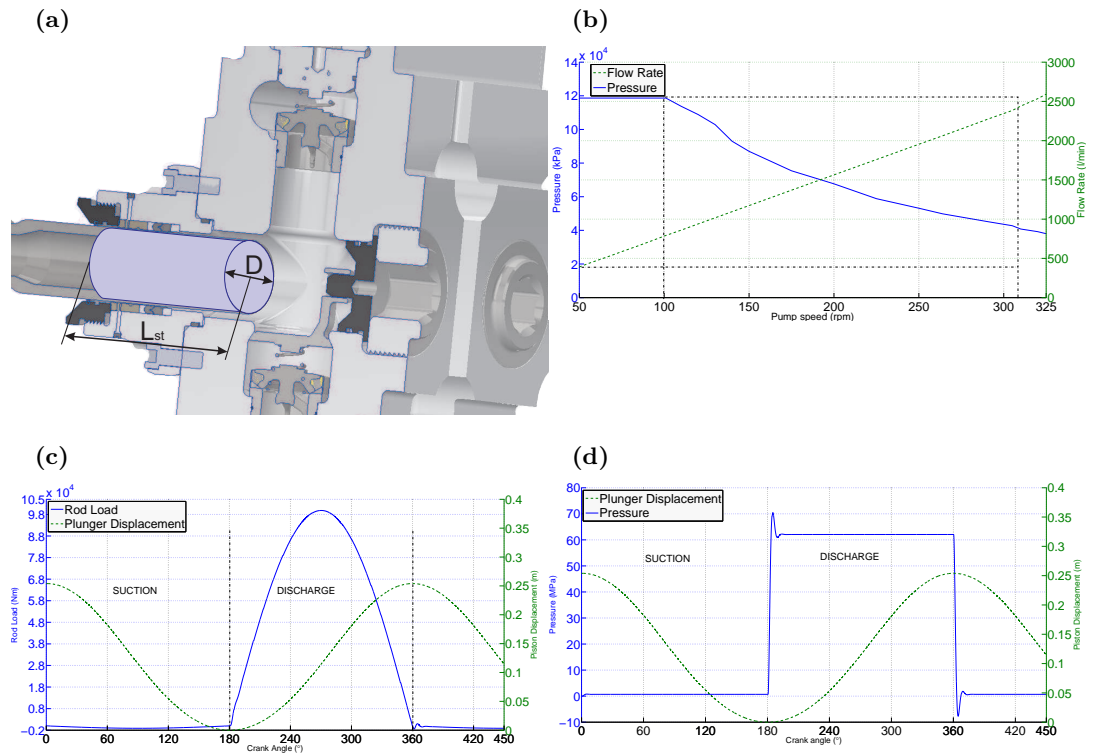


Figure 2.25: Cross section of the positive displacement pump (a) with speed and pressure ranges (b). Lower left and right graphs show the cyclic variations in rod load (c) and pressure seen during a single pumping stroke (d).

A pressure relief valve is located on the high-pressure part of the PD pump to prevent overpressurization and failure inside the chamber.

In a hydraulic fracturing operation, pumps must be capable of providing both high pressure and (at different times) high flow output. The initial phase of a fracturing stage, known as the ‘breakdown’ phase, requires a high pressure to initially crack the rock (in Figure 2.6 this is shown in the tenth minute of the stage). This duty lasts for only couple of minutes but it is crucial to the success of the entire operation. The next part of the operation (again, as shown in Figure 2.6) is referred to as the ‘fracture propagation’ or ‘extension phase’ [46]. In this phase, the cracks initiated in the ‘breakdown phase’ are propagated to create the desired fracture network necessary for maximum gas flow. Thus, this part of the hydraulic fracturing operation is also crucial as it directly determines the effectiveness of the well stimulation [47]. During this phase, the fluid pressure must be maintained at a lower level for a couple of hours while the flow rate is up to 6 times higher than in the breakdown phase. These flow rates are achieved either

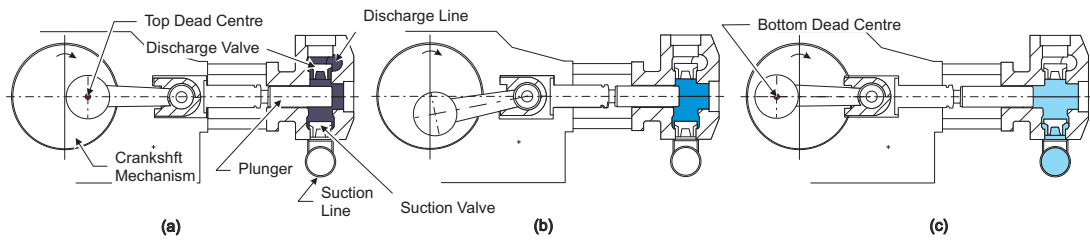


Figure 2.26: Three phases of a typical pd pumping cycle during suction stroke. (a) fluid is pressurised and delivered through the discharge valve. (b) decompression of the chamber as the plunger retracts. (c) pressure in the chamber is lower than the suction pipe and fluid enters through the suction valve.

by increasing the speed of the pump, Figure 2.25b, or (when the performance limits of individual pumps are reached) by introducing additional pumps to the operation. An experimental study by Fan [76] highlights pressure variation due to different injection flow rate dynamics. Negative effects of pressure oscillation are manifested in the form of unpredictable shale fracture development and are also damaging to the pumps and other process equipment generally used during hydraulic fracturing. Consequently, the relationship between injection pressure and injection flow rate is critical for successful well stimulation.

As previously noted, there is no advantage to designing larger pumps (rather than requiring a lower number of pumps), since, in order to be portable, their size is limited to the truck specifications in North America.

2.5.1 Operating principle of PD pump

A positive displacement pump in its simplest form consists of a pressure chamber, reciprocating plunger, an inlet valve that regulates fluid entering the internal pressure chamber, an outlet valve that regulates the exiting of the fluid from the pressure chamber and the power generator with the accompanying crankshaft mechanism that drives the reciprocating motion of the plunger, all of which are shown in Figure 2.26. Miller's work details some of the operating principles commonly associated with positive displacement pumps, [74] and the requirements in field operation are clearly documented by the American Petroleum Institute [75].

The operating cycle starts with the plunger retracting from TDC (top dead centre) position, illustrated in Figure 2.26. This configuration decompresses the internal cham-

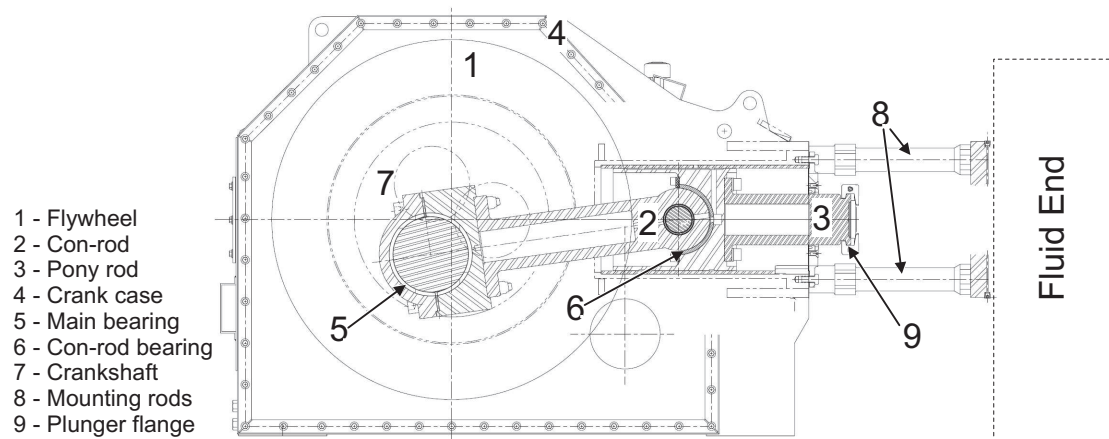


Figure 2.27: Cross section of the PD pump's power-end shows the crankshaft mechanism which drives the plunger motion. Main components are listed in the figure. The second part of the assembly (fluid-end) is mounted on the right.

ber and causes the suction (i.e. inlet) valve to open. At that point the pressure present in the suction line is greater than the pressure inside the chamber. The suction valve is held open until the plunger reaches BDC (bottom dead centre). Once the plunger starts moving away from BDC the compression stroke begins. The exact timing of the opening and the closing of both suction and discharge valves are dependent on the bulk modulus of the fluid. The outlet valve opens only when the pressure inside the internal geometry of the pump reaches the pressure in the discharge line. At this point the discharge valve opens and pressure balance is established. When plunger again reaches the TDC discharge is complete and the cycle begins again.

2.5.2 Power End design

The drive train is directly coupled to the power end part of the pump. In this section the rotational motion of the driveshaft is converted into linear motion of the plunger. In Figure 2.27 cross section of pump's power end is given. A list of the main components is displayed in Figure 2.27.

The power-end incorporates a fixed speed gearbox, not shown in Figure 2.27, that reduces the speed from the transmission unit by a set ratio. For the selected PD pump this ratio is identified in the table shown in Figure 2.24. Sets of bearings are assembled on each end of the connecting rod (con-rod). All plungers on a three-cylinder pump are offset by 120° . Crank radius defines plunger stroke in a way that stroke equals double

crank radius length. Rod-load is the limit of acceptable stress condition acting on the crankshaft via plunger, for specified pump rod-load is given in Figure 2.24.

The crankshaft is manufactured through forging process. The crank case which was previously machined and welded has in recent years undergone modifications in manufacturing process. New generation PD pumps have steel crank cases which are forged with minimum amount of welded structures.

Strength limitations

Bearings are critical components in the current power end assembly. Life of the bearing will depend on the operating conditions and the service life maintenance. Bearing life is expected to be up to 3,000 hours of operation with regular service every 500 hours [77].

The structural strength constraints of the pump can also affect operations in several ways, for example:

- Each pump has a pressure restriction due to the maximum rod load that its drive can transmit without buckling [78]. Each cylinder is controlled by a crankshaft that is powered from the diesel engine's driveshaft via the gearbox. [74].
- The pump housing is directly affected by periodic loads, particularly throughout the discharge stroke as shown in Figure 2.25c and 2.25d. The resulting strain frequently causes the pump housing to experience twisting and deflection.
- The cyclic loads on the structure, due to the drive mechanism, indicate that the power delivery (i.e. torque and speed) is non-linear [79]. The unsteady power delivery from the engine and transmission will impact on a pump's life through fatigue limits and shorter component life (e.g. bearings).

Vibration presents an additional phenomenon associated with current designs, resulting in problems of constructive interference. The previous investigation identifies that the fluctuation of the engine speed of ± 100 rpm is insufficient to control the fracturing process with adequate precision. Moreover, the life of other elements are strongly influenced by speed, load and vibration. The performance of machine elements such as

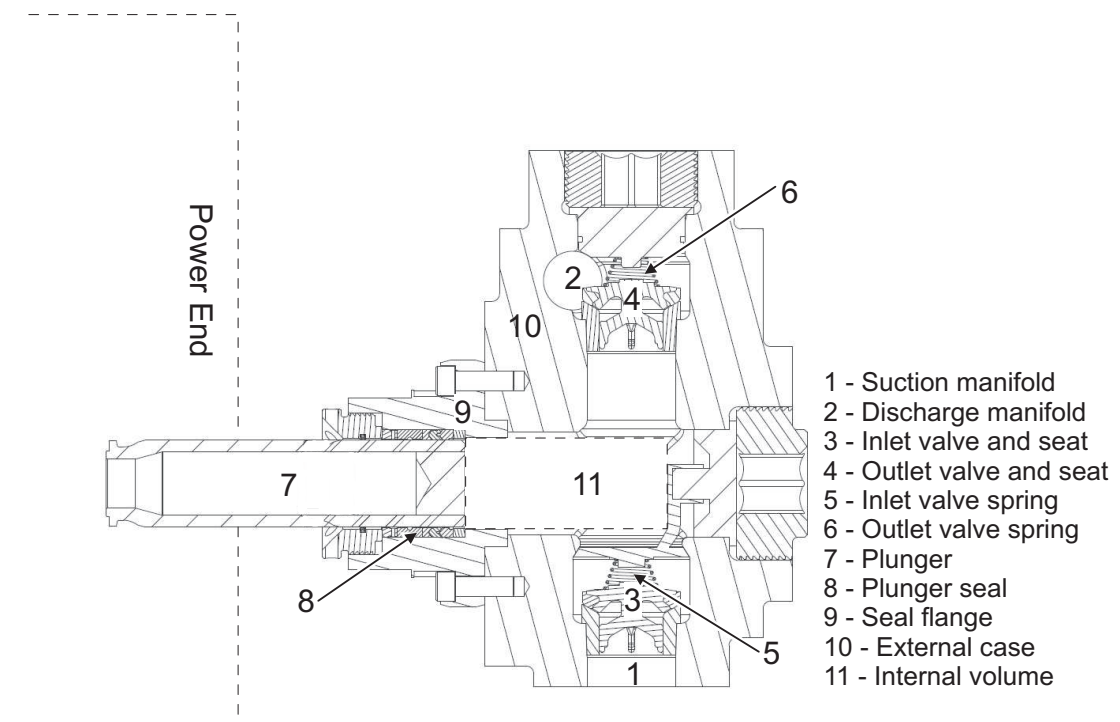


Figure 2.28: Cross section of the PD pump's fluid-end shows internal volume, cylindrical plunger and the set of poppet valves. List of key components of this section of the PD pump are listed.

bearing, drive couplings and driveshaft offset angle all have significant impact on the pump's overall performance.

2.5.3 Fluid End design

The next major component in PD pump assembly is the fluid-end where the reciprocating motion of the plungers sucks fluid inside the chamber and compresses it until the pressure reaches the outlet conditions. Main components of fluid end are shown in Figure 2.28.

Suction manifold supplies all cylinders with operating fluid. To prevent the liquid from cavitating (i.e. falling below atmospheric pressure) the inlet is pressurised by an external centrifugal pump located on the blender (section 2.3.2). The discharge manifold consists of chamber plenum that merges output from all cylinders in the pump. The discharge fluid is led back to the manifold trailer (as discussed in section 2.3.3). The inlet valve/seat assembly consists of a replaceable steel seat that is a part of the internal volume and the steel valve that is free to move, under the influence of

the pressure inside and outside the internal volume. The outlet valve operates on the same principle as inlet the valve. Inlet and outlet valve springs are pushed against the body of the valve which creates the preload force on the valve assembly. Preload on the inlet and outlet valve can be different in design.

A plunger is located inside each of the chambers, therefore, a three cylinder pump will have three plungers. The diameter of the plunger and crank radius (section 2.5.2) fully define the internal volume of the chamber and rod-load of the crankshaft. The plunger design has an internal bore, illustrated in Figure 2.28-7, to minimise the weight of the component and minimise inertia. Plunger seals are placed between the seal flange and the outer plunger circumference. Seals can be tightened to account for the high chamber (internal volume) pressure.

The external case is manufactured from stainless steel and different alloy steels through the process of casting. All internal volumes are machined.

Graphical representation of the internal volume is shown in Figure 2.28 for better understanding of the internal geometry.

Fluid limitations

Although fluid properties such as inertia or viscosity create theoretical boundaries for the flows and pressures that a pump can deliver, some of the most serious practical constraints are secondary to the movement of the fluid. For example, erosion is common even though pumps are manufactured from hardened-alloy or stainless steel. This is because, as described in Section 2.2.4, the frac-fluid is a slurry of water, chemicals and proppants, that erode and corrode the pump components in a number of ways [78].

- During the high flow operating regime sand and proppant particles cause erosion and wear in the fluid chamber [80].
- The addition of acid to the frac-fluid in some hydraulic fracturing operations causes corrosion that ultimately reduces the fatigue life of the pump [81].

Together, these processes wear the internal surfaces of the fluid chamber after a number of hours, leading to so-called pump "wash out". The effects of wear include leaking valves and deteriorated plunger seals. This limits the pressure at the outlet of the

manifold trailer (i.e. the inlet of the pump's suction chamber). Sealing failure can allow high-pressure fluid to propagate outside the pump in an uncontrolled way which is a serious risk for the operator and personnel on site. Pump leakage affects equipment efficiency and performance characteristics.

If the priming pressure coming from the manifold trailer drops below a critical threshold, cavitation problems occur in the fluid chamber [82].

Perhaps the most serious consequence is that wear varies in proportion to the fluid velocity [83],[84]. In other words a small increase in fluid speed might have a dramatic increase in the rates of erosion.

These issues lead to ineffective pumps, loss of volumetric efficiency and an unbalanced operation. These design challenges must be overcome to achieve a consistent flow pattern and avoid oscillation and vibration issues.

2.6 Environmental impact

Emissions are a key element of industrial impact so it is essential that onshore oil and gas develop scenarios for reduction of CO_2 similar to those adopted in other industries [85]. The methodology for doing this is well understood, for example, development of the computational model for estimating CO_2 emission from oil and gas extraction was discussed in Gavenas et al, (2015) which allowed the main source of greenhouse gas (GHG) emission to be identified, managed and mitigated [86]. Since it is forecast that gas will remain an important fuel into the future, it is important to minimise the emissions intensity of the shale gas extraction process in order for the resource to be developed in line with current targets for reduction of carbon emission.

Life cycle assessments (LCAs) are an important tool that can inform the relative carbon intensity of different energy choices, and identify means of reducing overall emissions. There is some uncertainty around the magnitude of greenhouse gas emissions from shale gas extraction and consequently the majority of reported shale gas LCAs have been performed using North American data and practices. Issues such as differences in assumptions and scope of the LCAs can make their results difficult to compare, and estimates of lifecycle emissions are evolving as new measurements become available and as commercial practices change in response to environmental regulation or techno-

logical advances. Furthermore, these LCAs must be adapted to the European context, which differs from North America in terms of the resource, environmental regulations, and social factors. A recent comparative meta-analysis of LCAs found that the median difference between electricity generated from unconventional and conventional gas in North America was 3% [87].

These results are similar to LCAs adapted for shale gas extraction in the EU [88]. Indeed, LCAs adapted for shale gas extraction in the UK [89] and Scotland in particular [90] find that the carbon intensity of shale gas could be lower than imported conventional natural gas. These LCAs identify that besides fugitive leaks of methane during gas extraction and transport, which could be the greatest source of greenhouse gas emissions from shale gas, the majority of greenhouse gas emissions arise from activities during the preparation of the well pad and construction of the well, rather than during gas production [90]. To further reduce the carbon intensity of shale gas and the environmental footprint of the industry, operators should seek to minimise the area of the well pad, the amount of surface infrastructure, size and mass of the construction materials, distances materials are transported, and the pad power requirements.

Local air quality, noise and traffic issues associated with hydraulic fracturing impact on communities local to shale gas developments, and concerns around these impacts are causing delays to planning applications in the UK and negatively affecting public acceptability of the industry [91]. The construction and operation of the surface facility requires significant truck movements and transport distances. For example in North America over 1000 truck round-trips are required for a single frac-site [92]. Diesel fumes from trucks, drilling, frac-pump engines and emissions from gas processing equipment can significantly reduce the air quality around a hydraulic fracturing site; both for the workers, and local residents [93]. Some significant air quality issues in North America are related to practices that would not be permitted in Europe due to environmental legislation (such as storage of flowback fluids in open ponds). The effect of diesel engines from trucks and pump engines will result in a decrease of local air quality as well as contributing to noise pollution. Recent work by Rodriguez et al (2013) measured fuel consumption and on site emissions for two hydraulic fracturing sites in North America, and found that the fracturing pumps contribute up to 90% of total emissions on-site.

The pumping equipment may also generate the most significant noise on site during the lifetime of the shale gas operations, depending on the number of pumps in operation at any time [91].

In North America, the development of surface hardware has, to date, largely been driven by the need for incremental improvements to enable hydraulic fracturing at higher pressures and greater depths. These requirements (high fluid pressure and transporting proppants into the well bore) place great demands on the mechanical structures of the pumps and therefore the pumps require frequent maintenance and have finite lives. However, there is no reason why the site machinery deployed in the EU needs to be designed to the same specifications as for the North American sites. For example, an enhanced pump design could contribute to reducing the environmental footprint of the well construction and completion, and also of any re-fracturing during the lifetime of the shale gas well. Given the relative infancy of the shale gas industry in Europe, it is timely to consider opportunities for improved design of required hardware.

2.7 Generation of improvement concepts

The literature review suggested nine areas in which technical development can benefit the hydraulic fracturing process. These are:

1. Process improvement could be achieved by implementing different control mechanisms that incorporate subsurface formation using such methods as microseismic feedback. Live microseismic feedback could enable better process control but the limitations are the unknown aspects related to implementation cost and market impact.
2. System control on site creates new possibilities for automated process operation. Technical feasibility presents a risk due to the lack of equipment's operational data and high research cost.
3. Several of the considered concepts, summarised in Table 2.2, could be categorised as "blue sky". An example of this is the feasibility of controlling the dynamics of pressure pulses towards the target zone.

4. Multiple small bore plungers could decrease hoop stresses and crankshaft loading. A key drawback of multiple small bore plungers is manifested in the high implementation cost.
5. In the current circumstances when application of hydraulic fracturing technology could be utilised worldwide, the questions of emission, noise pollution in inhabited areas and the physical scale of the operation present a potential bottle neck for technology acceptance.
6. A number of hypotheses have emerged from improved PD pump design, for instance, the ability to control the valve opening characteristic could influence cavitation suppression. Technical feasibility of servo controlled valves presents a possible risk.
7. A widely recognised concept in industry is the possibility of mixing slurry downstream of the high-pressure pumps. This concept will enable better preservation of high-pressure equipment on site. However, development cost is likely to be high due to limited technical feasibility and available expertise.
8. An alternative crack initiation method could be achieved by means of hypothetical downhole water expansion. Creating temperature differentials in the well utilises the energy of fluid expansion. Downhole water expansion is more challenging for a number of reasons, predominantly related to R&D time and technical feasibility.
9. The implementation of downhole microbores and timed pressure pulses can provide benefits to the process but at the same time carries the risk of extended development time. Although both have potentially high technological impact development cost is going to be high thus limiting the feasibility of the solution for this phase of project.

Table 2.2 illustrates a morphological chart of all the considered research directions. Design criteria, such as available research time, cost, technical feasibility and available expertise were used to evaluate impact and project outcome. Despite individual qualities of alternative research questions top surface operation has several key aspects that need to be considered in the phase of problem assessment.

Table 2.2: Morphological chart of future hydraulic fracturing development

Concept evaluation grid									
	1. Microseismic feedback	2. System control	3. Pressure pulsation waves	4. Multiple small bore plungers	5. Environmentally driven optimisation	6. Servo controlled valves in PD pump	7. High-pressure mixing	8. Downhole water expansion	9. Downhole micro-bores
Time (research)	✓	X	✓	✓	✓	X	✓	X	X
Time (development)	✓	✓	X	X	✓	X	X	X	X
Cost of investigation	?	✓	?	X	✓	✓	X	X	X
Risk	✓	✓	✓	X	✓	✓	✓	✓	✓
Market impact	?	✓	✓	✓	✓	✓	?	✓	✓
Technical feasibility	✓	X	X	?	✓	X	?	X	?
Commercial feasibility	✓	✓	✓	?	✓	✓	✓	X	X
Available expertise	✓	✓	?	✓	✓	✓	✓	X	X

The justification for selecting an environmentally driven pump design optimisation is attributed to its alignment with all the criteria, shown in Table 2.2. Optimisation will focus on improvement in energy systems specifically focusing on high-pressure pumps. This research will provide strong arguments for adaptation and wider application of hydraulic fracturing technology.

The surface operation presents one of the leading risks for public acceptance of hydraulic fracturing technology. Adgate (2014) report estimates a thousand return truck journeys over the course of an entire well stimulation process [92]. In addition, all positive displacement pumps mounted on individual trailer skids present the major part of all units on site [93]. Section 2.4.1 shows that all the pumps are powered by diesel engines. According to Rodriguez (2013), PD pumps on site contribute to 90% of diesel gas emission [93]. PD pumps also take the most of the space on site as shown in Table 1.1.

This research aims to execute a grid search optimisation algorithm for a redesign of a single pump unit and system of pumps. The best set of parameters are compared to current design and practices based on which an overall conclusion is made. The developed model will also prove to be beneficial for other solution ideas presented in Table 2.2.

2.8 Summary

The preceding discussion has shown that the machinery involved in hydraulic fracturing creates a broad spectrum of environmental impacts. Its mechanical design has been dictated by purely functional requirements of delivering specific pressure and flow, however, the hydraulic fracturing of the future will also have to minimise the environmental impact.

In this chapter basic concepts of oil formation and the different geological properties of rock associated with the process are discussed. Further literature examination is based around conventional and unconventional oil and gas recovery methods. The different phases of hydraulic fracturing operation starting with single, multiple stage design and a simple model of rock fracture mechanics (for establishing well requirements in terms of pressure and volume) are presented. These parameters will help to

establish benchmark values for typical process requirements on site. A brief overview of fluid composition and the auxiliary process equipment on site, including storage, transportation and fluid mixing units is also presented.

Risk and environmental constraints related to the process of hydraulic fracturing were identified by reviewing the practices involved.

Finally, using a morphological chart [94], the last section of the literature review presented the idea generation and concept selection for development in hydraulic fracturing. The conclusion of this qualitative analysis is in the identifying of the opportunities for reduction in environmental impact. Therefore, the optimisation of the equipment's design should be the objective of the research. This objective gives rise to two questions:

1. What modifications should be made to the design of the equipment?
2. What impact will the modifications have on the performance?

The following chapters develop system models that not only allow the optimisation of current design but also implement new design features that have potential to improve performance.

Chapter 3

Methodology

The literature review identified equipment optimisation as a feasible objective for the research. This chapter describes the methodology adopted to achieve this objective.

3.1 Research mode and strategy

After reviewing the taxonomy of research methodology proposed by [15] deductive research method was selected, as shown in Figure 3.1.

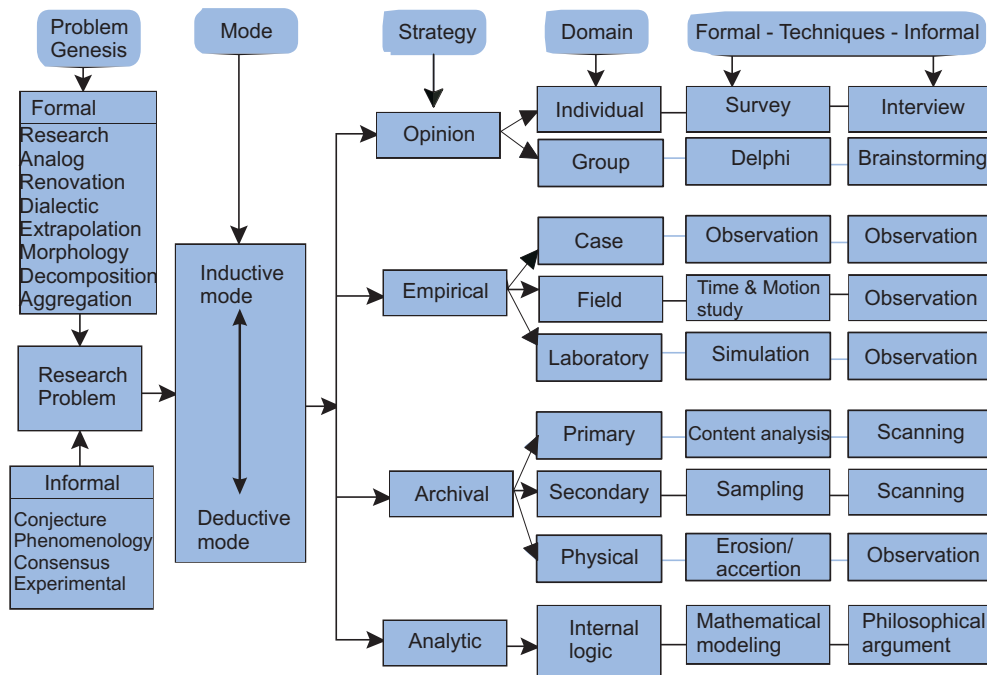
The process of hydraulic fracturing is designed to perform the function of well stimulation to increase productivity. Due to its nature, the engineering rationale will dictate that combination of physical measurements need to be compared and used to develop the analytical model.

Consequently, an empirical research strategy is appropriate as the work concerns a physical process. Because all the solutions and system improvement should be implemented on site it is essential to understand the current state-of-the-art.

Restrictions involved in the purely empirical approach are subject to operational limitation, so the repeatability is a risk. The need for robustness of the data (e.g. sensor issue and lack of precision instruments) is an inherent weakness of this method.

Constraints from the empirical strategy, such as limitation to real time event can be overcome by using an analytical alternative. Consequently replicating real-time event to a repeatable model will enable a higher degree of flexibility.

Limitations of the analytical strategy are predominately due to its limited fidelity.



Buckley J.W., B. M. H., Chiang Hung-Fu (1976). *Research Methodology & Business Decisions*

Figure 3.1: Framework of research methodology [15].

Analytical strategy on its own is hard to prove and may embody some logical error. The analytical strategy also risks the researcher's bias and temptation to focus on trivial factors, not providing the real answer for the process.

However, despite these problems it is clear that other research strategies, such as archival and opinion strategy, will not provide the quantifiable results that are needed, hence they can be excluded in the further analysis.

Therefore the combination of empirical and analytical approaches provides enough information for a successful research outcome. The following sections further expand on the manner in which these two strategies are to be applied in the field of hydraulic fracturing machinery.

3.2 Research domain

It has been established that empirical input from the field is essential to the overall understanding of the field operation and the subsequent refining of the model. All the system constraints and the operating practices will be embedded in the data. Obtained field data can be processed afterwards and examined using different mathematical tools.

However, owing to the nature of the hydraulic fracturing process, its high impact in the field and associated economical aspect, it can be concluded that a single, fully adaptable field model will not be possible for number a of reasons. Limitations in the data will imply that any change in the operational procedure will have to be reassessed. Equipment will work on site only in the way of an operator's established practice, making unknown the full scope of equipment variance.

The design and construction of the scaled model of a field setup, that can be operated fully and independently of external influences, may answer the insufficiency of field data. A laboratory research domain implementing scaled model will have the same operating principles and answer the questions determined in the problem identification section.

The third and final research strategy is required to be analytical. The development of such a computational model will enable flexibility and further practical implementation of knowledge and understanding stemming from two empirical strategies. The research domain of the analytical strategy is internal logic.

Ultimately the overall research domain consists of two empirical strategies - field and laboratory and an analytical internal logic.

3.3 Research technique

The final stage of the methodology discussion is analysing research techniques. Identified domains of research are field data, laboratory and internal logic; first two being empirical strategies and the last one analytical.

Although there are a number of different commercial suppliers of hydraulic fracturing pumps there is remarkable uniformity in their mechanical design (e.g. plunger diameter, speed, stroke length, etc.). Rather than simply adopting the industry's default values this research will investigate the "design space" of several critical interacting parameters to identify the optimum solution. To do this the following methodology is adopted:

1. Establish operational requirements for achieving successful well stimulation using an engineering approach presented in the literature review section 2.2.2.

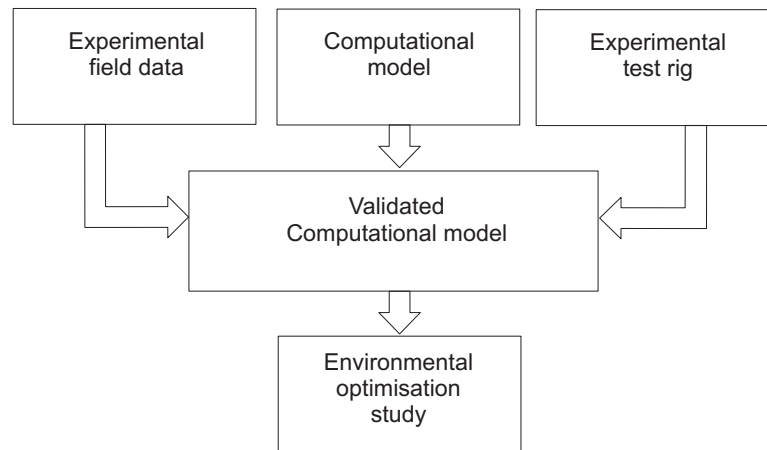


Figure 3.2: Methodology for optimisation development shows implementation of two experimental sets of data into a validated computational.

2. Identify the pressure and flow required to fracture low permeability rock at the required depths, presented in section 2.2.4;
3. Detail parts of the PD pump that determine mechanical performance;
4. Use the validated computational model for design space analysis;
5. Develop optimisation algorithm to explore possible efficiency improvements and identify best set of parameters;
6. Using the results from this study compare the power and performance requirements from the current and next generation of pumps;
7. Develop optimisation algorithm for site optimisation
8. Quantify the operational improvements between the optimised and the benchmark model.
9. Evaluate and discuss the environmental benefits that enhanced PD pump performance and system layout could offer for hydraulic fracturing operations;

Given the above strategy the crucial elements are computational model, model validation and pump/system optimisation, considering each of these in turn.

	Chapter: 4.1	Chapter: 4.2	Chapter: 4.3	Chapter: 4.4	Chapter: 7	Chapter: 8
	Drivetrain	Single cylinder	Valve dynamics	Multi cylinder	Validation	Optimisation study
MatLab model	•	•	•	•	•	•
CFD model		•	•		•	
Flowmaster model		•		•	•	

Figure 3.3: MatLab computational model validation was conducted in parallel with alternative modelling tools. Presence of each model in individual chapters throughout the thesis are identified.

3.3.1 Methodology for development of computational model

Every component seen on a frac-truck assembly is an independent subsystem. However, recognizing critical system parameters can, in the end, help towards better design and optimized pump performance. Therefore, the phased development of a computational model was done by implementing sequential design, validation and integration of individual parts into one pumping system. Modelling starts from power generators and progresses all the way to the internal parts of a single PD pump. Sections in this chapter will give emphasis on the most influential parts of the system such as:

- Engine to PD pump power transmission
- Internal fluid dynamics in a single cylinder
- Valve actuation analysis
- Chamber interaction in multi-cylinder pump

MatLab computational model is used throughout the thesis and in the Optimisation study, Chapter 8. Figure 3.3 identifies other methods used to validate the computational model in Chapters 4.1,4.2, 4.3, 4.4, 7, 8.

The sections in this chapter will be approached separately by identifying individual problems and opportunities relevant to the identified modelling scope. Each section has clearly defined aims and objectives to retain the focus on individual sections of the computational model. Mechanical overview of the system will be stemming from the data given in literature review sections 2.4-2.5 by providing additional information.

Validation of the fluid dynamics model will be provided in each of the sections to establish the ground truth. For this purpose a comprehensive Computational Fluid

Dynamic (CFD) model was used. A highly advanced model of single cylinder positive displacement pump was developed by A.Iannetti [95] in order to study cavitation and related phenomena. This model was fully validated against experimental data and will be used as a benchmark model.

Using fundamental numerical modelling and not the CFD is justified for three reasons; first of all the numerical model is efficient by being able to provide the analyst with reliable data, secondly, the fundamental numerical tool is also effective as it focuses on a critical part of the system and finally, it is cheap in terms of computational time and software licence.

The specific objectives for the computational model are:

- To create a computational model of a single cylinder PD pump driven by a rotary drive,
- Quantify the effects of varying the drive speed across a range of input speed, section 4.1
- Validate the output against a CFD [82] simulation for specific operating conditions, 4.2
- Analyse benefits of the improved valve dynamics, section 4.3
- Quantify the power losses in different plunger arrangements, section 4.4.

3.3.2 Methodology for model validation

Field data will focus on pump performance on site during hydraulic fracturing. In the research technique, pressure, speed and pump vibration will all be analysed. Pump pressure is a direct input to the system as shown in sections 2.2.2 and 2.2.4. Speed measurement is used to calculate pump flow rate. These two values together are the basic requirements for estimating the power consumption. In addition, pump vibration will be monitored through the use of accelerometers allocated to the specific sections of the pump. All the sensor data obtained during routine hydraulic fracturing operations will be subsequently post processed and analysed.

Laboratory tests will use a geometrically scaled replica of a genuine frac-truck assembly. Model will contain all the essential elements, such as power generator, speed

Computational model in Validation						
	Inlet pressure	Chamber pressure simplex	Chamber pressure triplex	Discharge pressure	Flow rate chamber	Flow rate total
CFD model		•			•	
Flowmaster model			•			
Field data	•			•		
Test rig data	•		•	•		•

Figure 3.4: Methodology for validating computational model using CFD model, Flowmaster[®] model, Field data and Test rig data.

variator and positive displacement pump as seen in full size applications. The pump will be instrumented with multiple pressure sensors, flow rate meter and speed sensor on the input driveshaft. Modularity and operation at different speeds and pressures are to be achieved from the system.

Not all necessary validation data can be derived from the experimental tests. Other two computational models (CFD and Flowmaster) are also used in the validating phase in Chapter 7. Different operating output from a PD pump include Inlet pressure, Chamber pressure (simplex and triplex), Discharge pressure and Flow rate (chamber and total).

3.3.3 Methodology for pump and system optimisation

To evaluate design space in PD pumps a Monte Carlo method is used for analysis of individual parameter data sets. In the first step Latin Hypercube Sampling is used to generate random samples of values in the interval [0,1] for each optimisation parameter. Such samples are then scaled accordingly in order to reflect realistic and physically meaningful parameter ranges, and model simulations are carried out for every randomly generated combination of parameters.

In the second step the desired model outputs characterising the PD pump, such as rod load, flow rate and power, are analysed. Simulations producing outputs which do not comply with the necessary performances are discarded.

Subsequently, the possibility for each of the retained model simulation to represent an optimum is assessed with the chosen criteria (for example pressure, flow rate and power).

Chapter 4

The Computational Model

In order to investigate the interaction of design parameters in a PD pump a computational model has been developed using the MATLAB and Simulink environments shown in Figure 4.4. Although many automotive and hydraulic examples have been reported in the literature [96], [97], [98] the author has found no investigation of reciprocating pump performance coupled with a hydrodynamic transmission. The formulation of the model combines analytical equations, lookup tables drawn from text books, manufacturers' product literature and the results of CFD simulations. The model was developed by progressively expanding the range of phenomena it incorporated. The following sections detail the key elements of the model as follows:

- Drive train modelling of a frac-truck assembly,
- Single cylinder model of a PD pump,
- Valve dynamics model in a PD pump,
- Multi-cylinder model of a PD pump.

4.1 Drive train modelling

The pump performance is strongly affected by the actual conditions in which the pump is operating. Different viscosity, different piston speed and output pressure all have a significant influence on the pump. P.J. Singh has published several papers [99],[100], [62] that discuss the performance of multi-cylinder pumps, most important of which is

the computational model designed to detect physical phenomenon that are present in the pumping cycle. The results illustrate how individual factors can be combined into a single model to represent a real pumping system with sufficient fidelity. Singh's work considers pump systems operating at a fixed speed [99], without investigating variable speed drive and its effect on improved pump operation. John E. Miller also presents a detailed analysis of individual PD pump performance [101]. His model considers suction conditions, valve dynamics and pulsation, effects of which can fundamentally change the pump's operation. However, he does not consider any speed fluctuations that are present during a pumping cycle or the possibility of using alternative methods for plunger actuation.

Issues with the rotary power transfer to the pump via the driveshaft have been previously acknowledged [102] to induce vibration and oscillation of mechanical components. This in turn greatly diminishes fatigue life of rotary components within a PD pump's power end. One way to summarise different loading conditions is to examine Figure 4.1 where typical PD pump mass flow rate output shows energy fluctuation during the pumping stroke. Fluid compression inside the cylinder is transferred to the crankshaft mechanism which is directly coupled to the transmission block of the frac-truck. Higher amplitude of a pulse wave will trigger higher torque demand and induce cyclic action in the pump operation. In turn, this phenomenon will affect the drive train with different speed/torque requirements.

The complete drive train model will primarily enable the investigation of the precise nature of the effect of internal fluid end dynamics on the drive train assembly. The model will, therefore, have to discretize individual components in the drive train which will enable modularity and increased flexibility in further development. Since previous sections 2.4.1 and 2.4.2 have identified specific component manufacturers all the available specification data can be embedded inside the computational model.

4.1.1 Drive train overview

The drive train used to power the fluid-end can be described as follows:

Engine: The engine size depends on the pump's power requirement. Losses in the power train and transmissions for powering auxiliary equipment must also be accounted for.

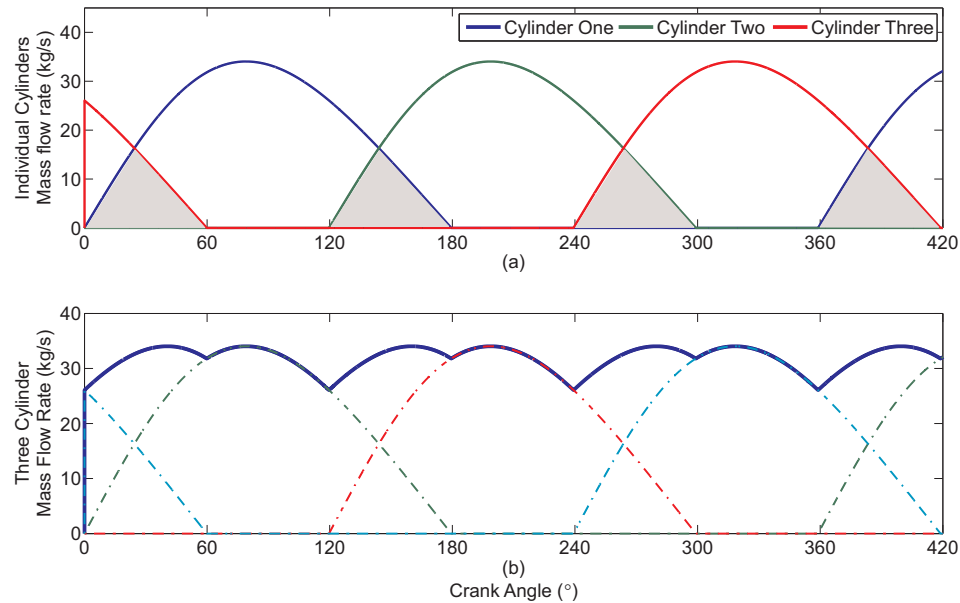


Figure 4.1: Mass flow rate from positive displacement pump. (a) individual cylinders offset by 120°. (b) integral mass flow from the entire pump. The dotted lines represent all the areas of mutual interaction amongst cylinders.

For example, engine cooling units are frequently powered by the same source as the pump itself and physically they can be as big as the actual engine which is clearly illustrated in Figure 2.19. The pump can operate in a variety of conditions, hot and cold climates and different altitudes, so in order to utilise maximum engine performance in real applications these factors should not be neglected. However, the computational model is using data provided by component manufacturers and assumes nominal environmental conditions. Field data will be used later to quantify the difference.

Transmission: The angular velocity of the engines drive shaft is too high for the pump operation. Speed reduction is needed therefore to create the high-torque low-speed input needed by the PD pumps.

Torque Converter - is a hydro coupling device that is used to multiply torque from the prime mover, in this case diesel engine. As previously explained in section 2.4.2 it is used to transmit power from the internal combustion engine to the gearbox and ultimately to the PD pump.

Gearbox - this unit handles power from the torque converter and delivers it to the next unit in the drive train, in this case the PD pump. Depending on the operating

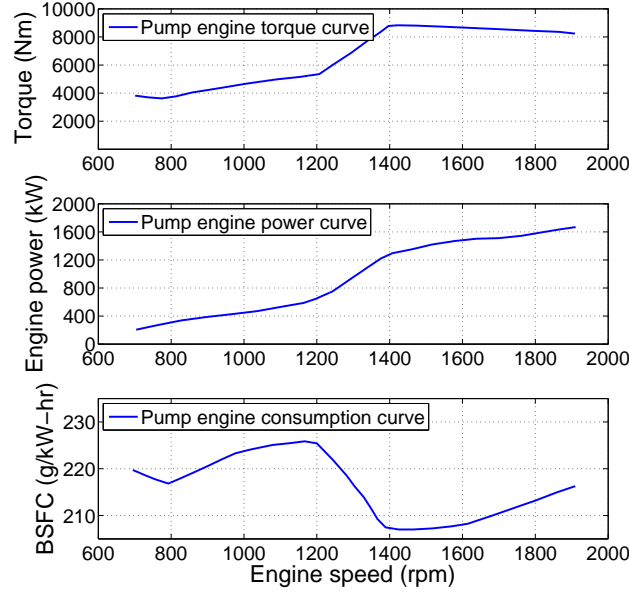


Figure 4.2: Extracted engine’s operational data [67]. Top: Torque curve at different operating speeds, Center: Engine’s power graph, Bottom: Engine’s brake specific fuel consumption

conditions the most appropriate gear ratio will be selected. Having more speeds allows operators to vary the flow intensity of the pump to meet specific well requirements. With the initiation of the pumping cycle the gearbox will start building from lower to higher gear regimes [, Chapter 9]shigley1988.

4.1.2 Drive train theory

Engine speed output is calculated using equation 4.1. The engine’s torque value (T_e) is read from the manufacturer’s lookup table, illustrated in Figure 4.2 and the variables I_e and T_i represent the engine’s inertia and the torque convertor’s impeller torque respectively.

$$\dot{N}_e = \frac{T_e - T_i}{I_e} \quad (4.1)$$

The engine is assumed to operate at a maximum power output. Therefore, throttle input is modelled as a step signal with “fully opened” as a final steady state value.

A brief recap on power transmission from the source (engine) to the PD pump.

Power is absorbed in the impeller and fluid inside the torque converter is accelerated from a relatively low velocity present near the centre to a high velocity that is at the outer diameter. The power capacity is proportional to the impeller's speed and outer diameter. Work done by the engine in accelerating fluid from low to high velocity is turned to kinetic energy. Kinetic energy is given up to a turbine in which fluid loses its speed while being guided back towards the centre of the chamber. From the turbine it enters a stator that changes its direction via the return flow between the turbine and the impeller. This direction change increases the momentum of the fluid, thereby increasing the torque capacity. From the stationary reaction chamber, it enters the impeller in a continuous process. Power from the engine is transferred to the PD pump via a torque converter and a gearbox. While the gearbox establishes mechanical the torque converter will create the flexible hydrodynamic coupling. Fluid flowing through impeller and turbine circuits inside the torque converter regulates the speed and the torque characteristics from the engine [69].

$$T_i = \left(\frac{N_e}{K} \right)^2 \quad (4.2)$$

Equation 4.2 calculates the impeller's torque (T_i) inside the torque converter unit by computing engine speed (N_e) and K factor.

$$K = \frac{N_g}{N_e} \quad (4.3)$$

Where the K factor is the ratio between the speed of the torque converter's turbine circuit (N_g) and the speed of the engine (N_e). Equation (4.3) and the K factor was obtained directly from OEM [71]. Note that speed from the torque converter's turbine circuit is equal to the gearbox's output speed. The simulink model uses a lookup table to link input speeds and output torque values.

To estimate torque and speed values from the gearbox (T_g, N_g), a gear ratio, as shown in Table 2.22, is introduced for each gear pair. Specified ratio directly modifies the torque from turbine and pump speed (T_t, N_p) using equations (4.4) and (4.5),

respectively.

$$T_g = R_g \cdot T_t \quad (4.4)$$

$$N_g = \frac{N_p}{R_g} \quad (4.5)$$

Torque value obtained from the transmission block is used to calculate the pump's speed in the same manner as in the engine block. But in addition, the pumps final drive (R_{fd}) and pump load (T_p) need to be accounted for. The final drive was identified in OEM specification sheets and it is given in Table 2.24. The pump load is derived from specific pressure conditions inside the well. Equation 4.6 describes this relation.

$$\dot{N}_p = R_{fd} \cdot (T_g - T_p) \quad (4.6)$$

Unlike the relatively smooth, continuous flow of the fluid through a centrifugal pump, the fluid flow through a piston pump occurs in a transitory dynamic manner referred to as the pumping cycle. The event that initiates this cycle is the linear movement of the piston. In the power end section of the pump the rotational speed of the input is converted into a linear movement of the piston. This movement can be modelled using equations 4.7-4.9 which includes the rod length of the crank shaft (L) and the crank radius (R). This enables the speed and acceleration of the piston to be calculated as follows:

Equation (4.7) relates piston displacement to crank angle during the suction and discharge stroke.

$$d_{pl} = R \cdot \cos(\omega t) + \sqrt{(L^2 - R^2 \cdot \sin^2(\omega t))} \quad (4.7)$$

Piston velocity is calculated using the piston position by equation (4.8).

$$v_{pl} = -R \cdot \sin(\omega t) - \frac{R^2 \sin(\omega t) \cos(\omega t)}{\sqrt{L^2 - R^2 \sin^2(\omega t)}} \quad (4.8)$$

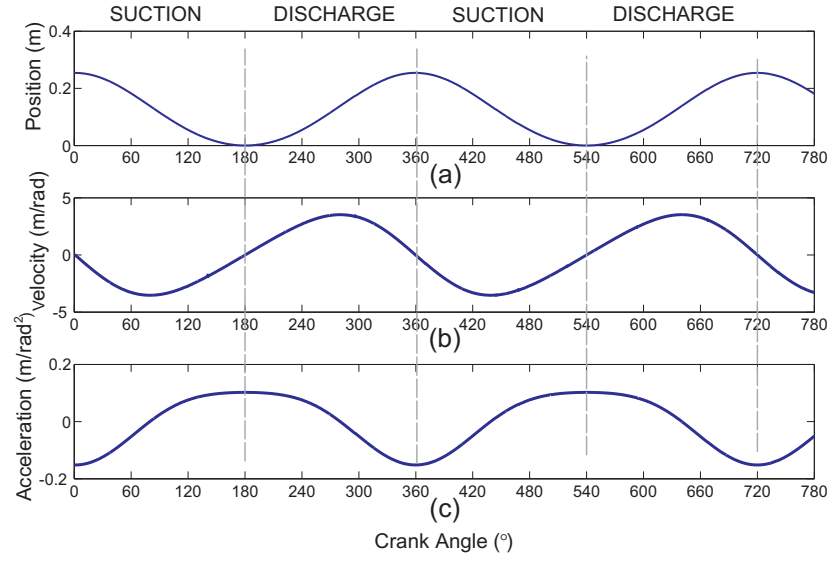


Figure 4.3: Suction and discharge pumping states are shown in the plunger motion plot. (a) plunger displacement is also referred to as plunger stroke (b) plunger velocity. (c) plunger acceleration.

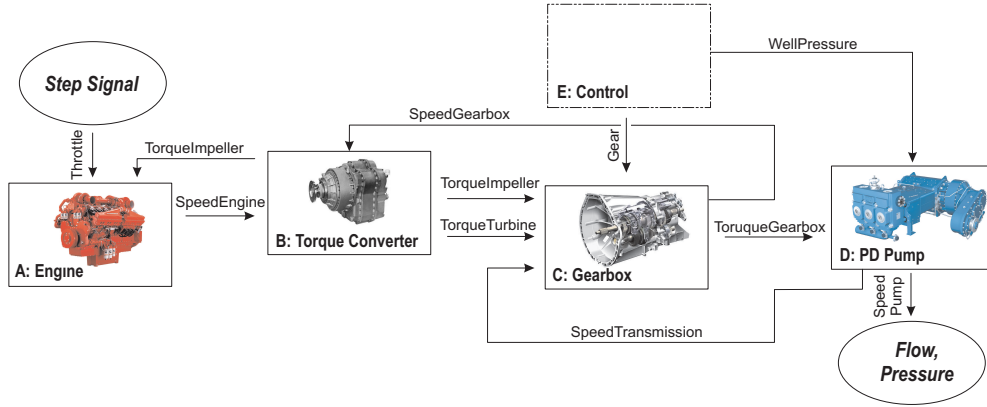


Figure 4.4: Hydrodynamic transmission in MatLab powering PD pump operation

$$a_{pl} = -R \cdot \cos(\omega t) - \frac{R^2 \cdot (\cos^2(\omega t) - \sin^2(\omega t))}{\sqrt{L^2 - R^2 \sin^2(\omega t)}} - \frac{R^4 \cdot \sin^2(\omega t) \cos^2(\omega t)}{(\sqrt{L^2 - R^2 \sin^2(\omega t)})^3} \quad (4.9)$$

Two pumping cycles of kinematic plunger motion are plotted in Figure 4.3

4.2 Single cylinder model

Figure 4.4 provides a schematic overview of the model.

A: Engine: The engine block uses a 2-D lookup table that is accessed via a throttle

state to return appropriate values from a torque/speed performance curve. `Throttle` step signal is the first input in the engine block, the second being the feedback signal from the `TorqueImpeller`. Once the speed is determined the result goes through a limited integrator and outputs engine speed (i.e. `SpeedEngine`).

B: Torque Converter: This block uses two 1-D lookup tables to compute both `TorqueTurbine` and `TorqueImpeller` values. Gearbox speed (i.e. `SpeedGearbox`) is fed back as an input and together with engine speed from Block A computes torque values.

C: Gearbox: This unit has four inputs. The first two are the output torque values from Block B (i.e. `TorqueImpeller` and `TorqueTurbine`). Transmission speed (i.e. `SpeedTransmission`) is being fed back as a third input parameter. Block C has single 1-D lookup table that is connected to Block E.

D: Pump: Torque value from the Block C (i.e. `TorqueGearbox`) is regulated with final drive ratio that is incorporated inside the power end of the pump. Subsequently, the torque value from piston loading is subtracted from Block C's torque. In this way the model takes into account dynamic loading that is present during a pump cycle. Lastly, torque is integrated to compute the pump's speed (i.e. `SpeedPump`).

E: Control: Finally, a `Gear` is assigned from the control unit (Block E). Changes in Block E output the gear and this information is sent to Block C. Because the pump is operating at a predefined well pressure dynamic load will be assigned from an external source. Block E, provides input pressure data (`WellPressure`) to the PD pump, Block D.

4.2.1 Validation

After the implementation stage the MatLab model was validated against a CFD simulation, previously published by [82] for a single stroke using the same boundary condition such as input pressure, output pressure and speed. Iannetti (2014) details CFD model convergence and validation against experimental data. Speed was kept constant throughout the initial testing process.

A pressure comparison is displayed in Figure 4.5. Simulation runs from a 0° crank angle which is the piston's TDC (Top-Dead-Center) position. The red curve displays a

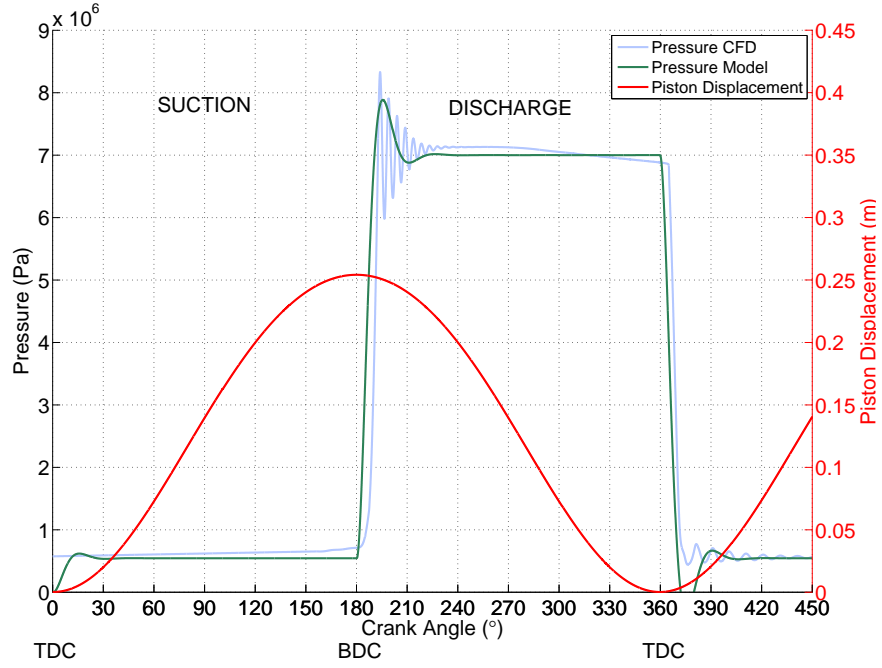


Figure 4.5: MatLab model pressure validation

piston movement with displacement values located on the right y-axis. BDC (Bottom-Dead-Center) is reached at 180° crank angle and the pump is doing a compression stroke until the next TDC. The other two curves represent the pressure inside the chamber. Due to the dynamic behaviour of the spring regulated control valves the CFD plot displays highly oscillatory movement around BDC. The MatLab model idealizes this by displaying only the fundamental operating parameters such as frequency (i.e. speed), minimum, maximum pressure values, peak overshoot and settling time.

The flow rate comparison graph is shown in Figure 4.6 where the simulation cycle starts from TDC, it reaches BDC at 180° crank angle and goes back to TDC at 360° crank angle. This graph compares two flow rate curves. One was obtained from CFD analysis whereas the other is derived from analytical equation (4.10).

$$\dot{m} = \rho \cdot \dot{V} = \rho \cdot v \cdot A_{pl} \quad (4.10)$$

Flow rate curves, illustrated in Figure 4.6, correlate well with the exception of the initial delay (because CFD takes into account fluid compressibility that induces delay

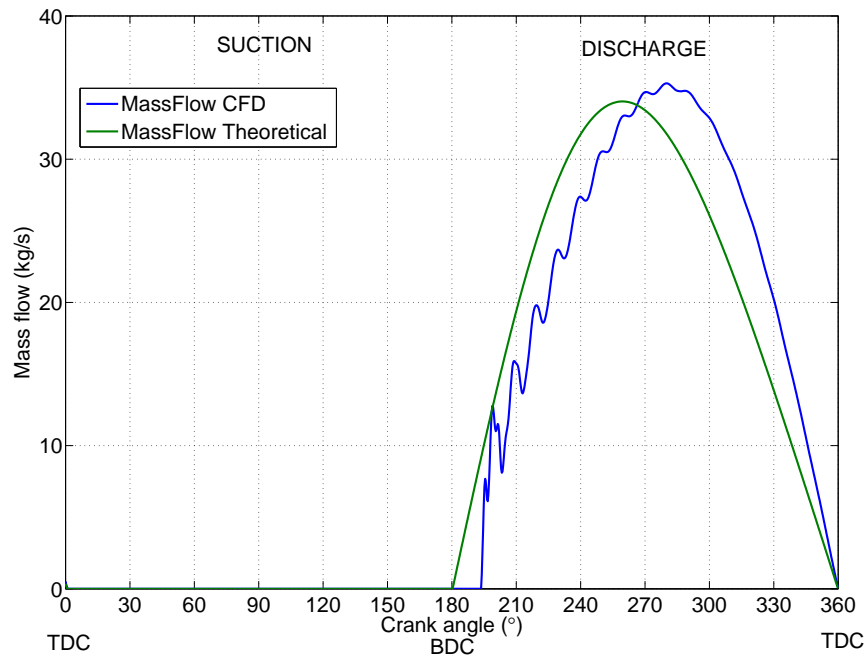


Figure 4.6: MatLab model flow validation

in the valve opening). Consequently, the CFD curve is offset from the theoretical one. In the context of this research it is important that the start, the end and the integral value of the outflow are all sufficiently accurate approximations.

4.2.2 Results produced by the single cylinder model

The single cylinder model was validated by modelling changes in the output of a PD pump's pumping cycle resulting from variable speed input. Taking into account these transitional changes allows engineering insights into the flow characteristics in-between the steady state values.

This model enables the investigation of the loading associated with the pressure variations in a PD pump. It is essential to consider how changes in a PD pump's discharge pressure affect loading on the crank shaft mechanism. Figure 4.7 displays dynamic speed response, triggered by gear change.

Since the piston loading is a cyclical function it is clear that speed does not reach a steady state even when a pump is running at a single speed (i.e. no gear changes). This slight speed variation indicates that a pump will not run at a constant speed. Figure 4.8 displays comparison figures between two different representations of the

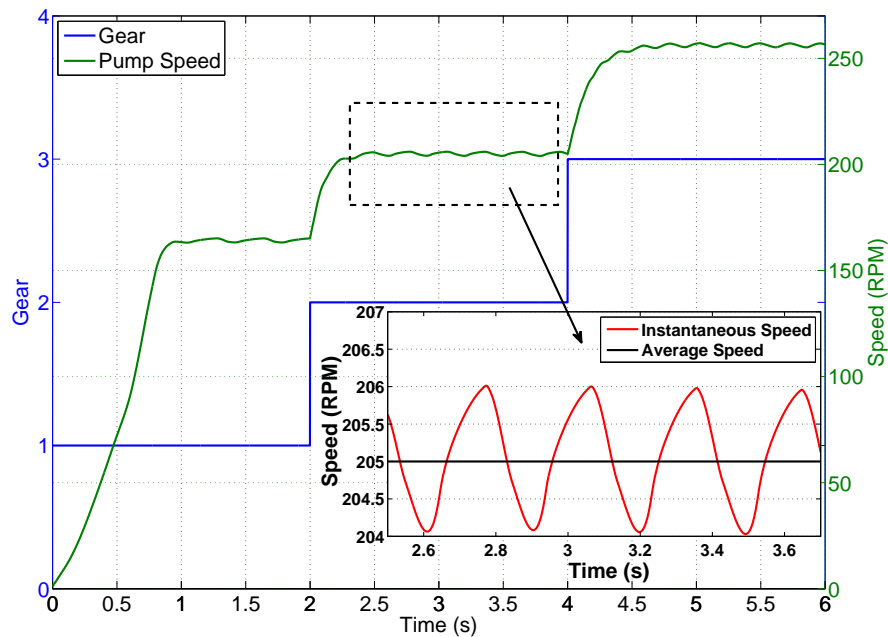


Figure 4.7: Pump Speed Inputs

pump's responses. The case study examines the mass flow rates resulting from the instantaneous speed and the constant average speed.

Figure 4.8 shows how the fluctuations in speed impact the fluid flow pattern. This assessment was conducted using second gear where speed values fluctuate from 204-206 RPM (Figure 4.7). When using an average value of 205 as a representative speed the upper part of Figure 4.8 shows the flow rates associated with two speeds, the average and the instantaneous one. The lower section of Figure 4.8 shows the mass flow rate profile for one stroke.

4.2.3 Discussion of a single cylinder model

From the results presented it can be concluded that speed fluctuation has a measurable effect on flow rate pattern. Consequently, capturing this realistic behaviour is essential for modelling pump performance. The essential parameter is taking into account the piston loading that is present in each stroke which effectively causes the pump to work at variable speeds so the piston speed is constantly accelerating and decelerating. This is creating added oscillatory phenomena and impacts the fatigue life of the mechanism. As a result, the mass flow rate of the pump is not consistent in each stroke. Moreover,

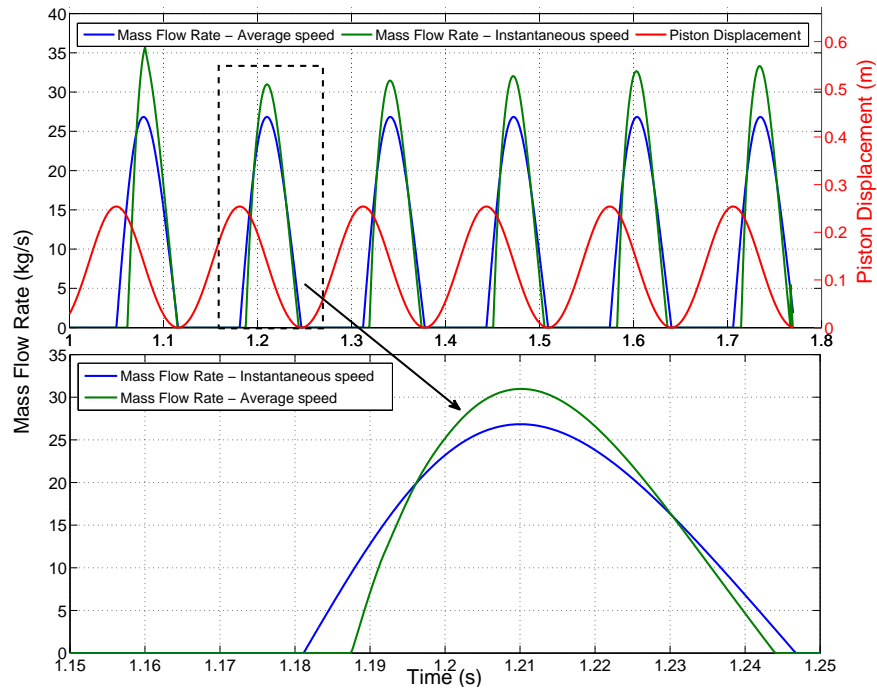


Figure 4.8: Results: Flow Rates at different rotational speed

the mass flow fluctuates with an accentuated high end curve profile. It also shows a distinct initialization delay from the theoretical estimation. Furthermore, it is apparent that in realistic conditions irregular flow is exhibited in shorter time segments.

Presented results are more accentuated in a simplex (one cylinder) pump. In multiple cylinder pumps, such as triplex, outputting to a common manifold may dampen this effect. The aim of this research was to realistically model conditions that are present in the actual systems and in the next phase this research will include additional cylinders and assess the effect of cylinder interaction during pumping.

4.3 Valve dynamics model

Current designs are dominated by mechanical systems (i.e. spring valves, crankshaft and con-rods) whose dynamic behaviour is fixed. Consequently, there are limits to what can be established experimentally either in the field or laboratory. Given this context author presents a computational model that combines relationships established by analytical (MatLab) and CFD analysis. The resulting model allows the impact of changes to the pump's control and design to be quickly investigated.

Although positive displacement pumps undoubtedly have many advantages they also have several engineering challenges associated with valve performance.

The fluid used in hydraulic fracturing applications is a complex medium that often has non-Newtonian fluid properties. Because the fracturing operation involves systematic adjustment of fluid suction, inlet condition will be affected by fluid alteration. A number of studies indicated the negative effects of insufficient suction pressure [99], [82] predominately manifested in forms of cavitation and extended unbalanced operation.

Inlet condition can also be affected by the fluid interaction within the pumping system. Operators in the field choose to operate pumps at different speeds to prevent cavitation. Common practice will see pumps operating closer to the blender, Figure 2.12, at higher angular velocity. This practice aims to minimize the negative effect of low suction pressure for pumps distanced from the blender that operate at lower pumping rates [49]. The inlet pressure condition is also affected inside a single PD pump. Pressure drop in the suction pipe can lead to cylinder “starvation” that induces cavitation. This can be controlled and suppressed by an accurate design of PD pump’s suction manifold [103].

Valve actuation in current designs is regulated entirely by the pressure change inside the cavity of the pumping chamber. This creates difficulties because changes in the fluid properties (i.e. density, bulk modulus) and operating conditions (flow rate and pressure) dictate valve opening and closing. Inlet and exhaust valves in the internal combustion engines have similar, “poppet valve”, construction as in positive displacement pumps. In contrast, the actuation of the inlet and exhaust valves, originally controlled via a camshaft movement [104], has in recent years had its efficiency boosted by mechatronic engine management systems (an example of which is discussed in other academic work [105]). However, these developments have not been implemented in positive displacement pump design.

4.3.1 Aims and objectives of the valve model

This study aims to study valve actuation in a PD pump by firstly analysing current systems and developing a model progression from basic to advanced.

Test cases will initially be conducted using instantaneous valve opening with actu-

ation timing predefined by a crankshaft angle. Pump outputs, such as pressure and mass flow rate, will be analysed and compared to the CFD validation test case done by A.Iannetti [95].

Subsequent model advancements will look into the force balance acting on the valve inside the fluid chamber. The pumping cycle will again be re-evaluated to assess changes in the performance output.

4.3.2 Valve system overview

In the current analysis, it is assumed that a constant drive speed is maintained with the torque stable and sufficient to drive the pump. Previous research shows that in reality speed of the drivetrain tends to oscillate around steady state value [79]. Rotational motion of the drive shaft power is transferred to a crankshaft mechanism that drives the pump's plunger. The full plunger cycle consists of two movements; firstly a plunger retraction stroke begins when the plunger moves from TDC to BDC and fluid gets sucked into the main pressure chamber; secondly when the plunger moves from BDC to TDC in compression stroke and fluid is pressurised inside the chamber before being delivered to the discharge side of the pump.

The cyclic pressure change in the chamber creates the primary force that dictates the valve motion. Other factors such as the retaining spring, valve geometry and valve mass also play an important role. However, the variations in force resulting from these factors are relatively small. Throughout the pumping cycle force generated by the pressure field due to the plunger motion is two orders of magnitude higher than the combined forces from the spring preload, spring stiffness and the valve inertia. Only during the transition states (valve opening or valve closing) do they have a significant effect on the system dynamics.

4.3.3 Valve computational modelling and model validation

The numerical model was established and validated using previous CFD analysis and experimental testing of the PD pump [106].

The experimental rig consists of a single chamber PD pump operating in a closed fluid loop. Main components of the system, in addition to the positive displacement

pump, are linear motor (generator), water tank and accompanying set of choke valves used to pressurise the system and regulate fluid circulation. A number of pressure sensors are in place to monitor the pump operation predominately focusing on the suction side of the pump. The flow rate is measured using the venturi effect and speed is assigned directly at the linear motor.

The valve model must incorporate following elements:

Piston kinematics

The conversion of rotational speed to linear motion is modelled using the kinematic equations of motion shown in equations 4.7 to 4.9.

Flow dynamics

The flow rate delivered during the compression stroke is given in equation 4.10 where the theoretical mass flow rate from a single chamber pump is calculated using fluid density ρ . The velocity of the plunger v_{pl} is obtained from the kinematic equation of motion and the cross-sectional area of the plunger is given as A_{pl} . Fluid density may vary in pumping cycle, however, for the purposes of this research a simplified version with constant density is applied.

Pressure dynamics

The exact measurement of the pressure inside a single chamber is more complex to model and validate. Experimental results available to the author [53] only record pressure from the common discharge line of the pump (i.e. the combined output of all three chambers together). Consequently, any model of the pressure variation within individual chambers could only be benchmarked against computational studies. Two earlier studies were used to create an analytical model of pressure change within a chamber; one using a high fidelity 3D CFD model [82] and the second one using a lumped parameter representation in a 1D fluid simulation system. Based on these the pressure field inside a single chamber was modelled by following equation 4.11.

$$\frac{dP}{dt} = -A_p \cdot \frac{dx}{dt} \cdot B \quad (4.11)$$

In the non-cavitating condition pressure is calculated based on displaced volume in the chamber and the bulk modulus of the fluid. Because pressure is dependent on the flow through the valve it will vary depending on the valve position. In Figure 4.5 pressure variation is compared to an established CFD model. The advantages of this lumped parameter model are reduction of computational time and the capability to couple this model to the drivetrain mechanics module, section 4.1, used to power the pump.

The benefit of using equation 4.11 (rather than the original CFD simulation) is that computational time is reduced without jeopardizing the accuracy of the model. Although the author recognises that specialized 1D fluid simulation software may give more flexibility of the model it is also important to integrate the response function with a model which is capable of simulating both fluid dynamics as well as drive train mechanics. The internally developed model can be translated and read in different computational languages.

Valve dynamics

Figure 4.9 displays the timing of the valve opening in the PD pump and its importance for subsequent analysis. Starting with the suction valve, shown in red in the circular chart on the right hand side of Figure 4.9, the plunger starts the retraction from TDC and the suction valve opens at approximately 15° of crank rotation. Meanwhile, the discharge valve is closed until the plunger has finally travelled past the BDC. Shortly after progressing past the BDC point, approximately 185° , suction valve is shut. The section where both valves are closed is variable and dependent on the pump's operating condition and fluid compressibility. The discharge valve finally opens and fluid is passing through to the outlet. The cycle is then reestablished and repeats for every crank rotation.

Illustration on the left-hand side of Figure 4.9 shows the plunger displacement in red (i.e. TDC to BDC travel) for two pumping cycles. The valve opening is instantaneous and coefficient variance between zero to one is designed to characterise the fully closed and fully opened position.

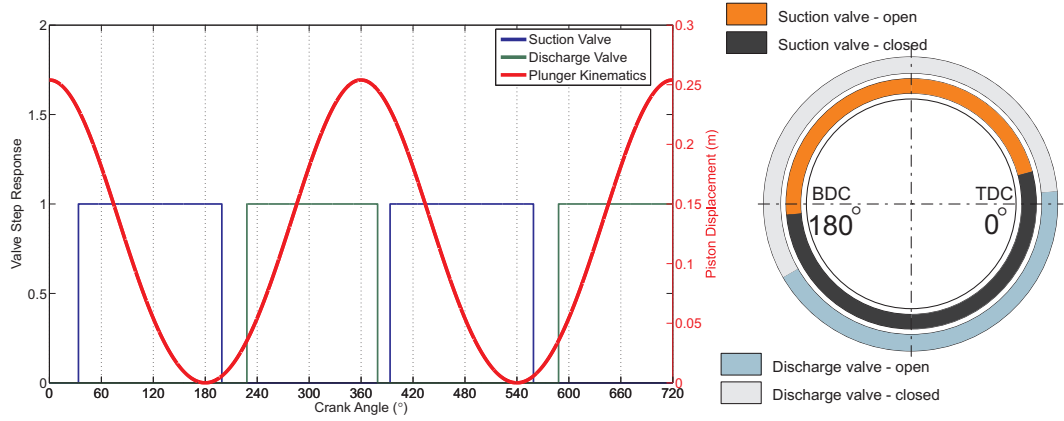


Figure 4.9: Suction and discharge valve actuation and timing

Valve opening during suction and discharge stroke are important parameters that determine the pump performance. Figure 4.9 shows instantaneous valve response assumption that results in a model which has insufficient accuracy. Adaptation of the valve dynamics will result in a more realistic fluid delivery model which can support such analysis.

Accurate valve behaviour can be obtained using principle equations of force balance [107]. Both suction and discharge valves are modelled as “poppet valves” that are entirely pressure regulated where the valve geometry provides most of the required data. Hydrodynamic forces acting on the valve are calculated using the pressure distribution on both top and bottom surfaces of the valve. Using the equations 4.12 - 4.13, valve motion is calculated based on the operating condition of the pump.

$$m \frac{d^2 h}{dt^2} = F_p - F_s \quad (4.12)$$

$$F_s = k \cdot (h_0 + h) \quad (4.13)$$

Figure 4.10 shows three characteristic cases for the suction valve dynamics. In the case where the valve is fully open pressure on the suction side is greater than the

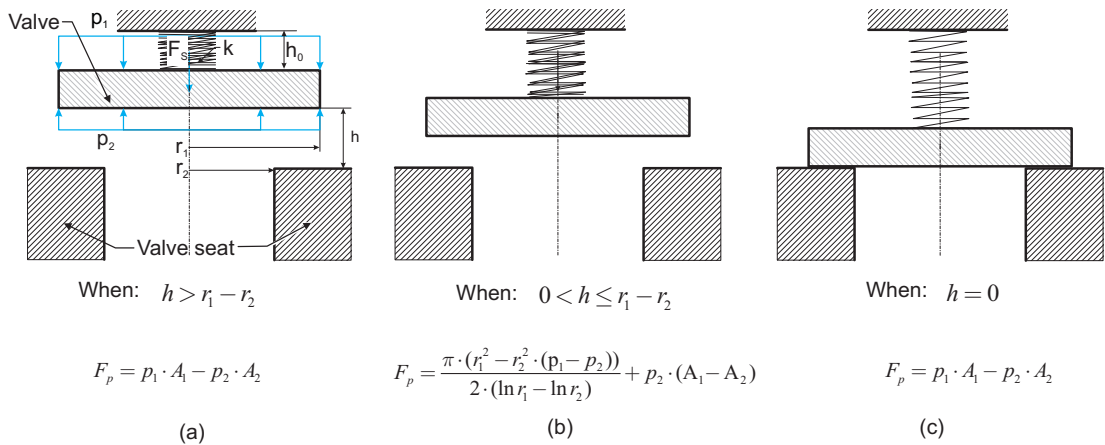


Figure 4.10: Three operating states of the valve; (a) fully open, (b) partially open, (c) closed

pressure inside the main chamber. When the valve is fully open fluid passes without obstruction. In case two when opening is $0 < h < r_1 - r_2$ the valve is in the transitional state between closed and fully open. In case three the pressure at the top of the valve is greater than the pressure field located on the suction side. This means that the pressure inside the chamber is higher than the pressure in suction manifold and therefore the valve will remain closed.

4.3.4 Results of valve model

Flow rate through the re-modelled “poppet” valve was computed and results can be seen in Figure 4.11. It is clear that valve modelling using the hydrodynamic effect resulted in a closer correlation to the outcomes of experimental testing.

Pressure from a single chamber through the re-modelled discharge valve is shown in Figure 4.12. Using the dynamics of the valve to calculate pressure during the discharge stroke produces results which show good agreement with the previously introduced benchmark model. The gradual decline of the pressure from $180^\circ - 360^\circ$ of crank angle demonstrates the system’s consistency with the CFD results.

4.3.5 Discussion of valve model

The potential benefits of valve control in a positive displacement pump are numerous. Currently, sudden pressure drops or pressure spikes in the suction and discharge line, cause unpredictable pump behaviour. In such cases, control of the exact timing of the

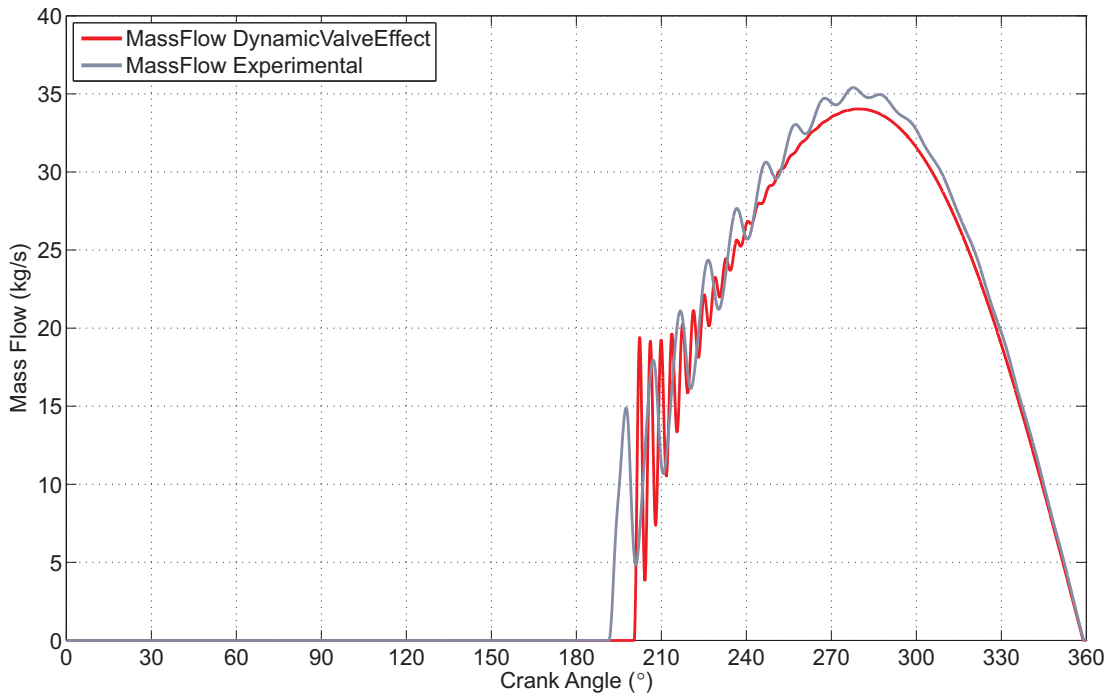


Figure 4.11: Mass flow rate during discharge stroke was modelled by using dynamic effect of the valve response

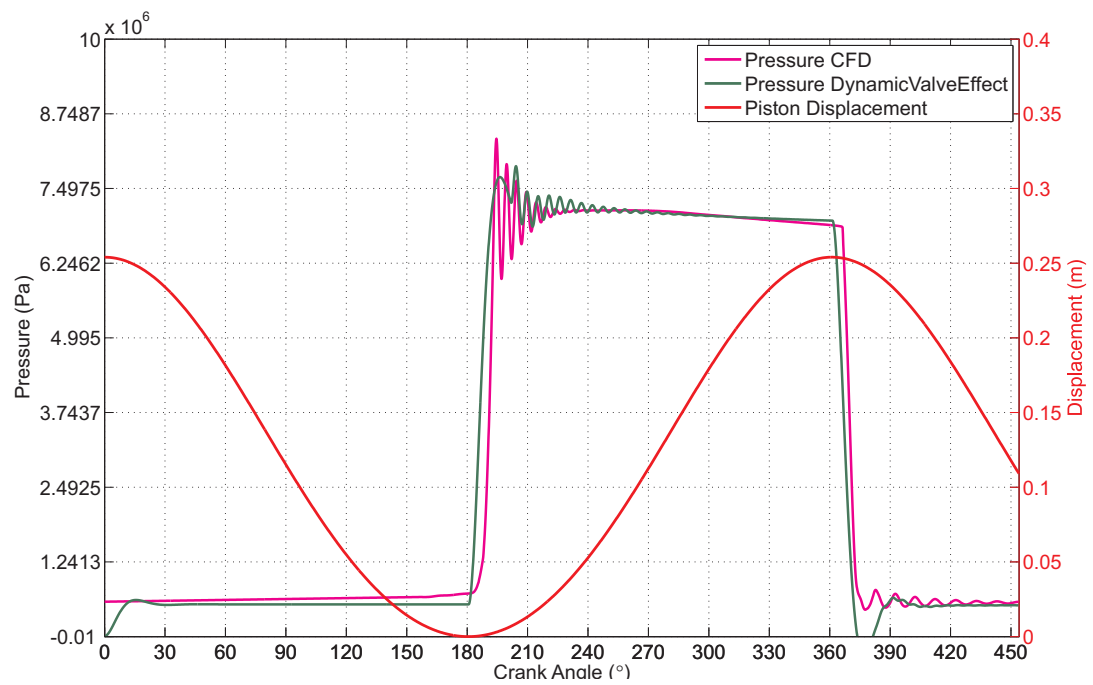


Figure 4.12: Pressure during discharge stroke using remodelled valve dynamics

valves opening and closing could greatly reduce the unwanted effect. Specifically, direct control of the valves could improve pump performance by:

1. Regulating the suction phase of the stroke in cases when the pressure in the inlet line is insufficient.
2. Enforcing early or late opening of the discharge valve depending on the operating condition (i.e. bulk modulus of the fluid).
3. Synchronization of the valves for individual chambers to dampen the accentuated pressure form.

The results suggest that modelling approaches used in this section can produce satisfactory results for studying the impact of design modification on the performance of multi-cylinder pumps. It can be seen that all the major elements, such as plunger kinematics, valve actuation and valve dynamics, that comprise a single pumping system can be represented effectively in a single computational model. All of the pump's output parameters can, therefore, be simulated and investigated. The model's credibility has been validated using an additional analytical model and the established experimental data sets.

This study concludes with the current state of the model that has been developed to describe the physical behaviour of the pump. By taking into account the precise timing of valve actuation the model can be used as a first step in the development of a control system for a positive displacement pump.

In the hydraulic fracturing applications PD pumps encounter a variety of dynamic changes in the system. One of the most common phenomena is sudden pressure change (e.g. a step change increase or decrease) when an impermeable barrier is encountered or when fracture occurs. Simulation in this computational model considers inlet and outlet pressures to be constant values. By doing so the simulation focuses on the dynamic behaviour inside the pump. Scope for future studies will be to model more complex hydraulic systems of PD pumps.

In conclusion, the quality of the results obtained present a solid foundation for the continual development of a closed loop, mechatronic control system for PD pumps.

4.4 Multi-cylinder model

Comprehensive development of a PD pump model needs to consider the common configuration of their cylinders in industrial systems. More cylinders are frequently operating in sequence to produce sufficient flow rate output. This analysis considers triplex (three cylinders) and simplex pumps.

The main engineering challenges will be presented in the following section together with proposed solutions. Final evaluation of PD pump performance will be considered by examining results of power consumption.

In the real pumping systems, where multiple pumps are operating on site, the dynamic of pressure pulse is complex and unpredictable. Pumps often operate at different speeds and thereby different flow rates enabling fluid flux from one unit to impede the flow from the unit operating at slower speed. Pressure fluctuation can initiate constructive interference in the form of superposition of pressure waves.

Computational fluid dynamics is designed to deal with highly complex geometries. The increase in physical size and introduction of more moving elements (motion from individual plungers) increases computational power and therefore computational time. Computation of single cylinder models can take up to several weeks which indicates that several pumps on site could possibly take months to solve. However, complex fluid structures can encounter systematic error in the calculation process and fail which presents a challenge for elaborate models.

The problem of finding the required computational power can be overcome by using High-Performance Computing (HPC) systems. However, the overall time requirements cannot be easily and sufficiently lowered as the time steps needs to be small enough to achieve the requisite of low Courant number and therefore computational stability.

Simplified analytic methods such as Johnston [108] and Edge [109], [110] were developed in times when the computational power available was scarce and gave no other option to the researcher. These methods consider compiling every element of a pumping system as a lumped parameter model where the information of its influence on the overall system is concentrated in a parametric function. For instance, the effect of a 90° elbow on the pipework is an empirical function of the pressure drop across the elbow against the mass flow rate. This method is usually referred to as 1D-CFD technique.

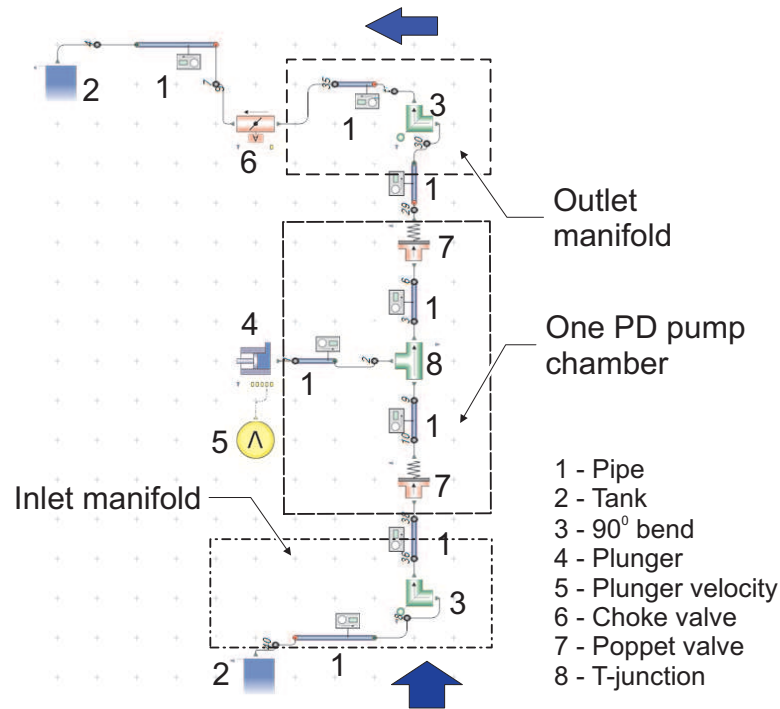


Figure 4.13: Single cylinder pump using lumped parameter model.

The mathematical model created results in a linear system where the only unknown is the static pressure in the network nodes (every node is placed between contiguous items of the network) and the mass flow rates in the pipework branches. This method, which requires low time (minutes) and power to solve, produces accurate results if the items included in the pipework are standard (e.g. elbows, orifices, junctions, straight pipes, etc.), however it loses accuracy in the presence of a non-standard item for which no empirical model is provided.

4.4.1 Modelling of a multi-cylinder PD pump

A commercial software package Flowmaster[®] was used to produce a 1D-CFD representation of a three-cylinder pump.

The Flowmaster model setup of a single cylinder pump is illustrated in Figure 4.13. The legend in Figure 4.13 details the functionality of all the elements in the model.

Water flows from the bottom tank through the pump chamber to the top tank, performing first the suction stroke and then the delivery stroke. During the suction stroke the chamber (dashed area) is filled as the plunger moves backwards and leaves

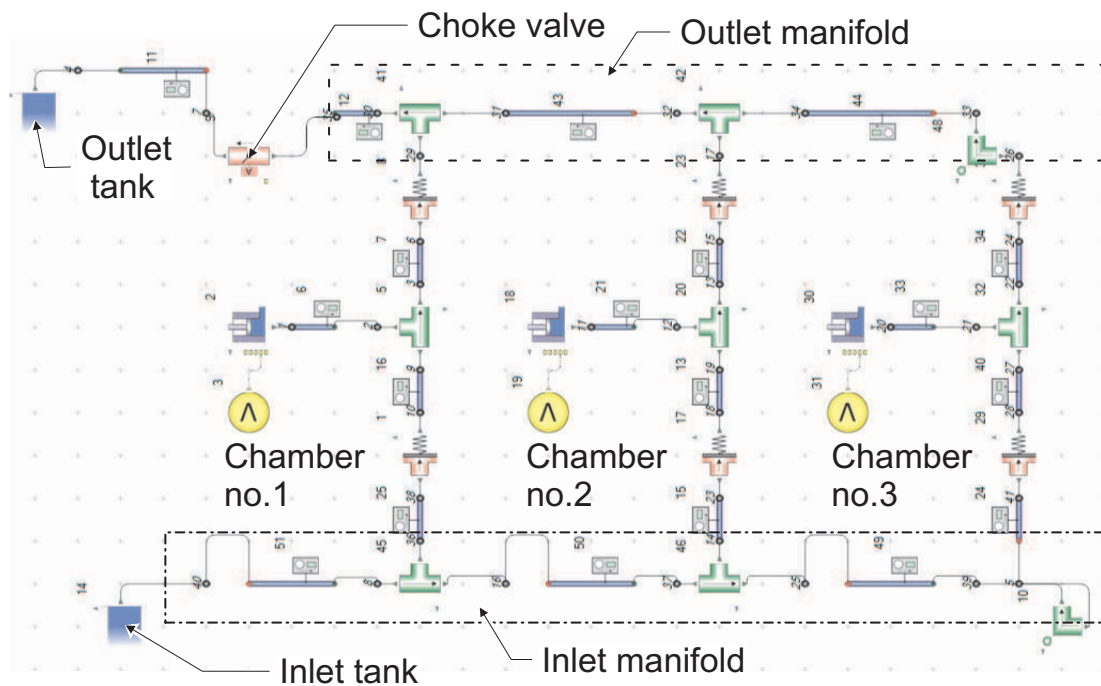


Figure 4.14: Triplex (three-cylinder) pump using lumped parameter model.

the displacement volume for the water to fill. The inlet and outlet valves are modelled as poppet valves for which the analyst has to specify the valve seat area, the valve disk area, the spring preload, spring rate and the valve loss coefficient factor as a function of the valve lift normalised with the max lift value.

The valve loss coefficient factor is essential to calculate the pressure drop across the valve against the valve lift. The estimation of the valve loss coefficient factor was carried out using 3D-CFD and [111]. The layout of the 1D system was decided in order to keep the model as close as possible to the physical apparatus which will be discussed later in the thesis, Chapter 6.

Before delivering to the outlet tank, a choke valve downstream of the outlet valve was utilised to increase the pressure. The choke valve opening was tuned in order to achieve the outlet pressure (measured in the node upstream the choke valve) of 200, 300 and 400 bar. Each of the pressures presents an individual test. The plunger velocity was imposed providing the code with the velocity-time function shown in Figure 4.3(b) generated using equation 4.8. The angular velocity was considered constant throughout the reference tests.

Evaluating the power consumption of one cylinder in a triplex experimental setup

was done using equation 4.14.

$$P_e = p_d \cdot A_{pl} \cdot v_{pl} \quad (4.14)$$

The three cylinder model shown in Figure 4.14 presents an extended version of the single-cylinder model where the suction and delivery pipe of the first, second and third chamber are connected to a singular suction and singular discharge manifold. Plungers two and three have a velocity offset of 240° and 120° respectively to match condition of the real device utilised in the experiments. In addition to the plunger velocity, the boundary condition for the inlet and outlet tank is set at a static pressure, the value of which was decided by the physical water level and the height of the base.

4.4.2 Results of a multi-cylinder PD pump model

In Figure 4.16 three of the performed reference tests are presented. The overall outlet pressure in the discharge manifold was evaluated during one pumping cycle (360°). The oscillation of the signal around the mean value is evidence of the interaction of the three chambers which takes place in the outlet manifold. One may assume that the simplified lumped parameter model accurately accounts the pressure frequencies but overestimates its amplitudes.

Amplified pressure oscillation is evident inside individual chambers, as shown in Figure 4.15. Each of the figures represents a different pressure history inside the cylinder number one. Test were performed at three reference pressures and data is displayed for one complete pumping cycle. When the outlet valve opens in chamber one the internal volume is subjected to the outlet manifold pressure where chamber two and three are delivering with a certain delay with respect to chamber one. As the overall rate of the water flowing through the discharge manifold is oscillating, following the plungers' velocities, the pressure resistance inside the manifold itself varies over time. This justifies the presence of the three bumps in the experimental and numerical pressure histories although in the former, their magnitude is significantly lower. The frequency and the distance between the three of them are established by the offset motion of the plunger two and three with respect to plunger one.

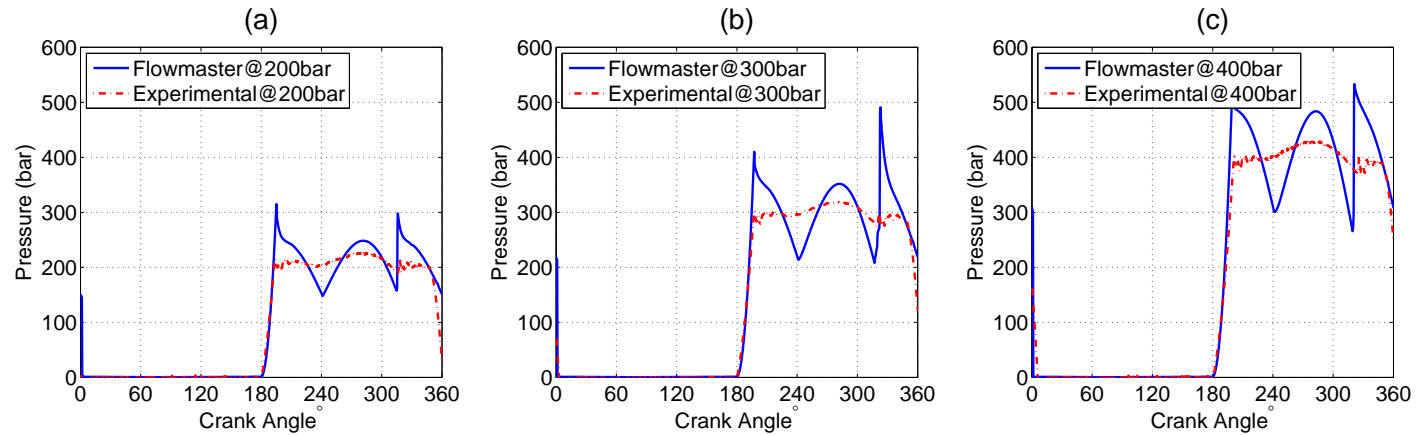


Figure 4.15: Chamber one pressure history was evaluated using lumped parameter model, shown in Figure 4.13 and experimental analysis for three test cases: 200 bar (a), 300 bar (b) and 400 bar (c). Tests were performed for a full pumping stroke.

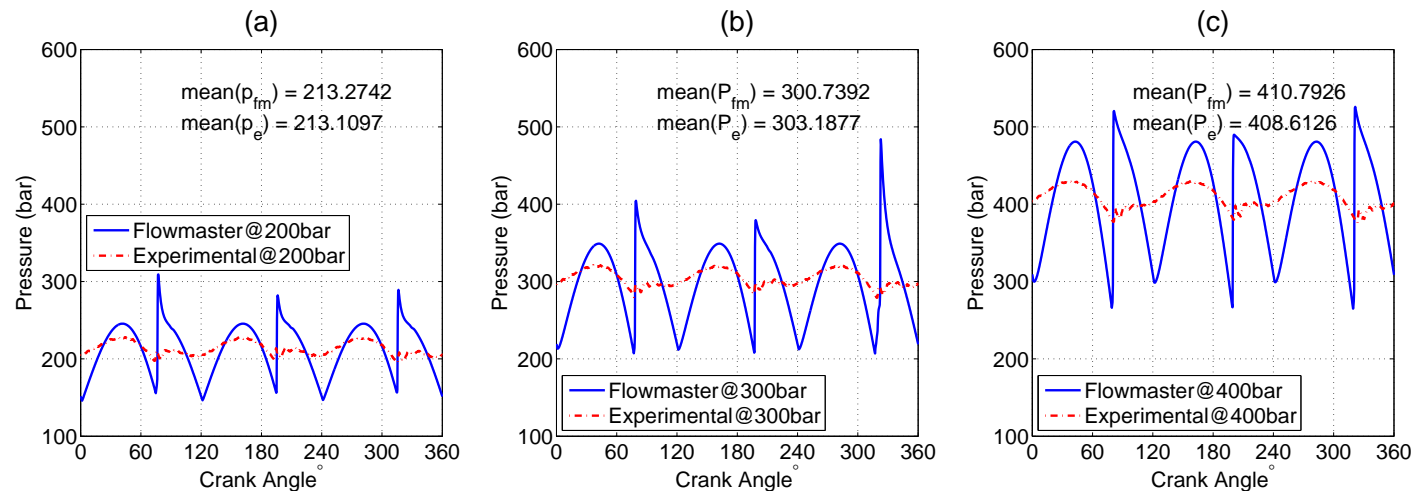


Figure 4.16: Experimental evaluation of a pressure field inside the common outlet manifold chamber in a triplex pump vs numerical evaluation of a common manifold chamber, illustrated in Figure 4.14, using a lumped parameter model. Three reference test were conducted at 200 bar (a), 300 bar (b) and 400 bar (c). The mean values of experimental and numerical pressures are displayed as p_e and p_{fm} respectively.

4.4.3 Power evaluation

Application of an accurate lumped parameter model of a complete multi-cylinder pump is justified by the need for estimating the performance of an entire pump. The interference among the chambers, makes the individual chamber analysis insufficiently accurate for this purpose.

In Figure 4.17 the computational lumped parameter model is presented. Each of the test cases was performed at a different outlet pressure which is directly proportional to the pump load factor. In each of the three test cases two main operating states were analysed; in the first, cylinder one was analysed in a triplex pump and in the second, the same cylinder was evaluated in a simplex pump. The hatched area presents the power loss that is taking place in the triplex pump due to cylinder interaction.

For instance, the lumped parameter model could estimate the power loss in the cylinders interaction. Figure 4.18 shows the power resistance calculated on the plunger for the three reference tests. The experimental data was evaluated by appraising the plunger in chamber one. By examining three test cases it is clear that the power requirement in one plunger in a triplex pump is higher than in a simplex pump (one cylinder) by approximately 25%, shown in Table 4.1 (third vs second column). It can be assumed that a single cylinder pump would need less than the same cylinder in a triplex pump of the same kind, or, conversely a triplex pump would need more than three times the power needed by each separate chamber. The power difference is represented by the power loss in the interaction.

Engineering rationale for this phenomenon is that at the beginning of the delivery stroke each plunger has to work against the high pressure created in the outlet manifold (generated by the delivery stroke of the other chambers). The novelty provided by the analysis methodology described in this section is the quantification of this power gap which can be examined in ‘Change(%)’ column of Table 4.1.

The validity of the lumped parameter model is clearly stated by comparing ‘Triplex pump’ columns from experimental and numerical analysis shown in Table 4.1. The power consumption values are remarkably close (approximately 2% differentiation) for each of the test cases indicating the high accuracy of the computational model.

For an absolute validation of the data in Table 4.1, the single cylinder lumped

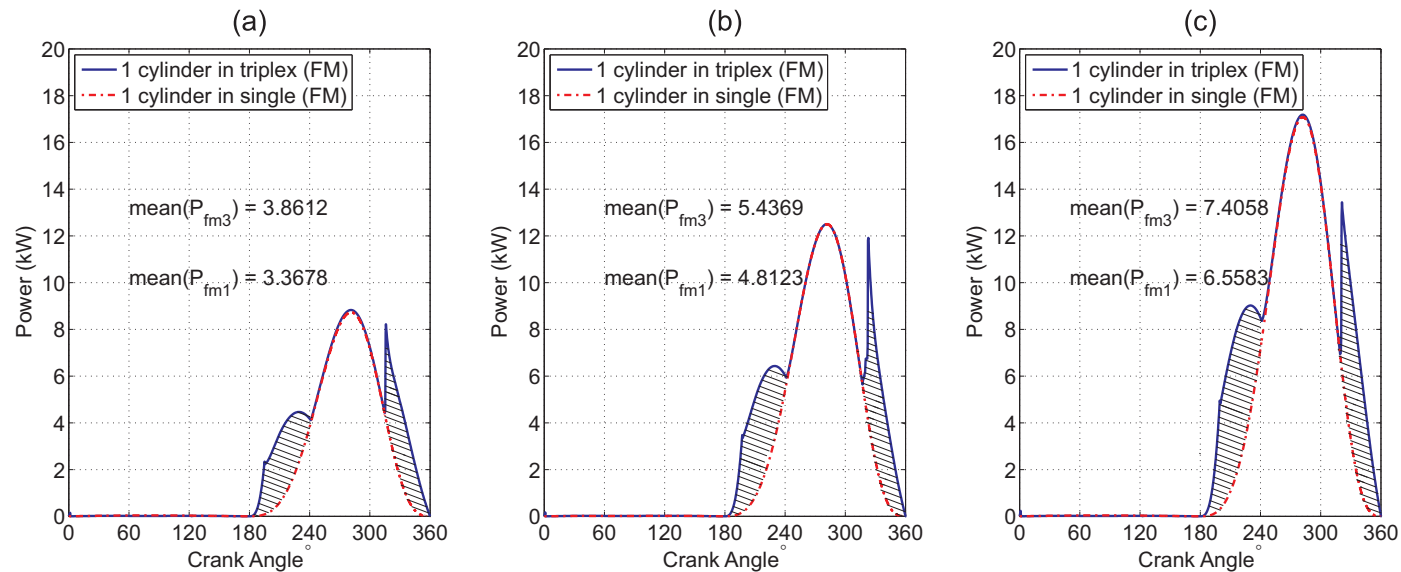


Figure 4.17: Power evaluation was performed using a lumped parameter model, presented in Figure 4.13 for one chamber at pressures: 200 bar (a), 300 bar (b) and 400 bar (c). The solid blue line shows the power of one chamber in a triplex pump and the red dashed line shows the power of one chamber in a simplex pump. The mean values, shown in the graph, indicate the difference in power consumption between simplex and triplex PD pumps.

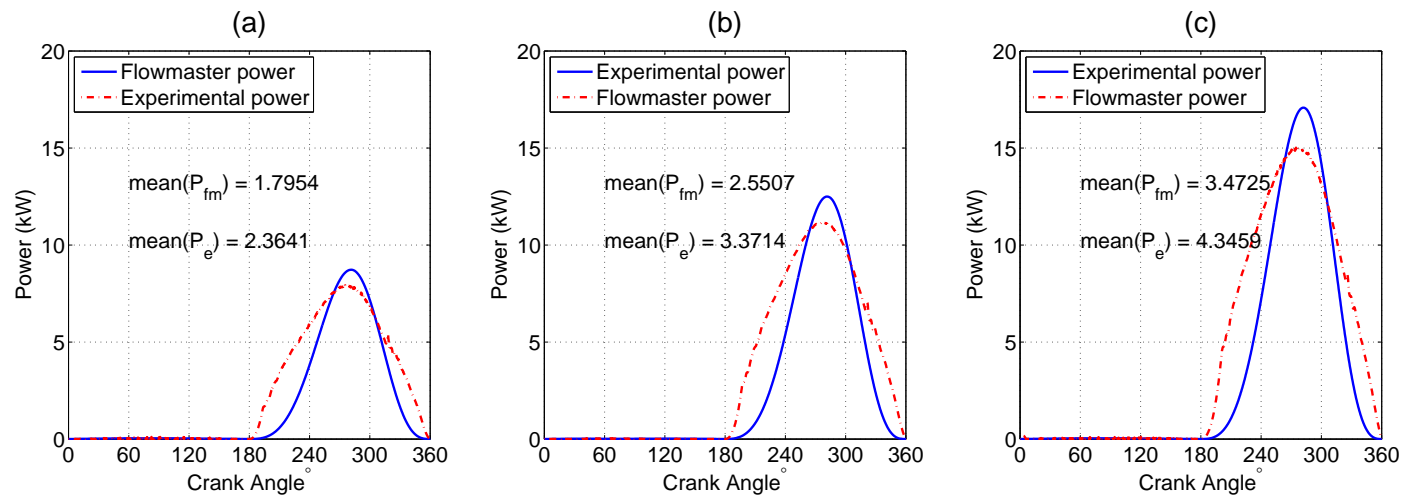


Figure 4.18: Experimental evaluation of one chamber in a triplex pump vs numerical evaluation of one chamber in a simplex pump (shown in Figure 4.14). Power consumption was measured and calculated at 200 bar (a), 300 bar (b) and 400 bar (c). Experimental and numerical mean power consumptions values are displayed for P_e and P_{fm} respectively.

Test	Mean power from one plunger (kW)				
	Lumped parameter model			Experiments	
	Triplex pump	Simplex pump	Change(%)	Triplex pump	Simplex pump
200	2.4181	1.7954	25.75	2.3641	N/A
300	3.3997	2.5507	25	3.3714	N/A
400	4.6098	3.4725	24.67	4.3459	N/A

Table 4.1: Summary of the power consumption from a single plunger. Lumped parameter model evaluated single cylinder consumption in triplex (three-cylinder) pump and simplex (one-cylinder) pump. Experimental data was only able to evaluate power consumption of single cylinder in triplex pump. Future studies will look into experimental power analysis of a single cylinder in simplex pump.

parameter model should be compared to a single cylinder experimental test. Experimental data is still unavailable as shown Table 4.1. From a computational lumped parameter model it can be seen, in Figure 4.17, that the estimation of the difference in power consumption made above is approximately 25%. The figures, in fact, show the numerical comparison between the three chambers and the single chamber lumped parameters model throughout the reference tests.

4.4.4 Discussion of a multi-cylinder PD pump model

The multi-cylinder pump section has demonstrated that one of the major challenges present in modelling PD pumps is the interaction between cylinders. Using 1D-CFD software it was proved that problem identification and performance changes in hydraulic systems are attainable using a combination of different commercial softwares. High-fidelity CFD codes show effectiveness in solving simplex pump designs. Multi-cylinder models are not affordable in industrial applications due to the high computational time. Lumped parameter models are ideal for a high-level system layout with multiple individual units and elements such as pumps, safety valves, hoses, etc. The synergy of two systems provides an optimal solution that takes into account high-level and in-depth analysis.

In the literature review section 2.3 site setup in hydraulic fracturing was discussed. Practically, layout of the PD pump on site is highly unpredictable and the absolute variance from site to site is common. This may cause enigmatic inconsistency in the operation. Recommendation for further study highlights the need to analyse the inter-

action between individual PD pump units on site as exceptionally important.

This research has illustrated how an application of commercial software can be used and customised to answer design requirements. Site variation can be overcome by in-depth analysis, standardisation and implementation of engineering solutions to the site.

4.5 Summary

Development of the optimised hydraulic fracturing system requires a fully functional computational model. Using the fundamental theory of PD pump operation this chapter describes the systematic development of a computational model of a frac-truck which incorporates both the dynamic behaviour of the drivetrain and the interaction of key components within a PD pump.

By identifying the individual components of a single frac-truck assembly the first section 4.1 shows the model of a drivetrain connected to a positive displacement pump. Subsequent phases of computational model development study fluid mechanics inside a PD pump's fluid end. A single cylinder model was improved by introducing valve dynamics and its impact on PD pump operation in section 4.3. The final phase of the computational model development, presented in section 4.4 of this chapter, shows a complete multi-cylinder model of a PD pump. The important outcome was illustrated in the power evaluation section results of which suggest further model development to assess the power consumption in current hydraulic fracturing systems.

Before this model can be implemented further in design optimisation studies it needs to be validated against field data and the experimental test rig.

Chapter 5

Field data

The computational model assumes constant environmental conditions (e.g. temperature, flow density and output pressure). This ideal situation may, or may not, produce significant errors relative to the real world. To quantify the differences this chapter reports the use of field data from a north American hydraulic fracturing site to compare with the output of the computational model.

The data, recorded by hydraulic fracturing pump's condition monitoring system shown in Figure 5.1, was used to make a comparison with the behaviour of the computational model.

5.1 Data acquisition methodology

As a part of the prototype trials of a condition monitoring system a number of pumps on a American frac-site were instrumented with a pressure sensors, a speed sensor, accelerometers on both power-end and fluid-end and a selection of pressure and temperature sensors for power-end lubrication. In addition to PD pump instrumentation, engine and transmission operation metrics were recorded to monitor drivetrain performance.

5.1.1 Sensor data

The selection of specific equipment sensors, to identify particular physical processes, is related to the nature of occurring phenomena. All reciprocating equipment can be

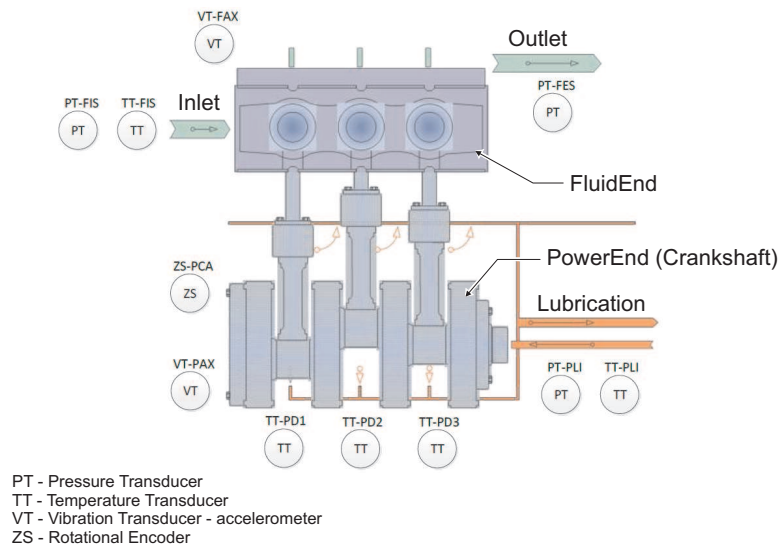


Figure 5.1: Sensor placement on the field unit

accurately converted to pumping frequency, therefore running the PD pump at higher speed will demand a higher acquisition rate from the sensors. For example, a higher acquisition rate is required for accelerometers to identify spectral energy at higher frequencies.

5.1.2 Location and well details

Field data was obtained from a pump operating in south Texas, Eagle Ford shale. In Figure 5.2 the location of the operational site is given in addition to the expected well conditions in the Eagle Ford shale. Well completions in this basin consist entirely of horizontal drilled wells and multiple stages. An average well has just over 1,800 cubic metres of fluid and slick water is predominately used. Proppants include different mesh sizes such as 100, 40/70 and 30/50 [112]. The majority of wells use sand, with some exceptions where resin-coated sand and low strength ceramic are used [113].

5.1.3 IMS gateway

The IMS gateway, shown in Figure 5.3, is a device used to acquire sensor data, perform signal processing and algorithmic calculations on the data and utilise its communication interfaces to send collected information up to a cloud server.

Data flow path, illustrated in Figure 5.4, is progressing through the following stages:

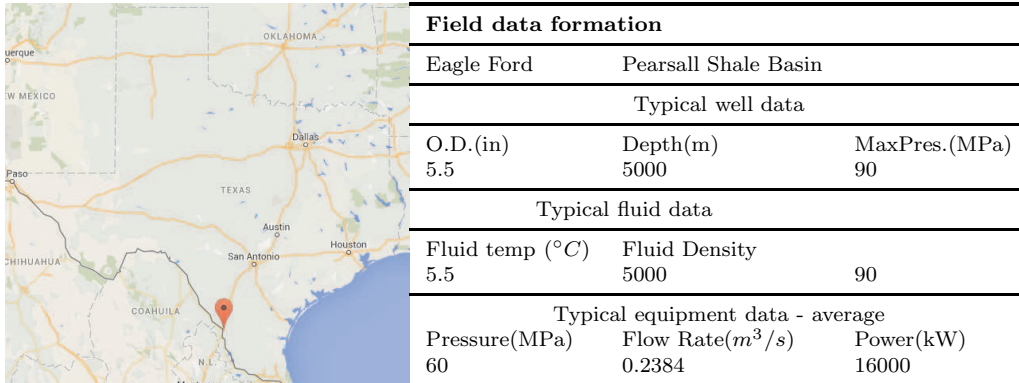


Figure 5.2: Field unit operates in Pearsall basin. Table shows typical well data associated with this location [114].

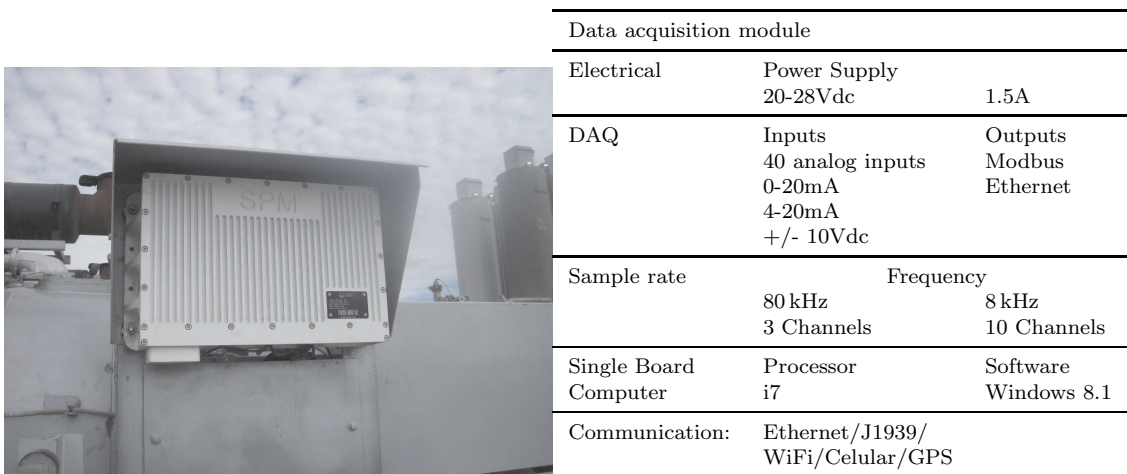


Figure 5.3: Data acquisition unit is installed in the field. Main characteristics are listed in the table.

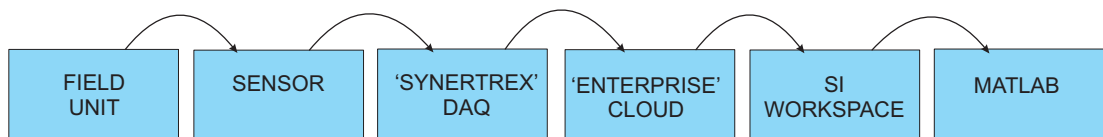


Figure 5.4: Methodology for data acquisition from the PD pump unit on site.

1. Signal conditioning changes transducer output into a readable value, which is followed by noise attenuation. For example a 4-20 mA value, obtained from the sensor, is converted into 0-5 VDC.
2. The signal conditioned data is then sent to one of the two data acquisition (DAQ) cards where the analog data is sampled and converted into a digital format that can be read by the Single board computer (SBC). Accelerometers are recorded at 4 kHz in DAQ card B and the remaining sensors are recorded at 1 kHz in DAQ card A.
3. The DAQ data is then sent to the SBC via USB interface. All the sensor data is stored in a database with time stamps and its respective sensor information (sensor type, units of measure, etc.)
4. Data is then saved to the solid state drive (SSD).
5. Data is finally uploaded to the cloud server or physically transferred by one of the field engineers. The main challenge with current DAQ system is the limited data storage space for high speed time series information. As a result the system is programmed always to erase the oldest data.

5.1.4 Acquisition and data storage

Stage data is stored using three different sampling rates. Low speed was used to capture the whole stage. Due to the length of the stage, which may run up to three hours of continual pumping, it was deemed sufficient to have 1 Hz sampling frequency to capture accurately well-head metrics. Sampling frequency of 1 kHz was used for all pressure sensors, temperature sensors and rotational encoders installed on the field unit. Finally, accelerometers on the PD pump's Power End and Fluid End were all acquiring data at 4 kHz owing to the rate of change and the induced equipment vibration on site.

One of the major challenges from the data acquisition side of the operation is the discharge pressure sensor, located on the outlet manifold of the pump, which may fail due to pressure fluctuation and the rate of pressure increase from individual cylinders. Increasing the speed of the pump will, by definition, require higher sampling frequency in order to capture all the trends in pressure oscillation.

5.1.5 Data transfer method

Physical data was downloaded using a specialised software, ‘SiWorkspace’, from the cloud to a local workstation where data was processed using a universal computational tool, MatLab. SiWorkspace is a configurable tool that currently has limited data processing capabilities and is presently being used only to download the data from the cloud.

5.2 Data analysis

The recorded operation of a single positive displacement pump, during one pumping stage. All the essential phases of the operation, such as pressure testing, formation breakdown and crack propagation, are illustrated in Figure 5.5.

The pressure, shown in Figure 5.5, is uniform across all PD pumps engaged in the process as well as at the wellhead itself. Flow rate is a function of speed and the choice was made to display only one variable and thereby maintain the comprehensiveness of the graph. Computation of the power consumption was added to the display as a function derived from the PD pump’s speed and pressure.

5.2.1 Methodology

Data is to be analysed by implementing following methodology:

- Data needs to be displayed in order to highlight all the sections where transitional states occur.
- Outlined time segment needs to be identified in time and all high frequency data is to be brought forward.
- Acquired high frequency data is to be analysed
- A conclusion needs to be made based on the analytical output.

In Figure 5.5 it can be seen that, although the first pressure signs are happening after the 20th minute of testing, the pump is engaged in operation at circa 38th minute. The reason for this is because the monitoring system on the frac-truck assembly is

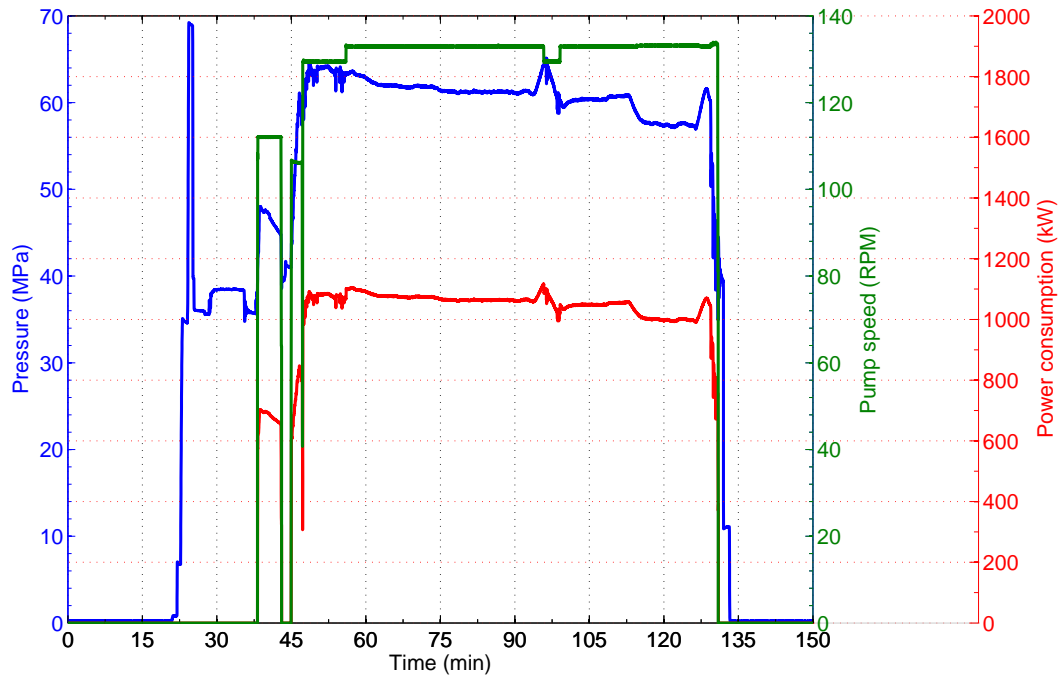


Figure 5.5: Pump metrics obtained during one pumping stage

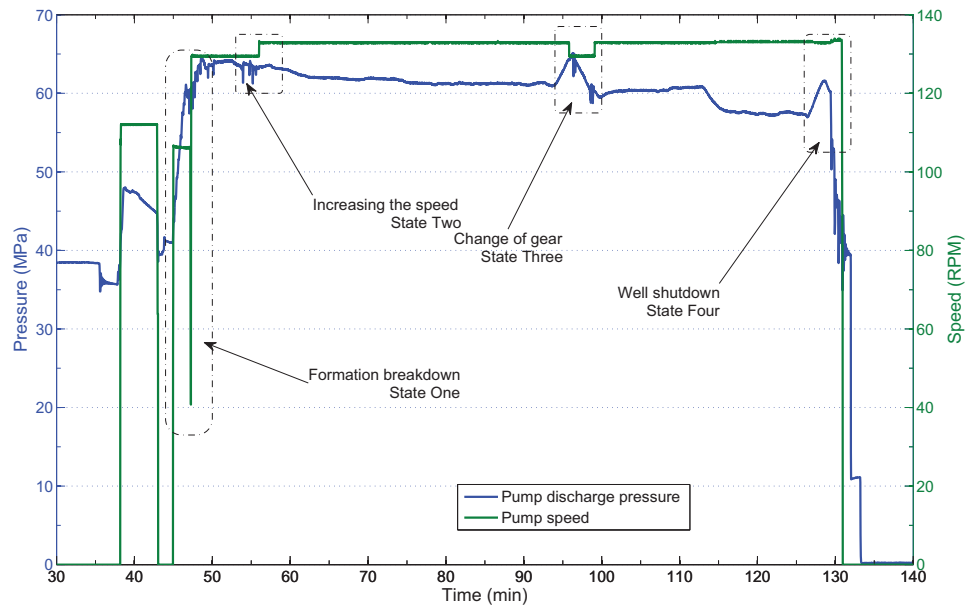


Figure 5.6: Identifying transitional parts of the stage

making a record even if the PD pump is not operating, provided that the diesel engine is running. The first step would therefore be to outline only the section when the pump is in motion.

The PD pump's pressure and speed are displayed in Figure 5.6. It is clear that changes occur in 44th, 53rd, 94th and 126th minute. All of the changes can be correlated to variations seen in the hydraulic fracturing stage. The highlighted areas will therefore be analysed further by using high frequency data. There hasn't been enough information to justify detailed discussion on each of the states as the analysis shows great similarities to one another.

Selected data shows operational measurements from two triaxial accelerometers (in the Appendix section A.1), suction (inlet), discharge (outlet) pressure and pump speed. Data is presented in the form of a continuous two minute range. Recorded metrics from two accelerometers are shown in three coordinate axes (X,Y and Z) at an acquisition frequency of 4 kHz. The remaining sensors, speed and pressure, are all acquiring at 1 kHz.

5.2.2 State one overview

Data segment in state one presents an actual formation breakdown. The event is followed by an obvious change in the pumping system. Using Figure A.2 from the Appendix A the precise time can be determined by identifying the point of the rapid pressure drop. This occurrence triggers the need to supply a higher flow rate to the well by increasing the PD pump speed or introducing additional units. In Figure 5.7 the increased PD pump speed is shown in bottom right subfigure.

It is clear that presenting data in this range is not the best approach if pressure pulsation and equipment vibration are to be investigated. However, the usefulness of this plot is to show a single event in the pumping dynamics and the response of a PD pump.

Values from a rotational encoder can be extrapolated to show 360° of crank rotation.

The operation in a steady state condition prior to formation breakdown shows the pump outputting results as seen in Figure 5.8.

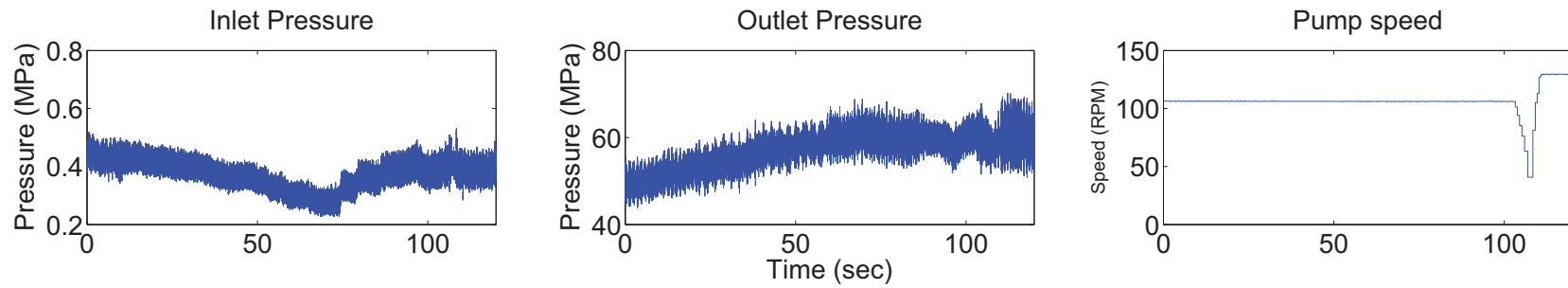


Figure 5.7: Pump metrics during formation breakdown - state one

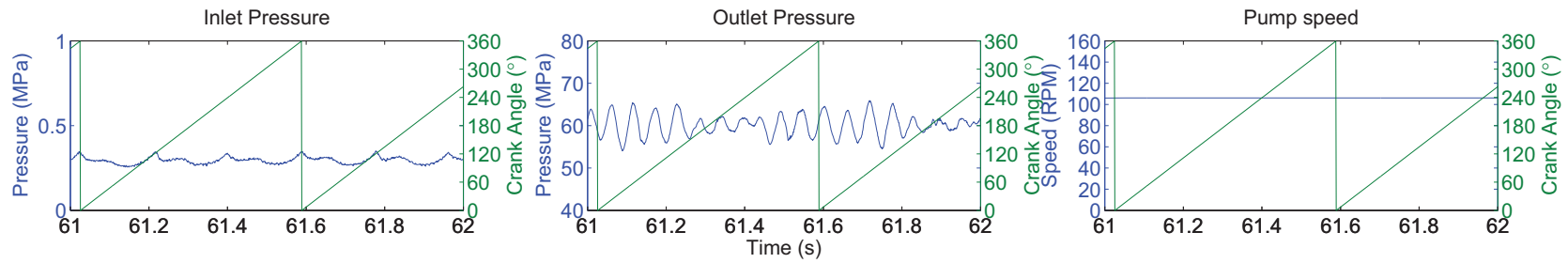
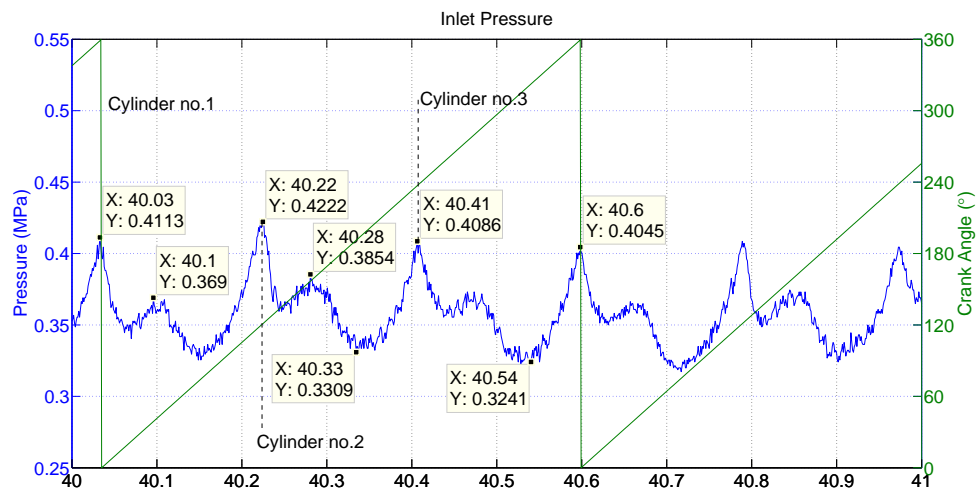


Figure 5.8: Pump metrics obtained in steady state conditions prior to formation breakdown - state one at one second

Table 5.1: Suction pressure operational metrics

Sensor	Peak (MPa)		Mean (MPa)	RMS (MPa)
	Positive	Negative		
Suction Pressure	0.5312	0.2273	0.3640	0.3674

**Figure 5.9:** Suction pressure on the inlet side of the pump during one pumping stroke

Suction pressure analysis

The PD pump's inlet pressure is a good indicator of a pump performance and can be used very efficiently for predicting cavitation. Data is processed and presented in the form of time series and frequency domain.

Table 5.1 shows peak pressure and mean values during one second.

One full pumping cycle is displayed in Figure 5.9 where pressure is shown in blue and plunger displacement, traveling from 0 to 360°, is shown in red on the right axis. It is clear that the pump is displaying three distinct pressure spikes which can be directly correlated to the three cylinder pumps. Pressure fluctuations, shown in Figure 5.9, are influenced by the opening and closing of the inlet valves which translates to the transient behaviour inside the inlet manifold of the PD pump. An instrumented PD pump was operating in the fleet of PD pump units so the possibility of suction pressure fluctuation due to system interaction must not be neglected.

It can be seen that peaks perfectly align with the crank angle position and the

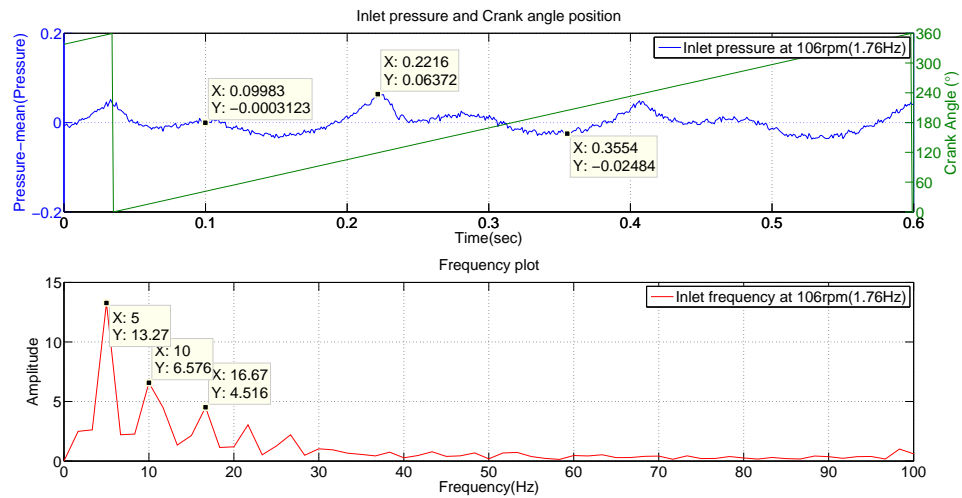


Figure 5.10: Frequency spectrum of the suction pressure on the inlet side of the pump during one pumping stroke

Table 5.2: Discharge pressure

Sensor	Peak (MPa)		Mean (MPa)	RMS (MPa)
	Positive	Negative		
Discharge Pressure	43.8088	70.1856	57.1819	57.3460

annotations in Figure 5.9 indicate precise timing of the individual cylinders during one pumping cycle.

The regular pattern of inlet pressure fluctuation can be seen in frequency plot, Figure 5.10. The frequencies conveying highest energy are at 5 Hz, 10 Hz and 16.67 Hz.

Suction pressure analysis in the frequency domain begins by taking identical time series data which was presented in the earlier figure.

Discharge pressure analysis

Time domain analysis of the discharge pressure has significance due to its influence on pump performance. Pressure was recorded at the discharge plenum located inside the PD pump. In the field operation the possibility that other PD pumps in the system are influencing the operation of the test unit needs to be considered.

Mean pressure during the recording time of two minutes, along with details on peak

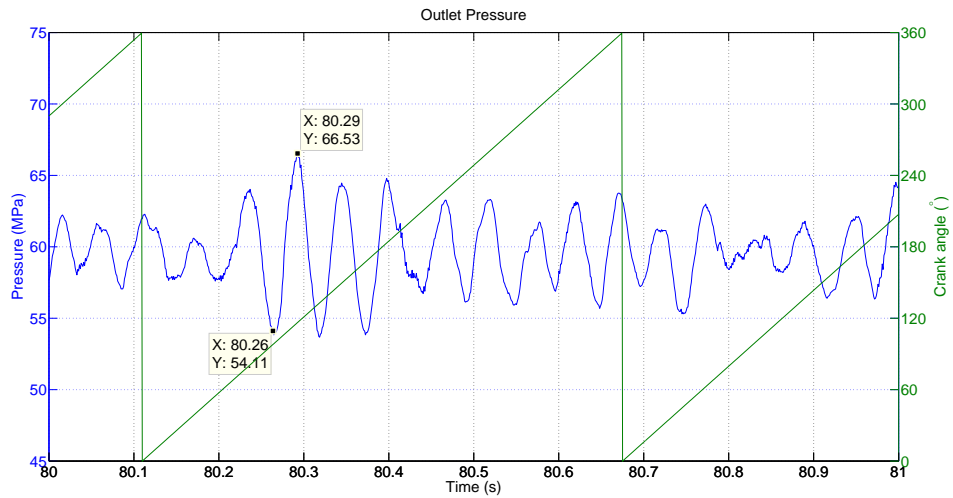


Figure 5.11: Discharge pressure inside outlet plenum of the pump during one pumping stroke

values, are shown in Table 5.2.

Figure 5.11 displays operation during one pumping cycle. The slow modulation of the outlet pressure can be the result of load and the flow rate. Overall complexity of the signal is shown in the Figure 5.11.

Peak to peak oscillation varies in the sampled period. A section from the later part of the recording shown in Figure 5.12 exhibits higher amplitudes. It is clear referring back to Figure A.2 that higher oscillation coincides with the increased speed of the pump.

Analysis in frequency domain for the discharge pressure was done on the identical time range of one second. Figure 5.13 displays results from this analysis.

The frequency spectrum, shown in Figure 5.13, depicts the impulsive nature in the low frequency part of the pressure signal. It is clear that the two strongest frequencies at 12 Hz and 18 Hz form approximately 7:1 and 10:1 ratio with plunger frequency of 1.76 Hz. This is a close estimate of the number of peaks and valleys in time series signal.

5.2.3 Data analysis summary

Synchronization in the time domain and alignment against the crankshaft position provides useful insight for understanding pump operations in the field environment. Clear analogy between different instrumental measurements can be seen and their relationship

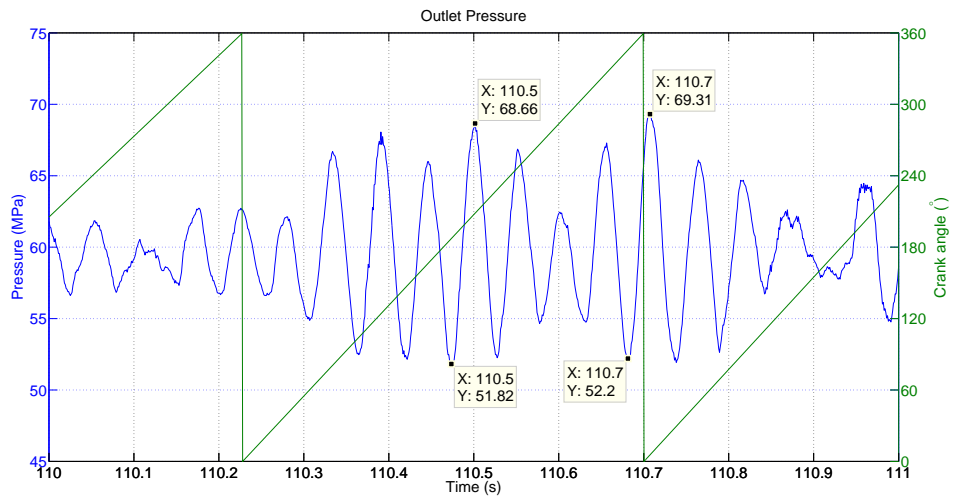


Figure 5.12: High amplitude variation of the discharge pressure inside the outlet plenum of the PD pump during one pumping stroke

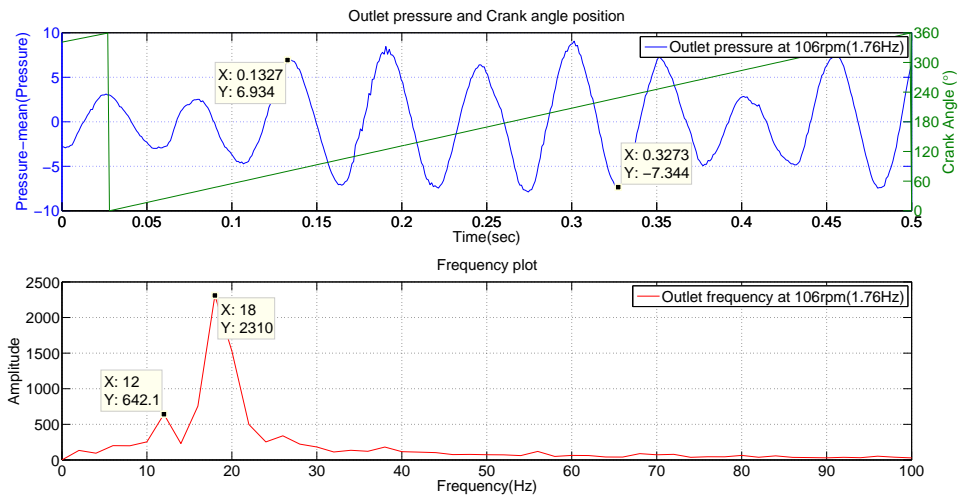


Figure 5.13: Frequency spectrum of the discharge pressure on the outlet side of the PD pump during one pumping stroke

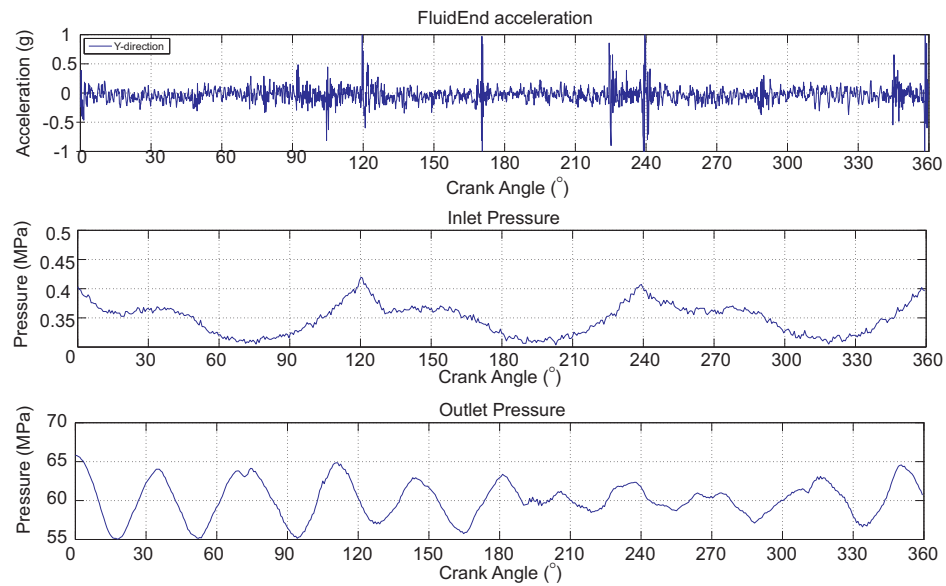


Figure 5.14: Important pump metric and their relationship during one full pumping cycle

has been presented in this section. In Figure 5.14 these observations are highlighted.

The accelerometer on the Fluid End in the direction of the y-axis shows equally spaced pulses that correlate well with angle of the crankshaft. Similarly, inlet and outlet pressure show strong association with the type of PD pump (i.e. triplex) in the output signal. Pressure variation is also presented and $\pm 10\%$ fluctuation is evident compared to the mean value.

5.3 Conclusion

In conclusion, data presented in this section shows current undertakings in the field to monitor site operation. This analysis has shown an important benefit of this approach in understanding field the operation and the opportunities for developing comprehensive system control on site.

From the analysis of the accelerometers (Appendix section A.1) it was shown that vibration across the length of the pump (in the direction of plunger motion) is emphasized compared to the remaining two orthogonal directions. This presents valuable information that needs to be further developed from a structural analysis point of view. Analogical field data analysis was previously done for wind turbines. The fatigue cycle

was measured and implemented in a computational model to assess possible improvements and design modification [115], [116]. One of the ways of implementing the PD pump field data analysis could be used for fatigue cycle assessment.

In pressure pulsation studies scenarios showing steady state and transitional operation were displayed and discussed. The magnitude of pressure saturation was shown in both cases and conclusions can be made with several research observations:

- Inlet and outlet pressure show cyclic variation during normal pump operation.
- Inlet pressure oscillation is more pronounced and may lead to cavitation if the pressure is reduced below a certain limit.
- The number of peaks in the inlet manifold during one pumping cycle is three which can be directly associated to three plungers.
- Outlet pressure peak to peak variation is approximately 20% in transient state (gear change) and 10% in steady state.
- The number of peaks in the discharge pressure history during one pumping cycle is nine

In the appendix, section A.2 the remaining data analysis graphs are given. Operational metrics in states two, three and four show negligible disparity to the detailed analysis of state one. All the remaining graphs are added to this brief section as a part of accompanying documents to avoid any repetition.

In chapter 7 the correlation between the computational model and the field data is presented.

Chapter 6

Pump test rig data

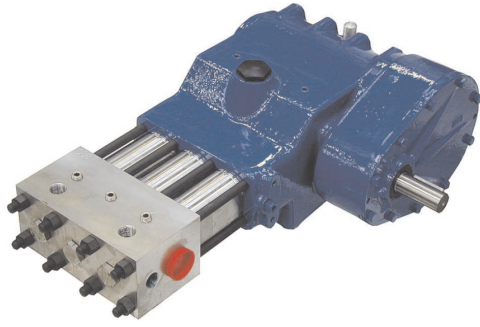
While field data verifies the magnitude of pumping parameters the test rig confirms their dynamic relationship as it is not feasible to run the full scale frac-site with varying parameters.

The objective of the test rig experiments was to assess the response of pressure and flow rate to varying speeds. Subsequent sections will correlate the results with values predicted by the computational model.

6.1 Test rig components

Replicating a PD pump operation, as seen in the field, starts by identifying the main elements of the assembly. A triplex PD pump is crankshaft driven with the same mechanical ratio between the main elements (i.e. crank diameter, con-rod length and diameter) to the full size original presented in section 2.5. An electric motor will be used to power the PD pump motion. A frequency variator will be used to provide variable motor speed and to enable the necessary operating flexibility. In addition to speed adjustment (the only form of control currently being used in PD pumps on site) the inclusion of pressure modularity will enable different loading conditions. This is an added feature not used on a real hydraulic fracturing site but necessary in the current lab setup to artificially simulate well pressure.

The main limitations of the system compared to the full size unit are in the operating fluid. Laboratory test rig uses water as opposed to typical slurry mixture which in



HPS 400 Pump specification	
Plunger Diameter (m)	0.022
Number of Plungers	3
Stroke (m)	0.045
Operating speed (rpm)	789
Gearbox ratio (-)	2.28:1
Displaced volume (m^3)	$1.7 \cdot 10^{-5}$
Maximum operating pressure (MPa)	40
Maximum flow rate (l/min)	41
Maximum power requirement (kW)	30

Figure 6.1: Essential operating parameters from the test pump [117]

reality can vary from water to high viscosity gel to multi-phase flows including solid particles.

The complete P&ID diagram of the test rig setup can be found in the Appendix, Figure B.2.

6.1.1 Pump

The key component of the test rig is the triplex positive displacement pump. Figure 6.1 summarises important parameters associated with the chosen PD pump. Pump is comparable to full size unit by several criteria: (1) Suction and discharge valves are regulated by pressure differential, (2) Ratio between crankshaft rod length and radius is the same to the full size unit, this is important for providing same sinusoidal plunger motion, (3) Fixed speed gearbox is also assembled as a part of pump unit.

Main differences between the scaled pump model and the full size unit are: (1) Pressure head is provided from an elevated tank, instead of a charge pump, (2) Maximum flow rate and pressure are not linearly proportional to the full size unit, (3) Speed of the model pump is higher than the full size unit. Suction head was sufficient and no cavitation was detected in any of the tests. Pressure and flow were expected to differ from the full size unit because of the difference in plunger size. Finally, pumping cycle is presented in crank angle degrees, therefore, difference in time measurement did not affect the data quality.

Model	Voltage		No load		Performance at max efficiency				Stall		Technical info		
	Range	Normal	Speed (r/min)	Current (V)	Speed	Current	Torque	Output	Torque	Current	Poles	Phase	Frequency (Hz)
Brook Crompton Series 10		400	4800		1489	51.2(A)		31.08(kW)			4	3	50

Table 6.1: Electric motor performance specification[118]

Normal ratings		No over-load use	Light-overload use	Heavy-duty use		Noise level dB(A)	Heat dissipation (W)	Air flow (m^3/h)	Type designation	Frame size (mm) HxWxD	Weight(kg)	
$I_{c.max}$ (A)	I_{max} (A)	$P_{c.max}$ (kW)	I_N (A)	P_N (kW)	I_{hd} (A)	P_{hd} (kW)						
72	86	37	69	30	49	22	65	810	250	ACS800-04-0040-3	602x265x276	32

$I_{c.max}$ - Rated current available continuously without overload availability at 40°C

I_{max} - Maximum output current for 10s at start, or as allowed by drive temperature. Max. motor shaft power is 150% P_{hd}

$P_{c.max}$ - Typical motor power in no-overload use

I_N - Continuous current allowing 110% I_N for 1-5min operation at 40°C

P_N - Typical motor power in light-overload use

I_{hd} - Continuous current allowing 150% I_{hd} for 1-5min operation at 40°C

P_{hd} - Typical motor power in heavy-duty use

Table 6.2: Variable frequency drive performance specification [119]

6.1.2 Motor

The pump is driven by an electric motor which was selected based on the maximum pump power requirements. The motor chosen for this application is rated at 37 kW and designed to operate at 1,800 rpm. Table 6.1 summarises key figures.

6.1.3 Inverter drive

The pump's operating speed is regulated using a frequency variator. Selected variable speed drive main characteristics are shown in Table 6.2.

6.1.4 Solenoid valve

Downstream flow restriction was implemented to increase the pressure inside the PD pump. The level of PD pump loading is directly proportional to the discharge pressure which is governed by using a pneumatic actuator. The chosen valve features electromechanical control of the pneumatic actuator by regulating the input current. Further explanation can be found in section 6.3.2. Figure B.1 in the Appendix presents technical drawing of the solenoid valve.

6.1.5 Tank

The PD Pump is operating in a closed fluid circulation system. The pump needs to be supplied with a constant source of clean water at ambient conditions. A 500 litre stainless steel water tank is provided within the specification and mounted directly above the PD pump on the assembly skid to provide pressure head. When fully filled it provides the PD pump with an inlet pressure of 1.13 bar absolute. Considering the fact that only a single pump will be operating in the system the pressure provided was sufficient to prevent any undesired cavitation. The water tank is fitted with an inlet point for initial filling from an external water supply source and an inlet float valve to prevent over filling.

6.1.6 Pipework

Other pipework includes selection of valves and hoses. A manually operated drain valve is installed to allow the system to be emptied when required. An additional, manually operated, ball valve is fitted to isolate the PD pump inlet from the tank. This ball valve also includes a limit switch to prevent the PD pump from operating if the valve is closed.

6.2 System requirements

The test rig is assembled on a single skid, in Figure 6.4 the main components are shown.



Figure 6.2: Skid assembly with major components

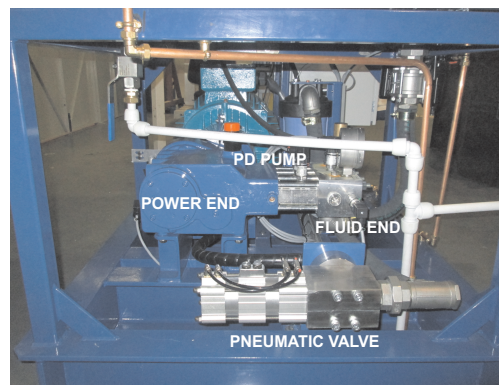


Figure 6.3: PD pump assembly with regulating pneumatic valve

Figure 6.4: Test rig assembly

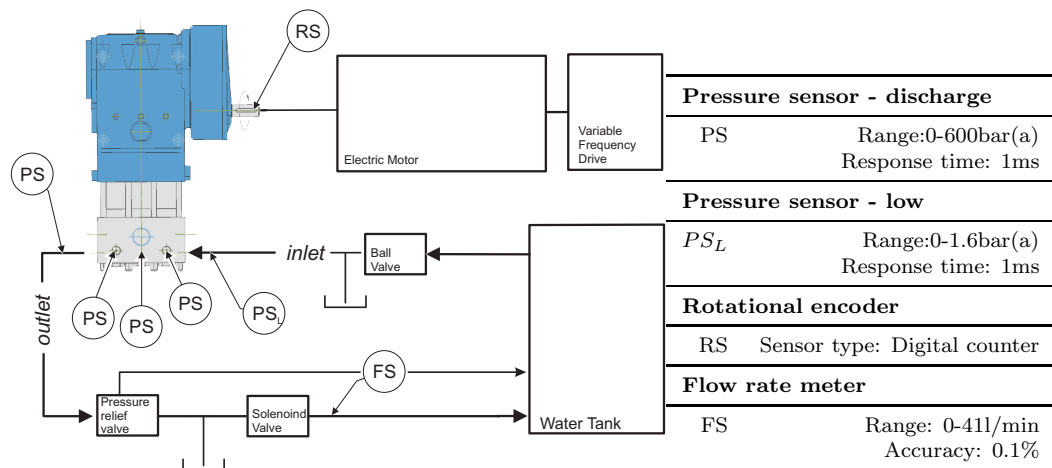


Figure 6.5: Test rig schematics and essential sensor information

The entire system operation can be concisely described as follows: the electric motor is operating at its optimum speed and is being directly coupled to the input shaft of the pump. Final gear reduction on the PD pump decreases shaft speed by a set gear ratio, as shown in Figure 6.1. Speed regulation is done by frequency alteration in the inverter (VFD) unit. Inside the power end of the pump rotational movement of the driveshaft is transferred into a linear motion of the plungers via the crankshaft. Fluid is being supplied to the pump from the tank by providing sufficient NPSH (net positive suction head). A choke valve is placed downstream of the pump and by gradual closing of the valve pressurisation in the pump outlet is achieved. Downstream of the choke valve pressure is approximately equal to the tank pressure. In the final phase, fluid is led back to the tank.

Once the detailed design had been agreed the test rig was manufactured by Hughes Pumps Ltd. and delivered to the University.

6.3 Instrumentation and data acquisition

A number of sensors are used in the current setup. Figure 6.5 represents a schematic of the test rig with the sensor location.

Pressure sensors			
Discharge		Suction	
Power supply (v)	10-30 DC	Power supply (v)	10-30 DC
Stainless steel wetted parts		Stainless steel wetted parts	
Number of sensors	4	Number of sensors	1
Output signal (mA)	4-20, 2-wire	Output signal (mA)	4-20, 2-wire
Pressure range (bar)	0-600	Pressure range (bar)	0-1.6
Accuracy	0.25% of span	Accuracy	0.25% of span
Allowable fluid temperature	-30 to +100° C	Allowable fluid temperature	-30 to +100° C
Response time	<1ms	Response time	<1ms
EN 10204 3.1 inspection certificate			

Table 6.3: Pressures sensors selected for this experimental setup [120]

6.3.1 Process control

Control of the PD pumps in the field during hydraulic fracturing consists solely of flow rate regulation that is a direct function of PD pump speed. The pressure, a second important parameter, is dictated by the condition inside the well. In the laboratory setup well condition needs to be simulated. This is achieved using a flow restricting valve.

Speed control

Motor speed is alternated using a variable frequency drive (inverter drive). Establishing connection with this unit was done in two ways; the control panel is equipped with speed control that can only be operated locally via an interface panel, secondly, the ModBus device on the VFD that enables control via the ethernet connection is added. The advantage of this feature is not only the ability to control the device remotely but also the direct PC interface with the unit that will enable further speed adjustment and feedback control. For the purpose of this experiment the first control method was adequate and sufficient to satisfy the test requirements.

Pressure control

Pressure in the system is regulated by a pneumatic pressure adjusting valve. This valve is installed on the PD pump's discharge to provide a restriction to the flow and thereby

generate a pressure in the system. The valve is adjustable by varying the air pressure acting on the valve (0-5 bar). The valve controls (manual) are embedded in the control panel of the PD pump. An alternative method includes an I/P (current to pressure) convertor and a solenoid valve, thereby, the air pressure acting on the valve can be adjusted remotely by a 4-20 mA signal.

6.3.2 Sensor implementation

Monitoring of the operation was done predominately using three types of sensors. In Figure 6.5 it can be seen that the monitoring of pressure variation was highlighted. To accurately measure plunger position a speed sensor was installed on the driveshaft. The overall pump output in terms of volumetric efficiency was monitored using a single flow meter.

Pressure sensor

The inlet pressure was monitored by installing one low pressure sensor on the suction side of the pump. One pressure transducer was fitted in each of the internal chambers (x3) to record the pressure changes during the pump operation. The pressure in each cylinder is expected to oscillate between 1 and 400 bar in every crank rotation. To monitor cumulative output from an entire triplex PD pump one pressure transmitter is to be fitted on the common discharge manifold. Table 6.3 provides all the relevant information for each of the pressure sensors. Sensor calibration certificate can be found in the Appendix, Figure B.3

Speed sensor

The pump's driveshaft was aligned at a precise position to determine plunger's starting point. Using the reflective tape and infrared sensor, pointed to the marked part of the driveshaft, the precise speed of the pump can be determined based on the number of pulses per minute. The device is outputting a digital counter signal. Detailed information on the sensor is available from the manufacturer's data sheets [121].

Flow sensor

A flow meter was included downstream of the solenoid choke valve. This is a stainless steel pelton wheel turbine flow meter, with 1/2" inlet and outlet connections. The output from the flow rate meter is fed to a digital display unit that was mounted to the door of the pump control panel and an output signal, 4-20 mA, was transmitted directly to an external DAQ device. The flow meter installed is operating with an accuracy of $\pm 2\%$ for the upper 90% of the range.

6.3.3 Safety and failure prevention

Operating the equipment demands fully understanding the system. Untrained handling can cause equipment failure and safety risks for nearby personnel. To prevent this from happening safety measures were taken which consist of the following:

- Level switch - water tank (low). To prevent the PD pump from running with an insufficient water supply level a switch was fitted that indicates failure in the system and prevents pump startup.
- Temperature switch - water tank (high). Because the energy from the PD pump is transferred to heat, safe pump operation is conducted at temperatures under $+70^{\circ}\text{C}$.
- Temperature switch - pump oil (high). Lubrication of the PD pump power end must not exceed $+42^{\circ}\text{C}$.
- Limit Switch - pump inlet feed valve. Placing the valve between the inlet of the pump and the tank is necessary to isolate the tank from the remaining part of the system. To prevent any attempt to operate the PD pump with the inlet valve closed an indicator switch was installed to send a warning signal to the operator.

6.3.4 Data acquisition

The signal from the sensor was processed using the National Instrument's USB DAQ devices. A high acquisition rate (10 kHz), collection of analog channels and the overall

Table 6.4: Data acquisition characteristics NI-DAQ[122]

USB-6210					
Input range (v)	Number of Channels			Resolution (bits)	MaxRate (kHz)
	Analog In.	Analog Out.	Digital I/O		
$\pm 10, \pm 5, \pm 1, \pm 0.2$	16	-	4DI/4DO	16	250

ease of use are features that align with the scope of the designed test rig. Key properties of this device are given in Table 6.4.

Control of the solenoid valve, via an electrical signal, was established by an analog output to the pneumatic actuator. For this purpose a secondary NI-USB device was used. More details can be seen in the specification sheet provided by the manufacturer [123].

6.4 Data analysis

The test overview lists all the test cases at all operating speeds and pressures. Table 6.5 summarises the entire test program. The performance variation of the PD pump test rig can be seen in the speed and pressure output.

Data sampling rate is 10 kHz for all pressure sensors. Analysis is conducted for the length of a single pumping cycle. Duration of the pumping cycle varies depending on the operating speed of the test pump.

Individual analysis will focus independently on inlet conditions, outlet conditions, chamber condition and volumetric flow rates. In Table 6.5 all the test cases are enumerated by establishing the main boundary conditions, i.e. speed and pressure.

6.4.1 Suction pressure

Analysis of the acquired inlet pressure data in time domain starts by presenting an overview of the pressure ranges and mean values for each of the 36 test cases.

In Table 6.6 the main results from all test cases are displayed. It can be seen that values are consistently within the range while excluding minor variances in particular operating conditions.

Visually displaying values from Table 6.6 results in the following Figure 6.6.

Table 6.5: Test outline

Test No.	Overall recording time (ms)	Pump	Motor Speed (rpm)	Pump Speed (rpm)	Pressure (MPa)	Fluid	Temp.(°C)
1	2000		600	263	5		
2	2000		600	263	10		
3	2000		600	263	15		
4	2000		600	263	20		
5	2000		600	263	25		
6	2000		600	263	30		
7	2000		600	263	35		
8	2000		600	263	40		
9	2000		700	307	5		
10	2000		700	307	10		
11	2000		700	307	15		
12	2000		700	307	20		
13	2000		700	307	25		
14	2000		700	307	30		
15	2000		700	307	35		
16	2000	HPS400	800	351	5	water	20
17	2000		800	351	10		
18	2000		800	351	15		
19	2000		800	351	20		
20	2000		800	351	25		
21	2000		800	351	30		
22	2000		800	351	35		
23	2000		900	395	5		
24	2000		900	395	10		
25	2000		900	395	15		
26	2000		900	395	20		
27	2000		900	395	25		
28	2000		900	395	30		
29	2000		900	395	35		
30	2000		1000	439	5		
31	2000		1000	439	10		
32	2000		1000	439	15		
33	2000		1000	439	20		
34	2000		1000	439	25		
35	2000		1000	439	30		
36	2000		1000	439	35		

It is clear, from observation of the plot in Figure 6.6, that higher pressure oscillation is seen at higher outlet pressures and with the increase of the operating speed.

Mainly all of the test cases at low outlet pressure have lower peak-to-peak variation compared to higher outlet pressures. Explanation for variation at higher outlet

Table 6.6: Inlet pressure

Test No	Peak (MPa)		Mean (MPa)	RMS (MPa)
	Positive	Negative		
1	0.1213	0.0872	0.1078	0.1079
2	0.1266	0.0822	0.1077	0.1079
3	0.1350	0.0801	0.1077	0.1080
4	0.1391	0.0757	0.1077	0.1080
5	0.1363	0.0758	0.1077	0.1080
6	0.1428	0.0759	0.1078	0.1082
7	0.1471	0.0731	0.1078	0.1082
8	0.1464	0.0695	0.1077	0.1082
9	0.1268	0.0837	0.1077	0.1080
10	0.1316	0.0808	0.1076	0.1080
11	0.1386	0.0719	0.1077	0.1082
12	0.1467	0.0757	0.1077	0.1084
13	0.1508	0.0678	0.1077	0.1085
14	0.1520	0.0665	0.1077	0.1086
15	0.1540	0.0624	0.1077	0.1087
16	0.1392	0.0719	0.1077	0.1086
17	0.1408	0.0650	0.1075	0.1086
18	0.1435	0.0615	0.1075	0.1088
19	0.1441	0.0582	0.1076	0.1090
20	0.1457	0.0570	0.1075	0.1090
21	0.1524	0.0538	0.1075	0.1092
22	0.1575	0.0506	0.1076	0.1095
23	0.1392	0.0783	0.1075	0.1081
24	0.1442	0.0747	0.1075	0.1083
25	0.1516	0.0696	0.1074	0.1084
26	0.1559	0.0639	0.1075	0.1087
27	0.1577	0.0624	0.1075	0.1089
28	0.1590	0.0597	0.1075	0.1091
29	0.1655	0.0592	0.1077	0.1095
30	0.1604	0.0679	0.1073	0.1085
31	0.1637	0.0638	0.1073	0.1088
32	0.1556	0.0629	0.1072	0.1087
33	0.1635	0.0596	0.1074	0.1090
34	0.1615	0.0580	0.1074	0.1091
35	0.1655	0.0559	0.1075	0.1092
36	0.1706	0.0529	0.1072	0.1092

pressures is due to the compressibility of the fluid at higher pressures. Higher compressibility means that during the suction stroke a suction valve will open later than usual.

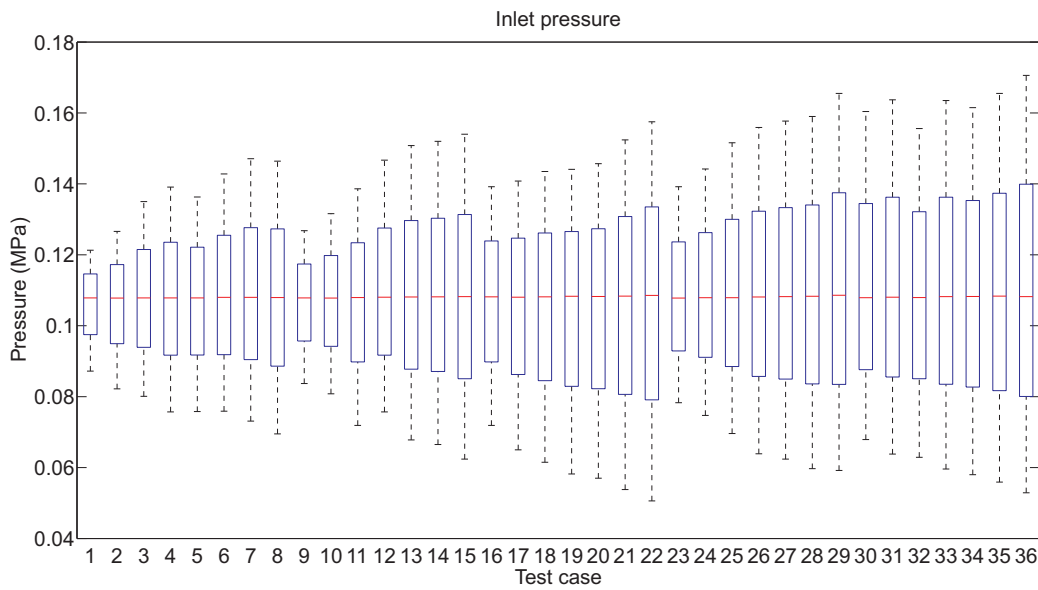


Figure 6.6: Inlet pressure variation showing most extreme values, 25th and 75th percentile and median

This phenomenon signifies that force equilibrium between pressure in the suction manifold and the chamber pressure is achieved later in the suction stroke at which point the plunger velocity is higher. At higher velocity valve opening will be more sudden and cause disruption in the flow pattern hence higher peak-to-peak oscillation.

Regardless of the peak variation the mean value stays relatively constant during all phases of the operation.

A single test case (No.18) was identified for further analysis in order to establish what is the operating envelope for the test rig model. Inlet pressure during one pumping stroke can be seen in Figure 6.7. The number of peaks is approximately five over the course of one pumping stroke.

Analysis of the frequency spectrum was performed on the limited length of the recorded inlet pressure signal. In Figure 6.8 the highest impact frequencies are displayed.

The peak with the highest energy, in Figure 6.8, correlates to the plunger frequency in 1:2 ratio.

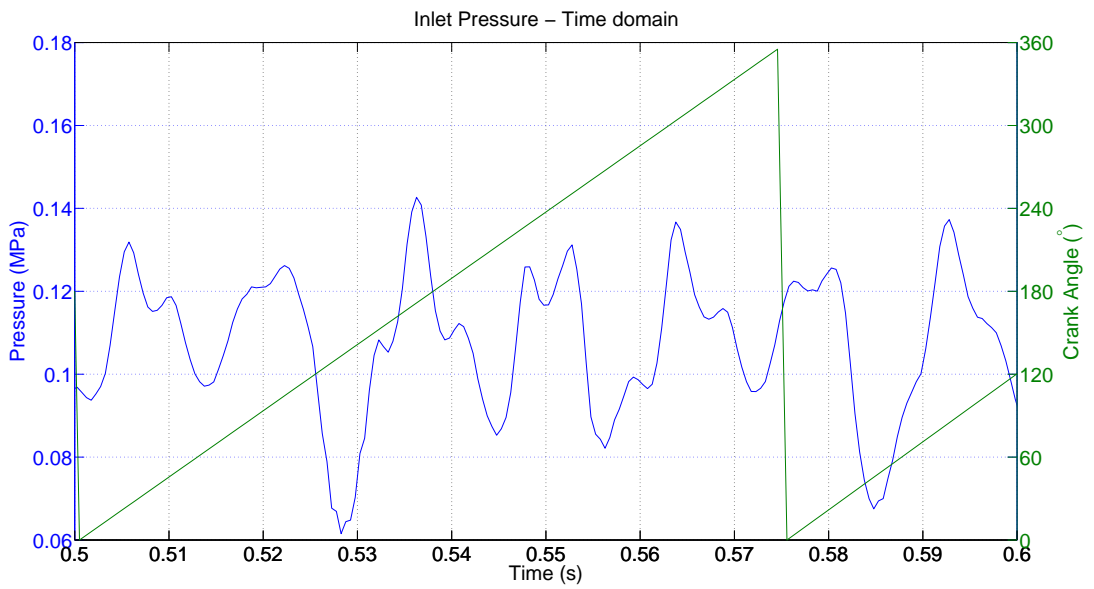


Figure 6.7: Inlet pressure during one pumping stroke in Test No. 18

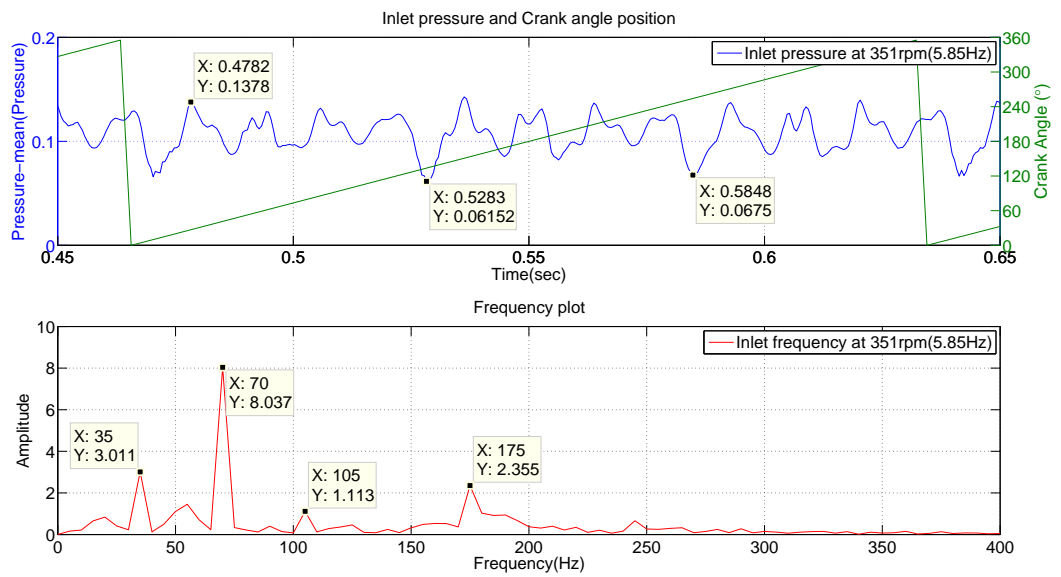


Figure 6.8: Frequency spectrum of the inlet pressure during one pumping stroke in Test No. 18

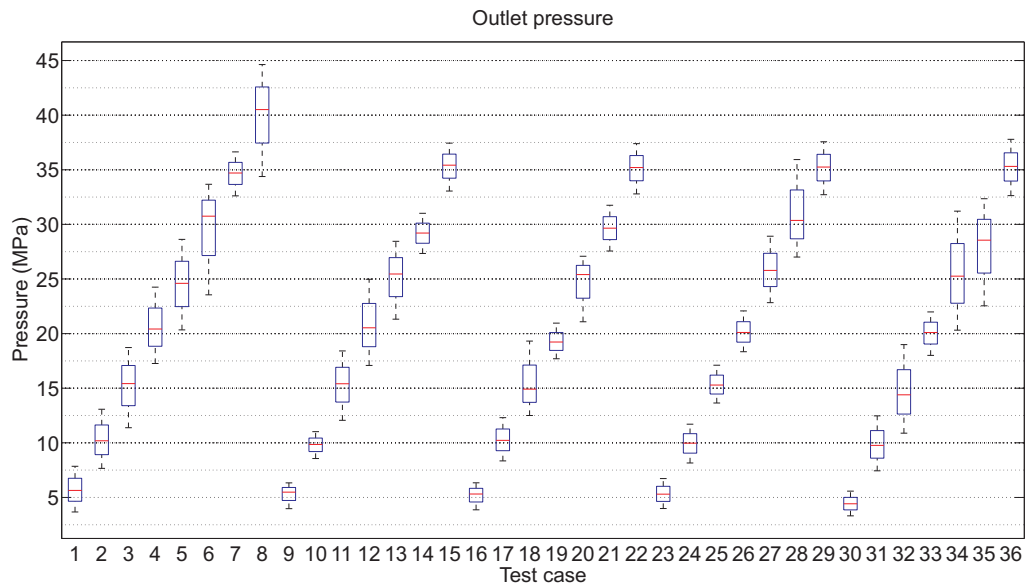


Figure 6.9: Outlet pressure variation showing most extreme values, 25th and 75th percentile and median

6.4.2 Discharge pressure

The outlet pressure from all three cylinders carries a high impact due to pronounced pressure variations which, unlike in low pressure inlet conditions, convey high energy. This is of particular significance in the field operation where discharge pressure pulsation causes excessive equipment vibration and requires a specialised handling procedure. The aim of this section is to examine and analyse the pressure fluctuations in scaled PD pump unit and discuss the operational variance.

The results from the discharge pressure analysis for all 36 test cases are displayed in Table 6.7.

In order to be able to recognize variations at different operating speeds and pressure a boxplot was generated and presented in Figure 6.9.

The information presented in Figure 6.9 shows different effects of pressure fluctuation at particular operating ranges. For instance, a higher amplitude variation can be seen in cases 6, 8 and 34. Evidence show that higher amplitude variations occur at higher pressures. Although, in some cases the peak-to-peak variation is quite low even at high pressure, for example cases 7, 14 and 22. There is a strong possibility that natural excitation is more pronounced at specific operating ranges.

Table 6.7: Outlet pressure

Test No	Peak (MPa)		Mean (MPa)	RMS (MPa)
	Positive	Negative		
1	7.8480	3.6696	5.6293	5.6522
2	13.0716	7.6577	10.1789	10.1955
3	18.7252	11.3840	15.4157	15.4279
4	24.2528	17.2649	20.4132	20.4251
5	28.6240	20.3388	24.5979	24.6112
6	33.6722	23.5486	30.7451	30.7594
7	36.6374	32.6146	34.7000	34.7128
8	44.6360	34.3813	40.5049	40.5215
9	6.3333	3.9710	5.4741	5.4919
10	11.0207	8.5596	9.8412	9.8561
11	18.4114	12.0610	15.4017	15.4153
12	24.9768	17.0820	20.5269	20.5410
13	28.4460	21.3173	25.4487	25.4627
14	31.0109	27.3390	29.1989	29.2119
15	37.4380	33.0520	35.4115	35.4264
16	6.3382	3.8673	5.3012	5.3212
17	12.3007	8.3471	10.2150	10.2324
18	19.3133	12.4984	14.9094	14.9257
19	20.9614	17.6973	19.2189	19.2324
20	27.0821	21.0825	25.3981	25.4126
21	31.7522	27.5614	29.6479	29.6628
22	37.3935	32.7900	35.1967	35.2135
23	6.7237	3.9834	5.2880	5.3087
24	11.7027	8.1519	9.9584	9.9769
25	17.1018	13.6474	15.2813	15.2965
26	22.0734	18.3397	20.0968	20.1125
27	28.9131	22.8345	25.7761	25.7935
28	35.9331	27.0055	30.3555	30.3743
29	37.5665	32.7159	35.2393	35.2593
30	5.5772	3.3113	4.4083	4.4303
31	12.4687	7.4378	9.7509	9.7745
32	18.9945	10.8799	14.3822	14.4029
33	21.9869	18.0062	20.0871	20.1055
34	31.2135	20.3141	25.2500	25.2722
35	32.3502	22.5453	28.5447	28.5668
36	37.7888	32.6319	35.2964	35.3199

Selecting one test case to represent one pumping cycle was decided arbitrarily. A single pumping cycle for case 6 can be seen in Figure 6.10. This case presents a single

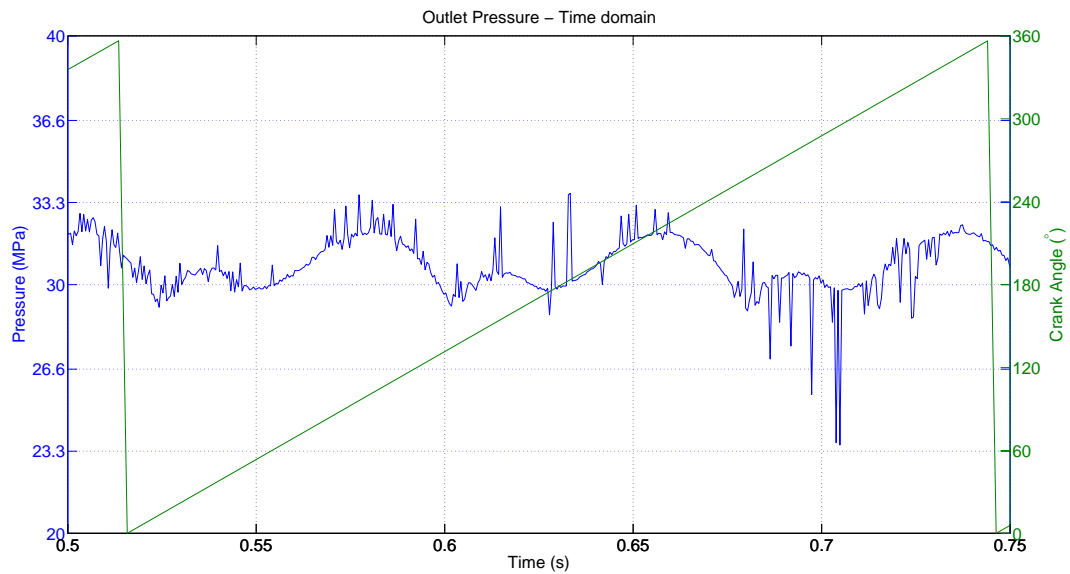


Figure 6.10: Outlet pressure during one pumping stroke in Test No. 6

pumping cycle recorded at the outlet manifold of the PD pump. The spikes in the time series data in Figure 6.10 could be a result of pressure sensor inaccuracy at acquisition speed of 10 kHz.

The frequency spectrum analysis for the outlet pump pressure was performed on the specified length of the signal. In Figure 6.11 dominant impact frequencies are displayed.

The peak with the highest energy, in Figure 6.11, correlates to the excitation frequency of the reciprocating plunger.

6.4.3 Internal chamber

Because of the highly transient pressure state inside a PD pump chamber and the passage from low suction to high discharge pressure there is a characteristic behaviour exhibited by the reciprocating motion of the plungers.

In Figure 6.12 pressure data was measured inside the individual PD pump chambers.

It can be seen that PD pump chambers have comparable performance to one another. The low pressure part of the cycle, seen during a suction stroke, is predominantly oscillating around 1 bar. Some difference can be seen at the middle cylinder where low pressure peaks fall below average pressure.

On the high-pressure side each of the cylinders exhibits three peaks where the middle

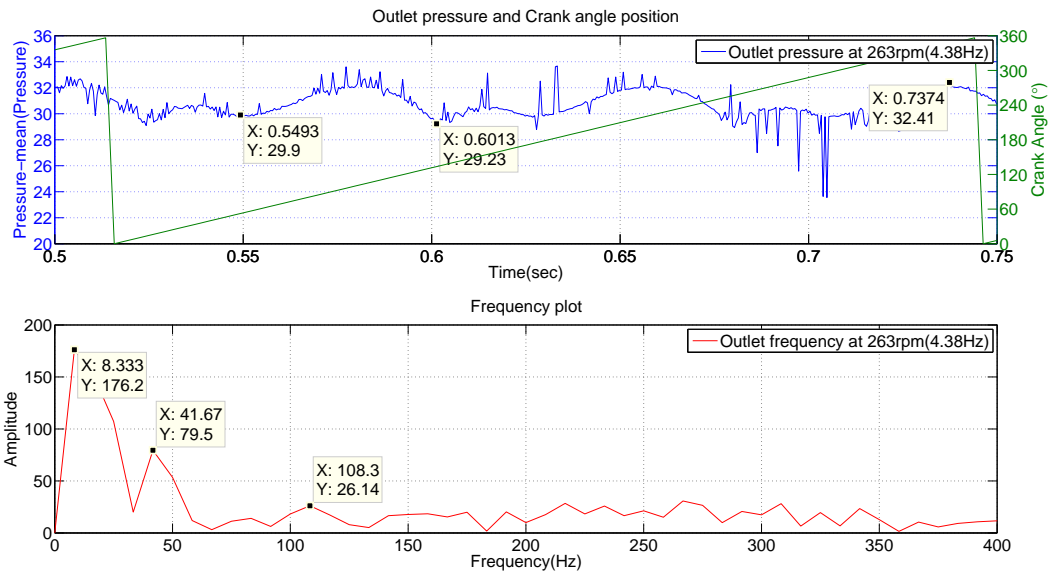


Figure 6.11: Frequency spectrum of the outlet pressure during one pumping stroke in Test No. 6

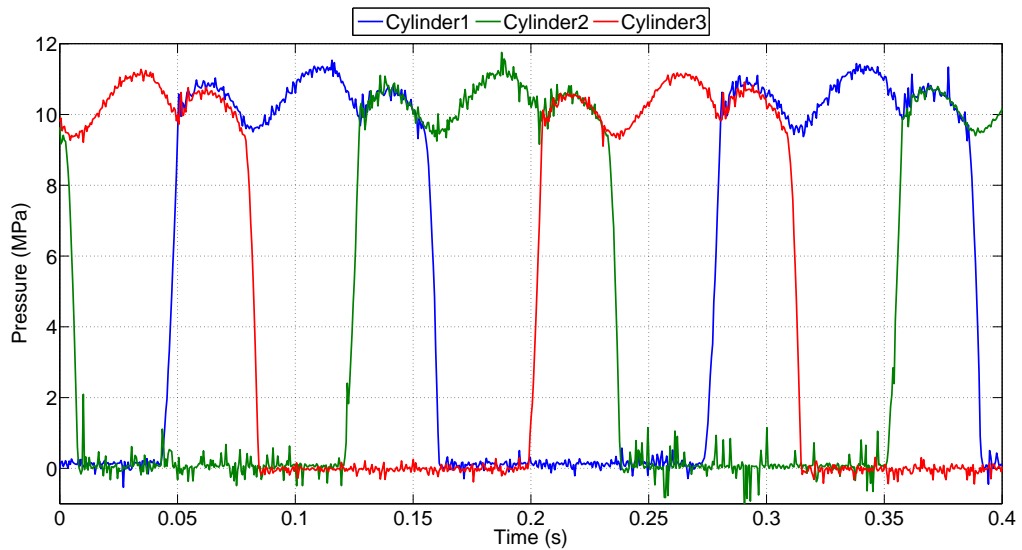


Figure 6.12: Chamber pressure from the internal side of the pump from all cylinders in Test No. 2

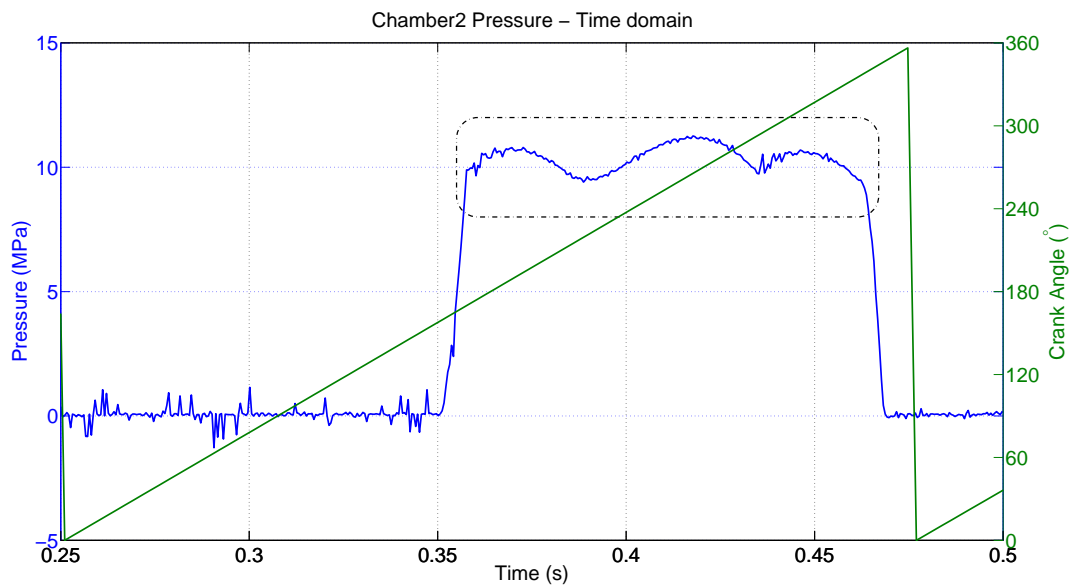


Figure 6.13: Chamber pressure from the internal side of the pump from only one cylinder in Test No. 2

peak is more dominant. Outlet pressure cylinder interaction can be seen in sections where the pressure patterns from two cylinders overlap.

The plotted pressure history of one PD pump chamber, together with the crank angle position of its reciprocating plunger, is shown in Figure 6.13.

A frequency analysis plot is displayed in Figure 6.14. Data was limited to the discharge part of the stroke, as shown in Figure 6.13 and subtracted from the mean value of the discharge pressure. In Figure 6.14 two plots display the manipulated time series and the evaluated frequency data. Results show that the most accented is the frequency of the plunger movement.

6.4.4 Flow rate

The second operational output from a PD pump is the flow rate. In the current setup the cumulative product of all three cylinders is recorded using a flow rate transducer. Due to the noisy signal output the results were averaged for ten recorded measurements at sampling rate of 1 kHz.

In Figure 6.15 the flow rate output from a triplex PD pump is presented.

The results show the accurate PD pump output which was compared to the number

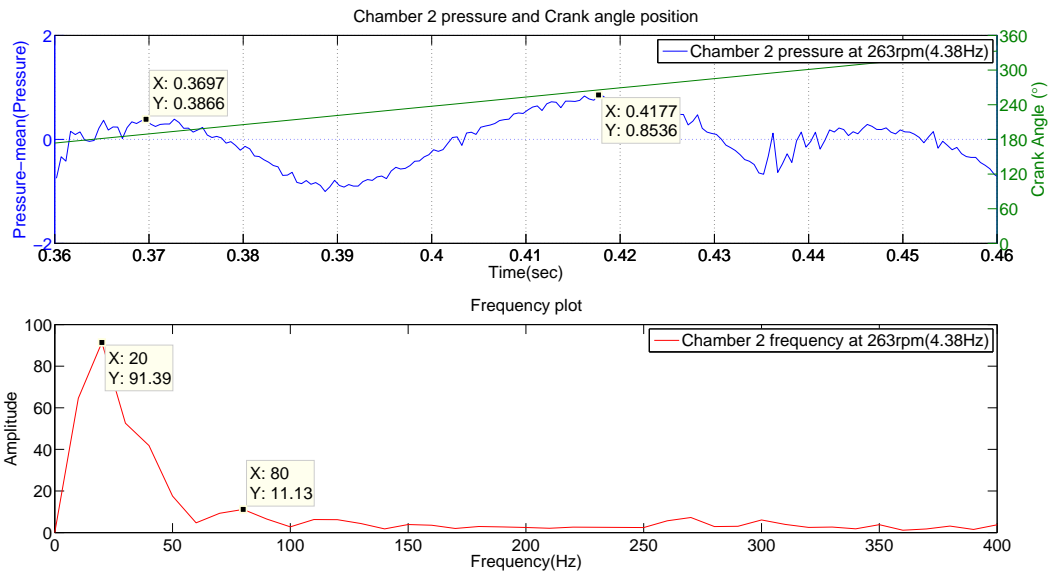


Figure 6.14: Frequency analysis in a single pressure chamber of a PD pump based on results from Test No. 2

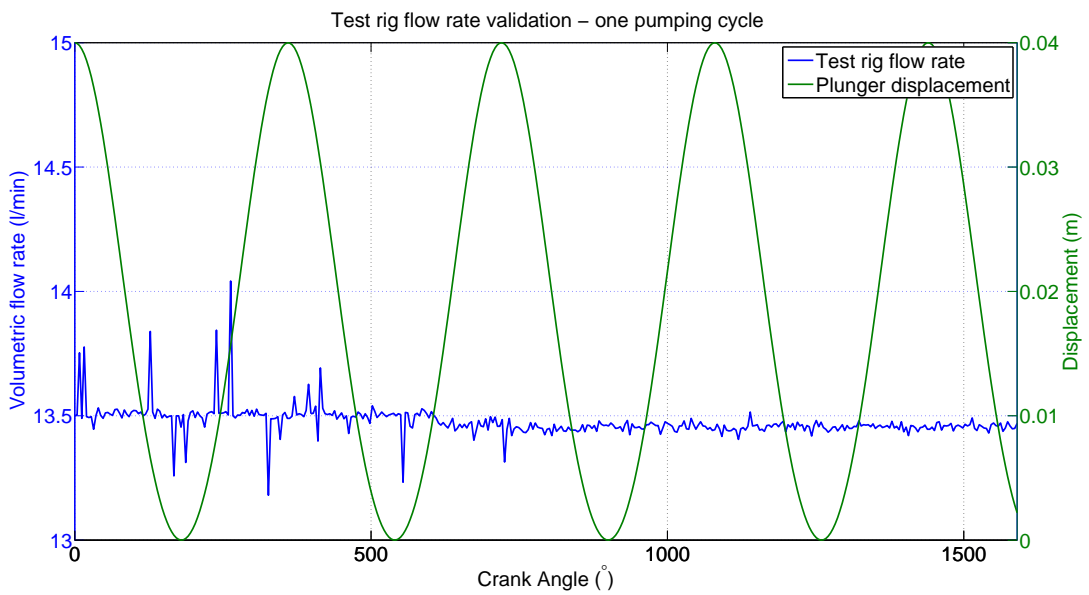


Figure 6.15: Overall volumetric flow rate output was measured and presented for the length of four pumping strokes.

of pumping cycles. In Figure 6.15, due to the position of the sensor in the hydraulic system, identifying an individual plunger action was not possible.

6.5 Summary

In this section the aim was to present the test rig design and advancements in the field of PD pump condition monitoring and control. The chapter was structurally divided into two parts; first the equipment selection, technical overview and operational functionality and the second data analysis, presentation and discussion.

Based on the operational practices seen in hydraulic fracturing a system design was selected to enable equipment scaling and process replication for a laboratory environment. Experimental priority was assigned to the scaled model of an original PD pump. Using the frequency variator and the pneumatic choke valve, the PD pump operates in a condition similar to the real fracturing site application. Owing to the fact that only one PD pump was tested the system interaction between multiple units was not evaluated which may be the subject for further development.

Performance metrics of a tested PD pump were classified into one of the three categories, pressure, speed and flow rate. Seven simultaneous measurements were made, four high-pressure (cylinder and discharge), one low pressure (suction), one flow rate and one plunger speed.

Results of the experimental model have indicated the following:

- Suction pressure is affected by individual plunger motion.
- Inlet pressure variation is influenced by the operating speed. At higher PD pump operational speeds the pressure variation will be higher. Pressure fluctuation could have possibly been avoided by using an additional pump to pressurize the inlet manifold.
- Discharge pressure displays a consistent number of pressure pulses during one pumping stroke. Discharge pressure variation does not indicate a relation to operating speed. Specific pressures show less peak-to-peak variation, for example 35 MPa shown in Figure 6.9.

- Speed measurement, using the digital pulse output, shows satisfactory results. Sensor measurements accurately correspond to the speed measurement displayed on the VFD. Aligning the crankshaft position with the speed pulse provided a precise indication of the plunger motion for an entire triplex PD pump.
- Flow rate measurement was designed to take into account the overall PD pump output. Recorded results accurately display the fluid flow rate. The initial expectation of being able to identify an individual plunger action was not accomplished. This may be accounted for by insufficient sensor accuracy or the complex flow in the discharge. A possible test rig modification could investigate locating the sensor on a different part of the hydraulic system.

Test rig model also enabled model validation comparison between Flowmaster[®] multi-cylinder design and the experimental setup, discussed in section 4.4

Experimental study has shown that reproduction of a full size PD pump is achievable in the laboratory environment. The ability to control external pressure state and PD pump speed from a local workstation enables operational flexibility that is not attainable in the field operation. Modularity of the PD pump test stand allows the addition of various instrumental measurements currently not possible in the field units. For example, the test rig was equipped with high speed pressure sensors on each of the cylinders and flow rate transducer, both of which are not used on PD pumps in the field. The test rig PD pump has a triplex design which could be modified for individual analysis of each of the chambers in isolation.

The next chapter quantifies the degree of correlation between the computational model, field and the test rig data.

Chapter 7

Validation

7.1 Problems and Opportunities

Before using the computational model to explore the design space it must be validated to ensure that it accurately predicts the behaviour of the system.

Measuring the model's accuracy will establish the level of the model's dependence on the experimental input. Quantifying the correlation factor will enable an estimation of the computational model's effectiveness.

7.2 Methodology

The validity of the results presented was established by performing a comparison study between two experimental tests and the results of the computational model. Research steps towards validating of the computational model consists of following:

- Choosing the appropriate statistical method to process the results
- Engineering evaluation of the presented data
- Discussion of results and identification of areas for improvement

7.3 Statistical model

The selected method for comparing the test cases and computational model was the Pearson's correlation coefficient, also known as the "product moment". This mathemat-

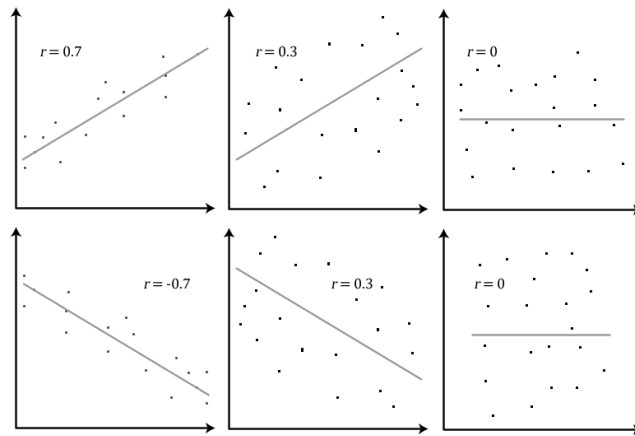


Figure 7.1: Theoretical understanding of the correlation value of product moment [125]

ical formulation evaluates the strength or the linear relationship between two variables of equal length.

The value of Pearson's correlation coefficient can vary from -1 to 1 where a value of zero indicates no association between the two variables. Positive and negative values of Pearson's correlation coefficient indicate different data association as seen in Figure 7.1. More detailed explanation of the importance of this measure is discussed by Taylor [124].

All the figures in this section, handling data comparison, will contain correlation coefficient factors embedded in the figure itself, expressed by r_{xy} . All values higher than 0.7 will be denoting strong correlation. Values between 0.3 and 0.7 are to be considered moderate in their strength and values below 0.3 can be regarded as weak.

Although the aim of this validation method is to confirm the accuracy of the model, which means comparison of the data in the same units of measurement, in reality this is not a limitation for Pearson's correlation coefficient. Variables can be measured in different units and a correlation can still be established. Pearson's correlation coefficient does not consider dependent and independent the variables as different.

Mathematical formulation of the Pearson's correlation coefficient is the covariance of the two examined variables divided by the product of variable's standard deviation.

The equation for Pearson's correlation coefficient can be simplified as shown in Equation 7.1. In this equation two data sets are assumed $x_1, \dots, x_i, \dots, x_n$ and $y_1, \dots, y_i, \dots, y_n$ each containing n data points.

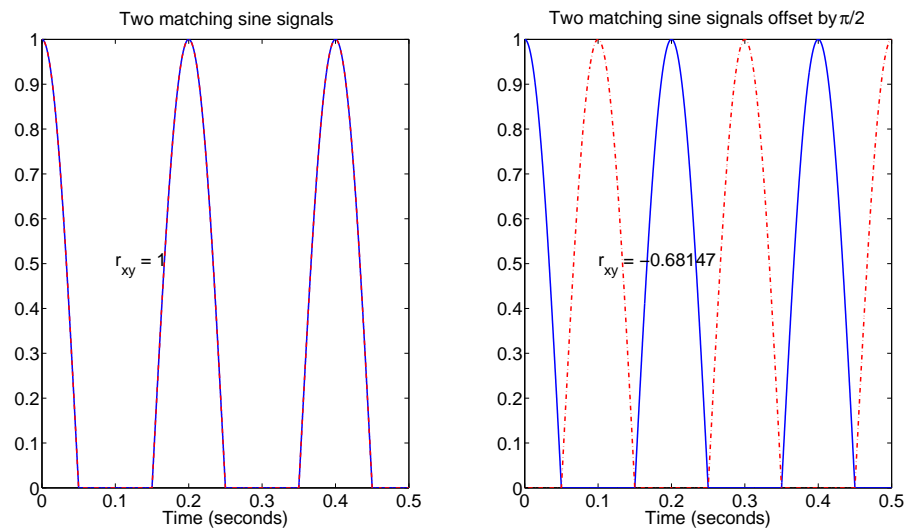


Figure 7.2: Problems with correlation coefficient in cyclic systems

$$r_{xy} = \frac{n \cdot \sum x_i \cdot y_i - \sum x_i \sum y_i}{\sqrt{n \cdot \sum x_i^2 - (\sum x_i)^2} \sqrt{n \cdot \sum y_i^2 - (\sum y_i)^2}} \quad (7.1)$$

Any uncertainty of this statistical method is its dependency on the precise phase synchronization of two examined models, an example of which is shown in Figure 7.2. Two identical signals were evaluated using Pearson's correlation coefficient. The results of which are embedded in the Figure 7.2. It can be seen that any phase offset can influence results significantly therefore it is important to align evaluated data sets in the best possible way.

7.4 Data analysis

Output from the computational model was compared against experimental and field data.

7.4.1 Suction pressure

Examining test rig data recorded on the inlet side of the pump and the computational model is the first step, Figure 7.3 shows correlation between the two data.

Data was plotted against crank angle and both y-axis show pressure values.

Table 7.1: Correlation data between test rig experimental and computational model for suction pressure

Suction pressure	mean	RMS	r_{xy}	RMSE $_{xy}$
Experimental rig	0.107	0.107	0.128	0.007
Model	0.110	0.110		

Table 7.2: Correlation data between field experimental and computational model for suction pressure

Suction pressure	mean	RMS	r_{xy}	RMSE $_{xy}$
Experimental field	0.358	0.359	0.491	0.054
Model	0.374	0.379		

Pressure field inside the suction chamber is expected to be influenced by the individual plunger motion. In the field data and the test rig data measurements triplex pumps were used, therefore, three transient pressure states are expected at equal offset of 120° of crank rotation.

First inspection of the data in Figures 7.3 and 7.4 shows higher level of pressure fluctuation in the test rig signal compared to the field data. In the test rig data, shown in Figure 7.3, three pressure spikes are identified at 30, 150 and 270 degrees of crank angle rotation which is associate with motion of individual plungers. Observed pressure fluctuation in the inlet manifold of test PD pump resulted in correlation data factor r_{xy} to be below 0.3 which indicates weak correspondence between the data. In Table 7.1 mean and RMS values show sufficient correlation between the experimental test rig and the computational model.

Suction pressure in the field conditions is affected by the complex system predominately influenced by the reciprocating plunger movement and the interaction from other elements of the hydraulic system. In Figure 7.4 association between computational model and the field data experiment is shown. In the field data pressure pulses are more recurrent with the exact phase offset of 120° of crank rotation.

In the field metrics inlet data, shown in Figure 7.4 was plotted for one pumping cycle so that all operational speed difference and time adjustments are avoided. The most accurate way of displaying and comparing results required data to be plotted with respect to crank angle.

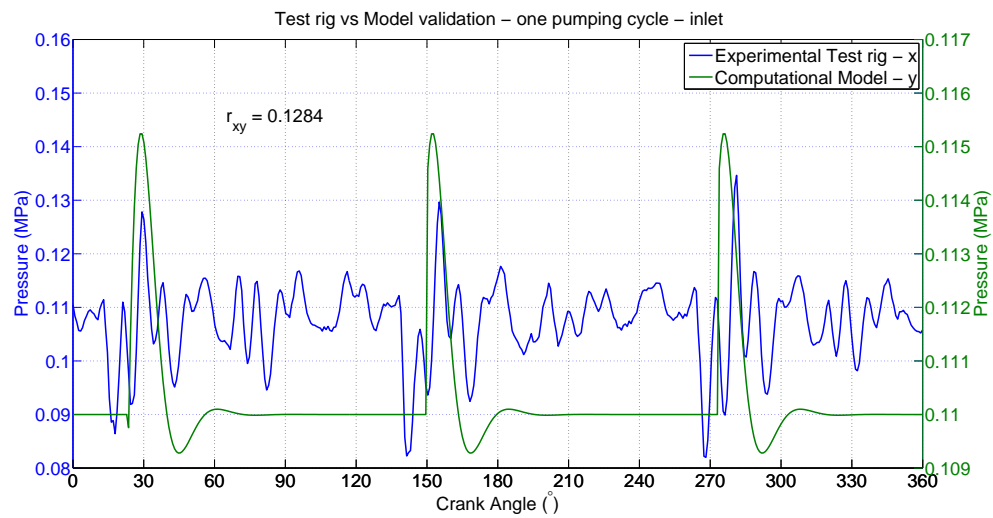


Figure 7.3: Comparison between test rig data and computational model. Correlation factor is stated as r_{xy}

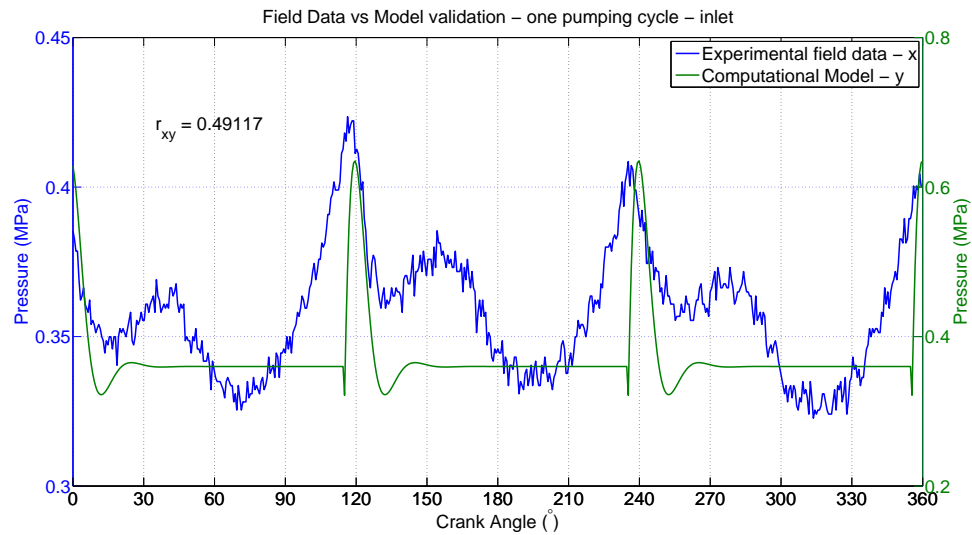


Figure 7.4: Comparison between the field data and the computational model. Correlation factor is stated as r_{xy}

The two dominant peaks associated with the plunger movement are synchronized and show a good relationship with the model. However the remaining part of the recorded field metrics were not captured in the computational model. The result of the correlation study, as illustrated in Table 7.2 is close to 0.5 which presents a moderate strength of correlation.

Table 7.3: Chamber pressure correlation data between the CFD and the computational model in a simplex PD pump

Chamber pressure		mean	RMS	r_{xy}	RMSE $_{xy}$
	CFD	46.01	55.29	0.989	4.757
	Model	46.09	55.85		

Table 7.4: Correlation data between experimental and computational model for chamber pressure

Chamber pressure		mean	RMS	r_{xy}	RMSE $_{xy}$
	Experimental	14.90	15.0937	0.988	1.16
	rig Model	14.47	14.76		

7.4.2 Chamber pressure

The profiles of the chamber pressure, suction pressure and discharge pressure are different. Essentially fluid phenomena inside the cylinder are creating a connection between the inlet and outlet by forming transition between low suction pressure and high discharge pressure.

A chamber pressure monitoring system is seldom carried out in the field operation. Results obtained from the actual hydraulic fracturing processes do not include internal chamber pressure, therefore this section will only look at the test rig experiments and the established CFD model discussed in section 4. The CFD model, previously compared in Figure 4.12, considers isolated chamber performance and the comparison between two models is shown in Figure 7.5.

The CFD model, developed for a simplex PD pump, considers the fluid pressurization due to the compressing action of the plunger without the added effect of chamber interaction. Plunger displacement is given on the right hand y-axis and it illustrates motion from BDC to TDC.

In Figure 7.5 pressure increase takes place after 180° and the main transient phenomenon can be seen in the oscillation (180° - 210°) prior to achieving pressure balance at the system's discharge pressure. The end of the discharge stroke sees the rapid pressure drop and the new cycle is reestablished. The computational model shows matching behaviour with a correlation coefficient of approximately 1 (which is considered high association between the two variables). Table 7.3 shows accurate model prediction of

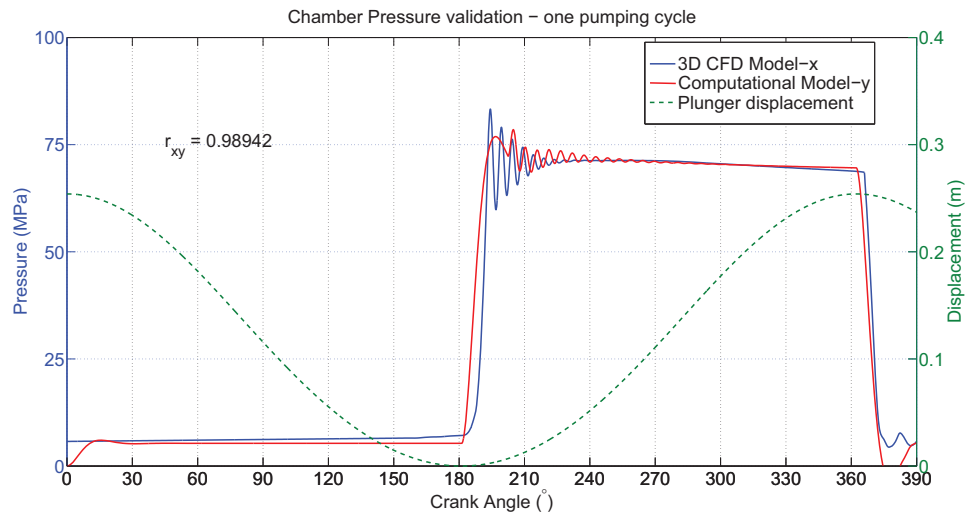


Figure 7.5: Cylinder pressure from the computational model and the more complex CFD design. Correlation factor is stated as r_{xy}

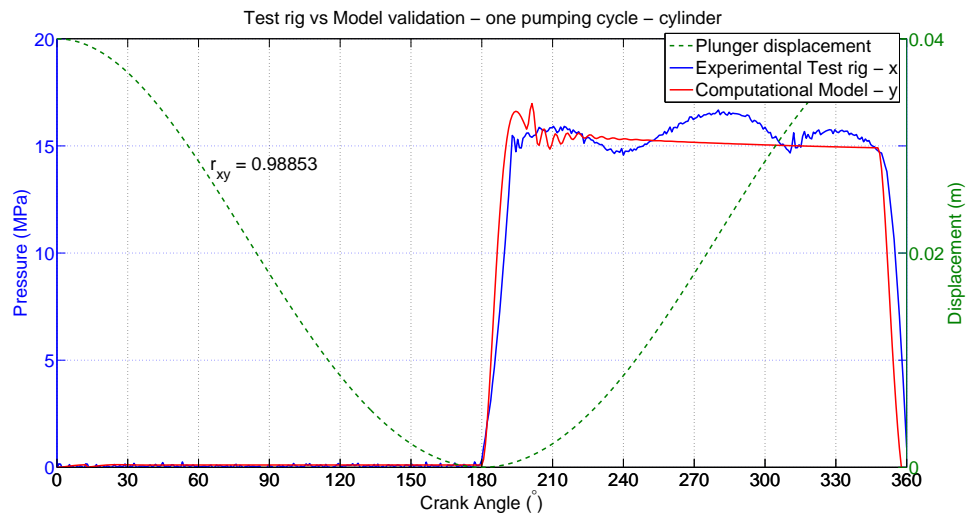


Figure 7.6: Cylinder pressure from inside one of the cylinders and its comparison to the computational model. Correlation factor is stated as r_{xy}

mean and RMS values.

The advantage of using a scaled size test rig was proved to be effective by enabling custom instrumentation, monitoring and control at different stages of a PD pump operation. Understanding cylinder performance will help establish an operating envelope to which all PD pumps need to be modelled.

In Figure 7.6 one pumping cycle is compared between the experimental test rig and the MatLab computational model of a simplex pump. Displacement motion is plotted on the right y-axis and for the comparison study the second (middle) chamber of the experimental PD pump was used. All chambers show close operational similarity as shown in Figure 6.12 and Table 7.4.

Plunger motion triggers a pressure increase in the chamber and Figure 7.6 illustrates a relationship between the computational model and the experimental data. Because the pressure trend in the computational model closely follows plunger motion and both sets of data are synchronized to the same operating speeds the correlation coefficient is high which denotes the high confidence between the experiment and the model.

A key difference in two sets of data is the outlet pressure value. In the CFD model the outlet pressure stays nearly flat during the discharge stroke due to simulation of the simplex (one chamber) pump. In reality, because of the multi-cylinder pump design, more than one plunger is compressing in one cycle of crankshaft rotation so the pressure field in the cylinder is dominated by other interfering elements, as explained in sections 2.5.1 and 4.4.

However, the same type of computational model was accurate enough to satisfy both single cylinder (simplex) and multi-cylinder (triplex) PD pump designs showing sufficient level of association. Increasing the precision of the model for demonstrating behaviour in multi-cylinder pumps will require more analysis and understanding of the accurate source for pressure variation seen in Figure 7.6.

A final chamber analysis was done for the triplex PD pump operating condition. In section 4.4 a 1D-CFD model was presented that takes into account the pressure interaction between chambers in PD pumps using Flowmaster[®] software. In Figure 7.7 a comparison was presented between the experimental results and the numerical model. Results show the correlation factor of 0.75.

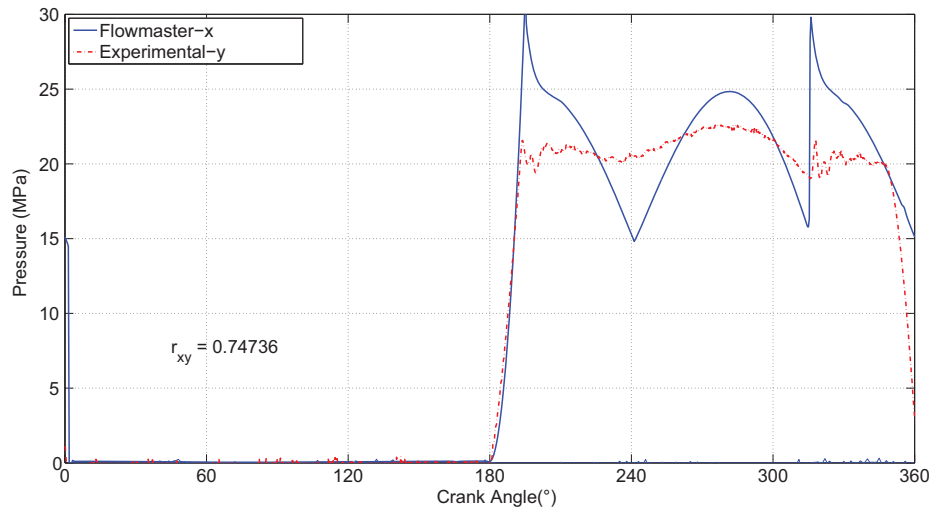


Figure 7.7: Comparison between one chamber numerical model and the experimental test rig in a triplex PD pump, correlation factor is give as r_{xy}

Table 7.5: Correlation data between experimental and computational model for discharge pressure

Discharge pressure	mean	RMS	r_{xy}	$RMSE_{xy}$
	Experimental rig	15.40	15.41	0.727
Model	15.36	15.40		

Examination of Figure 7.7 conclusion can be made that the pump design made using Flowmaster[®] overestimates pressure spikes and interaction between cylinders. Further model refinement could provide added fidelity to the multi-cylinder pump system.

7.4.3 Discharge pressure

The last section of pressure field appraisal in the computational model and experimental sets of data is related to the common discharge manifold located inside the PD pump. This section of the PD pump is directly connected to the downstream system so any change in pressure field downstream will affect the PD pump operation.

Evaluation the result will start by comparing the discharge pressure from a test rig PD pump to the computational model, shown in Figure 7.8. Both data sets (computational model and test rig results) are plotted against the crank angle to achieve sufficient accuracy.

The outlet pressure field is greatly dependent on the plunger velocity. A difference

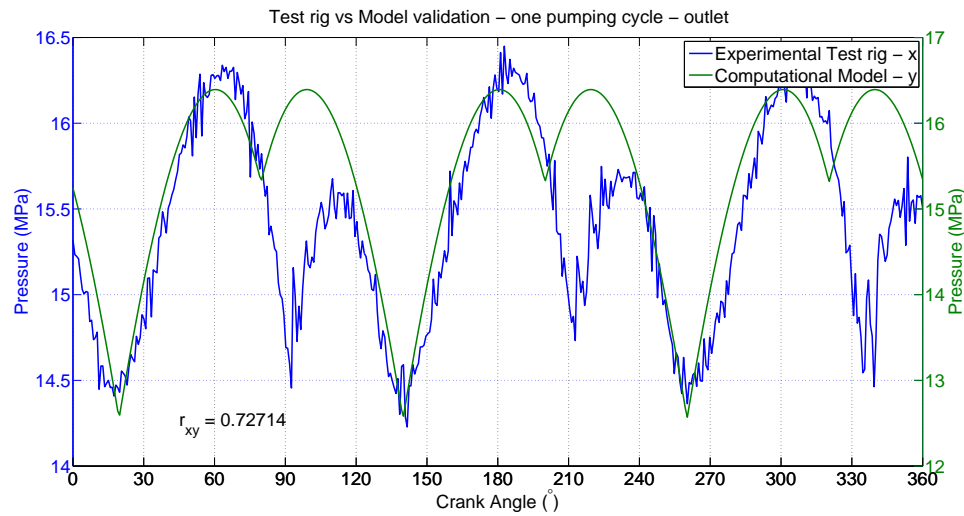


Figure 7.8: Outlet pressure from the test rig compared to the computational model. Correlation factor r_{xy} is 0.72

can be seen in the second pulse wave following the higher amplitude one. The model does not consider the variance between the two, clearly illustrated in the test rig data. The correlation factor presents a strong association between two sets of data, as shown in Table 7.5, which is satisfactory.

Following the same approach experimental field data is compared to the established numerical model. In Figure 7.9 one pumping cycle is illustrated and two sets of comparison data are plotted with respect to the crankshaft angle.

Unlike test rig data, where it was demonstrated that dominant pressure pulse is followed by a lower energy pulse, in the field experiment all discharge pulses vary in their intensity yet they are all equally spaced throughout one pumping cycle.

However, comparison between field data and the computational model shows weak association. Pressure drop seen at 0° , 120° and 240° , marking each plunger motion, is evident in both sets of data. Subsequently, results from correlation analysis illustrate this quite clearly. A factor close to zero, statistically speaking, signifies no relationship between data.

It is evident that analyzing field data on the outlet pressure chamber is more challenging. Owing to the fact that the pump is seldom operating isolated in the field it is fair to assume that there is a system influence on the presented results.

Despite the fact that Pearson's correlation coefficient shows insufficient association

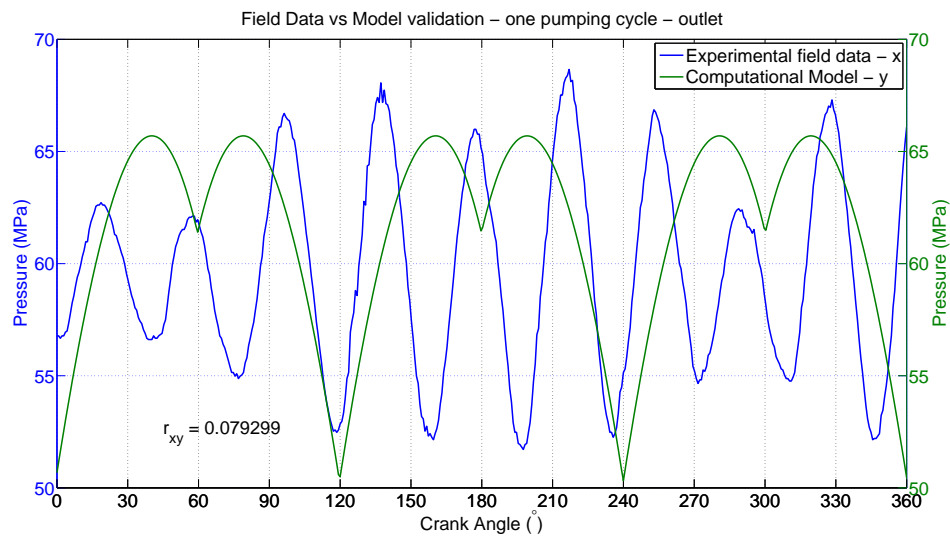


Figure 7.9: Outlet pressure recorded in the field and the computational model. Correlation factor is stated as r_{xy}

Table 7.6: Correlation data between the field data and computational model for discharge pressure

Discharge pressure	mean	RMS	r_{xy}	RMSE $_{xy}$
	Experimental field	59.60		
Model	61.57	61.72		

between the field experimental data and the computational model both mean and RMS values show consistency between the examined data sets as illustrated in Table 7.6. From the qualitative analysis standpoint the compared signals show similarities in amplitude variation, peak phase and mathematical mean value.

Several tests were conducted using a manufacturer's test facility (unconnected to a wellbore) in Texas and analysis of this data shows only three peaks per pumping cycle which, for the given operating speed, takes 0.46 seconds. Figure illustrating this test is given in the Appendix C.1.

Further optimisation model considers mean pressure output which means that the level of accuracy, of the discharge pressure, between field data and computational model should not affect the design accuracy.

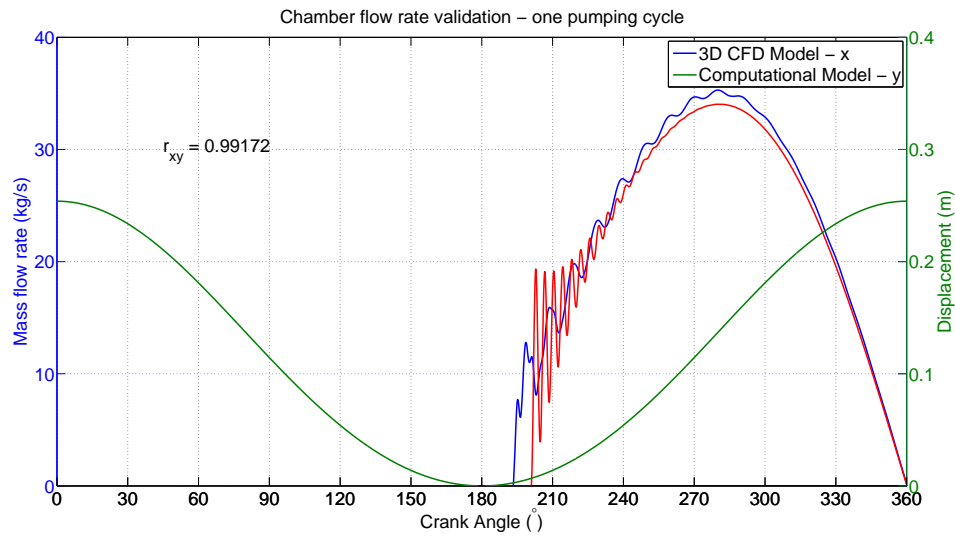


Figure 7.10: Comparing the computational model's flow rate response to the CFD. Correlation factor is stated as r_{xy}

7.4.4 Outlet flow rate

In addition to the pressure output mass flow rate is the second most important parameter in PD pump performance. Depending on the applications high-pressure or high-flow capacity may be required. In hydraulic fracturing both are critical and high demand is mandate for a specific part of the process.

Validation of mass flow rate is more demanding and challenging to measure and analyse especially if the effect of chamber interaction is to be taken into account. Mass flow is, in theory, related to plunger motion. The computational model relies on the reciprocating motion of the plunger to produce the integral of flow rate. In Figure 7.10, previously examined in Figure 4.11, a theoretical computational model is compared to CFD. Correlation coefficient shows a strong association in all aspects between the numerical computational model and the CFD simulation, shown in Table 7.7.

Measuring flow rate from the experimental test rig can only be achieved by accounting for the cumulative output from all three chambers. Discharge flow rate is the function of each of the plunger's reciprocating motion and the swept internal volume. Figure 7.11 shows flow rate measurement from the experimental test rig.

Data illustrated in Figure 7.11 shows approximately four pumping cycles, previously presented in Figure 6.15. Flow rate measurements obtained from the experimental

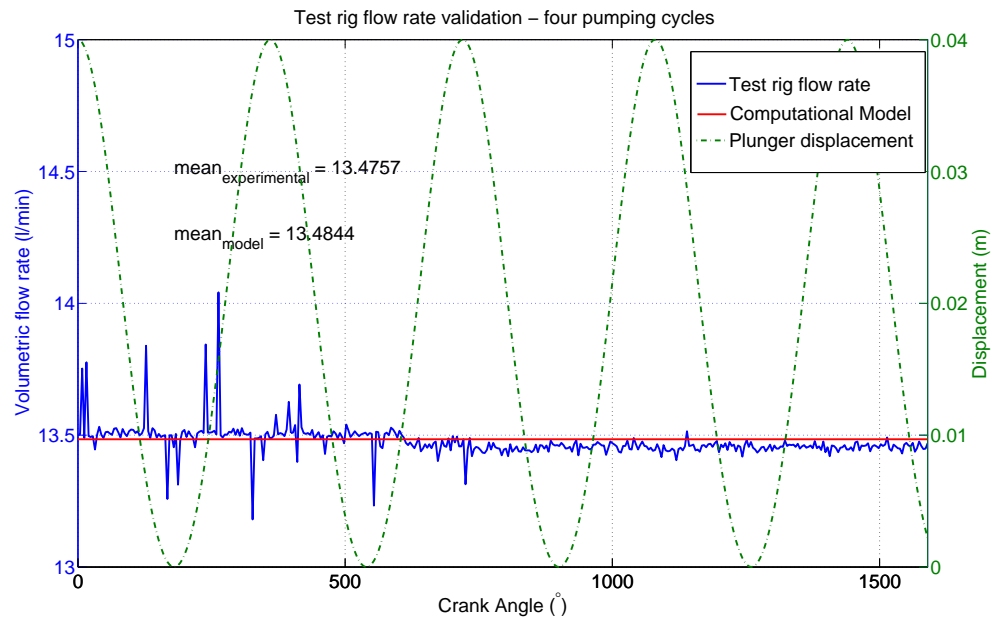


Figure 7.11: Comparing the flow rate from the test rig to the computational model. Correlation factor is stated as r_{xy}

Table 7.7: Correlation data between experimental and computational model for chamber flow rate

Chamber flow rate		mean	RMS	r_{xy}	$RMSE_{xy}$
	CFD Model		23.63 22.60	25.55 24.76	0.991

rig were averaged every ten values. The model is calculating integral value from all three cylinders and value is presented in litres per minute. The model is therefore outputting constant value at one operating speed. It can be seen in Table 7.8 that mean values show a well matched association between the computational model and the experimental test rig, up to a second decimal point (centilitre). The correlation coefficient was not applicable in the analysis as the computational model's constant average and recorded test rig data do not show same transient changes.

Table 7.8: Correlation data between experimental and computational model for discharge flow rate

Discharge flow rate		mean	RMS	r_{xy}	$RMSE_{xy}$
	Experimental rig		13.47	13.47	N/A
Model		13.48	13.48		

7.5 Summary

In conclusion, this chapter analyses, compares and discusses the results from the test rig, field data and computational model that were presented in earlier chapters (4,6 and 5). Key emphasis, in this chapter, was given to pressure and flow rate examination with one section covering relationships between the computational model and CFD data.

By identifying the statistical method a comparison between the experimental and numerical models was carried out. The operation was examined for one pumping cycle by measuring suction pressure, discharge pressure, chamber pressure and the output flow rate. Results show different levels of numerical association between the computational model and the experimental tests. Summary of all the individual validation data sets and their relationship to the computational model are listed as follows:

1. Field data comparison

- Results from the field data show moderate correlation to the computational model.
- Suction pressure shows good correlation to the computational model owing to the fact that a pressure spike is triggered from an oncoming plunger.
- Discharge pressure from the field unit shows an increased number of pressure peaks compared to results obtained in the lab setting.
- Peaks in the field data appear to be equally distributed during one pumping cycle.
- Chamber pressure was not measured in the field operation so could not be compared.
- Flow rate in the field condition is a function of PD pump speed. No physical measurements of flow rate are currently being carried out in the field, so again these could not be compared.

2. Test rig comparison

- Suction pressure from test rig data shows a highly oscillating trend and only some amplification can be seen at the points associated with the plunger

motion. The computational model is only accounting these timed 120° spikes as important operational variations.

- Discharge pressure from all cylinders matches the computational model verified with the high correlation factor.
- Chamber pressure in a triplex PD pump computational model shows more pronounced peak-to-peak variation compared to experimental test rig. Correlation was satisfactory.
- Chamber pressure in a simplex PD pump shows higher correlation coefficient to test rig's triplex PD pump due to less pressure variation in the computational model
- Test rig data shows satisfactory relationship compared to computational model.
- Flow rate measurement satisfies the evaluation criteria.

3. CFD comparison

- The majority of the approaches used for designing a computational model are similar to those employed in the complex CFD model.
- Chamber pressure for a single-cylinder (simplex) PD pump models shows strong association between CFD and the developed computational model.
- Mass flow rate for a simplex PD pump design indicates satisfactory correlation between CFD and the developed computational model.

In conclusion, validation between the different research domains proved to be very useful for quantifying the current level of fundamental understanding of PD pump performance. The aim was to evaluate an analytical model and compare it with experimental data obtained from the field data and a laboratory test rig. Field data contains valuable details, suction pressure and chamber pressure match well with the developed model. However, it raises questions related to the influence of the downstream discharge and the upstream suction system on an individual PD pump. The resolution of the identified issue exceeds the scope of this project.

Comparison between test rig data and the computational model shows satisfactory relationship. Chamber pressure, discharge pressure and outlet flow rate all show sufficient degree of accuracy in numerical and experimental simulation. Suction pressure proved to be extensively variable in the experimental test. Although the overall low pressure did not cause any cavitation future test rig development should consider priming the suction side of the PD pump (i.e. boosting suction pressure) to assess the nature of suction pressure fluctuation.

The computational model shows strong correlation to CFD results.

The overall conclusion is that the simplex model can reasonably be used for the optimisation study but the results must be understood to be limited until a full understanding of the pump's interaction with manifold and wellbore are available.

Chapter 8

Optimisation study

This chapter presents two optimisation studies: first for a single pump and then for a multi-pump system. Although Monte Carlo is used in both cases the first uses the computational model (detailed in Chapter 4) while the multi-pump study uses an approximate analytical model to represent the system's response to key design parameters.

Figure 8.1 illustrates schematically how parameters such as pumping pressure, speed, plunger diameter, stroke length and rod load all interact. The objective of the work reported in this chapter is to find the best combination of values. In other words could there be scope within the design space to select values that result in a smaller more compact pump more appropriate for the European transport specification, environmental and societal constraints? To investigate this thesis a numerical model was used to systematically explore the system's design space with the aim of optimising the size of the reciprocating components for a given pressure and flow.

This process of multivariable analysis has five steps:

1. Identify the functional requirements (i.e. specification) of a hydraulic fracturing pump
2. Define the system's model
3. Coarse grid exploration of the design space
4. Identification of possibilities for system improvement
5. Finer grid search through Monte Carlo optimisation

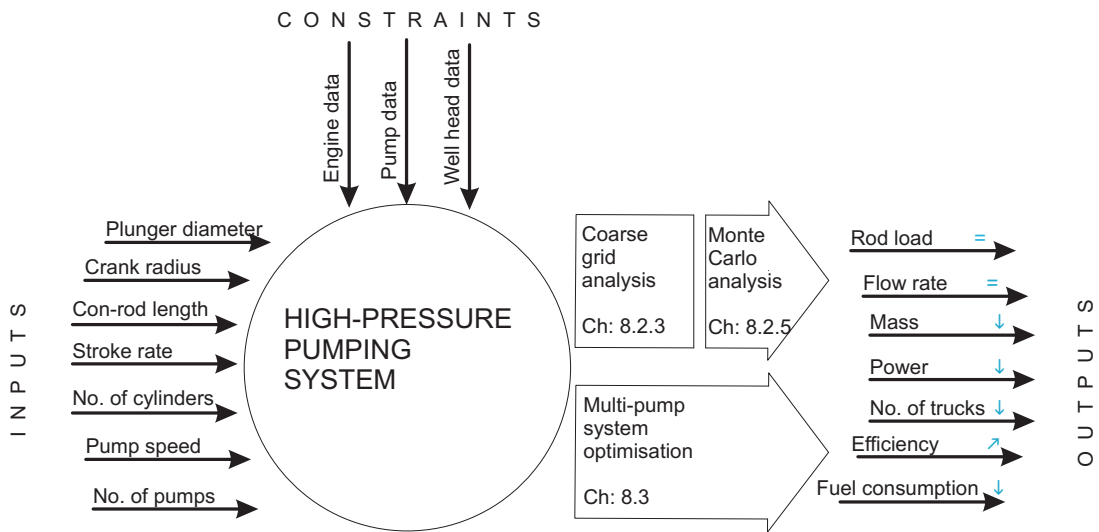


Figure 8.1: Process map for developing optimisation algorithm in high-pressure pumping systems

8.1 Hydraulic fracturing: functional requirements

To investigate the impact of the optimised design on a hydraulic fracturing process case studies are used. The mechanical properties associated with a rock formation in Woodford basin (Oklahoma) are summarized in Table 8.1[53]. Zhang [126] presents an “energy” study for which typical hydraulic fracturing was modelled using the STIMPLAN software [127]. The reservoir properties in the [126] study are similar to the recorded reservoir data used in our model. The analysis in this chapter will use a single stage in “Well 3’s” stimulation program, shown in Table 2.1, as a representative example for energy estimation.

8.1.1 Pumping period

The pumping rate for a single stage of hydraulic fracturing will be determined in advance of the propagation phase. The overall time is influenced by the size (width, depth and length) of the well and the mechanical properties of the rock (determined by rock type and depth). For this case study the time of the stage is set to 210 minutes (experience in North American shale reservoirs suggest that this estimate is toward the upper limits of a pump stage, i.e. longer than the average time required).

Formation Details—		Well 3 - Shale properties		
Formation	Woodford	Parameter	Variable	Value
Lithology	Shale	Depth (m)	H	4,649
Top MD(m)	3,522	Poisson's Ratio	ν	0.2
Bottom MD(m)	4,649	Vertical stress (kPa/m)	σ_v	0.2
Pore pressure (kPa)	39,330	Poroelastic constant	α	0.8
Pore pressure (ppg)	9.8	Pore pressure (kPa/m)	p_r	11.51
Fluid content	gas	Max. Horizontal stress (kPa)	σ_{Hmax}	72,180
Frac gradient	0.72	Tensile strength (kPa)	T	1,722
Total pump power requiremntns(kW)	14,155			
Breakdown pressure (kPa)	62,100			

Table 8.1: The case study shale formation properties are listed. This case study is used to quantify the potential impact of the optimal pump design. Values for North American shale are used due to lack of available data for European shale.

8.1.2 Pump pressure

The formation's breakdown pressure for this experimental well can be derived from equation 2.7 using the parameters in Table 8.1, and is approximately 62 MPa.

$$p_b = 3 \left[\left(\frac{\nu}{1-\nu} \right) (\sigma_V - \beta p_r) + \beta p_r \right] H - \sigma_{Hmax} + T - \beta p_r H = 62 \text{ MPa (9,000 PSI)} \quad (8.1)$$

For our case study, propagation pressure (p_p) is therefore approx. 43MPa (assuming a 30% reduction of the breakdown pressure). This pressure will be maintained throughout the propagation stage.

8.1.3 Flow rate

The total volume of liquid required for the fracturing operation (over the chosen 210 minute period) needs to be estimated to determine the magnitude of the flow rate. The total volume is the sum of the volume of liquid needed to fill the bore, calculated using equation 2.11 and the volume needed to push the proppant into the rock fissures. In order to calculate the volume of the production well casing it is necessary to define

both the measured depth of the well and the casing diameter. The standard production casing diameter is 73 mm ($2\frac{7}{8}$ ""). Using equation 2.11 the calculated volume of the well bore is 19,500 l. The combination of the calculated casing volume and the recorded field data suggests the total volume of pumped fluid for this example well stage is approximately 2.45 ML. It is interesting to note that the casing volume is only 0.7% of the overall fluid needs. In other words the casing volume is negligible compared to the quantity of fluid pumped into the rock during the fracture propagation stage.

The entire hydraulic fracturing process can be modelled using the calculated volume requirement parameter and formation breakdown pressure.

8.1.4 Pump Requirements

The pump pressure needed to fracture this well (62 MPa) is obtained from the mid-range of the performance curve of the pump, Figure 2.25b, confirms that the optimised pumps will be capable of delivering this required pressure to the wellbore. Given that the volume of liquid needed is approximately 2.45 ML and the time to deliver this volume is 210 minutes, the pumping rate must be 16,000 l/min. To generate this flow, a total of 14 positive displacement pumps would have to be used in parallel requiring a power of 25 MW.

8.1.5 Environmental Footprint

Having determined the overall fluid volume needed to fracture a single stage in the example well, and the number of pumps required to achieve these flow rates, it is important to consider the physical issues of delivering the equipment to site. One of the principal impacts on the local community is nuisance (noise and traffic) and air pollution from trucking [92]. Additionally, road traffic accidents (and subsequent spillages of e.g. frac-chemicals) are one of the most likely risks to the environment posed by hydraulic fracturing operations [5]. Thus the infrastructure for equipment delivery to the site has important implications for the environmental and social impact of hydraulic fracturing activities, which operators should seek to minimise.

A tanker, in accordance with EU road legislation [60], is able to transport a maximum of 32,000 litres of water or petrol (this volume is limited by mass restrictions). For

this case study, 78 water tankers would be needed to transport the required amount of fluid (outlined in section 8.1.3) to the well location. There will be additional trucks to transport the frac-chemicals and proppant - the volumes of which will be proportional to the total fluid volume pumped. However, the volume of both sand and chemicals required are an order, or even two orders of magnitude smaller than the water needed as discussed in section 2.2.4.

Due to strict road (load) and transport regulations, pump manufactures and final assembly companies are very conscious of the physical size of the frac-trucks. Council Directive 96/53/EC [60] specifies a maximum authorized dimension for national and international road traffic. Similarly pump assembly manufactures specify maximum overall dimensions of their units [59] to fit the size limits. These limits (designed for the North Americas) are approaching the very limit of the acceptable range for the European roads.

8.1.6 Case study summary

The mechanical properties of the rock and the time scheduled for each stage of the hydraulic fracturing largely dictates the amount of pumping hardware required. While it may be preferable to process a stage in a shorter time (for economic reasons and to reduce the period disturbance to local environment), doing so would require more pumps in operation at a given time. For the purpose of this study, an example of a hydraulic fracturing process from North America has been adopted. For this operation, 2.45 Ml ($2450 m^3$) volume of liquid must be delivered to the rock over a period of 210 minutes, requiring pump flow rates of 16,000 l/min. All the positive displacement pumps on the site individually must be capable of exceeding the formation breakdown pressure (62 MPa in this case study).

After the breakdown phase, pumping shifts from a low speed, high-pressure regime to a high speed, high flow rate (the propagation phase). The pumping profile associated with this case study is shown in Figure 8.2, which details the fluid pressure, flow rate and fluid density requirements. The case study demonstrates that an optimised pump could deliver adequate pressures and flows for a typical job.

The number of pumps and their duty cycle can be used to determine the power

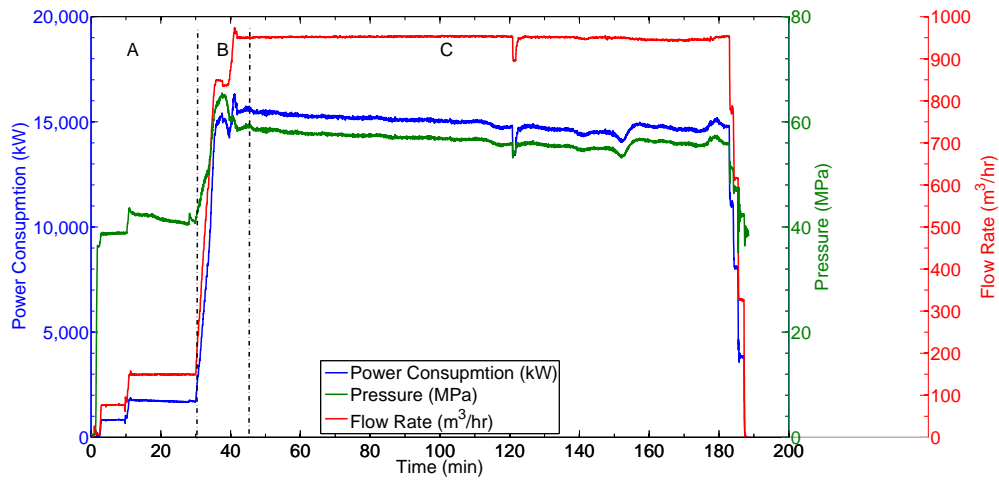


Figure 8.2: Experimental case study values (obtained from North American well stimulation operations) used to determine pumping requirements for hydraulic fracturing [53].

needed to run the site. These will determine both the traffic and environmental footprint of a single hydraulic fracturing stage. All the other variables present in the process such as sand and chemicals are affected by the size of the reservoir and the total water requirements.

8.2 Single pump optimisation

The following section details each step of this process.

8.2.1 Current design

Identifying performance parameter values from the current equipment performance is the first step in developing full multivariable analysis. Figure 8.3 shows hydraulic horsepower (HP) curve and the key design parameters used as a starting point for our analysis.

8.2.2 Model

A mathematical model, detailed in sections 4.2 and 4.3 was used to explore the design space using the parameters illustrated in Table 8.2.

The system's outputs are rod load (i.e. cylinder pressure) and flow rate. The rod

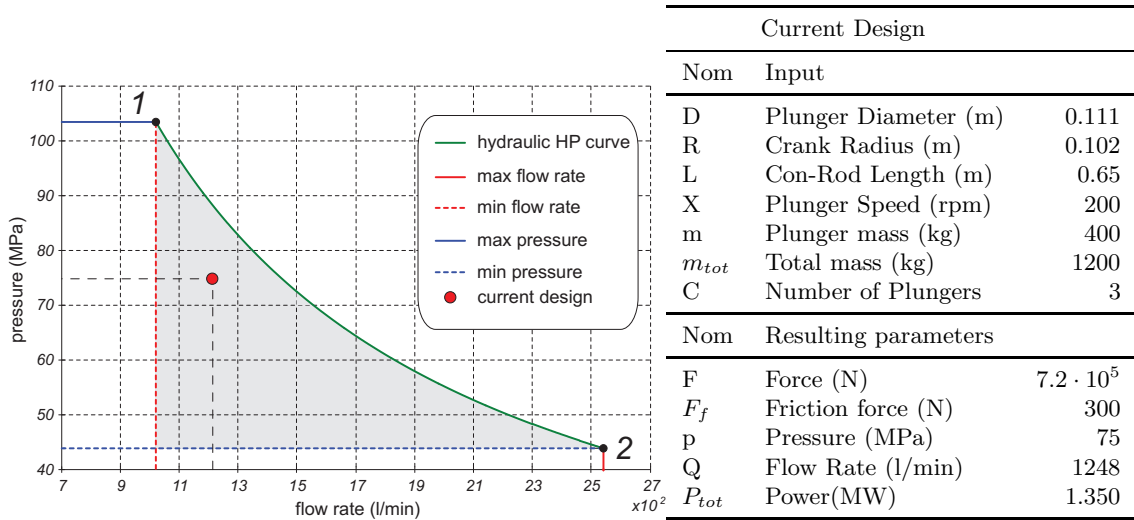


Figure 8.3: Pump’s operating range is shown in grey. Focusing on single operating point helps identify how can series of inputs and outputs be improved.

Table 8.2: The ranges of values used in the initial coarse grid exploration analysis to identify the range of performance values in current pump design.

INPUT					OUTPUT	
Description	Var.	Current Design.	Min	Max	Descr.	Var.
Plunger Diameter (m)	D_i	0.111	0.008	0.134	Rod Load	RL
Crank Radius (m)	R_j	0.102	0.01	0.164	Flow Rate	Q
Con-Rod Length (m)	L_k	0.650	0.05	0.750		
Stroke Rate (RPM)	X_l	300.0	100.0	700.0		
Number of cylinders	C_o	3	1	12		

load is a cyclic function dependent on the plunger placement during the operating phase. The rod load variation over one pumping cycle is shown in Figure 2.25c and modelled using equation 8.2.

$$RL(IN_{ijkl o}) = \frac{D_i^2 \pi}{4} \cdot \sin\left(\frac{2\pi \cdot X_l \cdot t}{60}\right) \cdot p \quad (8.2)$$

Similarly, flow rate also varies with the cyclic piston movement during the compression stroke. Integrating the discharge flow gives a single value that is associated with the internal displaced volume (Q), Figure 2.25a. The displaced volume from three cylinders over specified time (t) is defined by equation 8.3 (which assumes that there are no losses in the volumetric efficiency.)

$$Q(IN_{ijkl o}) = C_o \cdot \frac{D_i^2 \pi}{4} \cdot \left(-R_j \cdot \sin\left(\frac{2\pi \cdot X_l \cdot t}{60}\right) - \frac{R_j^2 \sin\left(\frac{2\pi \cdot X_l \cdot t}{60}\right) \cos\left(\frac{2\pi \cdot X_l \cdot t}{60}\right)}{\sqrt{L_k^2 - R_j^2 \sin^2\left(\frac{2\pi \cdot X_l \cdot t}{60}\right)}} \right) \cdot 998.2 \quad (8.3)$$

8.2.3 Coarse grid exploration study

Every combination of the five input parameters was generated (equation 8.4) [128] by incrementally varying them between minimum and maximum values that represent physical or functional limits to that quantity. Table 8.2 shows the values used in coarse grid exploration. Step size is 1% of the range.

$$IN_{ijkl o} = (D_i \quad R_j \quad L_k \quad X_l \quad C_o) \left|_{i=1}^{i=n_1} \right|_{j=1}^{j=n_2} \left|_{k=1}^{k=n_3} \right|_{l=1}^{l=n_4} \left|_{o=1}^{o=n_5} \quad (8.4)$$

The values of the connecting-rod length and crank radius are constrained by the ratio limit. Therefore, some values of $IN_{ijkl o}$ were excluded. The following equation

8.5 defines the combinations of parameters excluded by this design constraint.

$$IN_{ijkl o} = \left\{ D_i, R_j, L_k, X_l, C_o \mid \frac{L_k}{R_j} \leq 5.2 \text{ and } \frac{L_k}{R_j} \geq 2.8 \right\}$$

Where: (8.5)

$$i = 1 \dots n_1, j = 1 \dots n_2, k = 1 \dots n_3,$$

$$l = 1 \dots n_4, o = 1 \dots n_5.$$

The final multivariable space of possible PD pump designs can be represented as an array of input and output values, equation 8.6.

$$\begin{pmatrix} IN_{11111} & RL(IN_{11111}) & Q(IN_{11111}) \\ \vdots & & \\ IN_{1111n_1} & RL(IN_{1111n_1}) & Q(IN_{1111n_1}) \\ \vdots & & \\ IN_{n_1n_2n_3n_41} & RL(IN_{n_1n_2n_3n_41}) & Q(IN_{n_1n_2n_3n_41}) \\ \vdots & & \\ IN_{n_1n_2n_3n_4n_5} & RL(IN_{n_1n_2n_3n_4n_5}) & Q(IN_{n_1n_2n_3n_4n_5}) \end{pmatrix} \quad (8.6)$$

A discrete fixed step approach was adopted because incremental changes to the output (i.e. no step changes) make the impact of the parameters easier to distinguish.

8.2.4 PD pump design space results

Initial evaluation of the design space was done using five parameters. The fixed step size produced a characteristic design area in which incremental parameter alteration provided a specific result feature.

The results show that a wider plunger is associated with a relative increase in rod load as the pressure rises. Similarly, it is unsurprising that the stress on the crankshaft increases as the plunger area increases, where stress ultimately limits the maximum operating pressure. Since energy changes in the design parameters (i.e. plunger diameter, crank radius, con-rod, etc.) will result in different output characteristics, four areas of output characteristic can be identified in Figure 8.4.

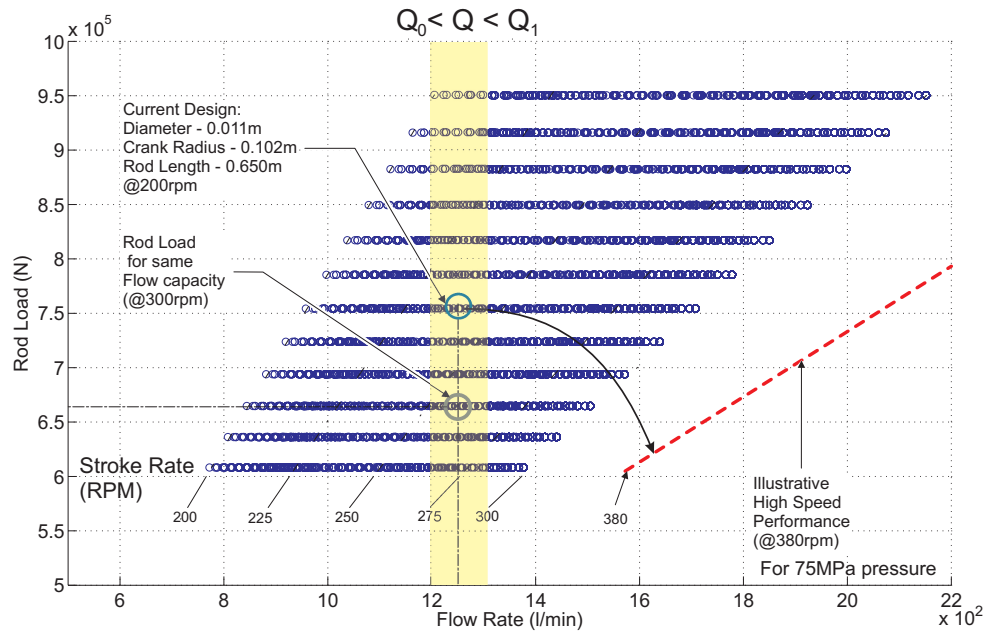


Figure 8.4: In this figure the current operating range was located with pump parameter plot for constant pressure. Each horizontal line is associated with a different plunger diameter. Similarly, each sloping vertical line presents a different speed parameter. The area highlighted in yellow presents boundary limits for the next phase of the optimisation

- Large plunger area and low speed (top left corner of Figure 8.4): low flow and high rod load performance.
- Medium - large plunger area and a range of speeds (top right corner of Figure 8.4): large variations in rod load and flow rate.
- Small - medium plunger area and mid to low speed (bottom left of Figure 8.4): relatively low rod load and low flow rates.
- Small - medium plunger area and high speeds (bottom right of Figure 8.4): relatively low rod load and high flow rates

For each area, the parameters can be expanded to explore in more detail the possibilities of different pump designs.

Low-order equations in the coarse grid optimisation study did not provide solution with local optimum between sample points. Increasing the number of evaluated data points in a more restricted design space will be the objective of the upcoming fine grid Monte Carlo analysis.

8.2.5 Monte Carlo optimization

The aim is to maximize flow rate while minimising the rod load. An optimized design needs to be able to deliver both high-pressure capability and sufficient flow capacity. Indeed, the flow rate of the pump is a significant factor in the overall time taken for a stage.

The next step would be to identify the possibility for obtaining the same level of performance with the improvements in the equipment footprint. This is to be achieved by running another simulation with the system's objective functions defined. The second phase of the multivariable analysis involves a more detailed exploration of the reduced parameter space identifier through the previous coarse grid search, section 8.2.3.

Optimisation was done using a Monte Carlo analysis with filtering to provide information about model sensitivity and parameter ranges around optimum values. The process has three distinct steps:

- Exploration of the reduced parameter space using a Latin Hypercube,
- Filtering and weighting the simulation according to the chosen criteria,
- Inferring the posterior distributions for each parameter according to the calculated weights.

The filtering has been conceived in order to explore the possibilities for improving the current design while maintaining the same performance output (i.e. flow rate). The flow rate represents the first objective function, boundaries for $(Q(ijkl))$ must be defined and only simulations returning flow rate values within the limits defined in equation 8.7 and highlighted in Figure 8.4 are to be retained.

$$Q_0 < Q(ijkl) < Q_1 \quad (8.7)$$

Values Q_0 and Q_1 present an acceptable range for the new design. These values are centred around the current operating range shown in Figure 8.3, where $Q = 1,4721/\text{min}$.

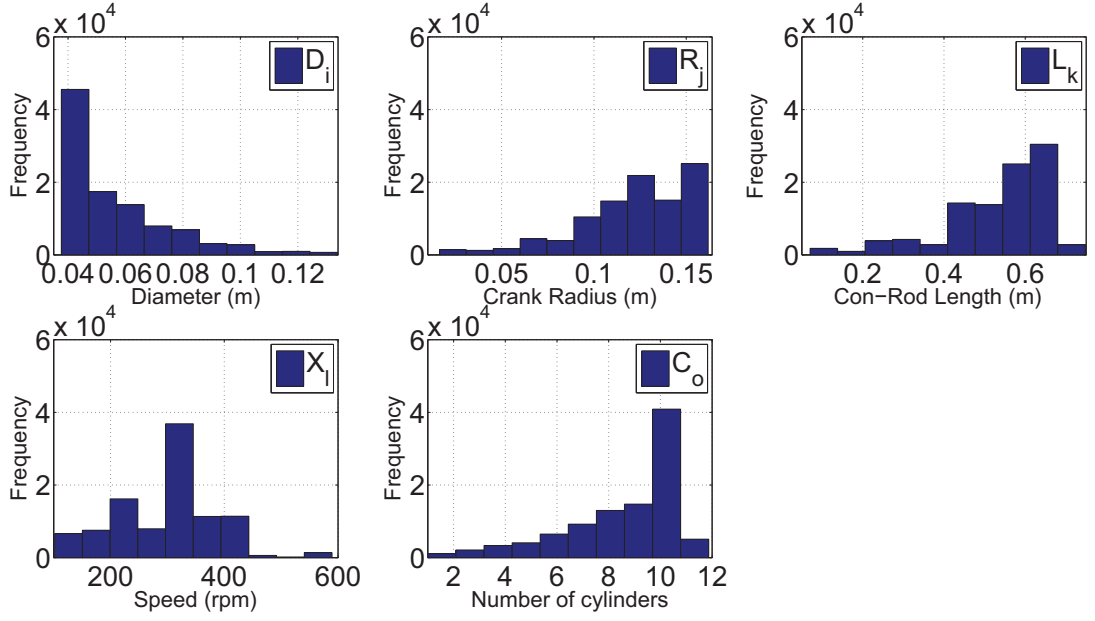


Figure 8.5: Histograms of the evaluated data. Four histograms identify optimum values for best performance. Con-Rod length is not as important as other variables because it is equally uniform in posterior as in prior distribution

The input vector weighting defines a score (or weight) to each retained simulation according to the probability that it would return the minimum rod load (i.e. the optimum).

$$f(RL(ijkl)) = \left(\frac{1}{RL(ijkl)} \right)^N \quad (8.8)$$

Rod load, equation 8.8, is the second objective function designed to weight the combination of parameters according to their minimum value.

The posterior distributions were inferred by sampling with replacement the simulation input vectors, defined by the initial Latin Hypercube design, with probabilities proportional to the calculated weights. The optimal value and range for each parameter was calculated by taking respectively the mode and the 95% confidence interval for such distribution. The value of coefficient N (in equation 8.8) was elected following a number of model trials. $N = 2$ was deemed to adequately define the posterior distribution.

Histograms illustrated in Figure 8.5 show optimised design characteristics for studied PD pump. All five parameters are displayed and impact on the performance varies

Comparison between two design states									
Nom	INPUT	Current	Optimised	% Change	Nom	OUTPUT	Current	Optimised	% Change
D	Plunger Diameter (m)	0.111	0.037	-194%	F	Force (N)	$7.2 \cdot 10^5$	$8.3 \cdot 10^4$	-860%
R	Crank Radius (m)	0.102	0.155	+52.6%	F_f	Friction force (N)	300	50	-600%
L	Con-rod Length (m)	0.650	0.640	-1%	p	Pressure (MPa)	75	75	-
X	Speed (rpm)	200	334	+67%	Q	Flow rate (l/min)	1248	1207	-3.2%
n	Number of plungers	3	11	+260%	P_{tot}	Power (MW)	1.350	1.288	-4.6%
m(kg)	Plunger mass	400	43	-89%					
m_{tot} (kg)	Total mass	1200	864	-28%					

Table 8.3: Optimised PD pump parameters, identified by the multivariable analysis, indicates a 4.6% energy and 28% mass saving.

as seen in presented graphs. Parameter variation is displayed on the individual x-axis. Frequency annotates the number of times in which particular design solution resulted with an optimal design. In the diagram where plunger diameter was assessed it is clear that the smallest value resulted in the best performance. Crank radius shows less variation finally settling on the optimal increase for the best output results. Optimised value for Con-Rod length coincides with current specification so no significant change was reported. Speed was increased towards the top end of the range. This is to be expected in order to maintain the same flow rate with lower swept volume resulting from smaller plunger diameter. Examination of the final histogram suggests an increase in number of cylinders. This is again oriented towards compensating for the loss in the individual cylinder volume.

The final estimation for new modelled parameter values can be seen in Table 8.3. In addition to the qualitative benefits the mechanical structure of the pump that will result

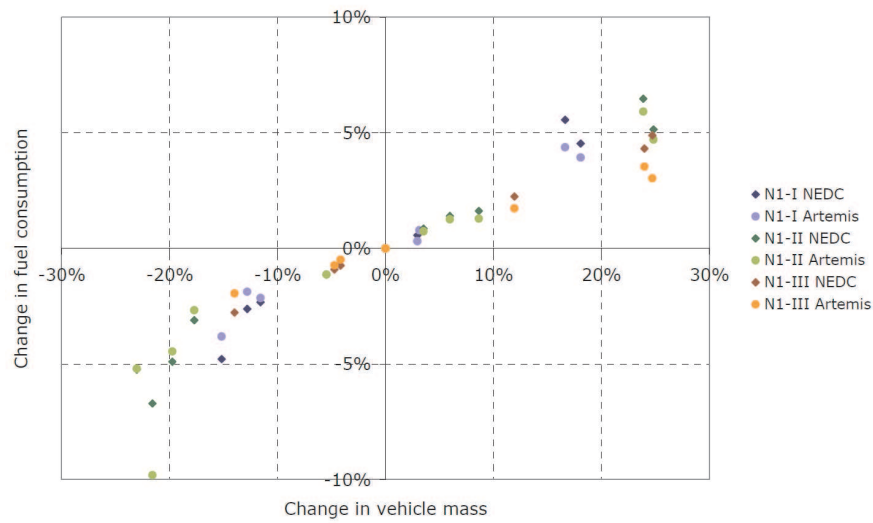


Figure 8.6: Effect of vehicle mass on fuel consumption in HGVs [130]

from the reduction in plunger diameter the analysis suggests a 4.6% energy saving.

8.2.6 Mass reduction

Opportunity to expand on previously done analysis considers the impact of novel design and its influences on the overall mass. Mass calculation can be assessed by using laws of scaling when examining optimised design. In equation 8.9 the formulation for plunger assembly mass evaluation is given.

The result analysis, presented in Table 8.3, suggest that plunger size should be reduced by three times. Mass of the resulting crank shaft assembly is a function of diameter cubed (square-cube law) [129].

New optimised design model predicts energy saving by using smaller diameter plungers while increasing the number of plungers in a single pump unit. In the following equation the main variables that determine pump mass are listed.

$$m_{tot} = \frac{D^2 \pi}{4} \cdot L_{pl} \cdot \rho \cdot a_c \cdot N_{cyl} \quad (8.9)$$

The main basis for this approach is to take account of the plunger diameter. As plunger diameter is a square function it is clear that it carries a high impact in this equation. Other constants such as crankshaft assembly constant and the assembly

support are also considered. The final result of mass evaluation is shown in Table 8.3.

Mass saving in a single pump unit is naturally reflected in the entire frac-truck assembly. Following assumptions are considered:

- A single PD pump weighs 5,400 kg and whole assembly weighs 30,800 kg (PD pump assembly takes 17.5% of the total mass)
- Assuming a 28% mass reduction in pump design the new pump weight will be 3,888 kg.
- The whole assembly would be reduced by 1,512 kg. So a new total weight would be 29,288 kg.
- The total truck weight reduction is 4.9%.

Therefore the second great advantage of the new design would be the weight reduction. Pump weight reduction has an influence on an entire truck assembly. Previous calculation estimates weight reduction of the frac-truck assembly to be approximately 5%. European commission and Institute for Energy and transport published a study related to heavy duty vehicles which quantifies the relationship between weight and fuel savings [130]. In Figure 8.6 graphical representation was reprinted to show results of this research. According to this publication 5% of weight reduction in heavy duty vehicles generates 1% fuel saving.

8.2.7 PD pump design space discussion

Figure 8.4 illustrates one projection of the five dimensional design space. Each point of the plot represents one set of input parameters. Two of the current functional (Flow Rate - Q) and physical (Rod Load - RL) limits are shown on the graph to illustrate the boundaries of the current design. The low gradient dashed line in 8.4 illustrates the impact of increasing the maximum pump speed by roughly 33% to 380 rpm.

Since pressure is directly dependent on the rod load limit, decreasing rod load requirements could achieve an increase in performance. Similarly, the same pressure output could be attained by optimizing the crankshaft to save weight and size.

The multi-variable model presented gives the initial basis for the optimized pump design. The advantage of this approach is the overall flexibility of the model and the

capability to implement any physical constraint of the real system. Evaluating design changes on the mass properties has resulted in the approach which has been presented to quantify the effect on mass reduction. Reducing the mass therefore benefits the complete system in several ways:

- Reduction of the physical properties of the units
- Decreasing the road damage caused by the truck load. Studies related specifically to the aspect of road haulage detail road deterioration due to excessive axial load [131],[132].

8.3 Multi-pump system optimisation

Optimising equipment on site to specific well requirements is an essential motivation for development of this model. The aim of this study is to understand the equipment requirements and respective loading condition which will result from an optimised system with higher efficiency. This study considers the different fuel consumption from two diesel engines at different operating conditions (PD pump loading) by defining boundary conditions associated with reservoir requirements, number of stages and operational brake-power available on site.

Number of constraints need to be considered in this model, for example, as shown in section 8.1, geology is closely related to the specific well requirements. This analysis aims to replicate performance from a typical North American well stimulation site. The focus of this study is analysing the pump engine and truck engine used to power and transport individual PD pump on site.

8.3.1 Methodology

The computational model is applied and further developed to assess its function on site level. To do this a simplified mathematical formulation of the pumping fleet have been implemented to include the required operational outputs, such as pressure and flow rate, with respect to engine emission and power consumption. The case study, presented in section 8.1, has shown pressure and volume demand for a single pumping

stage. Component manufacturers document the operational data for pump engine, truck engine and PD pump which will be used in the subsequent analysis.

Objective function will be defined based on the optimisation criteria, in this case, the aim is to minimise fuel consumption for a single fracturing stage by maintaining; flow rate in the range of current systems, operate each of the pump engines in the efficient range (i.e. beyond the point of maximum torque) and not exceed the maximum available power from each of the pump engines. Results should give an optimal solution for a single stage.

In order to test the validity of the optimised model benchmark values need to be defined. To do this hydraulic fracturing experts were asked to independently assess the presented case study in section 8.1 and propose an adequate pumping system capable of answering the well demands. Final step was to present and compare the optimisation results to one of the benchmark cases and quantify the operational improvements.

The summarised methodology of the site optimisation model includes the following steps:

- Mathematical formulation of the system
- Defining boundary conditions
- Defining objective function
- Presenting the results of the analysis

8.3.2 Multi-pump system modelling

Key elements of a PD pump are listed in Table 2.24. In order to compute flow rate and power consumption in a fleet of PD pumps equations are modified to include multiple units. Formulation of plunger velocity in equation 8.10 is a reproduction of equation 4.8 with the alteration of driveshaft speed to accommodate input in rotations per minute. Mathematical expression for PD pumps power and flow rate is illustrated in equations 8.11 and 8.12.

$$v_{pl} = -R_j \cdot \sin\left(\frac{2\pi \cdot X_l \cdot t}{60}\right) - \frac{R_j^2 \sin\left(\frac{2\pi \cdot X_l \cdot t}{60}\right) \cos\left(\frac{2\pi \cdot X_l \cdot t}{60}\right)}{\sqrt{L_k^2 - R_j^2 \sin^2\left(\frac{2\pi \cdot X_l \cdot t}{60}\right)}} \quad (8.10)$$

$$P_{tot} = n_p \cdot rms(v_{pl}) \cdot (m_{tot} \cdot rms(a_{pl}) + p \cdot A_{pl} + F_f) \quad (8.11)$$

$$Q_{tot} = n_p \cdot N_{cyl} \cdot \frac{D^2 \pi}{4} \cdot v_{pl} \cdot 998.2 \quad (8.12)$$

Based on the computed power consumption the optimisation method is developed by using the manufacturer's lookup table including BSFC (Brake specific fuel consumption). The derived value corresponds to a particular operating condition. Internal dimensions will be kept constant for this model having the speed and number of pumps as the only variables in the optimisation process. The speed of the pump is proportional to the power, as long as there is constant output pressure. Direct reading from the engine graph will produce $BSFC_s$ for a single pump. Once both values are derived multiplying the number of PD pump and consumption per single unit output indicates the consumption for the whole site (per fleet of PD pumps) - $BSFC_{tot}$, equation 8.13.

$$BSFC_{tot} = n_p \cdot BSFC_s \quad (8.13)$$

8.3.3 Boundary conditions

The following boundary conditions are necessary to define the optimisation model. The site requirement is based on a well stage presented in section 8.1. Each of the plotted data sets in Figure 8.2 is associated with power consumption, pressure and flow rate. Since successful well stimulation needs to deliver the required treating pressure and flow rate critical values have been identified and summarised in Table 8.4.

Similarly a frac-truck assembly with a pump engine needs to maintain the same size limit as in the already established equipment setup currently used in North America. This means that the pump power requirements must not exceed the power available from the driver (pump engine). For this model commercial engine metrics, shown in Figure 8.7, were used [67] in which the engine's torque, power and consumption are

Table 8.4: Frac site and engine boundary conditions

Frac site requirements		
Flow rate	Q_{tot}	$0.263 \text{ m}^3/\text{s} < x < 0.266 \text{ m}^3/\text{s}$
Pressure at wellhead	p	75 MPa
Truck requirements		
Pump engine power	P_{pow}	$< 1664 \text{ kW}$
Pump engine speed	E_{rpm}	$1400 \text{ rpm} < x < 1900 \text{ rpm}$

plotted against the engine's speed. The model, by default, considers an operation in an efficient regime at a selected speed range. This value, together with the power available from a pump engine, is shown in Table 8.4.

Finally, pump metrics used in the optimisation are employed from current hydraulic fracturing standards in North America. Internal geometry of the mechanical parts of a PD pump are outlined in Table 8.8. However two variables, pump speed and the number of pumps on site, present two main optimisation objectives in this analysis. Speed of the pump regulates the level of pump loading. Because downstream pressure is determined by the well condition keeping this pressure constant means that the pump engine speed is the only control variable of a PD pump loading. Second optimisation criteria is the number of PD pumps which determine the collective flow rate being delivered to the well. Remaining variables associated with the PD pump are shown in Table 8.8.

8.3.4 Defining objective function

The objective function is defined by applying the following criteria. First phase considers values only in the desired flow rate range.

$$0.263 < Q(i,j) < 0.266 \text{ m}^3/\text{s} \quad (8.14)$$

Power consumption from a PD pump must not exceed the pump engine power limit. Therefore power is limited so that:

$$P_{pow}(i,j) < 1664 \text{ kW} \quad (8.15)$$

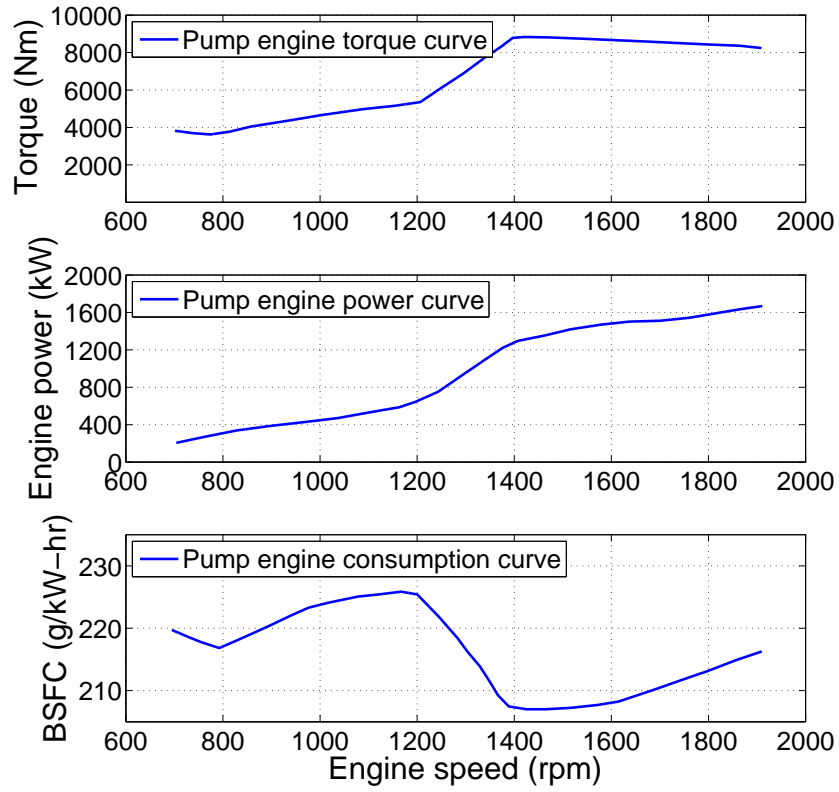


Figure 8.7: Engine performance was modelled using manufacturer’s data [67]

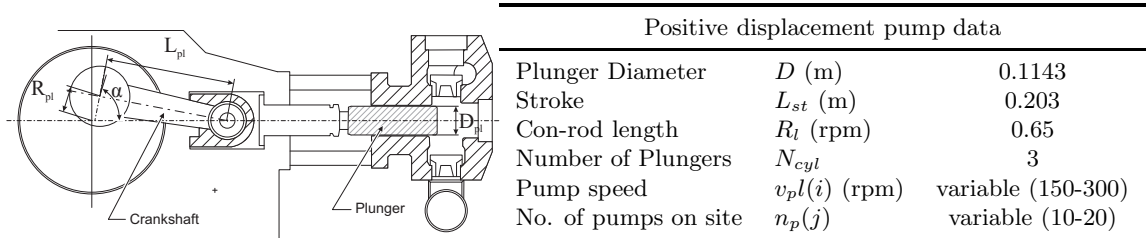


Figure 8.8: Defining pump simulation input data

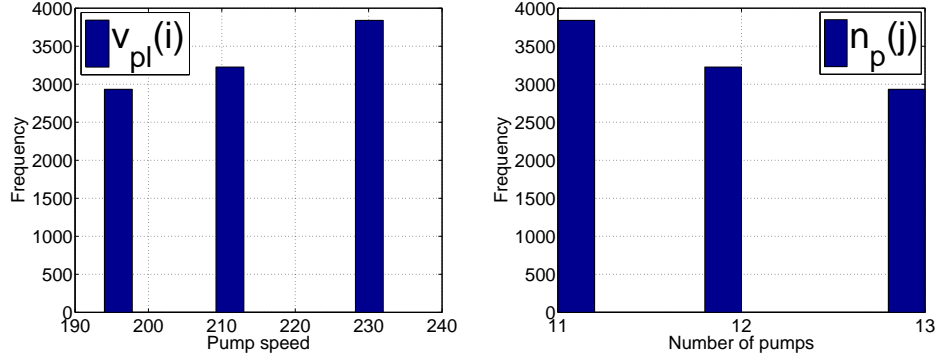


Figure 8.9: Optimisation results showing histograms of best operational practice on site in terms of number of PD pump and their operating speed

In addition, an engine is assumed to be operating in the efficient speed range. Therefore, engine speed is considered to be within the following range:

$$1400 < E_{rpm}(ij) < 1900rpm \quad (8.16)$$

Lastly, all pump parameters that satisfy the above criteria are scored (or weighted) according to the probability that it would result in the minimum fuel consumption for the entire site (BSFC). This assumption considers consumption from all the pumps on site with respect to their speed (i.e. throttle).

$$w(ij) = \left(\frac{1}{BSFC_{tot}(ij)} \right)^N \quad (8.17)$$

Posterior distribution was extrapolated by sampling with replacement the simulation's input vector that was defined initially using Latin Hypercube. Evaluating optimal value and the range for each of the simulated parameters was done by taking the mode and a 95% confidence interval for each distribution. The value of coefficient N was decided after a number of model trials. Value of N=2 was considered to be suitable for defining the posterior distribution.

8.3.5 Optimised model

Results shown in Figure 8.9 present the optimal solution for site management. It can be seen that a higher frequency denotes a better correspondence with the assigned boundary condition. A lower number of pumps and higher operating speed result in better energy use and lower emission factors.

The number of backup units is a percentage of the overall unit count on site. From private communication with the operators it was established that 25% of frac-truck assemblies should be kept as a backup [133], [134], [135]. The number of PD pumps on standby, for all test cases, is presented in Table 8.5.

Detailed analysis of the results shown in Table 8.5 illustrates three representative scenarios, a benchmark case study, and personal correspondence with experienced field operators. Simulation output displays three cases, shown in Figure 8.9, each of which is associated with the different number of PD pumps and the different loading ratios (throttle) driving a PD pump. In Table 8.5 simulation outputs are shown indicating that PD pump loading (throttle) is directly related to the PD pump speed. In the equation 8.12 it was shown that pump speed directly influences the flow rate output. Similarly, specific pump engine speed has its corresponding BSFC, as seen in Figure 8.7. The total consumption of fuel is derived from multiplying the overall number of PD pumps and the BSFC per individual pump.

The total consumption from three scenarios is now compared to the benchmark case. Full loading conditions in the benchmark example demonstrates 100% throttle position. Since all simulation cases run at lower pump speed, and therefore lower load, its throttle position is calculated based on maximum speed. Results show that case number 1 (11 PD pumps) has the best power consumption performance for the selected boundary conditions. This is the minimum number of units for this design specification. Analysis has shown that 10 PD pumps at full throttle speed would not meet the requirements. Number of units on standby, being a proportion of the overall unit count, will reduce to 3 backup PD pumps. This improvement is also reflected in the overall fuel saving seen in the last column of Table 8.5.

Table 8.5: Optimisation results for site management

Scenario	$[n_p]$ - No. of PD pumps (PD pumps on standby)	$[v_{pl}]$ - Pump speed [rpm]	Throttle [%]	Flow rate (single) [m ³ /s]	Flow rate (total) [m ³ /s]	Pump engine speed [rpm]	Pump engine power [kW]	Overall PD pump power on site [kW]	Pump engine consumption (single) [g/kW-h]	Pump engine consumption (total) [g/kW-h]	Consumption saving [%]
Operator 1[133]	16 (4)	246	100	0.0253	0.404	1881	1645	26320	215	3440	-3.8
Operator 2[133]	17 (5)	173	70.0	0.017	0.289	1356	1152	19584	210	3579	benchmark
Operator 3[134]	15 (4)	196	80.0	0.0201	0.301	1418	1307	19605	207	3105	-13.2
Operator 4[135]	18 (5)	148	60	0.0152	0.273	1308	985	17730	215	3870	+8.1
1	11 (3)	232	93.8	0.0237	0.264	1782	1561	17171	212	2339	-34.6
2	12 (3)	211	85.5	0.0219	0.263	1522	1424	17088	207	2487	-30.5
3	13 (4)	196	79.4	0.0203	0.265	1433	1322	17186	207	2691	-24.8

8.3.6 Multi-pump system optimisation summary

In conclusion it can be seen that each site needs to be considered as an individual engineering problem. Geological requirements and brake-power available on site are key determinants that need to be evaluated before commencing any well stimulation process. In this study a simplified model of pumping units was developed and presented indicating clear opportunities for improvement. Specifically, in this section a detailed analysis of PD pump energy use, together with its driver (pump engine), was presented. The importance of precise pump control is evident and improvements on site can be obtained with the right performance matching. Results of this study show that 34.6% fuel reduction can be gained with same equipment by keeping key components of the system in accordance with environmental aspects of hydraulic fracturing.

8.4 Assessing environmental impact

In order to evaluate the extended impacts of PD pump and site optimisation, associated carbon footprint must be identified for each of the components in the assembly. Table 8.6 quantifies the emission, weight and cost of the components comprising a single frac-truck assembly.

8.4.1 Input data - assumptions

The mass of a single PD pump and an entire frac-truck assembly was identified. In section 8.2.6 the results of pump optimisation were quantified in terms of mass reduction. The remaining components on a frac-truck assembly were not modified so the overall weight reduction will derive entirely from a PD pump.

The system optimisation has appraised improved site management to achieve reduced number of PD pumps on site. To understand the economic benefit the value of each of the frac-truck components, such as an engine, transmission and PD pump, were estimated by the industry's experts [136].

From an environmental perspective, each of the components on frac-truck assembly has associated noise which was modelled as part of the planning process for a proposed development in Lancashire, UK [7]. Cumulative noise from each of the frac-truck

Table 8.6: Environmental optimisation in hydraulic fracturing - input data

Elements of frac-truck assembly							
	Pump engine	Truck engine	PD pump	Auxiliary	Total	Source	
Weight (kg)			5,400	25,400	30,800	[65], [59]	
Cost (£)	168,000	105,000	175,000	367,500	815,500	[136]	
Noise (dB)	105		96	114	115	[7]	
Emission (g/hr)						[67], [68]	
CO ₂	1,176,278	217,210			1,393,488	[137], [138]	
PM	162.7				162.7	[137]	
CO	5,873	10.5			5,883	[139], [138]	
NO _x	11,914	1,281			13,195	[137], [138]	
HC	10,739	1.16			10,740	[139], [138]	
EC	78.8				78.8	[137]	
OC	99.0				99.0	[137]	
Embedded carbon (tonnes (CO ₂ e))			10.26	48.26	58.52	[140]	
Operational input data							
Well management			Transport management		Site management		
Wells on pad	Number of stages	Stage length (hours)	Travel time (hours)	Travel distance (km)	Operating frac-trucks	Frac-trucks on standby	
3	5	1.5	5	322	17	5	

assembly units can be numerically derived. A reduced number of units on site, discussed in section 8.3, will have the benefits of reduced noise levels and decreased radius of noise propagation.

Each of the frac-truck assemblies uses two main power generators, previously referred to as pump engine and truck engine. Pump engine is used predominantly to drive the PD pump operation on site during hydraulic fracturing and truck engine is

used to transport the frac-truck assembly to and from a site. The associated emission factors for each of the two engines were assumed using previously published laboratory tests [137], [138] and emission standards published by EPA (Environmental Protection Agency) [139].

The frac-truck assembly is predominately manufactured from steel, and the weight of different rubber and sealing elements is comparatively negligible. Therefore, the embedded carbon is evaluated based on the mass of current systems, using values from average global carbon emission from steel. [140].

All of the data in Table 8.6 is related to a single PD pump unit and its accompanying power systems. In order to scale the impact of developed optimisation algorithm size of well operation must be considered. Number of wells on a single pad, number of stages and length of operation at each stage was given in Table 8.6 based on current North American practices [37].

Reducing the weight of a frac-truck assembly will have environmental and financial benefits in terms of traffic and on site operation. Industrial upscaling in terms of time and distance of truck transport, based on [89], is required.

Finally, site management was considered with respect to the number of frac-truck assemblies on site, number of back-up systems and their operational regimes (low, medium, high). Based on the system optimisation in section 8.3 and Table 8.5, in-depth comparison between the two highlighted models will be presented.

8.4.2 Results

In section 8.2 PD pump optimisation resulted in mass and energy saving as summarised in Table 8.3. Evaluation of the energy saving and the improved emission, illustrated in Table 8.7 was done for a single frac-truck assembly and the fleet of 17 units.

Reduction in CO_2 emission was divided into two categories; transport and efficiency. Site transport assumes reduced fuel consumption for transporting lighter PD pumps. Site efficiency is based on improved pump design and the resulting power saving, illustrated in Table 8.3.

Reduction in CO_2 embedded is a function of the weight of a frac-truck assembly.

Reduction in emission of pollutants assumes the combined effect between lighter

and more efficient PD pumps. Effect of the lighter PD pump is seen in the truck engine saving as illustrated in Figure 8.6. More efficient PD pump indicate reduced emissions from a pump engine due to the lowered power demand.

Financial saving is the result of a lowered fuel consumption on site and in transportation due to lighter units.

Table 8.7: Environmental optimisation in hydraulic fracturing - results

PD pump optimisation - scenario 1			
Reduction in CO_2 emitted	Abbrev.	Per single Frac-truck	Per Frac-truck fleet (17)
Site transport	T	1.46 kg/hour	24.74 kg/hour
Site operation	E	54.11 kg/hour	919.85 kg/hour
Total		55.56 kg/hour	944.59 kg/hour
Reduction in CO_2 embedded		Per single Frac-truck	Per Frac-truck fleet (17)
Lighter PD pumps		2872.8 kg/pump	48.84 tonnes/fleet
Reduction in Pollutants		Per single Frac-truck	Per Frac-truck fleet (17)
NOx		560.85 g/hour	9.53 kg/hour
CO		270.26 g/hour	4.59 kg/hour
HC		2666.1 g/hour	45.32 kg/hour
Financial savings		Per single Frac-truck	Per Frac-truck fleet (17)
Fuel saving		17.49 £/hour	297.32 £/hour

In section 8.3 PD pump fleet performance on a hydraulic fracturing site was analysed. It was necessary to understand what is the best combination between a number of PD pumps on site and their operating regime (low, medium, high).

Site management results presented in Table 8.5 display a characteristic operating practice and the enhancements obtained through the computational model. A single benchmark model was selected, based on correspondence with operators, for comparison with the optimised model. The difference between the two operating states, highlighted in Table 8.5, is quantified in Table 8.8.

Reducing the number of PD pump units operating on a site has resulted in decreased

Table 8.8: Environmental optimisation in hydraulic fracturing - results

Site optimisation - scenario 2		
Reduction in CO_2 emitted	Abbrev.	Per Frac-truck fleet (from 17 to 11)
Site transport	T	8253.98 kg/hour
Site operation	E	1303.26 kg/hour
Total		9557.24 kg/hour
Reduction in CO_2 embedded		Per Frac-truck fleet (from 17 to 11)
Fewer PD pumps		82.08 tonnes/fleet
Reduction in Pollutants		Per Frac-truck fleet (from 17 to 11)
NOx		56.37 kg/hour
CO		0.46 kg/hour
HC		0.05kg/hour
Financial savings		Per Frac-truck fleet (from 17 to 11)
Operational saving		337.21 £/hour
Transporting saving		2,023.27 £/hour
Acquiring saving		£10,601,483

CO_2 emission. In Table 8.8, the optimised number of PD pump units on site will first of all require less units to be transported to site (T). In addition to the PD pump directly engaged in the process evaluation also considers backup units the number of which will be reduced as well. Although PD pumps will run at higher operating regimes, and therefore induce higher pump engine emission as shown in Table 8.5, the process will demand lower number of units altogether which produces a cumulative power saving. This is directly reflected on the optimised efficiency (E) and the reduced CO_2 emission in Table 8.8.

Embedded CO_2 , being proportional to the number of frac-truck units involved in the process, will decrease due to less units operating in real time and less units on standby.

Reduction in emission of pollutants assumes the combined effect of less PD pump operation and fewer PD pumps on standby. Each frac-truck assembly carries associated pollutants from pump engine and truck engine used to deliver frac-truck assemblies to and from a site. Quantified emission reduction for units in operation and units on

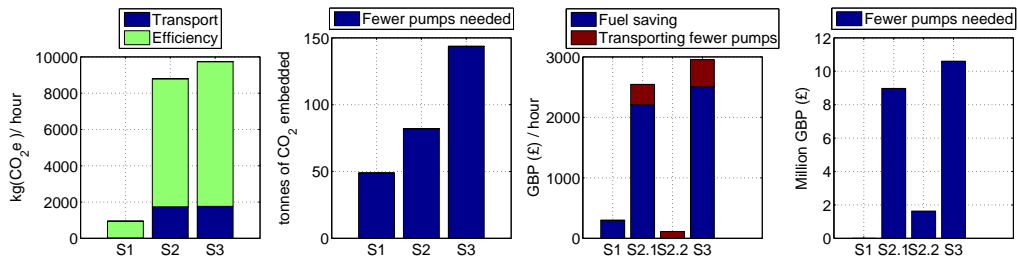


Figure 8.10: Quantified environmental and financial savings from PD pump optimisation (scenario 1), system optimisation (scenario 2.1 and 2.2) and their cumulative impact (scenario 3)

standby is displayed in Table 8.8.

Finally, financial saving associated with the improved site design is illustrated as follows; the operational running cost is reduced due to improved fuel efficiency with less operating PD pump, improved fuel consumption because fewer frac-truck assemblies are transported and reduced expenditure as additional frac-truck assemblies will not be required.

In Figure 8.10 the effect of the environmental impact was plotted for each of the two optimisation scenarios. Results show 17 PD pumps in fleet operation in scenario 1, the difference between the current and the optimised system (17-11 PD pumps) in scenario 2.1 and the effect of reduced standby units shown in scenario 2.2. In addition to PD pump optimisation (scenario 1) and the site layout optimisation (scenario 2) the aggregate of the two was also presented as scenario 3. Four charts, shown in Figure 8.10, display design and operational saving in the three scenarios. Reduced CO₂ emission, shown in the first plot on the right, is quantified for improved efficiency and transport. Second plot on the right evaluates the savings in the embedded carbon for the three scenarios in which the first bar accounts for the reduced weight from the optimised design, the second bar for lower unit demand and the third for their cumulative effect. Third and fourth plot on the right in Figure 8.10 detail the financial savings, third plot shows operational saving in the fuel and transport and the fourth presents the capital saving from having to acquire fewer frac-truck units.

8.5 Summary

The preceding discussions have clearly demonstrated that there is considerable scope for redesign of current hydraulic fracturing technology to create smaller, light units with lower environmental impact.

In the case study section 8.1 it was shown that using principle equation for characterizing well is sufficient to derive values for treating pressure and the operational flow rate.

Optimisation of a single PD pump, illustrated in section 8.2, has indicated redesign capabilities to improve operational performance. Early plunger pumps were designed to operate at pressures significantly less than current demands. Given the need for higher treating pressures there are clear advantages from increasing the pump speed and reducing plunger diameter. This reduction in rod load and cylinder stress will lead to a change in the required material properties of the pump frame and components. The analysis presented in section 8.2 has demonstrated that a 4.6% improvement in energy efficiency is theoretically obtainable by optimizing the relative proportions of the established design. Such a change would directly impact on the hydraulic fracturing site's fuel consumption and the associated CO_2 emissions.

Section 8.2 has shown conceptual mass improvement resulting from the novel PD pump design. Mass reduction of a single PD pump could be reduced by up to 28% in which case the overall frac-truck assembly will achieve 4.9% in weight reduction.

In section 8.3 the computational model further emphasizes the system response to well demands and the effect of fleet operation on levels of exhaust emissions. Emissions from pump and truck engines were modelled using previously published emission analysis. The engine model was integrated in the developed computational model of a PD pump. An optimisation algorithm identified the objective function and boundary conditions of the model. Results compare the optimised model to the selected benchmark scenario quantifying the fuel saving of up to 34.6% by operating PD differently to current practices.

Final section 8.4 summarises the results from the two optimisation scenarios by detailing the environmental aspects of improved PD pump design and site operation. Both optimisation models indicate possible system improvements. Reduced fuel con-

sumption and the novel site management system have environmental and economic benefits on the whole hydraulic fracturing site.

This chapter has outlined the engineering rationale for creating a compact, low energy hydraulic fracturing technology. The optimum PD pump and system design ought to be established for better process management and enhanced efficiency of the system. In short, key advances in hydraulic fracturing will come from the improved operation from equipment on site.

Chapter 9

Discussion and conclusion

This thesis has presented design optimisation studies of machinery used in hydraulic fracturing. Based on the developed computational and experimental model new engineering insights have shown the prospects of improving energy efficiency in the high-pressure slurry systems. Redesign of the current pumping system is necessary for the equipment adaptation and European use. This work has presented an optimisation algorithm that performs the re-evaluation of current systems quantifying the parametric modifications for specific hydraulic fracturing requirements in Europe. The study also shows empirical methods of quantifying emission levels on site associated with current drive systems and the opportunity to decrease the size of air and noise pollution on site.

The literature review section presented the global understanding of oil and gas formation and extraction. Well stimulation method focused on hydraulic fracturing and the engineering objectives that define this technology. Subsurface practices, such as well isolation, operation in stages and perforation methods, illustrate technological practices deployed in hydraulic fracturing. The calculation of downhole mechanics quantified the operational requirements that top surface process equipment needs to provide for successful well stimulation. Subsequent sections focused on surface equipment, their operating regimes, performance limitation and control on site. Positive displacement pumps, as equipment bearing the highest working impact, were analysed from a mechanical and fluid dynamic standpoint identifying critical areas and current design challenges. Based on the information presented the project's concern with envi-

ronmental questions was identified based on a morphological chart and the overview of different technical solutions.

Development of the environmentally driven optimisation required a detailed computational model that will be able numerically to assess different operational scenarios. Owing to the engineering setup used in hydraulic fracturing and the units with the highest impact, frac-truck assembly was chosen for further optimisation development. The methodology section identified the stages of model development and validation identifying the need for the experimental analysis.

The developed computational model considers power and transmission units driving the operation of a multi-cylinder PD pump. Results show a fully functional computational model that uses integrated solutions from CFD, lookup tables and fundamental physics of PD pump operation.

The validated computational model gives accurate and effective results for a relatively low calculation time (up to five minutes). This is an ideal result that can easily be modified by defining objective functions to compute an optimum solution. The first phase of model validation was performed using the experimental field data recorded in the actual hydraulic fracturing operation in North America. Results show an acceptable level of consistency between the two sets of data. The second phase of validation was conducted using the scaled-down experimental setup. Operational limitations that are inevitable in the actual field work were overcome by scaled-to-measure equipment. The computational model shows an accurate correlation in different operating states (i.e. speeds and pressures) with the scaled test rig setup.

Results of the optimisation studies show performance gains in a PD pump and the system of frac-truck assembly. An optimised parametric model of a single PD pump indicates a 4.6% efficiency saving through having different internal geometry of the fluid-end. New design has potential for mass saving due to reduced dimension of principal components (i.e. plunger diameter and crankshaft assembly). Mass reduction was quantified to be around 28% for a PD pump which transcends to 4.9% of the overall mass of the frac truck assembly.

Optimisation of the hydraulic fracturing site operation considered using the ideal number of frac-truck assemblies to minimise the fuel consumption and pollutant emis-

sion on the process location. A developed computational model was upgraded to account for emission data, as specified by equipment manufacturers. Based on the operational speed of the pump, which corresponds to engine loading, the consumption map was developed for a single frac-truck assembly. Satisfying the models' boundary conditions, for maintaining sufficient flow rate and pressure, the objective function of the optimised model concludes with the most appropriate number of frac-truck assemblies and their operational regime. Comparing optimisation results with current site operator's practices indicates savings in the number of units, fuel consumption (for transport and site operation) and pollutant emission. All the quantified reductions, shown in Table 8.7, are advantageous for the local community besides providing financial benefits to the site operator.

Research presented in this thesis was done for specific operating condition and predefined system considerations. For example, in the section 2.2.4 uniform rock structures were considered. Evaluating heterogeneous shale structure would have deviated from the selected research path. Subsurface frac-fluid pumping was also assumed to have same flow characteristics as in measured surface operation. Validating pressure waves downstream of the wellhead was not possible but recommendation for future research is the analysis of pressure waves in long pipe sections.

Fluid properties in all simulations is assumed to be water although, as previously discussed in section 2.2.4, parts of the pumping stages will use different density fluid as well as solid particles. Experimental test rig does not allow more complex fluid operation. Possibility for future work may lie in evaluating fluid impact on specific parts of the system.

Modelling of pumping and drivetrain system was established using current automatic transmissions to replicate field practices. Even though this research led to conclusion that more dynamic systems need to be considered this work concludes with recommendation for further research and model expansion.

Field data evaluation was limited to one pumping unit. More in-depth field analysis will need to consider multiple frac-truck assemblies during hydraulic fracturing processes.

Power evaluation on site was considered only for PD pumps. Auxiliary equipment,

such as blenders, sand auger and suction pumps, were not considered due to their relatively low power share (less than 5%). Time for equipment processes on site was based solely on fluid injection downhole. Well preparation activities, such as wireline, perforation and equipment testing was not under investigation. Recommendation for further work may consider financial and time constraints related to operating schedules on site.

For the case study evaluation in section 8.1 North American shale basin was used. To date on-shore oil and gas exploration in Europe is still in early stages with limited quantities of operational results. Site practices and pumping schedules discussed in this work are also affiliated with the North American shale. The ongoing work of external agencies and institutions will develop operational guidelines for test wells in the UK.

The environmental impacts were constructed using diesel engine data previously recorded in academic literature. In cases where laboratory testing was not available official emission guidelines were used. Diesel emission on site could vary depending on the quality of filtration system and the engine rating which exceeded the scope of this analysis. Despite many challenges associated with the on-site air quality measurements this work has proved that there is a great opportunity for improved equipment operation which demands further experimental work and field testing.

9.1 Key developments

To enable equipment redesign and its application in Europe this work has developed and validated a computational model which is able to assess the performance of a parameterized representation of a PD pump used in hydraulic fracturing. The computational model was designed by implementing data from academic and commercial literature and validated through an iterative process using experimental field data and an experimental test rig. The final phase of the computational model has demonstrated the model's ability to evaluate on-site practices and demonstrate changes for improved energy efficiency.

Key milestones in the project development are:

- Mapping the process requirements that need to be met on site, i.e. pressure and

flow.

- The simulation of the operating conditions in a PD pump.
- The analysis of the experimental field data to validate the computational model.
- The design and construction of the scaled-down test rig to enhance model validation.
- The acquisition of the test rig and field data to verify the computational model.
- The application of the computational model to perform a multi-variable optimisation process.
- The calculation of the emissions on site using the computational model.

9.2 Contribution to knowledge

The main contributions to knowledge of this work are:

- The quantification of the internal PD pump design changes by varying mechanical geometries using the established computational model.
- The specification and commissioning of a laboratory test rig whose behaviour is analogous to a full scale frac-pump.
- Holistic view of fracturing machinery impacts
- The quantification of the effect of different speeds and loading conditions on engine emission from a single and multiple frac-truck assemblies.

9.3 Future work

Based on the output from this thesis a number of future projects can be identified which could:

1. Develop a better understanding of flow and pressure interaction between individual frac-truck assemblies on site; current hydraulic fracturing sites lack sufficient

control of discharge pressure. Due to the cyclic nature of the discharge pressure propagation it is possible that a measurable size of energy is lost between individual units. Further experimental data development should consider introducing pressure measurements on critical parts of the pumping network.

2. Installation of accelerometers on current test rig setup which will enable comparison with previously recorded and analysed field data.
3. Expand the computational model to include different drive and transmission systems by replacing current finite ratio gearboxes. Numerical modelling of infinitely variable PD pump speed will increase the efficiency of the frac-truck assembly by allowing the pump engine to operate at its optimum power/consumption regime.
4. Implement closed loop control system to utilise higher efficiency from the current systems. The developed scaled-size test rig can be upgraded to dynamically control boundary conditions, such as speed and pressure. This will enable further studies to be undertaken related to PD pump response to a sudden operating change commonly found in real hydraulic fracturing applications.
5. Improve levels of CO_2 and pollutant emission on site. Further on-site experimental measurement is recommended to understand the realistic emission per frac-truck assembly.
6. Expand the computational model to include sound pressure level from individual field components. Alternative mechanical solutions should also be rated according to noise emission. The developed scaled-size test rig can be upgraded to evaluate different noise prevention systems in a controlled laboratory environment which will improve the understanding of noise propagation and noise attenuation on a hydraulic fracturing site.
7. Develop a simplified hydraulic fracturing process calculator by integrating the key performance inputs (engine, PD pump, well data) and the resulting outputs (flow rate, fuel consumption, CO_2 and pollutant levels, etc.) that can be used to quickly assess the results of different site configurations.

8. Expand the current experimental setup by constructing a new scaled PD pump assembly which will enable system analysis and interference between individual units to be performed. A new system could be constructed with a different transmission system to assess the advantages of infinitely variable hydrostatic drive.
9. Experimentally verify the influence of different valve dynamics on the PD pump operation. The current laboratory setup can be modified by introducing external actuators to drive the valve motion. Providing proof of these concept on the scaled unit will justify the investigation and development on a full size PD pump.
10. Integrate top surface operation with downhole rock mechanics by injecting high-pressure fluid into a compressed rock specimen and monitoring crack formation and propagation. The current experimental test rig is modular and transportable to the site which adds to the flexibility of the system.

References

- [1] International Energy Agency - IEA. Golden rules for a golden age of gas, world energy outlook special report on unconventional gas. Paris, France, 2012. [URL](#).
- [2] M. E. Biresselioglu, T. Yelkenci and I. O. Oz. Investigating the natural gas supply security: A new perspective. *Energy*, 80: 168–176, 2015. [DOI:10.1016/j.energy.2014.11.060](https://doi.org/10.1016/j.energy.2014.11.060).
- [3] ASME. Fracking: A Look Back by Michael MacRae, [online], Accessed: 17 April 2014, 2012. [URL](#).
- [4] EEC. A Brief History of Hydraulic Fracturing [online], Accessed: 17 April 2014, 2012. [URL](#).
- [5] Mair, R., Bickle, M., Goodman, D., Koppelman, B., Roberts, J., Selley, R., Shipton, Z., Thomas, H., Walker, A., Woods, E. Shale gas extraction in the uk: a review of hydraulic fracturing. royal society and royal academy of engineering. <http://www.raeng.org.uk/>, 2012. RS-RAEng.
- [6] Parliament UK. Environmental impact of development of shale gas in the uk (online). <http://parliament.uk>, 2015. Accessed: 04 Jun 2015.
- [7] Cuadrilla Bowland Ltd. Lancashire shale gas exploration sites. Regulation 22 Information - Noise, 2015. [URL](#).
- [8] I. J. Karassik, W. C. Krutzsch, W. H. Fraser and J. P. Messina. *Pump handbook*, volume 3. McGraw-Hill New York, 1986.
- [9] B Davies. Forward Concepts for plunger pump design. SW1072 Design report from TH Consultantants Ltd , 2011.
- [10] ETSU, AEAT PLC. Study on improving the energy efficiency of pumps. European Commission, 2001. [URL](#).

-
- [11] T. Fleiter, W. Eichhammer and J. Schleich. Energy efficiency in electric motor systems: Technical potentials and policy approaches for developing countries. United Nations - Industrial Development Organization, Vienna, Austria, 2011. [URL](#).
- [12] L. Cao, S. Mantell and D. Polla. Design and simulation of an implantable medical drug delivery system using microelectromechanical systems technology. *Sensors and Actuators A: Physical*, 94(1): 117–125, 2001. [DOI:10.1016/S0924-4247\(01\)00680-X](#).
- [13] M. Hu, H. Du and S. Ling. A digital miniature pump for medical applications. *Mechatronics, IEEE/ASME Transactions on*, 7(4): 519–523, 2002. [DOI:10.1109/TMECH.2002.805620](#).
- [14] FIA. Formula one - power unit regulations. <http://www.fia.com/>, 2014.
- [15] Buckley, J. W., M. H. Buckley and H. Chiang. Research Methodology & Business Decisions. National Association of Accountants, 1976.
- [16] O. Shale. Yen et al. *Developments in Petroleum Science*, 5: 187–189, 1976. ISBN: 978-0444552938.
- [17] J. S. Seewald. Organicinorganic interactions in petroleum-producing sedimentary basins. *Nature, International weekly journal of science*, pages 235–246, 2003. [DOI:10.1038/nature02132](#).
- [18] Pennsylvania, Department of Conservation and Natural Resources. Thermal maturation and petroleum generation, 2014. [URL](#).
- [19] Susan Pater, Kim McReynolds, and Kristine Uhlman. GEOLOGIC PROCESSES, 2012. Web-site:[URL](#).
- [20] Ward Cameron. Bricks and mortar the rocks that make up the rockies (online). Accessed: 30 March 2016. [URL](#).
- [21] G. E. Manger. Porosity and bulk density of sedimentary rocks. Technical report, USGPO, 1963. [URL](#).
- [22] PetroWiki. Tight gas reservoirs (online). Accessed: 29 February 2016, 2015. [URL](#).
- [23] C. D. J. Poupon, A.; Clavier. Log analysis of sand-shale sequences a systematic approach. *Journal of Petroleum Technology* 22, 07, 1970.
- [24] National Energy Technology Laboratory. Geologic Storage, 2010. [URL](#).

-
- [25] Schlumberger. Oilfield glossary - primary recovery (online). Accessed: 30 March 2016. [URL](#).
- [26] Energy Information Administration - EIA. Drilling sideways – a review of horizontal well technology and its domestic application. DOE/EIA-TR-0565 Distribution Category UC-950, 1993. [URL](#).
- [27] Rafael Osorio. Oil reservoir performance (online). Accessed: 31 March 2016, 2016. [URL](#).
- [28] Paul Glover. Reservoir drives(online). Accessed: 31 March 2016, 2016. [URL](#).
- [29] C. Cook, S. Jewell *et al.* Reservoir simulation in a north sea reservoir experiencing significant compaction drive. *SPE Reservoir Engineering*, 11(01): 48–53, 1996. [URL](#).
- [30] D. Brouwer, J. Jansen, S. Van der Starre, C. Van Kruijsdijk, C. Berentsen *et al.* Recovery increase through water flooding with smart well technology. *SPE European Formation Damage Conference*. Society of Petroleum Engineers, 2001. [URL](#).
- [31] S. Kokal and A. Al-Kaabi. Enhanced oil recovery: challenges & opportunities. *World Petroleum Council: Official Publication*, 2010: 64–69, 2010. [URL](#).
- [32] S. Thomas. Enhanced oil recovery-an overview. *Oil & Gas Science and Technology-Revue de l'IFP*, 63(1): 9–19, 2008. [URL](#).
- [33] R. Veatch *et al.* Overview of current hydraulic fracturing design and treatment technology—part 1. *Journal of Petroleum Technology*, 35(04): 677–687, 1983. [URL](#).
- [34] H. A. Nasr-El-Din, S. M. Al-Driveesh, K. M. Bartko, H. H. Al-Ghadhban, V. Ramanathan, S. K. Kelkar, M. M. Samuel *et al.* Acid fracturing of deep gas wells using a surfactant-based acid: Long-term effects on gas production rate. *SPE Annual Technical Conference and Exhibition*. Society of Petroleum Engineers, 2006. [URL](#).
- [35] H. O. McLeod *et al.* Matrix acidizing. *Journal of Petroleum Technology*, 36(12): 2–055, 1984. [URL](#).
- [36] S. Reed. Managing the Risks From Hydraulic Fracturing and Oil and Gas Development Of the Marcellus Shale Region. *Westlaw Journal*, 32, 2012. [URL](#).
- [37] G. E. King and Apache. Hydraulic fracturing 101: What every representative environmentalist regulator reporter investor university researcher neighbor and engineer should know about estimating frac risk and improving frac performance in unconventional gas

- and oil wells. *SPE Hydraulic Fracturing Technology Conference*. Society of Petroleum Engineers, 2012. [URL](#).
- [38] Twin Disc. A guide to - Hydrodynamic Drive Applications. Racine, Wisconsin, 1960.
- [39] Calfrac Well Services. Shale Fracturing Operations, Technical Expertise and Achievements, 2014. [URL](#).
- [40] Daneshy Consultants International. Hydraulic fracturing to improve production. Tech101, 2010. [URL](#).
- [41] N. Warpinski and M. B. Smith. *Recent Advances in Hydraulic Fracturing*, volume 12. SPE Monograph Series, 1989. ISBN:978-1-55563-020-1.
- [42] EPA. Evaluation of impacts to underground sources of drinking water by hydraulic fracturing of coalbed methane reservoirs. Washington DC, USA, 2004. [URL](#).
- [43] ICP. Well Completion Procedures in US, 2012. Experimental Field Data.
- [44] Halliburton. Stimulation handbook. Halliburton Energy Institute, 2006.
- [45] DECC - Andrews, I.J. The Carboniferous Bowland Shale gas study: geology and resource estimation. British Geological Survey for Department of Energy and Climate Change, London, UK, 2013. [URL](#).
- [46] B. Haimson, C. Fairhurst *et al.* Initiation and extension of hydraulic fractures in rocks. *Society of Petroleum Engineers Journal*, 7(03): 310–318, 1967. [URL](#).
- [47] M. K. Hubbert and D. G. Willis. Mechanics of hydraulic fracturing. 1972. [URL](#).
- [48] M. A. Biot. Thermoelasticity and irreversible thermodynamics. *Journal of Applied Physics*, 27(3): 240–253, 1956. [URL](#).
- [49] M. J. Economides, K. G. Nolte, U. Ahmed and D. Schlumberger. *Reservoir stimulation*, volume 18. Wiley Chichester, 2000. ISBN: 978-0471491927.
- [50] J. M. Carcione and F. Cavallini. Poisson’s ratio at high pore pressure. *Geophysical prospecting*, 50(1): 97–106, 2002. [URL](#).
- [51] American Petroleum Institute - API. Water Management Associated with Hydraulic Fracturing - HF2, 2010. [URL](#).

-
- [52] K. B. Gregory, R. D. Vidic and D. A. Dzombak. Water management challenges associated with the production of shale gas by hydraulic fracturing. *Elements*, 7(3): 181–186, 2011. [URL](#).
- [53] Fluid Lab. Experimental results - 1714311. Texas, USA, 2011.
- [54] A. Vengosh, R. B. Jackson, N. Warner, T. H. Darrah and A. Kondash. A critical review of the risks to water resources from unconventional shale gas development and hydraulic fracturing in the united states. *Environmental science & technology*, 48(15): 8334–8348, 2014. [URL](#).
- [55] A. Kondash and A. Vengosh. Water footprint of hydraulic fracturing. *Environmental Science & Technology Letters*, 2(10): 276–280, 2015. [URL](#).
- [56] R. D. Gdanski, J. D. Weaver, B. F. Slabaugh *et al.* A new model for matching fracturing fluid flowback composition. *SPE Hydraulic Fracturing Technology Conference*. Society of Petroleum Engineers, 2007. [URL](#).
- [57] California Department of Transportation. California vehicle code (online). Accessed: 1 April 2016, 2016. [URL](#).
- [58] Texas Department of Motor Vehicles. Texas size and weight limits (online). Accessed: 1 April 2016, 2016. [URL](#).
- [59] NRG Manufacturing. 2500 HP Frac Pump Unit. Tomball, Texas, USA, 2013. [URL](#).
- [60] European Communities. Council Directive 96/53/EC. Official Journal of the European Communities, Brussels, Belgium, 1996. [URL](#).
- [61] Stewart and Stevenson. Accu Frac PC, Automated Blender Controller - Operation Manual, 2005. Stewart and Stevenson Control System Group, 10750 Telge Road, Houston, Texas 77095.
- [62] P. J. Singh and S. D. Able. Determination of npshr for reciprocating positive displacement pumps-a new approach. *PROCEEDINGS OF THE INTERNATIONAL PUMP USERS SYMPOSIUM*, pages 131–142. TEXAS A&M UNIVERSITY SYSTEM, 1996.
- [63] WeirSPM. QEM3000 Well Service Pump. Weir SPM web-site: www.weiroilandgas.com, Fort Worth, Texas, USA, 2015. [URL](#).
- [64] Stewart and Stevenson. Intelligent pump control - operation manual, 2005. Stewart and Stevenson Control System Group, 10750 Telge Road, Houston, Texas 77095.

-
- [65] WeirSPM. SPM pump product catalog. Weir SPM web-site: www.weiroilandgas.com, Fort Worth, Texas, USA, 2015. [URL](#).
- [66] Dragon. Products. ltd. Mobile frac pump stimulation unit, 2012. [URL](#).
- [67] CAT Engine specification. 3512c hd offshore well service engine, 2011. [URL](#).
- [68] Mercedes-Benz. OM 501LA, 2002. [URL](#).
- [69] H. Wirry, R. Bachmann and M. Dundore. *Guide to Hydrodynamic Drive Applications*. Twin Disc, Racine, Wisconsin, 1961.
- [70] Twin. Disc. Products for gas and oil Industry, 2013. Web-site:[URL](#).
- [71] Twin Disc Inc. Engine - torque converter performance characteristics. USA, 2011.
- [72] Allison. Transmission. 9800 series Performance Data, 2012. Web-site:[URL](#).
- [73] TWS 2250HD Well Service Pump. Weir SPM web-site: www.weiroilandgas.com, Fort Worth, Texas, USA, 2009. [URL](#).
- [74] J. E. Miller. *The reciprocating pump: theory, design, and use*. John Wiley & Sons, 1987. ISBN 0471854670, 9780471854678.
- [75] American Petroleum Institute. 674 Positive Displacement, Reciprocating, Pumps. API Standard, 1995.
- [76] T.-g. Fan and G.-q. Zhang. Laboratory investigation of hydraulic fracture networks in formations with continuous orthogonal fractures. *Energy*, 74: 164–173, 2014. [doi: 10.1016/j.energy.2014.05.037](https://doi.org/10.1016/j.energy.2014.05.037).
- [77] M. HybridTM. Technical Manual - Well Service Pump Triplex and Quintuplex Models . MSI web-site: www.diwmsi.com, Alice, Texas, USA, 2016. [URL](#).
- [78] I. J. Karassik, W. C. Krutzsch, W. H. Fraser and J. P. Messina. *Pump handbook*. 1986. ISBN: 9780080560052.
- [79] A. Josifovic, J. Corney and B. Davies. Modeling a variable speed drive for positive displacement pump. *Advanced Intelligent Mechatronics (AIM), 2014 IEEE/ASME International Conference on*, pages 1218–1223. IEEE, Besanon, France, July 8-11, 2014. [URL](#).

-
- [80] Z. Guanghong, D. Hongyan, Z. Yue and L. Nianlian. Corrosion–erosion wear behaviors of 13cr24mn0. 44n stainless steel in saline–sand slurry. *Tribology International*, 43(5): 891–896, 2010. [doi:10.1016/j.triboint.2009.12.021](https://doi.org/10.1016/j.triboint.2009.12.021).
- [81] The National Physical Laboratory. Pumps and valves. Guides to Good Practice in Corrosion Control, 2000. [URL](#).
- [82] A. Iannetti, M. T. Stickland and W. M. Dempster. A computational fluid dynamics model to evaluate the inlet stroke performance of a positive displacement reciprocating plunger pump. *Proceedings of the Institution of Mechanical Engineers, Part A: Journal of Power and Energy*, 2014. [DOI:10.1177/0957650914530295](https://doi.org/10.1177/0957650914530295).
- [83] H. Meng and K. Ludema. Wear models and predictive equations: their form and content. *Wear*, 181: 443–457, 1995. [URL](#).
- [84] C. A. R. Duarte, F. J. de Souza and V. F. dos Santos. Mitigating elbow erosion with a vortex chamber. *Powder Technology*, 288: 6 – 25, 2016.
- [85] J. Rootzén and F. Johnsson. Co 2 emissions abatement in the nordic carbon-intensive industry—an end-game in sight? *Energy*, 80: 715–730, 2015. [DOI:10.1016/j.energy.2014.12.029](https://doi.org/10.1016/j.energy.2014.12.029).
- [86] E. Gavenas, K. E. Rosendahl and T. Skjerpen. Co 2-emissions from norwegian oil and gas extraction. *Energy*, 90: 1956–1966, 2015. [DOI:10.1016/j.energy.2015.07.025](https://doi.org/10.1016/j.energy.2015.07.025).
- [87] G. A. Heath, P. ODonoughue, D. J. Arent and M. Bazilian. Harmonization of initial estimates of shale gas life cycle greenhouse gas emissions for electric power generation. *Proceedings of the National Academy of Sciences*, 111(31): E3167–E3176, 2014. [URL](#).
- [88] Forster, D., Perks, J. Climate impact of potential shale gas production in the eu - final report (final report - review no. issue 2). 2012. [URL](#).
- [89] D. J. MacKay and T. J. Stone. Potential greenhouse gas emissions associated with shale gas extraction and use. *London, UK: Department of Energy and Climate Change*, 2013. [URL](#).
- [90] Bond, CE., Roberts, J., Hastings, AFSJ., Shipton, Z., Joao, E., Tabyldy, K., Stephenson, M. Life-cycle assessment of greenhouse gas emissions from unconventional gas in scotland. 2014. [URL](#).

-
- [91] New York State Department of Environmental Conservation. Well permit issuance for horizontal drilling and high-volume hydraulic fracturing to develop the marcellus shale and other low-permeability gas reservoirs. <http://www.dec.ny.gov/>, 2011.
- [92] J. L. Adgate, B. D. Goldstein and L. M. McKenzie. Potential public health hazards, exposures and health effects from unconventional natural gas development. *Environmental science & technology*, 48(15): 8307–8320, 2014. [URL](#).
- [93] G. Rodriguez. *Air emissions characterization and management for natural gas hydraulic fracturing operations in the united states*. Master’s thesis, University of Michigan, 2013. [URL](#).
- [94] S. Pugh. *Total design: integrated methods for successful product engineering*. Addison-Wesley Wokingham, 1991. ISBN: 978-0201416398.
- [95] A. Iannetti. *A numerical and experimental study on cavitation in positive displacement pumps and its application in valve design optimization*. Ph.D. thesis, University of Strathclyde, 2015.
- [96] T. Zackrisson. Modeling and simulation of a driveline with an automatic gearbox. *Master’s thesis, Royal Institute of Technology, KTH*, 2003. [URL](#).
- [97] MATLAB. Modeling an automatic transmission controller. *Simuling - Stateflow documentation*, 2016. [URL](#).
- [98] MATLAB. Fixed-displacement hydraulic pump. *Simscape fluids - documentation*, 2016. [URL](#).
- [99] P. J. Singh and N. Madavan. Complete analysis and simulation of reciprocating pumps including system piping. 1987.
- [100] P. J. Singh and W. K. Chaplis. Experimental evaluation of bladder type pulsation dampeners for reciprocating pumps. 1988.
- [101] J. E. Miller. *The Reciprocating Pump - Theory, Design and Use*, volume Second Edition. Krieger Publishing Company, Malabar, Florida, 1995. ISBN 0-089464-599-4.
- [102] TNO Science and Industry. Api 674 analysis for reciprocating pumps. web-site: <https://www.tno.nl/>, 2013.
- [103] WeirSPM. Pressure Pumping Systems. Weir SPM web-site: www.weiroilandgas.com, Fort Worth, Texas, USA, 2015.

-
- [104] W. Woods and S. Khan. Paper 3: An experimental study of flow through poppet valves. *Proceedings of the Institution of Mechanical Engineers, Conference Proceedings*, volume 180, pages 32–41. SAGE Publications, 1965. [URL](#).
- [105] J. Zhao and R. J. Seethaler. A fully flexible valve actuation system for internal combustion engines. *Mechatronics, IEEE/ASME Transactions on*, 16(2): 361–370, 2011. [DOI:10.1109/TMECH.2010.2043850](https://doi.org/10.1109/TMECH.2010.2043850).
- [106] A. Iannetti, M. T. Stickland and W. M. Dempster. A cfd and experimental study on cavitation in positive displacement pumps: Benefits and drawbacks of the fullcavitation model. *Engineering Applications of Computational Fluid Mechanics*, 10(1): 57–71, 2016. [URL](#).
- [107] D. S. Miller. *Internal flow system*. BHRA, 1990. ISBN: 978-0956200204.
- [108] D. Johnston, K. Edge and N. Vaughan. Experimental investigation of flow and force characteristics of hydraulic poppet and disc valves. *Proceedings of the Institution of Mechanical Engineers, Part A: Journal of Power and Energy*, 205(3): 161–171, 1991. [URL](#).
- [109] Edge, KA and Boston, OP and Xiao, KCS and Longvill, KCMJ and Burrows, KCCR. Pressure pulsations in reciprocating pump piping systems part 2: Experimental investigations and model validation. *Proceedings of the Institution of Mechanical Engineers, Part I: Journal of Systems and Control Engineering*, 211(3): 239–250, 1997. [DOI:10.1243/0959651971539777](https://doi.org/10.1243/0959651971539777).
- [110] K. A. Edge, O.P. Boston, S Xiao, M.J. Longvill, C.R. Burrows. Pressure pulsation in reciprocating pump piping systems: Part2. 1997.
- [111] A. Josifovic, A. Iannetti, J. Corney and M. Stickland. A new engineering procedure for positive displacement pump performance analysis based on 1d and 3d cfd commercial codes. *Journal of Fluids Engineering*, 2016.
- [112] C. L. Cipolla, E. Lolon, M. J. Mayerhofer, N. R. Warpinski *et al.* The effect of proppant distribution and un-propped fracture conductivity on well performance in unconventional gas reservoirs, 2009.
- [113] S. Ron Martin, S. Jason Baihly, S. Raj Malpani and S. Garrett Lindsay. Understanding production from eagle ford-austin chalk system, 2011. [URL](#).

-
- [114] R. Martin, J. D. Baihly, R. Malpani, G. J. Lindsay, W. K. Atwood *et al.* Understanding production from eagle ford-austin chalk system. *SPE Annual Technical Conference and Exhibition*. Society of Petroleum Engineers, 2011. [URL](#).
- [115] B. Jouan, S. Bergholz and J. Rudolph. Fatigue monitoring approaches for power plants. *ASME 2014 Pressure Vessels and Piping Conference*, pages V001T01A035–V001T01A035. American Society of Mechanical Engineers, 2014. [URL](#).
- [116] S. Bergholz, J. Rudolph and A. Willuweit. Famos 4 wind a new method for the fatigue monitoring of wind energy plants. *Procedia Engineering*, 133: 84–89, 2015. [URL](#).
- [117] Hughes Pumps. HPS400 High Pressure Triplex Pump - technical paper (online). Accessed: 08 Jun 2015, 2015. [URL](#).
- [118] Brook Crompton. W cast iron motors - technical paper (online). Accessed: 28 Jan 2016, 2015. [URL](#).
- [119] ABB. Abb industrial drives - technical paper (online). Accessed: 08 Jun 2015, 2015. [URL](#).
- [120] WIKA. WIKA S-10 pressure sensors - technical paper (online). Accessed: 08 Jun 2015, 2015. [URL](#).
- [121] Honeywell Sensing and Control. Hoa series infrared reflective sensor - technical paper (online). Accessed: 22 Jan 2016, 2016. [URL](#).
- [122] National Instruments. 6210 Bus-powered M Series Multifunctional DAQ for USB - technical paper (online). Accessed: 25 Jan 2016, 2016. [URL](#).
- [123] National Instruments. 6008 Bus-Powered Multifunction DAQ USB - technical paper (online). Accessed: 25 Jan 2016, 2016. [URL](#).
- [124] R. Taylor. Interpretation of the correlation coefficient: a basic review. *Journal of diagnostic medical sonography*, 6(1): 35–39, 1990. [URL](#).
- [125] Leard Statistics. Pearson product-moment correlation, 2016. [URL](#).
- [126] Y.-J. Zhang, Z.-W. Li, L.-L. Guo, P. Gao, X.-P. Jin and T.-F. Xu. Electricity generation from enhanced geothermal systems by oilfield produced water circulating through reservoir stimulated by staged fracturing technology for horizontal wells: A case study in xujiaweizi area in daqing oilfield, china. *Energy*, 2014. [doi: 10.1016/j.energy.2014.10.073](#).

-
- [127] StimPlan. Integrated 3d fracture design and analysis. Tulsa, OK 74136, USA, 2012. [URL](#).
- [128] J. F. Hair, R. L. Tatham, R. E. Anderson and W. Black. *Multivariate data analysis*, volume 6. Pearson Prentice Hall Upper Saddle River, NJ, 2006. ISBN: 978-0130329295.
- [129] C. Van Dam, R. Chow, J. Zayas and D. Berg. Computational investigations of small deploying tabs and flaps for aerodynamic load control. *Journal of Physics: Conference Series*, volume 75, page 012027. IOP Publishing, 2007.
- [130] European Commission - JRC Scientific and technical report. Parameterisation of fuel consumption and co2 emissions of passenger cars and light commercial vehicles for modelling purposes, 2011. [URL](#).
- [131] Metropolitan Transport Research Unit. Heavy goods vehicles - do they pay for the damage they cause?, 2014. [URL](#).
- [132] NVF committee Vehicles and Transports. Road wear from heavy vehicles, 2008. [URL](#).
- [133] J. Leszek. private communication, 2015.
- [134] H. Clarke. private communication, 2015.
- [135] C. Green. private communication, 2015.
- [136] T. Stewart. private communication, 2015.
- [137] V. Jayaram, M. Y. Khan, W. A. Welch, K. Johnson, J. W. Miller and D. R. Cocker. A generalized approach for verifying the emission benefits of off-road hybrid mobile sources. *Emission Control Science and Technology*, pages 1–10, 2016.
- [138] C.-L. Myung, A. Ko, J. Kim, K. Choi, S. Kwon and S. Park. Specific engine performance and gaseous emissions characteristics of european test cycle and worldwide harmonized driving cycle for a heavy-duty diesel engine. *Journal of Mechanical Science and Technology*, 27(12): 3893–3902, 2013. [URL](#).
- [139] EPA. Final regulatory impact analysis: Control of emissions from nonroad diesel engines. Washington DC, USA, 1998. [URL](#).
- [140] WorldSteel association. Sustainability indicators (online). Accessed: 16 April 2016, 2014. [URL](#).

Appendix A

Appendix

A.1 Field data

In addition to the speed encoder (measuring the PD pump's RPM) and discharge pressure sensor, location of which can be seen in Figure 5.1, the pump is also instrumented with two accelerometers. In Figure A.1 their precise orientation and placement on two main subsections of the pump, power-end and the fluid-end, can be seen.

A different amplitude of vibration can be seen in Figure A.2. Vibration in the direction of x-axis on PE is an order of magnitude higher than in the other two. Y-axis on FE is also showing a similar amplitude difference compared to others. Dominant acting forces are coincident, both are oriented facing each other which is to be expected because power is continually being balanced between PE's crankshaft and FE's plunger assembly.

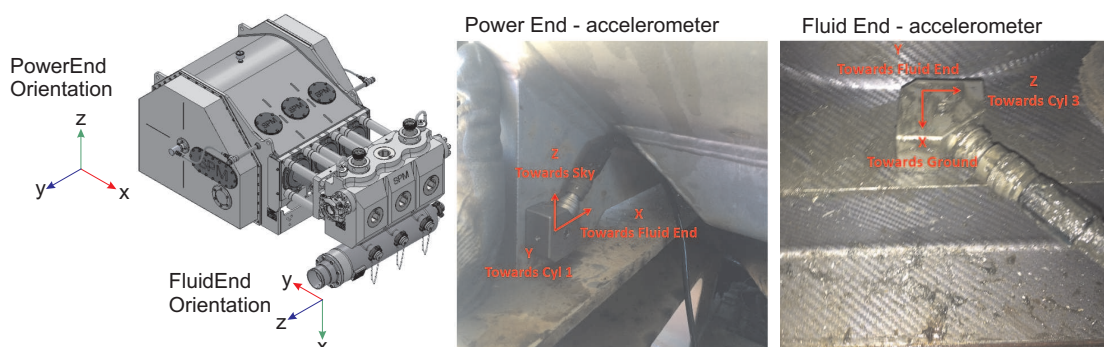


Figure A.1: Orientation of accelerometers on the PD pump

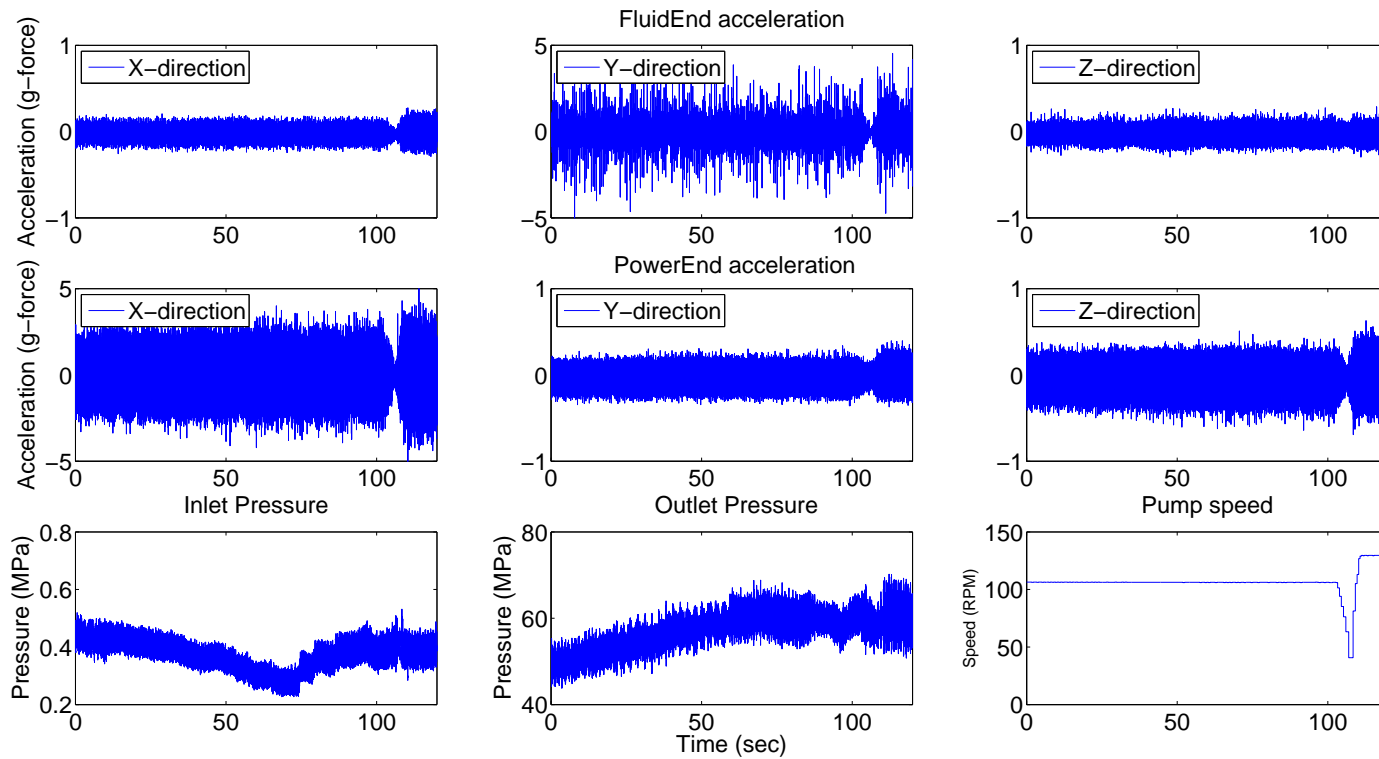


Figure A.2: Pump metrics during formation breakdown - state one

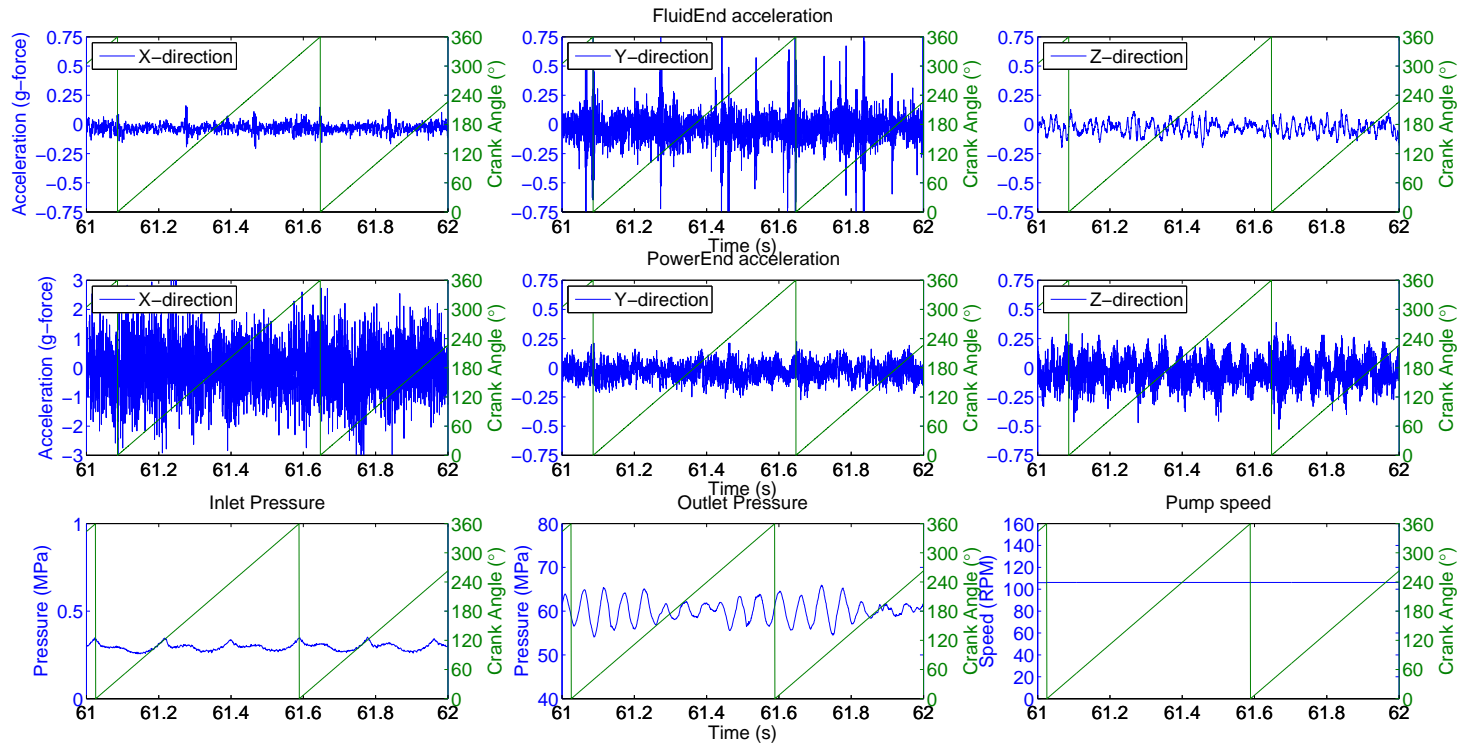


Figure A.3: Pump metrics obtained in steady state conditions prior to formation breakdown - state one at one second

Table A.1: Data from tri-axial accelerometer located on the PD pump's Power End

Sensor	Peak (g)		Mean (g)	RMS (g)
	Positive	Negative		
x-accelerometer	5.0947	-5.0063	-0.0309	0.8373
y-accelerometer	0.3945	-0.3698	-0.0283	0.0805
z-accelerometer	0.6283	-0.6920	-0.0305	0.1172

A.1.1 Power End Tri-axial accelerometer

Time domain analysis of the crankshaft accelerometer in state one is shown in Table A.1.

Analysis in time domain demonstrates significantly higher energy in the x-axis of the crankshaft assembly. Calculating RMS values shows approximately 10 times more energy in x-axis compared to y-axis and 7 times more energy than in the z-axis.

Peak values are mostly symmetrical in positive and negative magnitude. Mean values are relatively low in all three orientations.

There has not been enough evidence to prove interaction between the vibration in the three axes, so it can be concluded that each of the axes is to be considered as an independent function. Because of the comparatively high energy in one direction further PE accelerometer analysis and discussion will focus solely on the x-axis.

Time series data obtained from the PE accelerometer can be further developed by implementing double integration thereby evaluating crankshaft displacement. Noisy signal was processed with 50 Hz filter. Final result can be seen in Figure A.4.

Analysis in the frequency domain of the accelerometer in x-axis is displayed in Figure A.5.

A.1.2 Fluid End Tri-axial accelerometer

Time domain analysis of the accelerometer placed on the Fluid End chamber in the state one is shown in Table A.2.

Once again energy in the direction of one of the axes is visibly higher compared to the other two. Further analysis will take into account this measurement. Displacement can also be evaluated using double integration of the acceleration. Figure A.6 shows

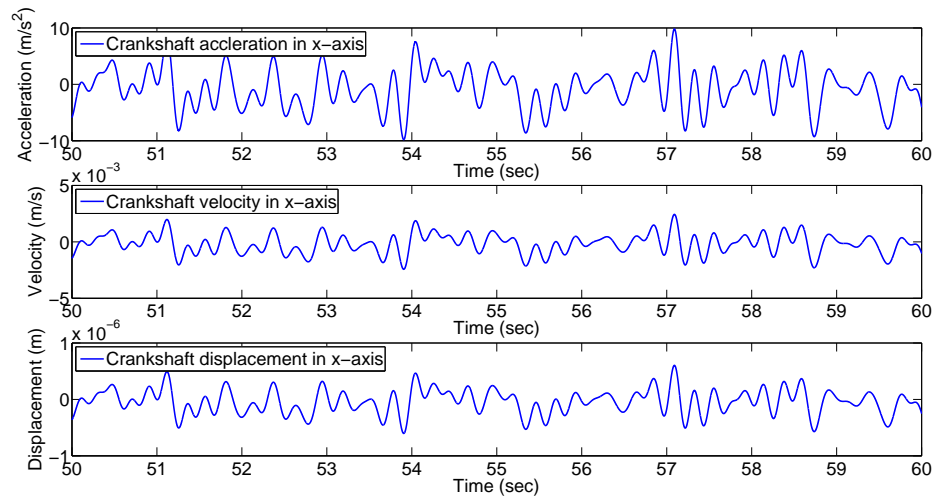


Figure A.4: Crankshaft accelerometer and data metrics displaying velocity and displacement

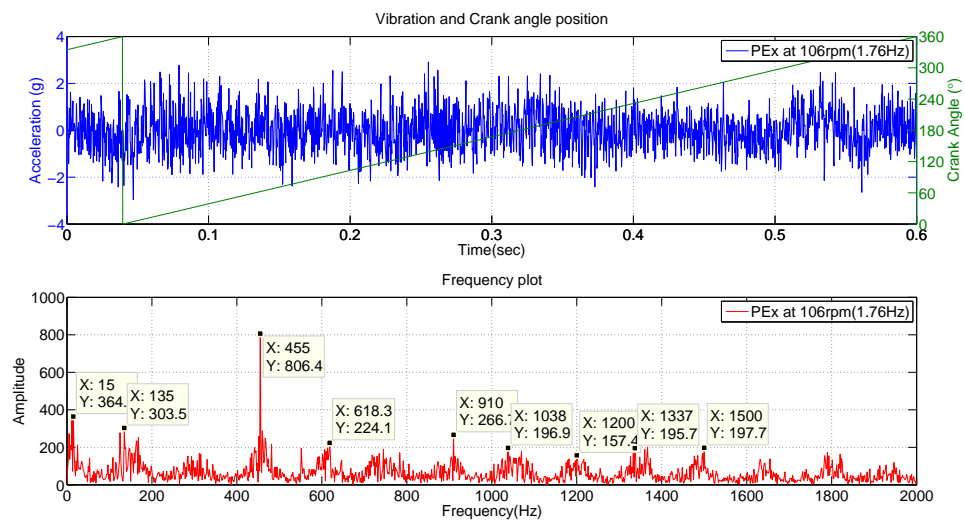


Figure A.5: Frequency plot of accelerometer placed on the PD pump’s Power End in the direction of the x-axis

Table A.2: Data from tri-axial accelerometer located on the PD pump’s Fluid End

Sensor	Peak (g)		Mean (g)	RMS (g)
	Positive	Negative		
x-accelerometer	0.2745	-0.2877	-0.0305	0.0498
y-accelerometer	4.6588	-5.4990	-0.0322	0.1769
z-accelerometer	0.2871	-0.2940	-0.0290	0.0681

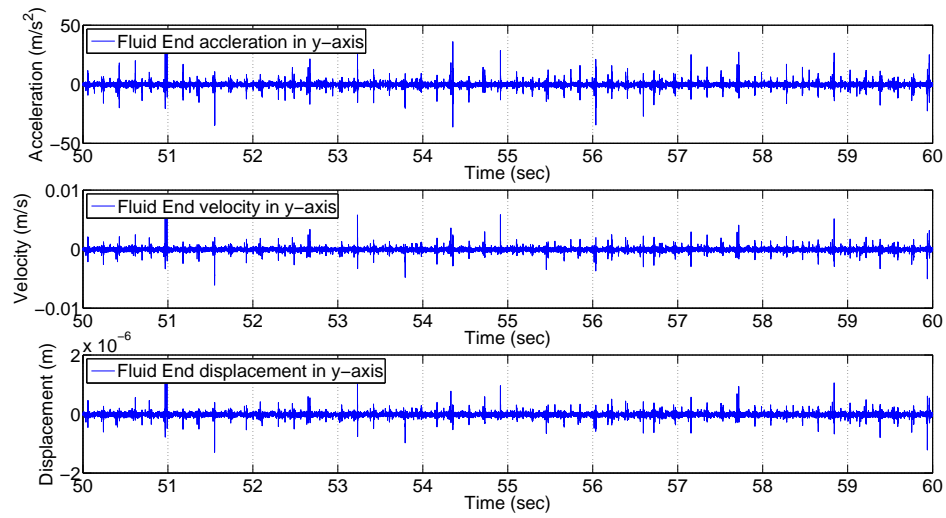


Figure A.6: Acceleration, velocity and displacement plot from accelerometer located on the Fluid End in the direction of the y-axis

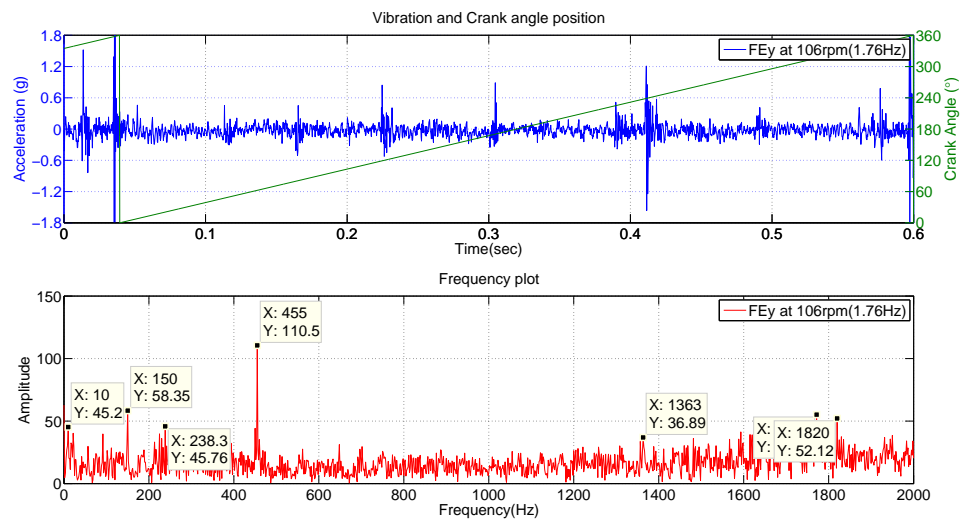


Figure A.7: Frequency analysis plot from accelerometer located on the Fluid-end of a PD pump in the direction of the y-axis

Fluid End displacement over the course of ten seconds.

Because of the nature of the signal it was decided that no filtering is needed as it will affect the final output. Because of this it is clear that pulses are equally spaced. This means that a pump running at a constant speed will produce synchronized pulses that correspond well with the plunger movement inside the pump. This effect is naturally more prominent on the Fluid End side of the pump because of the closeness to the reciprocating source (plunger) and the operating medium (slurry).

Analysis of the Fluid End accelerometer in the frequency domain can be seen in Figure A.7. Data presented is taken from the same time segment as in the analysis of the crankshaft metrics.

A.2 Operational states two, three and four

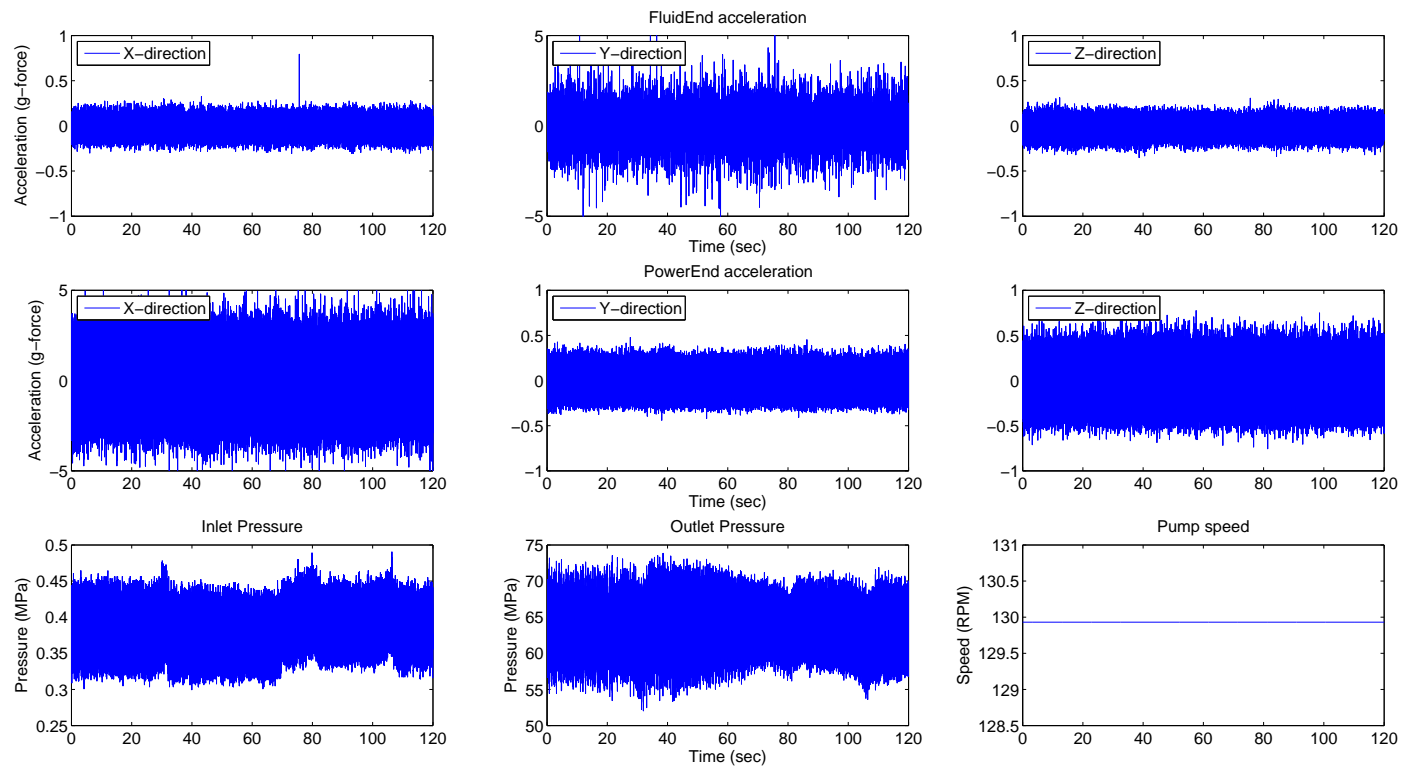


Figure A.8: Operating metrics in the state two

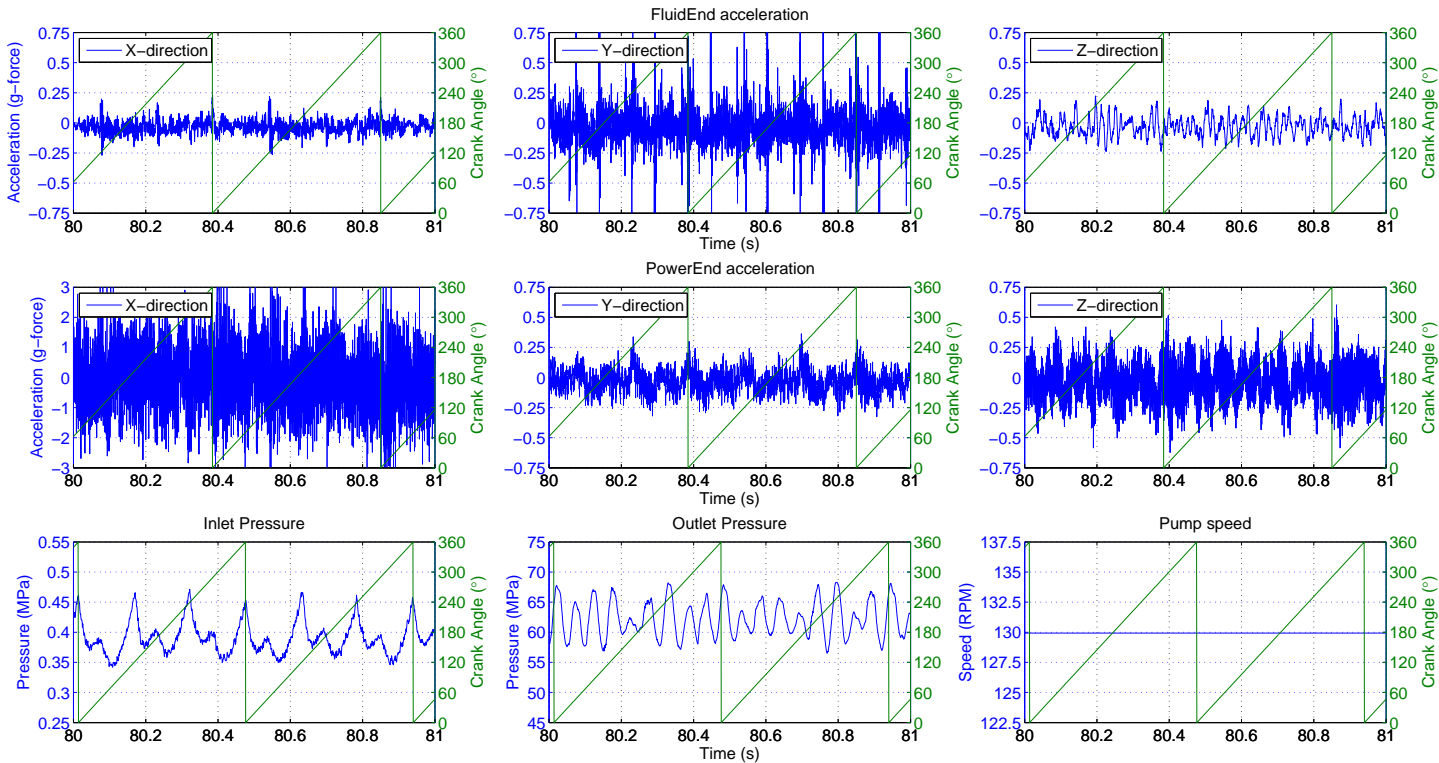


Figure A.9: Operating metrics in the state two - one second data

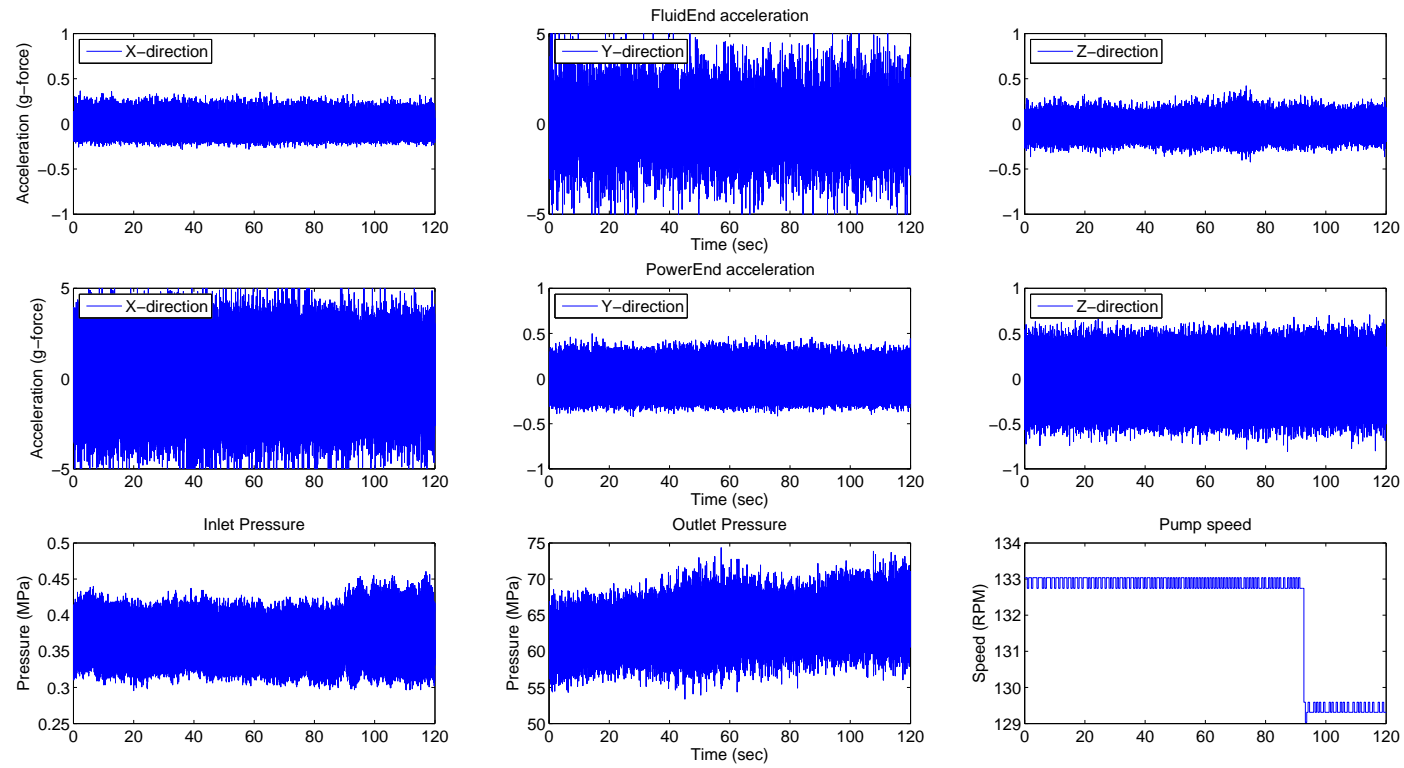


Figure A.10: Operating metrics in the state three

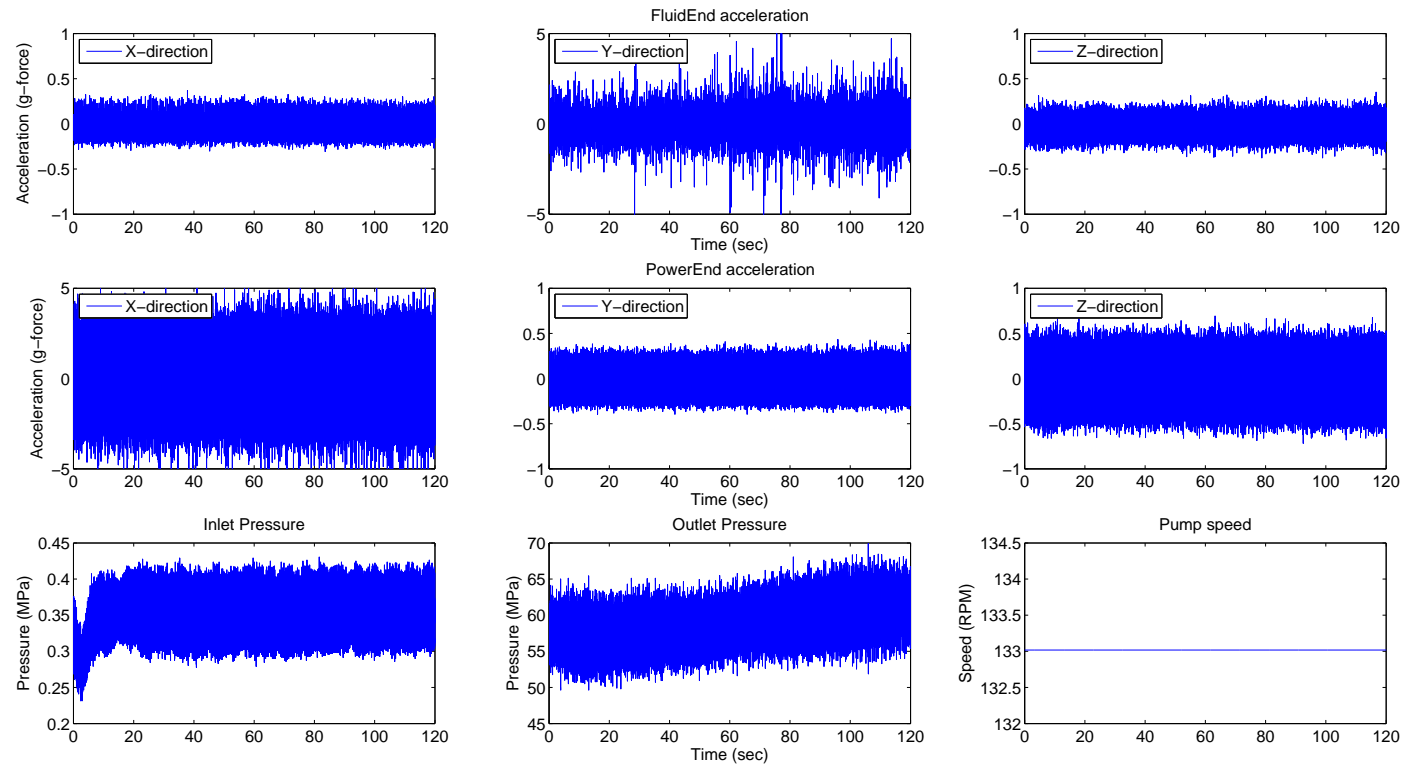


Figure A.11: Operating metrics in the state four

Appendix B

Test rig components

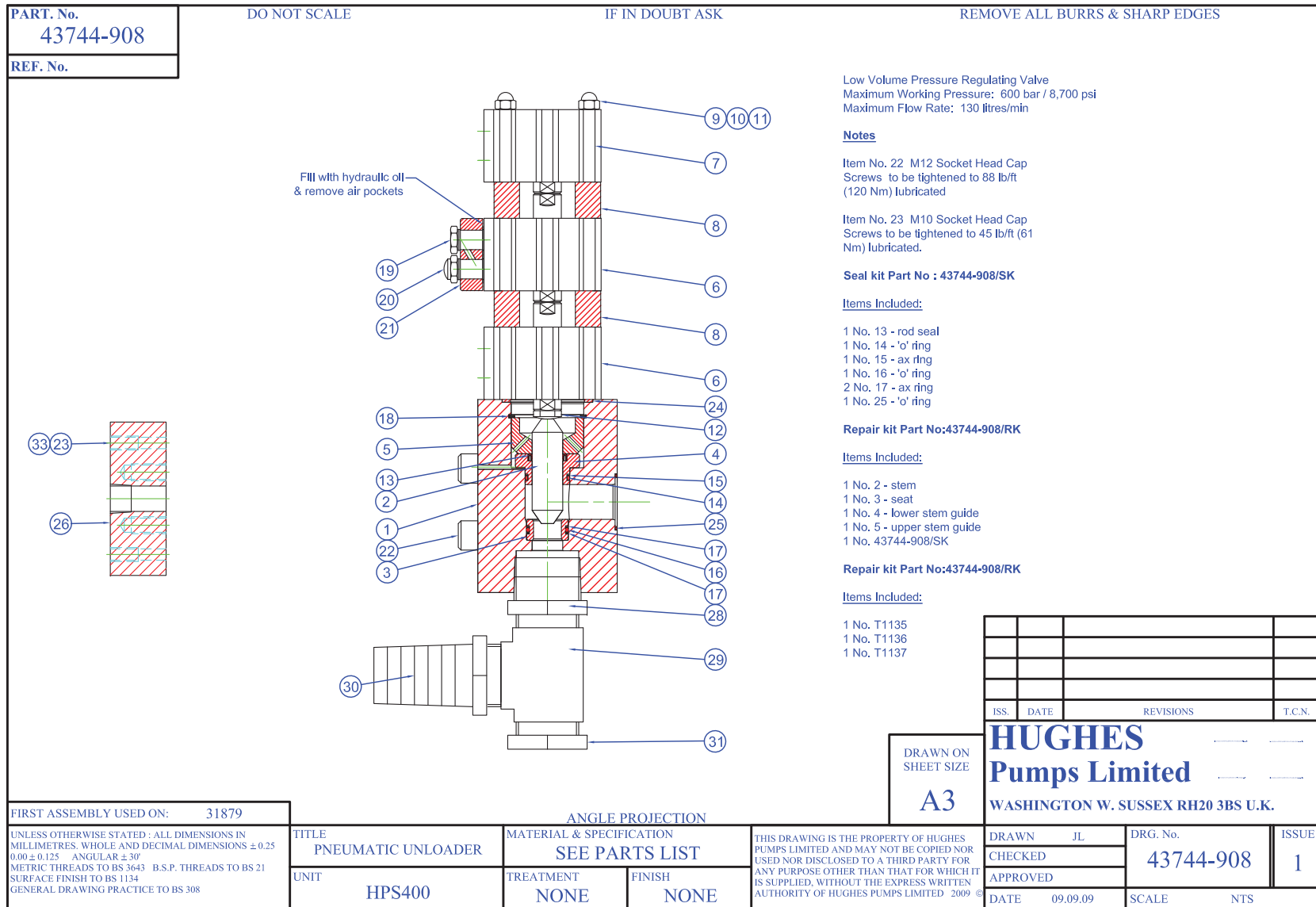


Figure B.1: Pneumatically actuated pressure adjusting valve to generate back pressure for the pump

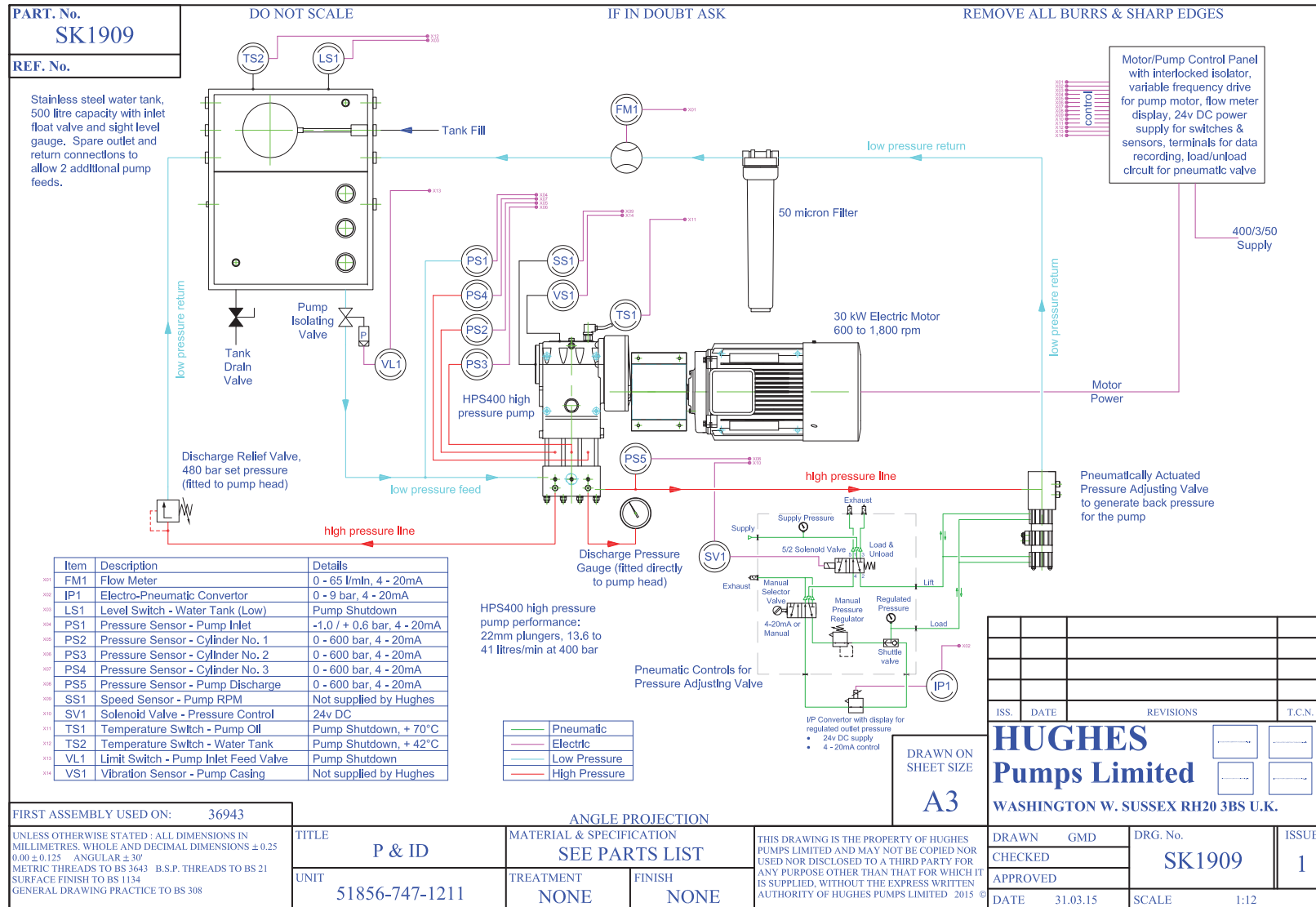


Figure B.2: P&ID schematic of the test rig



Piezoresistive Pressure Transmitter

Prod.No: 222305.2974

TYPE : PAA-23 / 2bar / 8465.1

SN : 543896

OUTPUT : 0 ... 10 V



RANGE : 0 ... 2 bar abs

Linearity	-0.03	%FS(Lnorm)	bar abs	
Max.Pressure	3	bar abs	0.00	
Supply	13 ... 32	V DC	0.50	
Comp.Temp.Range	-10 ... 80	°C	1.00	
			1.50	
			2.00	

1 : GND
2 : +OUT
3 : +Vcc

07.01.2016

1
BC

KELLER Druckmesstechnik

CH-8404 Winterthur, St.Gallerstrasse 119

D-79798 Jestetten, Schwarzwaldstr.17



Piezoresistive Pressure Transmitter

Prod.No: 222305.2352

TYPE : PA-23 / 600bar / 8465.1

SN : 151611

OUTPUT : 0 ... 10 V



RANGE : 0 ... 600 bar

Linearity	0.09	%FS(Lnorm)	bar	
Max.Pressure	900	bar	0	0.00
Supply	13 ... 32	V DC	150	2.49
Comp.Temp.Range	-10 ... 80	°C	300	4.99
			450	7.50
Atm. Pressure	1000mbar abs		600	10.01

1 : GND
2 : +OUT
3 : +Vcc

07.01.2016

1
BOS

KELLER Druckmesstechnik

CH-8404 Winterthur, St.Gallerstrasse 119

D-79798 Jestetten, Schwarzwaldstr.17

Appendix C

Validation

Two pumping cycles from a PD pump were recorded in test facilities in the USA. Pump is operating at 130 rpm which translates to 0.46 seconds per crank rotation. It can be seen that pump is showing three distinctive pressure pulses per single crank rotation.

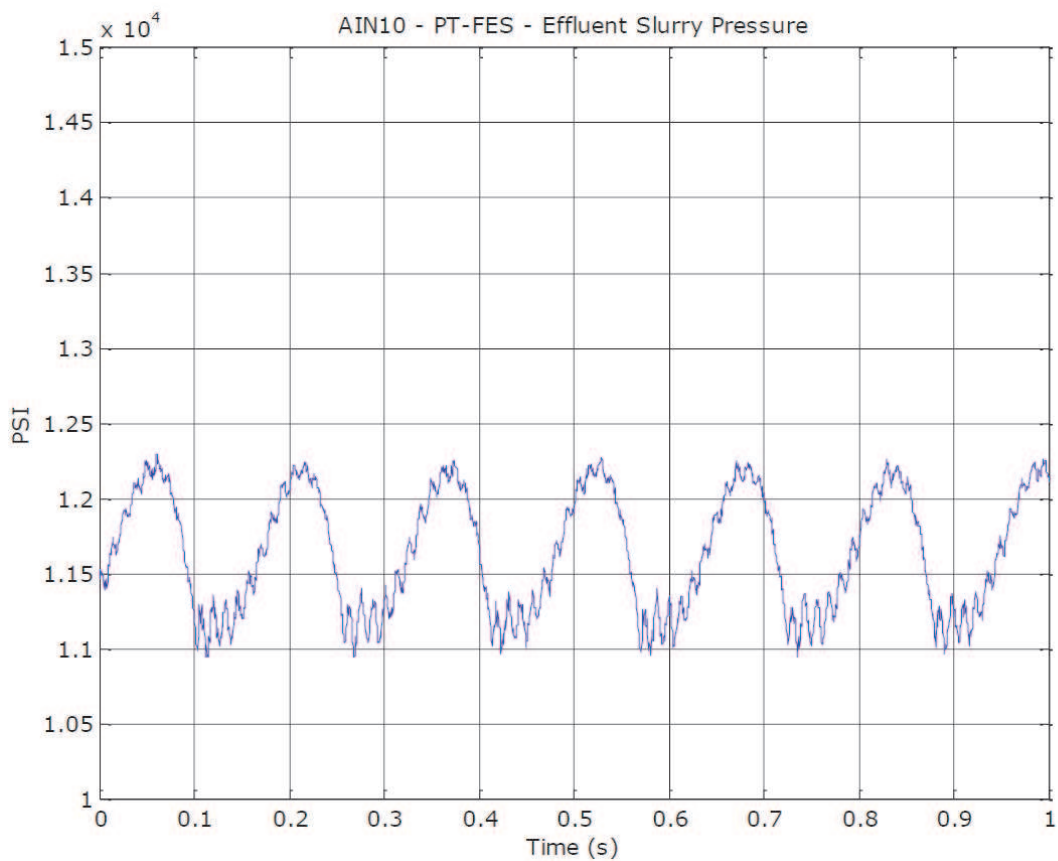


Figure C.1: Factory test rig data from full size experiment conducted in the USA.